Mandibular Mass Properties in Mammalian Terrestrial Herbivores

Adrian Maurice O'Driscoll

PhD

The University of Hull and The University of York

Hull York Medical School

October 2025

Thesis Abstract

This thesis investigates the determinants, mechanical implications, and evolutionary significance of mandibular mass distribution in ungulate-grade mammals. The mass properties of the mandible (i.e., mass, centre of mass, and rotational inertia) govern the energetic efficiency of mastication and the mechanical stresses acting on the masticatory system. Despite their importance, these properties remain poorly quantified in comparative studies. Here, new computed tomography (CT) based and surface model-based methods are developed and validated to estimate mandibular mass distribution with high precision and reproducibility. Validation against an established analogue method demonstrates close agreement, confirming that CT-derived estimates are accurate and data derived from either method are statistically interchangeable.

Using these techniques, interspecific and ontogenetic datasets of ungulate-grade mammals (Orders Artiodactyla, Perissodactyla, Proboscidea) were analysed to evaluate scaling relationships between anatomical and mechanical metrics (i.e., mandible length, mass, centre of mass, rotational inertia, masseter insertion area, mechanical advantage of the adductor musculature). Results show that rotational inertia scales with positive allometry relative to mandible length, indicating that larger taxa possess disproportionately higher resistance to angular acceleration. Adjustments for habitual head posture reveal that an anteriorly downward mandible orientation reduces effective rotational inertia and the mechanical cost of chewing, an effect which is most pronounced in grazing and large-bodied species. Additional analyses show that the masseter insertion area and mechanical advantage scale isometrically, maintaining functional efficiency across size ranges. Comparative results from extinct and extant taxa demonstrate continuity in these biomechanical patterns through the Cenozoic, linking morphological diversity to ecological adaptations in feeding behaviour and energetics.

Collectively, the findings establish a robust methodological and theoretical framework for integrating mandibular mass distribution into functional and evolutionary analyses of mammalian masticatory mechanics. The study highlights the interplay between biomechanics, ecology, and evolution in shaping the morphology, function, and performance of the mammalian mandible.

Contents

List of Figures

List of Tables

Acknowledgements

An enormous thank you must be given to Dr Laura Fitton, without who this thesis would not have been written, and who can always be relied upon to go the extra mile.

I would also like to show my appreciation for Prof Nathan Jeffery, who provided the initial idea that led to this project and whose supervision was critical during the first three years of my PhD.

Conference Presentations

The Annual Symposium of Vertebrate Palaeontology and Comparative Anatomy 2022. “The Effect of Mass Distribution on the Mammalian Mandible”. *Poster Presentation.*

The Annual Symposium of Vertebrate Palaeontology and Comparative Anatomy 2023. “External Morphology or Internal Anatomy - Assessing Determinants of Mandibular Mass Distribution”. *Oral Presentation.*

Anatomical Society Winter Meeting 2024. “Biological and Mechanical Implications of Mandibular Mass Distribution in Terrestrial Mammalian Herbivores (Orders Artiodactyla, Perissodactyla, Proboscidea)”. *Oral Presentation.*

Progressive Palaeontology 2024. “Biological and Mechanical Implications of Mandibular Mass Distribution in Terrestrial Mammalian Herbivores - An Evolutionary Perspective from Eocene to Present”. *Oral Presentation.*

Author's Declaration

I declare that this thesis is a presentation of original work and I am the sole author. This work has not previously been presented for a degree or other qualification at this University or elsewhere. All sources are acknowledged as references.

1. Introduction

The evolution of the mammalian masticatory system represents a major functional development in vertebrate evolution. Arising from the transition between non-mammalian synapsids and early mammals, this system enabled the mechanical processing of food to become more efficient and controlled. Mastication, defined as the rhythmic and cyclic breakdown of food by coordinated movements of the jaws and teeth, is central to the mammalian mode of life. It supports high metabolic demands associated with endothermy and sustained activity, and it has facilitated extensive dietary diversification across the clade.

The masticatory apparatus integrates skeletal, muscular, and neural components into a single biomechanical system. The mandible functions as the principal load-bearing element, transmitting forces generated by the adductor musculature through the temporomandibular joint to the dentition. The morphology and mechanical performance of this structure reflect the balance between competing requirements for rigidity, dietary specialisation, and efficiency. Variation in mandibular morphology and mass distribution therefore provide an important record and avenue for study of evolutionary and functional adaptation.

This chapter establishes the conceptual framework for the study. It examines the defining characteristics of mammalian mastication, outlines the organisation of the masticatory system, and identifies the features that distinguish it from other vertebrate groups. It then reviews previous research on mandibular form and function, introduces the concept of mass properties and their mechanical significance, explains the rationale for using ungulate-grade mammals as a comparative model, justifies the necessary inclusion of head posture in studies of mandible mechanics, and explores the past diversity of ungulate-grade mammals and their extreme mandible morphologies. The chapter concludes with a statement of the study's aims, which seeks to validate a computed tomography-based method of estimating mass distribution using voxel-specific material densities and investigate the determinants of mandible mass distribution, and investigate the biological and mechanical implications of mass properties on the mechanics of the mandible, the effect of head posture, and mandibular mass properties in megafaunal mammals throughout the Cenozoic.

1.1 Overview of the Mammalian Masticatory System

Mastication, the mechanical breakdown of food by the teeth, is not unique to mammals, but its efficiency and precision are. Mammalian mastication is facilitated by a suite of key anatomical

adaptations: the transformation of the lower jaw into a single dentary bone; the establishment of the temporomandibular joint (TMJ); the evolution of precise dental occlusion; and the diversification of dental form and function (Crompton, 1962; Turnbull, 1967; Herring, 1993). Collectively, these traits permit controlled, repetitive, and forceful chewing, allowing mammals to exploit a wide range of dietary resources and environments.

The masticatory system is an integrated complex comprising the mandible, dentition, jaw adductor musculature, temporomandibular joints, and associated neural control mechanisms (Herring, 2001). The mandible acts as both a structural lever and a dynamic oscillating element, transmitting muscular forces through the TMJ to fracture food between the teeth. Central pattern generators in the brainstem coordinate rhythmic jaw motion, while sensory feedback from muscle spindles, tendon organs, and periodontal ligaments fine-tune the force and timing of each cycle (Ross et al., 2007; Ross et al., 2009).

The mammalian mandible is a bilaterally symmetrical, U-shaped bone formed entirely by the dentary. Each side consists of a horizontal body or corpus housing the molar row and a vertical ramus bearing the coronoid, condylar, and angular processes. The symphysis joins the two halves, or hemi-mandibles, at its anterior end. This architecture reflects both evolutionary simplification and functional specialisation (Crompton, 1962; Turnbull, 1967).

Mechanically, the mandible operates as a third-class lever system, with the TMJ as the fulcrum, the masticatory muscles applying input forces, and the teeth delivering output at the bite point (Herring, 1993). The relative positions of these elements determine mechanical advantage of the masseter and temporalis, balancing bite force against jaw-closing velocity. Carnivores often exhibit long, slender mandibles optimised for speed and shearing, whereas herbivores, particularly ungulates, possess deep mandible bodies for large masseter insertions and reinforced symphyses that resist bending and torsional stresses from transverse chewing (Janis, 1990; Williams et al., 2007).

The adductor musculature, the masseter, temporalis, and pterygoids, control the movement of the mandible during mastication. The masseter, often present in multiple layers, provides the muscular force for jaw elevation and transverse movement, especially in herbivores where grinding dominates the chewing cycle (Turnbull, 1967; Williams et al., 2007). The temporalis contributes to vertical bite force and jaw stabilisation, while the medial and lateral pterygoids generate mediolateral motion, crucial for maintaining occlusal contact during power strokes. Together, these muscles enable the complex, three-dimensional jaw movements characteristic of mammalian mastication.

Compared to non-mammalian vertebrates, mammals display unique masticatory features. The evolution of the dentary-squamosal joint and dentary bone replaced the multi-element lower jaws of earlier synapsids (Barghusen and Hopson, 1970)., reducing kinematic complexity and allowing more precise control. In combination with heterodonty and occlusal precision, this reorganisation established the foundation for the diversity of feeding strategies observed in mammals.

1.2 Evolutionary and Functional Significance of Mammalian Mastication

Mammals occupy a broader diversity of ecological niches than any other animal clade, a success owed in part to their ability to process food efficiently through mastication. Endothermy, or the maintenance of a constant internal body temperature, reflects the high metabolic rates that characterise the clade (Grigg et al., 2022; Buckley et al., 2012). Sustained activity, whether in foraging, predator avoidance, or migration, requires a consistent and high-energy intake. Consequently, the mammalian feeding apparatus has evolved to extract maximal energy from food through mechanical breakdown prior to digestion, and its as a highly efficient mechanism, delivers a high ratio of calories ingested per calories expended during mastication.

Endothermy also imposes substantial energetic demands on the brain and musculature. The mammalian brain is a metabolically expensive organ and accounts for a large portion of total energy consumption (Raichle and Gusnard, 2002). Increases in relative brain size are correlated with elevated basal metabolic rates (Isler and van Schaik, 2006). Similarly, muscle performance benefits from endothermy as enzymes function optimally within stable thermal ranges, and oxygen delivery is sustained at high rates (Dauncey and Ingram, 1988; Schulte, 2015). These physiological conditions create a selective pressure for energy-efficient food processing. Effective mastication therefore reduces the mechanical work required to process food, saving energy for neural and locomotor functions while increasing feeding throughput.

Mammalian mastication is distinguished from that of other vertebrates by its rhythmicity, occlusal precision, and muscular coordination. In reptiles, feeding typically relies on inertial or static pressure mechanisms, with limited control of occlusion. Birds, while capable of cranial kinesis, rely on keratinous beaks for the breakdown of food material and lack post-canine occlusion. Mammals, by contrast, evolved the capacity for controlled chewing cycles with direct neural modulation of muscle recruitment and force production (Herring, 1993; Ross et al., 2009).

Among extant mammals, ungulates exemplify the extreme adaptation of the masticatory system for processing fibrous plant material. Their highly specialised dentition (i.e., selenodont and lophodont molars) produce efficient shearing and grinding surfaces, while transverse jaw motion enhances particle reduction, both necessary processes for the breakdown of tough fibrous vegetation. Analogous solutions occur outside Mammalia, including in herbivorous dinosaurs such as sauropods, which evolved convergent strategies for coping with abrasive vegetation (Sereno et al., 2007; Taylor et al., 2009).

1.3 Mass Properties, Rotational Inertia, and Scaling

Mass properties describe how mass is distributed within a structure and how well it resists linear and angular acceleration. These include total mass, the position of the centre of mass (CoM), and the moments and products of inertia that quantify resistance to angular acceleration (Zhang et al., 2001; Zhang et al., 2002). In the mandible, these properties determine how efficiently it can be accelerated and decelerated during each chewing cycle.

The mandible is repeatedly rotated about the TMJ thousands of times per day. Its morphology affects its function adaptations and structural strength but also its inertia (Ross et al., 2017). Early measurements of mass properties relied on physical models, but advances in computed tomography (CT) have enabled high-precision estimation of mass distribution and inertial parameters. Studies on pigs and humans revealed that bone density is consistent and that the COM lies close to the molar region, a position balancing muscular and occlusal loads (Zhang et al., 2001; Zhang et al., 2002).

Comparative research has established clear scaling patterns between aspects of mandibular morphology and its mass properties. In primates, rotational inertia scales with positive allometry relative to mandibular length, meaning larger mandibles resist angular acceleration disproportionately more than predicted by geometric similarity (Ross et al., 2017). Deepened corpora and robust symphyses, while increasing stiffness, also elevate inertia by shifting mass away from the axis of rotation. This creates a functional trade-off between strength and dynamic efficiency.

Recent research investigated if inertia, as the physical resistance to angular motion, dictates chewing rate. If the mandible behaved as a simple passive oscillator, larger species would chew much more slowly than they do. Instead, chewing cycle duration scales only modestly with

body size, suggesting that neuromuscular control and muscle stiffness control chewing rate and frequency (Ross et al., 2009).

Larger herbivores operate with more massive, high inertia mandibles but compensate by adjusting chewing rhythm and muscle activation (Ravosa et al., 2010). The result is a system that maintains performance efficiency across scales, which stand outs as a key reason for the evolutionary success of mammalian mastication.

1.4 Ungulate-Grade Mammals as a Model System

Ungulate-grade mammals provide an ideal model for investigating relationships between mandibular morphology, mass properties, and function. Their mandibles and dentitions exhibit a wide range of structural and ecological adaptations, making them ideal subjects for a comparative biomechanical study of this kind.

Ungulate dentition illustrates the evolutionary consequences of abrasive diets. Grazers such as equids and bovids possess hypsodont teeth (i.e., high-crowned molars adapted to resist wear from grass phytoliths and exogenous grit) while browsers typically retain brachydont dentition suited to softer vegetation (Damuth and Janis, 2011; Williams and Kay, 2001). Hypsodont taxa not only differ in crown height but also in the proportion of enamel and dentine, influencing mandibular mass distribution. The greater mass of hypsodont teeth and reinforced bone along the molar row likely shifts the COM posteriorly, altering rotational inertia.

Functional morphology also varies across feeding types. The deep corpus and fused symphyses in grazers resist torsional loads generated during transverse grinding, while more gracile, flexible mandibles in browsers facilitate varied jaw movements (Turnbull, 1967; Ross et al., 2017). These contrasts provide a natural experiment in form–function relationships: how mass distribution, mechanical strength, and neuromuscular control co-evolve to maintain efficient mastication under different ecological pressures.

Ungulates thus offer a framework for exploring the evolutionary relationships between mandible morphology, mass properties, and dietary specialisation. Their diversity of jaw forms, muscle architectures, and dental morphologies makes them an ideal comparative model for investigating the biomechanics and morphofunctional evolution of the mammalian mandible.

1.5 Head Posture and Mass Properties

Head posture influences the spatial orientation of the cranium and mandible, the direction of muscle forces, and the mechanical loading of the mandible during feeding. The habitual position of the head determines the gravitational and muscular conditions under which mastication occurs, and therefore affects mandibular rotational inertia and the muscular force necessary to move the mandible during mastication. Comparative studies have demonstrated that the orientation of the lateral semicircular canal (LSC) provides a broad indication of habitual head posture in mammals. In ungulates, LSC orientation correlates with neutral head position, though the relationship is influenced by phylogeny and ecological factors (Benoit et al., 2020). Rhinocerotids illustrate this pattern: grazing species such as the white rhinoceros exhibit downwardly inclined skulls, while browsing taxa maintain a more horizontal orientation (Schellhorn, 2018). Similar phylogenetic constraints are evident in other clades, such as Xenarthra, where variation in LSC orientation reflects both ancestry and ecology (Coutier et al., 2017).

From a functional standpoint, habitual head posture modifies the orientation of bite forces and muscle vectors during mastication, thereby influencing the distribution of stresses in the mandible (Ross et al., 2007). Species feeding with the head lowered, such as grazers, experience loading patterns distinct from those of browsers that feed at or above shoulder height. Over evolutionary timescales, these consistent differences in mechanical environment may contribute to the development of deeper mandible bodies, reinforced symphyses, and increased rotational inertia (Ross et al., 2017).

Consideration of head posture is therefore necessary in studies of mandibular biomechanics and mass properties. It defines the mechanical framework within which masticatory forces act and provides context for interspecific variation in mandible form and function.

1.6 Extreme Mandible Morphologies without Extant Analogues

The extant diversity of ungulate mammals represents only a fraction of the ecological and morphological variation achieved by the group earlier in the Cenozoic. Today, extant ungulates, composed of the Orders Artiodactyla and Perissodactyla, include approximately 220 species; there are roughly 200 extant artiodactyl species (Rubes et al., 2012) and 17 extant perissodactyl species (Price and Bininda-Emonds, 2009). The ungulate radiation in open grassland ecosystems during the Neogene gave rise to a broad spectrum of grazers and mixed feeders.

Despite being the basal ungulate diet, browsing is comparatively less abundant, as grazing and mixed feeding evolved later after extensive grasslands appeared approximately 25 million years ago (Janis, 2008). However, their contemporary diversity contrasts with the far more substantial taxonomic, morphological, and ecological diversity evident in extinct ungulate-grade mammals that characterised much of the Paleogene and Neogene.

During the early Cenozoic, ungulate-grade mammals underwent multiple endemic radiations. In South America, for instance, the South American Native Ungulate (SANUs) orders Litopterna and Notoungulata paralleled true ungulates in body size, dentition, and limb specialisation, but were phylogenetically distinct (Cassini et al., 2017; Püschel et al., 2022). Similarly, the afrotherian lineages Proboscidea, Embrithopoda, and Hyracoidea diversified rapidly following the Paleocene-Eocene transition, forming an early assemblage of large herbivores with varying jaw architectures and feeding strategies (Gheerbrant, 2009; Gheerbrant and Tassy, 2009). In Eurasia and North America, during the Eocene, across the Oligocene, and into the Miocene numerous rhinocerotid, equid, and proboscidean species filled a continuum of browsing, grazing, and mixed-feeding niches (Cerdeño, 1998; Janis et al., 1998). Each of these lineages exceeded the range of mandibular morphologies found among living ungulates, reflecting greater diversity of functional adaptations and ecological strategies.

Several extinct ungulate-grade taxa possessed mandibular morphologies unlike those of extant relatives, with direct consequences for masticatory mechanics and mass properties. For instance, in rhinocerotids, for example, early Miocene genera such as *Stephanorhinus hundsheimensis* and *Dihoplus bethlehemsis* exhibit a shallower mandibular body, less reinforced symphyses, and less ventrally deflected rami than their modern analogues (Cerdeño, 1998; Pandolfi et al., 2020), reflecting a mandible which have been lighter and less resistant to torsion, consistent with lower bite forces and less repetitive grinding indicating mixed or browsing diets (Bargo et al., 2009; Ballatore and Breda, 2013; Schultz et al., 2020). By contrast, later Pleistocene rhinoceroses such as *Elasmotherium sibiricum* evolved very deep and robust mandibles associated with hypsodont molars and inferred grazing habits (Kosintsev et al., 2019). The most extreme mandible morphology among the rhinocerotoids belong to the Oligocene Paraceratheriidae. *Dzungariotherium* and *Paraceratherium* were among the largest terrestrial mammals known with body masses that may have exceeded 20,500 kg (Li, Jiangzuo, and Deng, 2022). This group ubiquitously exhibited brachydont cheek teeth, indicative of a browsing diet (Janis, 2008). Despite having a relatively small skill compared to its body size, the paraceratheres possessed an extremely elongate mandible (Li, Jiangzuo, and Deng, 2022) which

imposed unique mechanical demands on its relative enlarged masseter despite its relative narrow structure and proportionally small cheek teeth (Zhanxiang and Banyue, 2007).

A similarly broad morphological range is seen in proboscideans. The browsing Miocene mammutids and gomphotheres possessed relatively low-crowned molars and slender, tusked mandibles, contrasting with the more massive, shortened mandibles of later grazing species such as Pleistocene *Mammuthus* species and the mixed feeding extant elephants (Larramendi, 2016; Shoshani and Tassy, 2005). Recent work on early proboscideans indicates that their mandibles transitioned from elongate, "shovel-tusked" forms in basal species to shortened, reinforced, and more robust forms as the trunk elongated and became the primary food gathering organ (Liu et al., 2008; Li et al., 2024). These changes reflect a shift in feeding mechanics from mandible-to-trunk mediated food gathering, reducing direct loading on the mandible and altering its mass distribution and moment of inertia. An exceptional deviation from this general trend occurs in *Deinotherium*, a large, primarily browser that persisted from the Miocene to the Pleistocene across Africa and Eurasia (Shoshani and Tassy, 2005; Huttunen, 2004). Unlike most proboscideans, *Deinotherium* possessed a mandible bearing a pair of large, curved, mandibular tusks that grew from the lower incisors. These tusks projected ventrally and posteriorly from the symphysis rather than dorsally or anteriorly, as in the shovel-tusked gomphotheres (e.g., *Gomphotherium*) and amebelodonts (e.g., *Platybelodon*, *Amebelodon*). The mandibular symphysis was elongate and unfused, while the horizontal ramus was relatively shallow, indicating a mandible designed for controlled movement and precision feeding rather than heavy mechanical grinding (Gheerbrant and Tassy, 2009; Huttunen, 2002; Li et al., 2024). The adductor musculature was proportionally small, as indicated by the area for masseter and temporal insertions, though considerably larger than in *Prodeinotherium*. Even though both genera exhibit practically identical mandible morphologies, the primary difference between enlarged size in *Deinotherium*, it is assumed the power of the masticatory apparatus was enhanced or made more efficient when compared to *Prodeinotherium* (Huttunen, 2002).

Among the SANUs, variation in mandibular robustness likewise affected masticatory performance. *Toxodon*, for example, exhibits a high mechanical advantage in jaw-closing muscles and a shortened lever arm for the masseter, promoting powerful but slower chewing (Cassini et al., 2012). Increasing robustness necessitates increasing bone mass and therefore inertia, paralleling trends in artiodactyl, perissodactyl, and proboscidean grazers. In contrast, the more slender mandible possessed by litopterns would have favoured lighter, faster jaw movements suited to selective browsing.

Across these groups, increased mandibular mass is associated with repetitive mastication of fibrous and abrasive food material, illustrating a recurring link between structural reinforcement of the mandible, rotational inertia, and dietary adaptation.

1.7 Statement of Aims

The aim of this thesis is to investigate the determinants, functional significance, and evolutionary implications of mandibular mass distribution in mammalian herbivores, with a particular focus on ungulate-grade taxa. Through four research chapters, digital methodologies for estimating mass distribution will be established and validated, the scaling of mass properties with mandible functional anatomy and the role of head posture on the mechanical costs of mastication investigated, and finally, these analyses will be expanded to the fossil record by integrating extinct megafaunal taxa.

Chapter 2 – Determinants of the Mass Distribution of Mineralised Tissues in the Mammal Mandible and Assessing Methods for Estimation of Mass Properties

This chapter aims to develop non-destructive digital methods for estimating mandibular mass properties (i.e., mass, centre of mass, rotational inertia) using computed tomography (CT) and surface-scan data, and validate these methods via statistical comparison with an established analogue method.

Chapter 3 – Biological and Mechanical Implications of Mandibular Mass Distribution in Ungulate-Grade Herbivores (Orders Artiodactyla, Perissodactyla, Proboscidea)

This chapter aims to quantify the scaling relationships between mandibular mass properties and anatomical and mechanical metrics related to mastication across a broad sample of extant ungulate-grade mammals.

Chapter 4 – Habitual Head Posture and Associated Behaviours as Adaptations to Mitigate the Mechanical Effects of Mandible Mass Distribution

This chapter aims to evaluate the influence of habitual head on modulating the mechanical costs of mastication, and whether the compensatory effect of head posture on mandibular mass properties is associated with body size, dietary strategy, or phylogenetic affinity.

Chapter 5 – Mandibular Mass Distribution in Cenozoic Megafaunal Ungulate-Grade Mammals

This chapter aims to extend these analyses to the Cenozoic fossil record by incorporating extinct megafaunal ungulate-grade mammals and their ecological analogues, to test whether the scaling relationships identified in extant species represent fundamental biomechanical constraints or are influenced by ecology and dietary strategy and phylogenetic constraint.

2: Determinants of the Mass Distribution of Mineralised Tissues in the Mammal Mandible and Assessing Methods for Estimation of Mass Properties

2.1 Introduction

2.1.1 Past Studies of Mandibular Mass Distribution, Parallels to Limb Mass Distribution, and Considerations for Mastication Studies

2.1.1.1 Past Studies of Mandibular Mass Distribution

A relatively small body of literature exists that is concerned with the distribution of mass in the mammalian mandible (Zhang et al. 2001; Zhang et al. 2002; Ross et al. 2009; Ross et al. 2017). Consequently, the existing literature is relatively constrained in terms of its scope; being limited to an ontogenetic series of domestic miniature pigs (Zhang et al. 2001) and to primates (Ross et al. 2017), including humans (Zhang et al. 2002), and concerned only with broad-scale mass properties rather than fine-scale variation in distribution. The scope of these studies is therefore limited in mandible morphology, diet, and behaviour, being concerned only with variation in a single species (Zhang et al. 2001; Zhang et al. 2002) and the scaling of rotational inertia across a relatively restricted range of mandible morphologies and size (Ross et al. 2017).

Zhang et al. (2001) used CT scanning to specify mass properties of the pig mandible. The authors found positive correlations between estimated mean bone density and age, and that the centres of mass and geometric centres were near the midline, an expected result as it can be assumed each hemimandible is a mirror of the other, but with the geometric centre consistently located slightly more anteriorly than the mass centre. This suggests the variation of material density in the mandible varies, and that the mass centre is more proximal than geometry alone would suggest.

A later study investigating chew cycle scaling in 35 primate species (Ross et al., 2009) estimated the mandibular moment of inertia, which is directly influenced by the distribution of mass. When total mass is equal, a more distal distribution produces greater rotational inertia than mass located more proximally. Ross et al. (2009) found that anthropoids exhibited longer chew cycles than non-primate mammals of comparable mandible length, which they attributed to increased rotational inertia resulting from enlarged mandibular symphyses. In a subsequent study, Ross et al. (2017) used computed tomography to quantify mandibular mass properties in

31 primate species (nine prosimians and 22 anthropoids) and examined how rotational inertia scales with mandible length and mass, its variation among similarly sized mandibles, and its relationship with chew cycle duration. They reported that the moment of inertia scales with positive allometry relative to jaw length and that anthropoid mandibles have relatively higher rotational inertia than those of prosimians. However, they concluded that mass-related momentum effects have negligible influence on the scaling of primate chew cycle period. Their hypothesis that incorporating more precise estimates of moment of inertia would improve predictive models for chew cycle duration was not supported, as this approach resulted in less accurate scaling relationships. Nevertheless, the relatively low mass and short mandibles (approximately 0.02–0.16 m) of primates likely contribute to their small moments of inertia compared with larger herbivores possessing longer and heavier mandibles (approximately 0.7m in *Ceratotherium simum*), in which mass-related momentum effects may play a more significant role in determining chew cycle duration.

2.1.1.2 Parallels with Limb Mass Distribution

Although these primate data are limited in scope, they highlight the broader relevance of mass distribution to other biomechanical systems. The mechanics and dynamics of the limbs during locomotion parallel that of the mandible during mastication, in the way that stride length parallels gape and stride frequency parallels chew cycle frequency. Despite the lack of attention placed on mass distribution in masticatory studies, mass distribution and mass properties have been well studied with respect to locomotion (Raichlen, 2004; 2005a; 2005b; Taylor et al., 1974; Grand, 1977; Myers and Steudel, 1985; 1997). As such, it seems likely that mass distribution plays as significant a role during mastication as it does during locomotion. These parallels justify the inclusion of mass properties in mandible mastication studies.

During locomotion, increased limb length usually amplifies the influence of angular momentum. This energy-saving mechanism, however, is not utilised in chewing systems. As such, it is not expected that incorporating moment of inertia in mastication studies will result in less accurate predictions of chew-cycle scaling (Ross et al., 2017). This may be because chewing uses a much smaller proportion of total energy expenditure than locomotion and so a proportionally smaller amount of energy would be saved (Ross and Iriarte-Diaz, 2014). However, this statement was made regarding primates, which exhibit a small mandible size range compared to ungulate-grade animals. While large primates spend a considerable proportion of their time feeding, defined as the time spent moving food to the mouth, chewing, and

swallowing, 54.2% in *Gorilla gorilla* (Lehmann et al., 2008) and 55% in *Pongo pygmaeus* (Fox et al., 2004). As well as having a substantially larger mandible size range, ungulate-grade mammal mandibles are also proportionally longer. These animals, especially large-bodied species, therefore, experience much greater mandible rotational inertia than primates. They also spend a significant proportion of their time chewing, 33% of their time in the case of *Bos taurus* and 49% for *Ceratotherium simum* (Dittrich, 2007).

2.1.1.2.1 The implication for energy efficiency in herbivores

Due to these factors, having larger jaws and spending a considerable portion of their time chewing, ungulate-grade herbivores use a substantial proportion of their energy on mastication. As body size and therefore metabolic demands change, feeding systems and behaviours necessarily change to meet the metabolic demands of the organism (Ross et al., 2009). Therefore, it would be expected that ungulate-grade herbivores utilise energy-saving mechanisms and adaptations. A proximal centre of mass offers reduced rotational inertia and therefore reduced muscular torque during mastication. With increasing mandible size, it would be energetically beneficial to shift the centre of mass more proximally which would offer proportionally greater energy savings. Large-bodied species with distal centres of mass, and therefore high rotational inertia, would benefit from high mechanical advantage of the masseter and therefore greater torque per unit of muscular force.

2.1.1.2.2 The Limb Mass Distributions and efficiency

Posterior centres of mass, which concentrate mass proximal to the body, are associated with limbs used solely for locomotion while more anterior, or distal, centres of mass are associated with the use of the distal section of the limb for additional functions including grasping, climbing, and prey capture. Cursorial mammals typically have a higher stride frequency (Alexander and Jayes, 1983) and more proximally heavy limbs than non-cursors (Grand, 1977; Myers and Steudel, 1997; Raichlen, 2004). In this way, it seems clear that cursoriality is associated with a proximal distribution of mass in the limb.

Ungulates are prime examples of animals which have optimised their limbs for cursoriality. They achieved this by concentrating limb musculature close to the body, which places most of the limb mass proximal to the axis of rotation, while reducing the distal segments of the limb. The reduction of the distal segment to a hoof maximally reduced the distal mass of the limb while

retaining locomotory function. By distributing the mass of the limb proximally, the moment of inertia of the limb is reduced, thereby reducing the work incurred and energy expended during each stride.

However, despite marked differences in limb morphology and mass distribution, cursors employing distal limb segments for non-locomotor functions, such as domestic cats and cheetahs (Hudson et al., 2011; Raichlen, 2005a) incur similar locomotor energy costs to species with proximally concentrated limb mass, seemingly optimised for energetic efficiency, such as gazelles (Taylor et al., 1974).

This might be explained in that cursors with distally heavy limbs have a lower stride frequency than other cursorial mammals (Alexander and Jayes, 1983). In this way, though each stride incurs a greater energetic cost, the lower number of strides required to cover the same distance results in similar overall energy expenditure. Primates, while not cursors, possess distally heavy limbs, and have optimised the distal segments of their limbs for arboreal locomotion and object manipulation (Raichlen, 2005a). This suggests when the limb is used only for terrestrial locomotion, a proximal mass distribution is favoured, but when survival is dependent on other functions, there is a trade-off which results in a more distal distribution of mass.

Limb mass distribution is also associated with changes in limb function and stride frequency during ontogeny in primates. While primates have more distally distributed limb mass compared to most other mammal groups, there is a shift in distribution pattern, from distal to proximal, during the transition from dependent travel to independent locomotion. This shift is more pronounced when it coincides with a transition to terrestrial locomotion (e.g., infant baboons) rather than arboreal locomotion (e.g., macaques) (Raichlen, 2005a; 2005b). This supports the notion that the distribution of mass is directly linked to function, and that species which utilise terrestrial locomotion benefit more from a proximal distribution of mass than species which use the distal segment of the limb for other rigorous tasks. It is predicted that this pattern is reflected in the mandible, with a distal-to-proximal shift in mass distribution during ontogeny due to size-related changes and across the transition from milk feeding to solid food. This shift will likely vary between species due to differences in the timing of this transition, between infant and adult morphology, and in adult diet composition.

2.1.1.2.3 Mass-specific total power

Mass-specific total power is the sum of internal power (the muscular power required to move the limbs relative to the body) (Hildebrand and Hurley, 1985; Dellanini et al., 2003; Raichlen, 2006) and external power (the power required to move the limbs and body centre of mass) (Heglund et al., 1982; Minetti et al., 1999; Raichlen 2006) normalised to body mass. This measure does not differ between mammals with both distally and proximally heavy limbs during locomotion due to a trade-off between stride length and frequency (Raichlen 2006). Low stride frequency reduces limb velocities and therefore decreases internal power while associated long strides increase the vertical displacement of the centre of mass and therefore increases external power. This suggests non-cursorial mammals and those with distal mass distributions are reducing their stride frequency to minimise total mechanical power output and total energetic cost. In fact, adding weights to the distal limb segments of humans and dogs increases the natural period of limb oscillation, leading to increased stride durations (Raichlen, 2005a).

This parallels mass-specific total power involved in mastication, where internal and external power can be understood in terms of the muscular and energetic components of food processing. Internal power in mastication is the power output involved in moving the mandible during a chew cycle. This includes the power generated by the contraction of the jaw adductor musculature and the energy involved in the elastic components of the masticatory apparatus. External power in mastication refers to the power output required to fracture food particles, or the bite force required to break down food, and the displacement and deformation of the mandible due to reaction forces. The expected trade-off in mastication is those taxa with proximal mass distributions have a high chew frequency but smaller food volume per chew cycle. Similarly, those with more distal mass distributions, have low chew frequency but higher bite force, which allows them to process a higher volume of food per chew cycle. Irrespective of chew cycle frequency and duration, a distinction is expected between those taxa with a preference for selective, low-volume feeding optimised by minimising the moment of inertia of the mandible to facilitate low-energy cost per chew cycle, and those taxa which engage in bulk feeding, which is facilitated by high bite force and a more robust mandible which necessarily increases its inertial moment. Furthermore, it is expected that larger-bodied taxa with heavy mandibles, which are typically bulk feeders, will demonstrate proportionally proximal mass distributions as a way of mitigating the inertia of the mandible. In simple terms, highly selective feeders will exhibit proportionally low rotational inertia while bulk feeders exhibit proportionally high rotational inertia despite proximal mass distributions.

Behaviours other than mastication which utilise the mandible must also be considered when studying mandibular mass properties. Primates also use their jaws for non-feeding behaviours (e.g., fighting, threat displays) in which artiodactyls typically do not engage. Those that do, such as the members of Hippopotamidae and Suidae (i.e., pigs and their close relatives), are outliers and have specialised tusks and distinct anterior dentition affecting their mass distribution. These impose functional demands on mandibular morphology that do not facilitate mechanically efficient mastication and food manipulation.

These patterns of function and mass distribution indicate similar trade-offs between internal and external power exist for the mammalian mandible. If animals which are optimised for cursoriality exhibit proximally heavy limbs, then taxa which are adapted for reduced energy expenditure during mastication will have proximally heavy mandibles. Similarly, animals with limbs specialised for a secondary function, such as prey capture, arboreal locomotion, or object manipulation, have limbs with a distal mass distribution. Therefore, it is expected that animals with mandibles adapted for functions other than mastication, such as rooting, threat displays, or combat, will exhibit distal mass distributions.

2.1.2 Mass properties and musculoskeletal adaptation

Mass properties are linked with musculoskeletal adaptions in that different adaptations confer mass in different areas of the mandible. A large masseter insertion adds mass proximal to the TMJ, the mass added by the cheek teeth varies by the length and position of the molar row as well as by tooth size and degree of hypsodonty, and bulk feeding of tough vegetation adds density to the bone along the molar row to resist the stress and strain of chewing while large incisors and canines add mass distally. The presence of a diastema, depending on its length and robusticity, will add differing amounts of mass and contributions to the rotational inertia of the mandible. By extending the distance from the anterior teeth to the TMJ, the centre of mass could be shift distally, increasing mandibular rotational inertia. In contrast, a lightly built diastema may add functional length to the mandible, especially useful for selective feeders, without significantly adding to the total mass and rotational inertia. These mass properties (mass, centre of mass, rotational inertia) often closely correlate with morphology, feeding, and phylogeny (Ross et al, 2009; Ross et al, 2017).

In summary, centre of mass is a fundamental anatomical and biomechanical parameter, essential to studies of locomotion (Macaulay et al., 2017), and this study suggests it is an equally important consideration when studying mastication. However, this aspect of

mastication mechanics is understudied. An interspecific study of adult individuals across multiple mammalian orders encompassing diverse dietary behaviours and a broad range of jaw sizes and morphologies would contribute substantially to understanding the role mass distribution plays in mandible mechanics and function. Additionally, an intraspecific ontogenetic study of mass distribution and associated mechanics and anatomies, would allow investigation of the parallels between functional shifts associated with changes in mass distribution, as observed in locomotory studies, but also in determining if any size-related changes observed in the broad interspecific study are simply the result of size or are influenced by functional demands. This study suggests analogies between the mechanics of mastication and locomotion and associated functional adaptations in the mandible and limbs provide a convenient avenue for these investigations.

2.1.3 Mass Distribution Data Collection from Computed Tomography – Summary

Popular methods for collecting mass distribution data, such as suspension or physical sectioning, are either destructive or low-resolution and are not reliably accurate or precise. The compound-scales method (Clemente, 2014; Macaulay et al, 2017) is repeatable, more accurate than suspension methods, and sufficient for estimating a centre of mass. This method involves using two identical bench scales placed on a level, stable table and aligned with one another. Small support structures are placed on the centre of each scale to minimise the area of which the weight of the specimen is dispersed and either a beam or platform, depending on the size of the specimen, is placed atop the supports perpendicularly to the long axis of the table such that it rested on them evenly. Next, the specimen is placed on the platform with the long axis parallel to that of the table and platform, and the posterior end of the specimen aligned with the end, or proximal edge, of the platform. Knowing the distance from the centre of the supports to the edges of the scale weighting surface, the distance between the centres of the supports, and the mass registered on each scale, the centre of mass with respect the proximal edge of the platform can be calculated. However, this method does not allow for the investigation of variation in centre of mass due to changes in tissue or internal structure, or a detailed look at the distribution of mass, only an estimate of the mass centre. Some studies have used medical imagining technologies, such as CT-scanning, to produce a high-resolution image series to construct a mass distribution along one or more axes of the mandible, which follows similar principles to physical sectioning but is not destructive and produces higher resolution data. Studies which have utilised CT-scanning in studies of mandible mass properties, such as Zhang et al. (2001, 2002) and Ross et al. (2017) used three-dimensional computed tomography to

estimate jaw mass, mean bone density, anatomical location of mass and geometric centres, and moment of inertia in ten dry osteological specimens of miniature pig (*Sus scrofa*) mandibles (Zhang et al. 2001) and estimate mass properties in primates (Ross et al. 2017).

Zhang et al. (2001, 2002) included a phantom consisting of four tubes of KH_2PO_4 solution of different densities to perform a calibration linear regression, the coefficients of which allowed for a bone mineral density to be assigned to each voxel. Ross et al. (2017) assigned air and enamel Hounsfield unit values of -1,000 and 6330, which was the average value of all enamel voxels in scans which included a water phantom, and linearly interpolated between those values for all other voxels.

Partial volume averaging is an effect that occurs when a CT scan voxel contains more than one material. When this occurs, the voxel is assigned a single Hounsfield unit based on the average X-ray attenuation of all the materials in that voxel. In clinical settings, if a voxel contains two tissues of different densities (e.g., cortical bone and muscle), the assigned Hounsfield unit will fall between the real values associated with those tissues. This can negatively affect image quality by blurring the boundaries between tissues and around small structures, and critically for mass distribution studies, distort attenuation values. Accurate Hounsfield units for each voxel are essential for assessing bone mineral density in clinical settings, but also when estimating mass distributions of hard tissues.

Zhang et al. (2001, 2002) attempted to mitigate partial volume averaging by submerging the mandibles in water, rather than air, before scanning; as water is denser than air, the contrast boundary between cortical bone and water is less sharp than with air and reduced partial volume averaging occurs. Partial volume averaging can also be mitigated by scanning at a higher resolution, as the larger the voxel, the greater the degree of partial volume averaging. However, this must be done at the time of scanning and so cannot always be accounted for if the study sample is composed of scans from multiple sources or from previously established databases. In which case, an alternative method would be to select representative voxels from each identifiable material and linearly regress the grayscale value of these voxels against known material densities to generate the calibration coefficients. Computed tomography has more utility compared to other methods as it distinguishes regional mineral and tissue variations, while earlier studies assumed a homogenous material density or were finite element based with tissue properties, either osseous or dental, were assigned to each element (Langenbach and Hannam, 1999), which is lower resolution than a CT scan and the material properties at a point are inferred rather than explicit. Zhang et al. (2002) applied the CT methodology established in

their earlier work to a collection of eight osseous human jaw specimens with adult dentitions. The authors aimed to study cause and effect in the human masticatory system which required specification of mandible mass properties. In both the pig mandible and human mandible, they found linear relationships between mandible length, the actual and estimated masses, and moments of inertia, which might suggest this is a consistent trend despite different morphologies. Further analysis of a wider range of sizes and morphologies would be needed to support this hypothesis.

The effect of mass distribution in the mammalian mandible is understudied and not well understood. Before this latent aspect of masticatory mechanics can be studied in any depth, a consistent method of collecting mass distribution data must be detailed and validated. In this chapter, we detail a process which improves upon previous methods in terms of resolution and accessibility and propose alternative methods for estimating broad-scale mass properties.

For mandibular mass distribution to become a commonly utilised metric, a reliable method of collecting mass distribution data from the mineralised tissues of the mandible, which is accurate, precise, repeatable, and non-destructive must first be established.

2.2 Hypotheses, Research Questions, Objectives

The mandible's phenotype reflects its evolutionary history, ontogeny, and functional plasticity. These factors, in turn, influence its mass distribution through muscular forces and mechanical stresses. These stresses are incurred by the muscular forces involved in moving the mandible and producing bite force as well as the reaction forces during a biting and mastication, food acquisition, combative and defensive behaviours, and even the muscular force required to hold the jaw closed at rest. These stresses arise from to the muscular forces that move the mandible during mastication and generate bite force. Additional loading occurs due to reaction forces during mastication and food acquisition, as well as during combative and defensive behaviours. Even at rest, isometric muscular contraction is required to maintain jaw closure. The mechanics of mastication influence these three phenotypic aspects, each of which contribute, in various degrees, to the distribution of mandibular mass.

The taxa investigated in this study, all being ungulate-grade mammals, have homologous mandibles. Some of these differences are proportional, such as a long or short dentary, molar row, or edentulous region, tall or short ramus, and the relative sizes of the coronoid and condyle. These affect the area available for muscular attachments and the length of the lever

arms which determine mechanical advantage. Other differences are due to the presence or absence of a feature, such as a pronounced diastema, or the specific dental formula, including the lack of anterior teeth (*Diceros*, *Ceratotherium*) or proportionately very large canines and incisors (*Hippopotamus*).

By including only the hard mineralised elements of the mandible (i.e., bone and teeth), this study accounts for only part of the total mass of the masticatory system, which also comprises soft tissues including the adductor musculature, tongue, mylohyoid, marrow, tendons, and cartilage. However, this project attempts to establish a simple foundational model for understanding a limited set of variables associated with mandible mass distribution which can later be developed and adapted to address more sophisticated research questions. In limiting this study to hard tissues, a wider study sample was allowed to be constructed from dry osteological specimens. Attempting to construct a study sample which exhibits the size range and morphological diversity of the one investigated here while accounting for both the hard and soft tissues of the mandible would have been impossible due to time and financial constraints as well as limited specimen availability.

2.2.1 Hypothesis 1 – the hard tissue anatomy of the mandible does not meaningfully contribute to mass distribution.

The mass distribution of the mandible is controlled by aspects of its phenotype, namely the internal anatomy, meaning the variation in mineral density and spatial distribution of hollow spaces filled by soft tissue and fluid during life, and the external morphology. The hard tissue anatomy of the mandible is comprised of mineralised tissues, principally cortical and trabecular bone, with small amounts of enamel, dentine, and cementum. These tissues have different densities, which vary within known ranges. These vary between species due to adaptation throughout its evolution, incurring different sets of stresses during life, physiologic bone loads and how voluntary behaviour leads to non-traumatic bone fractures resulting in improved bone-strength safety factor (Frost 1996; 2003). These behaviours are often related to feeding and vary within species due to genetic variation and different experiences during development in terms of mechanical stress, diet, and nutrition. The external morphology is also the result of its evolutionary history but as the result of very different demands. Variation in dentition, length of the molar row, size of the ramus and angle, presence or absence of diastema and anterior teeth, and the relative and absolute sizes of the coronoid and condylar processes arose due to muscular and skeletal adaptations to diet and mechanical demands. To

what degree each of these aspects of phenotype contribute to mass distribution is not understood.

To investigate the extent to which anatomical variation in mineralised tissues influences mandibular mass distribution, a methodology is presented for acquiring high-resolution mass distribution data using computed tomography (CT). This approach is based on the principle that grayscale values in CT images scale linearly with material density.

This data is validated by testing CT derived centres of mass against those estimated using an established analogue method of estimating centre of mass, the compound-scales method specified in Clemente (2014) and Macaulay et al. (2017). Similarly, volumetric distributions generated by assigning a uniform density to each voxel enable testing of whether variations in the relative densities of constituent materials produce an appreciable effect; in essence, this will test the relative anatomical locations of the mass and geometric centres as in Zhang et al. (2001, 2002) and Ross et al. (2017).

2.2.2 Hypothesis 2 – the internal architecture of the mandible, defined as the medio-lateral and supero-inferior distribution of mineralised tissues and internal cavities, has negligible effect on longitudinal mass distribution.

The mammalian mandible is not a solid body of compact bone. The medullary cavity is an internal region of the mandible composed of trabecular bone, marrow, blood vessels, and the nerve which innervates the teeth.

The size and shape of the medullary cavity likely relates to the distribution of mineralised tissue around the long axis of the mandible. The amount and distribution of mineralised tissue determines the structural resistance to bending and torsion, while simply the amount of mineralised tissue influences moment of inertia. This distribution varies between species due to differences in mandible size and morphology, but also within species as bone models during development and plastically remodels during adulthood subject to a variety of mechanical stresses.

Dry osteological specimens, such as the ones used in this study, do not retain the marrow, nerves, and blood vessels of the medullary cavity, which is represented by a hollow void. In this way, the mineralised tissue alone underestimates the total mandible mass during life, but at times, such as when studying a palaeontological sample, mineralised tissue is all that is available. However, I hypothesise the medio-lateral and supero-inferior distribution of

mineralised tissues in the osteological specimen do not affect the mass distribution along the long axis, nor do the volumes of the internal hollow voids, suggesting external morphology is the primary determinant of mass distribution, and variation in internal anatomy contributes comparatively little. If internal tissues density contributes minimally to mass distribution, then surface-based models may also provide sufficiently accurate estimates, offering a faster and more accessible alternative for future studies.

2.2.3 Hypothesis 3 – Mandible length is expected to scale linearly with the position of the mandible's centre of mass.

It is hypothesised here that mandible length scales linearly with centre of mass in ungulate-grade animals. If Hypothesis 1&2 are supported, this would indicate that variation in the internal anatomy and architecture of the mandible do not meaningfully contribute to differences in its mass distribution. Consequently, the external morphology of the mandible would represent the principal determinant of mass distribution. Additionally, if this relationship holds, variation in the medio-lateral and supero-inferior morphology would have little influence in the longitudinal distribution of mass. In which case, simple linear metrics may offer a practical proxy for estimating mass distribution. This hypothesis will be tested by examining the scaling relationship between mandible length and centre of mass using linear regression. If a linear relationship is found, but with a non-unity slope, further adjustments or comparative analyses will be explored.

2.3 Materials and Methods

A series of four methods were used to estimate the mandible centres of mass for two study samples.

The first sample consisted of an interspecific selection of 40 hemimandible specimens, incorporating 31 species of functionally diverse terrestrial mammalian herbivores and generalist omnivores (Suids) belonging to the Orders Artiodactyla, Perissodactyla, and Proboscidea (Table 2.1). Some specimens downloaded from the online repository MorphoSource, and those scanned at The York Hospital, Wigginton Road, were available only as either a left- or right-hemimandible. To standardise the sample, complete mandibles were digitally separated into paired hemi-mandibles.

The second sample consisted of a 4-stage ontogenetic and intraspecific sample consisting of 15 individual black rhinoceros, *Diceros bicornis*, ranging from neonates to old adults (Table 2.2). In keeping with the process undertaken for the interspecific sample, each complete mandible was divided into paired hemi-mandibles.

The different natures of these two datasets address different types of scaling. Interspecific scaling, considered across adult individuals of different species, varies due to evolutionary adaptations and functional diversity, but may be affected by biomechanical and phylogenetic constraints. Ontogenetic scaling reflects anatomical changes during development due to changes in material properties, muscle forces, and function (e.g., weaning).

Including each set of paired hemi-mandibles expanded the total sample size, increasing the statistical power of linear regression. However, paired hemi-mandibles from the same specimen violates the independence assumption underpinning linear regression. To address this, a mixed-effects model that includes specimen identity as a random effect was tested against standard linear regression. In each case, the random variance was close to zero, indicating the paired data can be considered independent.

In the case of the interspecific sample, where only some specimens were represented by paired hemi-mandibles, including all hemi-mandibles (n = 40) rather than only single hemi-mandibles (n = 33) marginally increased the statistical power of the linear regressions without significantly violating independence.

In the case of the ontogenetic sample, using paired hemi-mandibles (n = 30) or complete mandibles (n = 15) produces statistically indistinguishable standard linear regression (OLS) results. The choice was made to continue with paired hemi-mandibles to keep the methodology consistent across both samples, rather than the more conservative complete mandible approach.

Table 2.1. List of species included in adult interspecific sample. Specimens selected for the CoM-CT validation subsample are denoted by an asterisk(*).

(Museum abbreviations: 1) zmh - Zoologisches Museum Hamburg, University of Hamburg, Hamburg, Germany. 2) zmb - Museum für Naturkunde, Berlin, Germany. 3) usn:mamn - National Museum of Natural History, Smthsonian Institution, Division of Mammals. 4) TMM - Texas Memorial Museum, Austin, Texas, USA)

Specimen No.	**Species**	**Scanner Type**	**Scanning Facility - Institute**	**Digital Repository**	**Equipment Used**	**Software Versions**	**Original Voxel Size (mm)**	**Final Voxel Size (mm)**	**Voltage (kVp)**
zmh-s:2552	*Ceratotherium simum*	Clinical CT	Universitätsklinikum Hamburg Eppendorf (UKE)	MorphoSource	Philips Brilliance 64 CT Scanner	N/A	0.6510	2.9686	120.0
zmh-s:8273	*Dicerorhinus sumatrensis*	Clinical CT	Yxlon International	MorphoSource	Yxlon CT Modular	N/A	0.2300	1.7573	N/A
zmh-s:9379	*Diceros bicornis*	Clinical CT	Oregon Imaging Centers	MorphoSource	Philips Brilliance 64 CT Scanner	N/A	0.9777	2.8107	120.0
Z.2009.152*	*Rhinoceros unicornis*	Clinical CT	Small Animal Hospital, Royal (Dick) School of Veterinary Studies, University of Edinburgh	---	Siemens SOMATOM Definition AS	Syngo CT VA48A	0.6000	2.1440	120.0
zmb:70335	*Equus quagga (burchelli)*	Clinical CT	Oregon Imaging Centers	MorphoSource	Philips Brilliance 64 CT Scanner	N/A	1.0000	1.0178	140.0
usnm:mammals:241009	*Equus grevyi*	Custom CT Scanner	High-Resolution X-ray Computed Tomography Facility, University of Texas at Austin	MorphoSource	North Star Imaging NSI Custom Build	N/A	0.2707	1.8758	210.0

Specimen No.	Species	Scanner Type	Scanning Facility - Institute	Digital Repository	Equipment Used	Software Versions	Original Voxel Size (mm)	Final Voxel Size (mm)	Voltage (kVp)
York Specimen (UoY -CT-001)*	*Equus caballus*	Clinical CT	The York Hospital, Wigginton Road	---	Siemens SOMATOM Definition AS+	Syngo CT VA48A	1.0000	1.8060	120.0
York Specimen (UoY-CT-002)*	*Equus caballus*	Clinical CT	The York Hospital, Wigginton Road	---	Siemens SOMATOM Definition AS+	Syngo CT VA48A	1.0000	1.4056	120.0
TMM-M-16 (left)	*Tapirus terrestris*	Custom CT Scanner	High-Resolution X-ray Computed Tomography Facility, University of Texas at Austin	MorphoSource	North Star Imaging NSI Custom Build	N/A	0.2996	1.3925	210.0
TMM-M-16 (right	*Tapirus terrestris*	Custom CT Scanner	High-Resolution X-ray Computed Tomography Facility, University of Texas at Austin	MorphoSource	North Star Imaging NSI Custom Build	N/A	0.2996	1.3925	210.0
York Specimen (UoY -CT-004)	*Bos taurus*	Clinical CT	The York Hospital, Wigginton Road	---	Siemens SOMATOM Definition AS+	Syngo CT VA48A	1.0000	1.5960	120.0
kupri:z928	*Cephalophus* sp.	Clinical CT	Primate Research Institute, Kyoto University	Digital Morphology Museum	---	---	0.4000	0.5008	---
usnm:mammals:199074	*Damaliscus lunatus jimela*	Custom CT Scanner	High-Resolution X-ray Computed Tomography Facility, University of Texas at Austin	MorphoSource	North Star Imaging NSI Custom Build	N/A	0.3308	1.2385	220.0

Specimen No.	Species	Scanner Type	Scanning Facility - Institute	Digital Repository	Equipment Used	Software Versions	Original Voxel Size (mm)	Final Voxel Size (mm)	Voltage (kVp)
usnm:mammals:367429	*Redunca arundinum*	Custom CT Scanner	High-Resolution X-ray Computed Tomography Facility, University of Texas at Austin	MorphoSource	North Star Imaging NSI Custom Build	N/A	0.3427	0.8801	190.0
usnm:mammals:291836	*Rupicapra rupicapra*	Custom CT Scanner	High-Resolution X-ray Computed Tomography Facility, University of Texas at Austin	MorphoSource	North Star Imaging NSI Custom Build	N/A	0.2420	0.6486	190.0
usnm:mammals:336264	*Saiga tatarica*	Clinical CT	High-Resolution X-ray Computed Tomography Facility, University of Texas at Austin	MorphoSource	Varian Medical Systems , ACTIS CT scanner with FeinFocus X-ray source	N/A	0.4500	0.7308	450.0
usnm:mammals:164562	*Tragelaphus scriptus*	Custom CT Scanner	High-Resolution X-ray Computed Tomography Facility, University of Texas at Austin	MorphoSource	North Star Imaging NSI Custom Build	N/A	0.2420	0.7066	190.0
TMM M-454	*Sus scrofa*	Clinical CT	High-Resolution X-ray Computed Tomography Facility, University of Texas at Austin	MorphoSource	Varian Medical Systems, ACTIS CT scanner with FeinFocus X-ray source	N/A	0.4500	0.9540	N/A
usnm:mammals:145297	*Sus barbatus*	Custom CT Scanner	High-Resolution X-ray Computed Tomography Facility, University of Texas at Austin	MorphoSource	North Star Imaging NSI Custom Build	N/A	0.2244	1.3051	200.0

Specimen No.	Species	Scanner Type	Scanning Facility - Institute	Digital Repository	Equipment Used	Software Versions	Original Voxel Size (mm)	Final Voxel Size (mm)	Voltage (kVp)
York Specimen (UoY-CT-005)*	*Sus domesticus*	Clinical CT	The York Hospital, Wigginton Road	---	Siemens SOMATOM Definition AS+	Syngo CT VA48A	1.0000	1.1592	120.0
usnm:mammals:a36000	*Phacochoerus africanus*	Custom CT Scanner	High-Resolution X-ray Computed Tomography Facility, University of Texas at Austin	MorphoSource	North Star Imaging NSI Custom Build	N/A	0.3308	1.1644	220.0
TMM M-2052	*Lama glama*	Custom CT Scanner	High-Resolution X-ray Computed Tomography Facility, University of Texas at Austin	MorphoSource	North Star Imaging NSI Custom Build	N/A	0.7000	1.0052	N/A
usnm:mammals:278681	*Lama glama*	Custom CT Scanner	High-Resolution X-ray Computed Tomography Facility, University of Texas at Austin	MorphoSource	North Star Imaging NSI Custom Build	N/A	0.1658	1.0505	150.0
York Specimen (UoY-CT-006)*	*Camelus sp*	Clinical CT	The York Hospital, Wigginton Road	---	Siemens SOMATOM Definition AS+	Syngo CT VA48A	1.0000	1.9768	120.0
Z.2009.72.1 (left)*	*Camelus bactrianus*	Clinical CT	Small Animal Hospital, Royal (Dick) School of Veterinary Studies, University of Edinburgh	---	Siemens SOMATOM Definition AS	Syngo CT VA48A	0.6000	1.7520	120.0
Z.2009.72.1 (right)*	*Camelus bactrianus*	Clinical CT	Small Animal Hospital, Royal (Dick) School of Veterinary Studies, University of Edinburgh	---	Siemens SOMATOM Definition AS	Syngo CT VA48A	0.6000	1.7520	120.0

Specimen No.	Species	Scanner Type	Scanning Facility - Institute	Digital Repository	Equipment Used	Software Versions	Original Voxel Size (mm)	Final Voxel Size (mm)	Voltage (kVp)
Z.2008.35 (left)*	*Hippopotamus amphibius*	Clinical CT	Small Animal Hospital, Royal (Dick) School of Veterinary Studies, University of Edinburgh	---	Siemens SOMATOM Definition AS	Syngo CT VA48A	0.6000	2.3408	120.0
Z.2008.35 (right)*	*Hippopotamus amphibius*	Clinical CT	Small Animal Hospital, Royal (Dick) School of Veterinary Studies, University of Edinburgh	---	Siemens SOMATOM Definition AS	Syngo CT VA48A	0.6000	2.3408	120.0
Unregistered (left)*	*Hippopotamus amphibius*	Clinical CT	Small Animal Hospital, Royal (Dick) School of Veterinary Studies, University of Edinburgh	---	Siemens SOMATOM Definition AS	Syngo CT VA48A	0.6000	2.5680	120.0
Unregistered (right)*	*Hippopotamus amphibius*	Clinical CT	Small Animal Hospital, Royal (Dick) School of Veterinary Studies, University of Edinburgh	---	Siemens SOMATOM Definition AS	Syngo CT VA48A	0.6000	2.5680	120.0
usnm:mammals:374880	*Mazama americana*	Custom CT Scanner	High-Resolution X-ray Computed Tomography Facility, University of Texas at Austin	MorphoSource	North Star Imaging NSI Custom Build	N/A	0.2134	0.7204	190.0
usnm:mammals:246649	*Odocoileus hemionus*	Custom CT Scanner	High-Resolution X-ray Computed Tomography Facility, University of Texas at Austin	MorphoSource	North Star Imaging NSI Custom Build	N/A	0.2134	0.9919	190.0

Specimen No.	Species	Scanner Type	Scanning Facility - Institute	Digital Repository	Equipment Used	Software Versions	Original Voxel Size (mm)	Final Voxel Size (mm)	Voltage (kVp)
usnm:mammals:246649	*Rangifer tarandus*	Custom CT Scanner	High-Resolution X-ray Computed Tomography Facility, University of Texas at Austin	MorphoSource	North Star Imaging NSI Custom Build	N/A	0.2433	1.4131	190.0
York Specimen (UoY-CT-007)*	*Giraffa sp*	Clinical CT	The York Hospital, Wigginton Road	---	Siemens SOMATOM Definition AS+	Syngo CT VA48A	1.0000	2.2596	120.0
GH3.21 (left)*	*Okapia johnstoni*	Clinical CT	Small Animal Hospital, Royal (Dick) School of Veterinary Studies, University of Edinburgh	---	Siemens SOMATOM Definition AS	Syngo CT VA48A	0.6000	1.6448	120.0
GH3.21 (right)*	*Okapia johnstoni*	Clinical CT	Small Animal Hospital, Royal (Dick) School of Veterinary Studies, University of Edinburgh	---	Siemens SOMATOM Definition AS	Syngo CT VA48A	0.6000	1.6448	120.0
usnm:mammals:282308	*Antilocapra americana*	Custom CT Scanner	High-Resolution X-ray Computed Tomography Facility, University of Texas at Austin	MorphoSource	North Star Imaging NSI Custom Build	N/A	0.3118	1.0763	190.0
Z.2001.147 (left)*	*Elephas maximus*	Clinical CT	Small Animal Hospital, Royal (Dick) School of Veterinary Studies, University of Edinburgh	---	Siemens SOMATOM Definition AS	Syngo CT VA48A	0.6000	2.2384	120.0
Z.2013.148.1 (left)*	*Loxodonta africana*	Clinical CT	Small Animal Hospital, Royal (Dick) School of Veterinary Studies, University of Edinburgh	---	Siemens SOMATOM Definition AS	Syngo CT VA48A	0.6000	2.2384	120.0

Specimen No.	Species	Scanner Type	Scanning Facility - Institute	Digital Repository	Equipment Used	Software Versions	Original Voxel Size (mm)	Final Voxel Size (mm)	Voltage (kVp)
Z.2013.148.1 (right)*	*Loxodonta africana*	Clinical CT	Small Animal Hospital, Royal (Dick) School of Veterinary Studies, University of Edinburgh	---	Siemens SOMATOM Definition AS	Syngo CT VA48A	0.6000	2.2384	120.0

Table 2.2. List of *Diceros bicornis* specimens included in intraspecific ontogenetic sample. Specimens selected for the validation subsample are denoted by an asterisk(*). All specimens were loaned from the National Museum of Scotland and scanned at the Royal (Dick) School of Veterinary Studies, University of Edinburgh.

Specimen No.	Species	Scanner Type	Scanning Facility - Institute	Equipment Used	Software Versions	Original Voxel Size (mm)	Final Voxel Size (mm)	Voltage (kVp)
Z.2021.46.38	*Diceros bicornis*	Clinical CT	Small Animal Hospital, Royal (Dick) School of Veterinary Studies, University of Edinburgh	Siemens SOMATOM Definition AS	Syngo CT VA48A	0.6	0.9664	120
Z.2021.46.8*	*Diceros bicornis*	Clinical CT	Small Animal Hospital, Royal (Dick) School of Veterinary Studies, University of Edinburgh	Siemens SOMATOM Definition AS	Syngo CT VA48A	0.6	1.0240	120
Z.1953.57*	*Diceros bicornis*	Clinical CT	Small Animal Hospital, Royal (Dick) School of Veterinary Studies, University of Edinburgh	Siemens SOMATOM Definition AS	Syngo CT VA48A	0.6	1.2880	120
Z.2021.46.17 *	*Diceros bicornis*	Clinical CT	Small Animal Hospital, Royal (Dick) School of Veterinary Studies, University of Edinburgh	Siemens SOMATOM Definition AS	Syngo CT VA48A	0.6	1.3984	120
Z.2021.46.15 *	*Diceros bicornis*	Clinical CT	Small Animal Hospital, Royal (Dick) School of Veterinary Studies, University of Edinburgh	Siemens SOMATOM Definition AS	Syngo CT VA48A	0.6	1.3872	120
Z.2021.46.9*	*Diceros bicornis*	Clinical CT	Small Animal Hospital, Royal (Dick) School of Veterinary Studies, University of Edinburgh	Siemens SOMATOM Definition AS	Syngo CT VA48A	0.6	1.4480	120
Z.2021.46.12 *	*Diceros bicornis*	Clinical CT	Small Animal Hospital, Royal (Dick) School of Veterinary Studies, University of Edinburgh	Siemens SOMATOM Definition AS	Syngo CT VA48A	0.6	1.6192	120

Specimen No.	Species	Scanner Type	Scanning Facility - Institute	Equipment Used	Software Versions	Original Voxel Size (mm)	Final Voxel Size (mm)	Voltage (kVp)
Z.13.6.84	*Diceros bicornis*	Clinical CT	Small Animal Hospital, Royal (Dick) School of Veterinary Studies, University of Edinburgh	Siemens SOMATOM Definition AS	Syngo CT VA48A	0.6	1.5840	120
Z.2021.46.13	*Diceros bicornis*	Clinical CT	Small Animal Hospital, Royal (Dick) School of Veterinary Studies, University of Edinburgh	Siemens SOMATOM Definition AS	Syngo CT VA48A	0.6	1.7120	120
Z.2021.46.7*	*Diceros bicornis*	Clinical CT	Small Animal Hospital, Royal (Dick) School of Veterinary Studies, University of Edinburgh	Siemens SOMATOM Definition AS	Syngo CT VA48A	0.6	1.7248	120
Z.2021.46.10*	*Diceros bicornis*	Clinical CT	Small Animal Hospital, Royal (Dick) School of Veterinary Studies, University of Edinburgh	Siemens SOMATOM Definition AS	Syngo CT VA48A	0.6	1.1714	120
Z.2021.46.3*	*Diceros bicornis*	Clinical CT	Small Animal Hospital, Royal (Dick) School of Veterinary Studies, University of Edinburgh	Siemens SOMATOM Definition AS	Syngo CT VA48A	0.6	1.7024	120
Z.2021.46.5*	*Diceros bicornis*	Clinical CT	Small Animal Hospital, Royal (Dick) School of Veterinary Studies, University of Edinburgh	Siemens SOMATOM Definition AS	Syngo CT VA48A	0.6	1.8448	120
Z.2021.46.4*	*Diceros bicornis*	Clinical CT	Small Animal Hospital, Royal (Dick) School of Veterinary Studies, University of Edinburgh	Siemens SOMATOM Definition AS	Syngo CT VA48A	0.6	1.6720	120
Z.2021.46.6*	*Diceros bicornis*	Clinical CT	Small Animal Hospital, Royal (Dick) School of Veterinary Studies, University of Edinburgh	Siemens SOMATOM Definition AS	Syngo CT VA48A	0.6	1.8000	120

2.3.1 Compound-Scales Method for Estimating Centre of Mass

Access to physical specimens is expensive and may limit the sample size available for study. The advent of online repositories such as *MorphoSource* has enabled researchers to freely share CT-scans and digital models of previously scanned specimens, greatly expanding the number of specimens available for study. The method presented here for collecting mass distribution data from hard mineralised tissues, wherein CT scan grayscale density is used as a proxy for material density (CoM-CT), has not previously been tested for accuracy and precision.

To do this, the new computed tomography method was validated against the previously established compound-scales method. The computed tomography method was used to estimate the centres of mass for a 17-specimen subsample (Table 1) of the interspecific sample (Table 1) and a 12-specimen subsample of the ontogenetic study sample (Table 2) using the established compound-scales method. Specimen selection for the validation subsample was dependent on availability of the physical specimen, which is necessary for the compound-scales method, and in the case of the ontogenetic subsample, left-side hemi-mandibles which were able to stand with physical supports were selected. Three *Diceros bicornis* hemi-mandibles were not able to stand freely in a stable position without physical supports which would have affected the results obtained from the compound-scales method, as such only specimens able to stand freely were selected.

Macaulay et al. (2017) assessed three methods (suspension, scales, and digital modelling) for estimating centre of mass for accuracy and repeatability. They found the scales method to be the most accurate, closely followed by digital modelling (CT-based) and suggested these methods could provide accurate and consistent centre of mass estimations. Following Clemente et al. (2014) and Macaulay (2017), the compound-scales method was used to estimate the centre of mass and compare these values with CT-derived estimates to assess accuracy. Each specimen was measured three times using both scales and digital methods to assess precision and repeatability.

Two bench-scale setups were used, one for smaller specimens (OHAUS scale C11P9 (OHAUS Europe GmbH, Heuwinkelstrasse 3, 8606 Nänikon, Switzerland); 0.005kg resolution, 9kg capacity) and one for larger specimens (OHAUS scale C11P75; 0.05kg resolution, 75kg capacity). The scales were aligned with one another such that the front surface of both scales was parallel to the table edge. A platform on which the specimen was placed sat atop the scales and spanned the distance between them. To minimise the contact surface area between

the platform and scales and maximise point pressure on the scales, a support axis was placed in the centre of each scale, under the platform, perpendicular to the long axis of the table. Here, the support was a small dimension stainless steel rod affixed to the bottom of the platform. The scales were then positioned to allow approximately 20–30 mm overhang between the plank ends and the centre of the supports (Figure 2.1).

2.3.2 Validation of New Methodologies

In clinical and experimental research settings, new methodologies and measurement techniques are frequently developed to provide indirect measures where direct measurement is impractical or to replace older, established methods. For a new technique to replace an existing one, the two must first be evaluated for their level of agreement, i.e., whether they produce results sufficiently similar be used interchangeably.

This differs from calibration, in which empirically known quantities are measured by a new method and compared directly with their true values. When neither method provides an unequivocally correct measurement, the comparison focuses instead on the degree of agreement rather than accuracy against a known standard. If two methods are shown to agree within acceptable limits, their data may be combined to create larger, more robust, aggregate datasets.

A common but misleading approach to method comparison is the use of correlation coefficients. A correlation coefficient close to 1 indicates that two datasets are linearly related, but it does not demonstrate agreement. Two methods may correlate perfectly yet differ systematically, for example, if they measure the same variable in different units. The apparent strength of correlation also depends on the range of values in the dataset: a wider range inflates the correlation coefficient, even if the underlying disagreement between the two methods remains constant.

This study aimed to development new methodologies for estimating mass distribution and mass properties in the hard mineralised tissues of the mammalian mandible. To obtain a reliable assessment of agreement between new methods and an already established for estimating centre of mass, the Bland–Altman Analysis (Altman and Bland, 1983; 2010) was used. This method evaluates the extent to which a new measurement technique deviates from an established one. The process followed in this study process began by examining whether the two datasets are linearly related with a slope close to 1. While first performing linear regression

is not strictly necessary, it acts as a way of assessing if the two datasets have a linear association, and if the slope was not near 1, it becomes clear the two datasets are not in agreement without performing the more involved Bland-Altman Analysis. If this conditions awas met (i.e., the data are have a linear relationship with a slope close to 1), the differences between methods are plotted against their means, allowing investigation of any systematic relationship between measurement error and the true (but unknown) value. Because the true value is not known, the mean of the two methods serves as the best available estimate.

Agreement can be summarised by the mean difference (đ), representing bias, and the standard deviation of the differences (s). Most differences should fall within the limits of agreement, defined as đ ± 1.96s. When these limits are clinically or biologically acceptable, the two methods can be regarded as interchangeable. A consistent bias, if present, can be corrected by subtracting đ from the new method's results. These limits are specific to the analysed sample and must be recalculated for other datasets or populations.

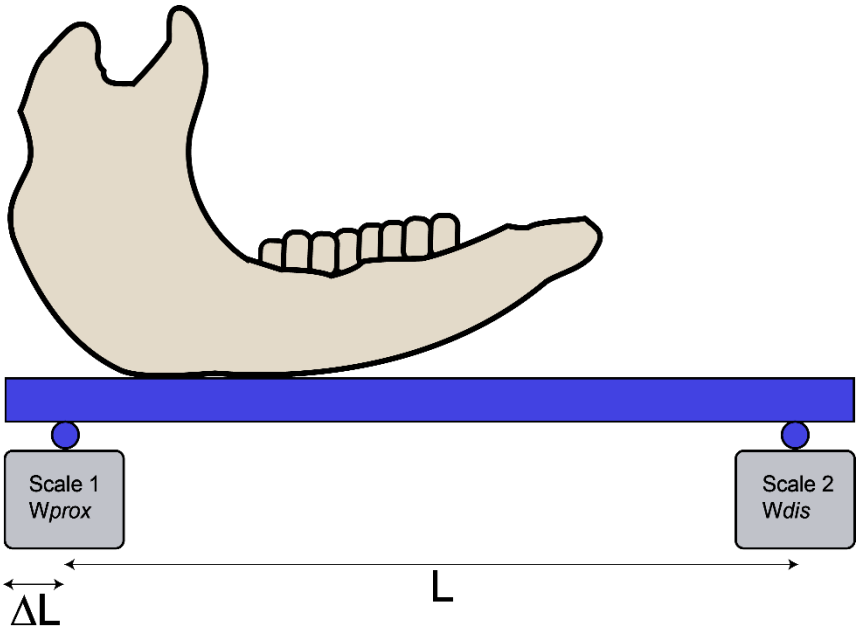

Figure 2.1. Diagram of equipment and specimen set-up for the "compound-scales" method of centre of mass estimation.

Both scales were then tared, and the specimen placed on the platform with the posterior surface of the condyle aligned with the proximal end of the platform. Measurements were taken using a metre rule of the distance between the centre of the supports (L), the distance from the

proximal edge to the proximal support (ΔL), and the mass values (W_{prox}, W_{dis}) read from each scale. The scales-method estimated centre of mass (CoM_{sc}) was then calculated from:

$$1) \quad CoM_{sc} = \left(W_{dis} * \frac{L}{(W_{prox} + W_{dis})} \right) + \Delta L$$

This process was repeated three times for each specimen, and three times with the specimen placed at the distal end rather the proximal, to ensure a reasonable degree of repeatability and precision, which produced identical results. The values obtained from the compound-scales methodology were compared against those estimated from CoM-CT using Bland-Altman Analysis.

2.3.3 CT-Based Methods – Linearly Regressed Material Density and Homogenous Density

2.3.3.1 CT-Based Methods - Linearly Regressed Material Density

To produce images appropriate for collecting high resolution mass distribution data which represent the tissue variation in the mandible, computed tomography was chosen over other imaging modalities. Firstly, it was essential that the modality was non-destructive and high resolution, which ruled out any sectioning methods. Secondly, any images or volumes produced needed to capture internal structure, which precluded surface scans even though these are more widely available from established online repositories. Finally, computed tomography (CT) was chosen over magnetic resonance imaging (MRI). MRI produces volumetric data and provides excellent contrast for soft tissues, but it does not generate a measurable signal from mineralised tissues such as bone or enamel when using a standard scanner. CT, by contrast, accurately represents variations in hard-tissue density, making it the more appropriate modality for studying mandibular mass properties.

The computed tomography (CT) scans listed in Table 1. and Table 2., were inspected for completeness in both *Avizo (Version 2021.1)* (Thermo Fisher Scientific, 2021) and the *Fiji (Version 1.54p)* variant of *ImageJ* (Schindelin et al. 2012). Specimens were chosen with considerations regarding phylogeny, overall size, and dietary category. In the case that no complete specimen was available for a given taxon, specimens were chosen such that a digital composite of a complete hemimandible could be made from combining incomplete hemimandibles from the same individual. There were occasions where this was impossible, and

a semi-complete mandible was included out of necessity, the details of which are supplied in the appendix.

Each volume was saved as an .tiff image stack and, in the case of 16-bit scans, converted to 8-bit. CT scanners capture X-rays from many different angles as the scanner rotates about the object which are computed processed to form cross-sectional slices and stacked, which creates a three-dimensional representation of the object. Hounsfield units (HU) are the default measure of radiodensity used in CT scanning, and are typically calibrated with water, 0 HU, and air, -1000 HU. Hounsfield unit image stacks are 12-bit, displaying 4,096 grayscale units, but can be padded to 16-bit, displaying 65,536 increments of grayscale, by storing the 12-bit data in a 16-bit format and filling in the missing bits with zeros. This allows for compatibility with 16-bit computer and image analysis systems and retains the high resolution of 12-bit imaging while increasing the grayscale graduation, making different tissues more easily distinguishable. However, higher-bit-depth images require more storage, and greater processing demands than lower-bit-depth images. As some scans obtained from online repositories were available only in 8-bit, which display only 256 grayscale units, it was necessary to convert all image stacks to 8-bit to maintain consistency across the sample. Unless already scaled, as in the case of DICOM files, the image resolution was specified using the voxel dimensions provided in the scan parameters for each image stack. Each volume was then orientated to a standardised orientation. This orientation is described as the z-axis parallel to a plane defined as containing the occlusal surface of the most anterior dentition, typically the incisors, and the most posterior molar, typically M3, and the x-axis defined as the plane containing the posterior surface of the condylar processes and perpendicular to the z-axis. This was performed in *Fiji* using the plugin *TransformJ* (Meijering et al., 2001). Each stack was then resliced along the z-axis to 250 slices In *Fiji* using the *ResliceZ* function. This standardised the stack length, allowing for comparisons to be made later using rank tests when comparing the shape of the mass distributions between two species, which require an equal number of datapoints in each dataset being compared, and reduced the size of the image file considerably allowing for greater ease-of-use and processing on less powerful hardware. However, re-slicing also increased voxel size, by increasing the z-dimension of the voxel. As each scan was performed separately, either coming from a variety of sources, or in the case of the scans performed at the Royal (Dick) School of Veterinary Studies, the technician made constant adjustments between scans to optimise clarity and minimise noise, which occasionally reduced z-axis resolution and increased the potential for partial volume averaging error; this was an unfortunate but necessary result as partial volume averaging can be mitigated at a later stage while the noise effects drastically obscured the

image and the true X-ray attenuation throughout the image. Measures taken to mitigate this error and account for partial volume averaging are described later. Next, the TIFF stacks required editing and masking, using the *Segmentation Editor* plugin (by Johannes Schindelin, Francois Kusztos, and Benjamin Schmid), to remove artefacts, crania, and other materials included during scanning. Mandibles were digitally separated into left and right hemi-mandibles using the *Segmentation Editor* plugin.

Once correctly oriented and standardised to a consistent slice number, the image stacks were ready for data collection. Firstly, grayscale values were collected in *Fiji* for each of the major materials present: dentine, enamel, cortical bone, and air. These values were linearly regressed against values within a known density range for these materials (dentine = 0.00196 g/cm^3; enamel = 0.00269 g/cm^3; cortical bone = 0.00191 g/cm^3 (Grimal and Laugier, 2019); air = 0 g/cm^3), and the regression coefficients recorded. This allows a density value to be assigned to each voxel in the volume. Next, a threshold value is selected which acts as the cut-off point between bone and air. The number of voxels per slice after thresholding (n) was recorded in a .csv file. This boundary is affected by partial volume averaging, and this cut-off acts as a form of mitigation by discarding any voxels below the threshold. This was done by the full-width half-maximum (FWHM) method for refining the boundary between two materials (Bettinardi et al., 2014). This value was checked using the histogram function in Fiji, which shows each major material as a noticeable peak or plateau in the plot. It is critical to select an accurate and appropriate threshold to minimise the over-estimation of mandible mass by reducing the effect of partial volume averaging. Most of these concerns are addressed later in the sensitivity and validation sections of this chapter. Then, using the plugin *Macro-code-slice-count.ijm,* the voxels of each grayscale value in each slice were counted, the *graycount*, and saved as a .csv file. These values were ported into an *Excel* spreadsheet containing the voxel resolution and regression coefficients specific to the scan in question. Using the voxel dimensions (x, y, z) to calculate a voxel volume (V), and voxel density (D) from the grayscale-material density regression, a mass is assigned to each voxel and summed for each slice.

$$2) \quad V = x * y * z$$

$$3) \quad D = a + (b * \text{grayscale value})$$

Where the intercept (a) and the slope (b) were obtained from linear regression. The voxel mass (m), mass per slice (s) and the total mass (M) were then determined from:

$$4) \quad m = D * V$$

$$5) \quad \mathrm{s} = \sum_{i=1}^{n} m_i$$

$$6) \quad \mathrm{M} = \sum_{i=1}^{250} s_i$$

The mass per slice was then plotted across the mandible length, from the posterior surface of the condyle at 0% to the most anterior tip of the symphysis or incisors, if present in the taxon, at 100%, to visualise a distribution of mass along the long axis of the mandible. Volumetric data, essentially a mass distribution of homogeneous material density, was also collected by assigning a mass of 1 g/mm^3 to each *graycount* voxel and plotted similarly to the mass distribution. The centre of mass along the z-axis, or long axis, was delineated as the slice at which the mandible could be divided into two sections of equal mass, and the volumetric centre was calculated at the point at which the mandible could be divided into two sections of equal volume.

2.3.3.2 CT-Based Methods - Homogenous Material Density

The locations of the centre of mass and centre of geometry will be compared to assess if they are positionally aligned.

Two similar, but distinct, CT-based methods will be used to estimate the locations of the mass centre and geometric centre; 1) the previously described CoM-CT method which uses a linearly derived grayscale proxy for voxel mass, 2) a variation of the CoM-CT method which instead assumes a homogenous density for all voxels, which, in effect, produces a centre of volume or geometric centre, referred to in this study as CoV-CT. The resulting mass centres and geometric centres resulting from each of the two methods will then be tested for agreement using Bland-Altman Analysis.

If the two methods are in agreement this will demonstrate the locations of the mass centres and geometric centres are in close proximity. This implies variation in the material density of the hard tissues of mandible has a negligible effect on its mass distribution.

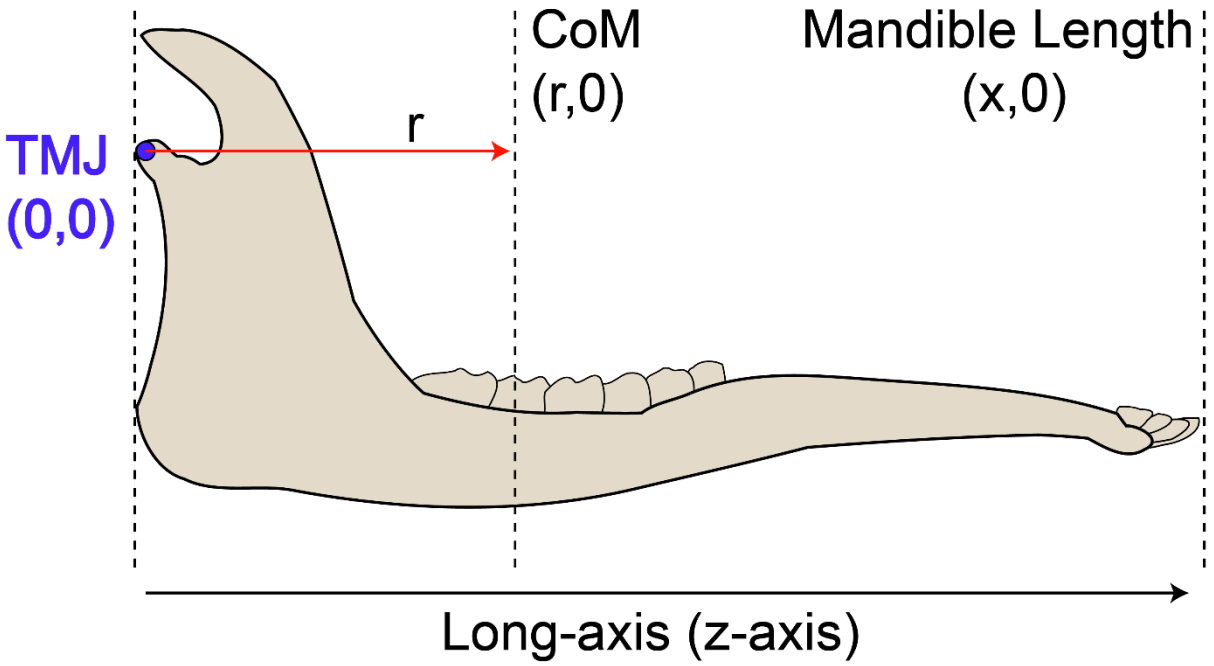

Figure 2.2. The centre of mass along the z-axis expressed as the perpendicular distance between the vertical planes which contain the most posterior surface of the condylar process or ramus or angle of the mandible and the centre of mass.

2.3.4 Surface Centre of Mass Estimation Method Using Blender

To investigate if the internal architecture of the mandible (i.e., the medio-lateral and supero-inferior distribution of mineralised tissues and interval cavities) meaningfully affects longitudinal mass distribution, the centres of mass estimated from the CoM-CT method were compared against geometric centres along the longitudinal axis a from surface model derived method. Surface models were generated from each hemi-mandible CT-scan in the *Fiji* (Schindelin et al., 2012) *3D Viewer* plugin (Schmid et al., 2010) by importing the CT stack, selecting the surface rendering mode, and exporting as an .stl file. Surface models capture the complete external geometry of a specimen and, as such, represent it as a solid model that does not account for internal voids as CT scans do. These voids would have been occupied by marrow, nervous tissue, and fluids during life and appear as voids in CT scan reconstructions of the mineralised tissue. Consequently, surface models yield a total volume that is greater than that of corresponding CT-derived models for the same specimen.

The centre of mass for each hemi-mandible surface model was estimated in *Blender* (Version 3.1; Blender Foundation, 2022) by importing the surface file and aligning the long axis of the

model with a chosen axis, in this case, the z-axis, with the posterior end of the model at position zero. The surface was converted to a mesh by right clicking the object and selecting *Convert to Mesh*. This allowed modifiers to be applied to the object. The *3D Print ToolBox* add-on was enabled, and the volume of the model was calculated by selecting *Volume* within the *Statistics* section of the *3D Print Toolbox* panel. Next, a plane was added by pressing *Shift + A* to open the *Add* menu and choosing *Plane* within the *Mesh* submenu. The plane is perpendicular to the z-axis my default, and was scaled to a size larger than the hemi-mandible model in its x- and y-dimensions and 0mm in its z-dimension, and moved unilaterally along the z-axis by adjusting its *Scale* and *Location*, both in the *Object Properties* panel *Transform* submenu, until there was no spatial overlap of the two objects and the plane was positioned beyond the anterior extent of the hemi-mandible model. Next, the hemi-mandible model was selected, and a *Boolean Modifier* was added by clicking the *Modifier Properties* tab in the *Properties* panel, selecting *Boolean* from the *Add Modifier* submenu, and setting the *Operation* to *Difference*. Within the *Boolean Modifier* panel, the *Operand Type* was set to *Object*, and within the *Object* drop-down menu, the plane was selected. The plane was then moved along the z-axis until it intersected with the anterior end of the hemi-mandible surface model. The hemi-mandible model was re-selected, and the *Boolean Modifier* was applied. This process removes the anterior portion of the hemi-mandible model which behind the bisecting plane. The volume of the remaining portion of the hemi-mandible model was calculated as before. If this new volume was less than exactly half of the initial volume, the plane was moved further towards the posterior end of the hemi-mandible model by a small amount. Precision was ensured by making fine adjustments to the plane's *Location*, within the *Object Properties* panel *Transform* submenu. This process was repeated iteratively until the new volume of the retained portion of the hemi-mandible model was exactly half of the initially calculated volume. Finally, the plane was selected and its *Transform* submenu inspected. The x- and y- locations were zero, as expected, while the z-location gave the perpendicular distance from the origin to the plane which divided the hemi-mandible model in two halves of equal volume. This value was the surface model derived longitudinal geometric centre or CoM-Surface.

This process was repeated for each of the specimens in both the interspecific sample (Table 1) and the ontogenetic sample (Table 2). The resulting geometric centres were compared across the corresponding centres of mass calculating using the CoM-CT method and tested for agreement using Bland-Altman Analysis.

If the two methods are in agreement this will demonstrate the locations of the CoM-CT derived mass centres and CoM-Surface derived geometric centres are in close proximity. This would

imply variation in the internal architecture of mandible has a negligible effect on its mass distribution.

2.3.5 Jaw Length as a Proxy for Centre of Mass

Jaw length, defined as the horizontal distance between the anterior tip of the central incisor (or the most anterior point of the symphysis in taxa without incisors) and the most posterior point of the ramus or condyle, whichever has the most posterior extent. Mandible mass and moments of inertia can be estimated from mandible length in pigs (Zhang et al., 2001), humans (Zhang et al., 2002), and primates more generally (Ross et al., 2017) as mass and length are linearly correlated. As mandible length is strongly associated with mass properties in these taxa, it may be a relationship that holds across mammals generally. Ungulate-grade mammals provide an interesting case study for this relationship as their mandible anatomy is homologous, they exhibit a wider range of mandible morphologies and sizes than any of the previous tested groups.

Mandible length was calculated for each species in both the interspecific (Table 1) and ontogenetic groups (Table 2) by multiplying the z-direction voxel dimension by the number of slices in the CT image stack. These values were then linearly regressed against centre of mass estimated from the CoM-CT method. If mandible length scales linearly with centre of mass in ungulate-grade animals, length alone may serve as a practical proxy for centre of mass. Additionally, if this relationship holds, it suggests variation in the medio-lateral and supero-inferior morphology of the mandible has little influence on its longitudinal distribution of mass, and mandible length alone is the primary determinant of mass properties in the ungulate-grade mandible.

2.4 Results

2.4.1 Results 1 – Interspecific Sample

2.4.1.1 Interspecific Sample – CoM-CT Validation

The aim of this analysis was to validate a new method for estimating centre of mass from computed tomography using voxel grayscale as a proxy for material density (CoM-CT).

Linear regression (Figure 3. A) demonstrates a strong positive relationship ($y = –0.00972 + 1.09x$; adjusted $R^2 = 0.97$) between centre of mass estimated by the compound-scales method and

CoM-CT. However, the slope slightly greater than 1 (1.09) and the small negative intercept suggest a systematic bias, where the compound-scales method tends to result in marginally lower CoM estimates at smaller values and slightly higher at larger values

The Bland-Altman plot (Figure 3. B) illustrates agreement between the two methods. The mean bias (central line) is close to zero (approximately –0.01), indicating minimal systematic difference overall. The scatter of points around this line shows random variation across the measurement range, with no clear trend suggesting proportional bias. The limits of agreement (outer lines) encompass all data points, demonstrating that differences between the methods are small and consistent.

Together, the two plots indicate that CoM-CT estimates are highly comparable and statistically interchangeable with those derived from the compound-scales method. As CoM-CT and compound-scales derived data are interchangeable, this validates CoM-CT as an accurate new method, and as a standard against which the other new methodologies (CoV-CT; CoM-Surface) can be compared.

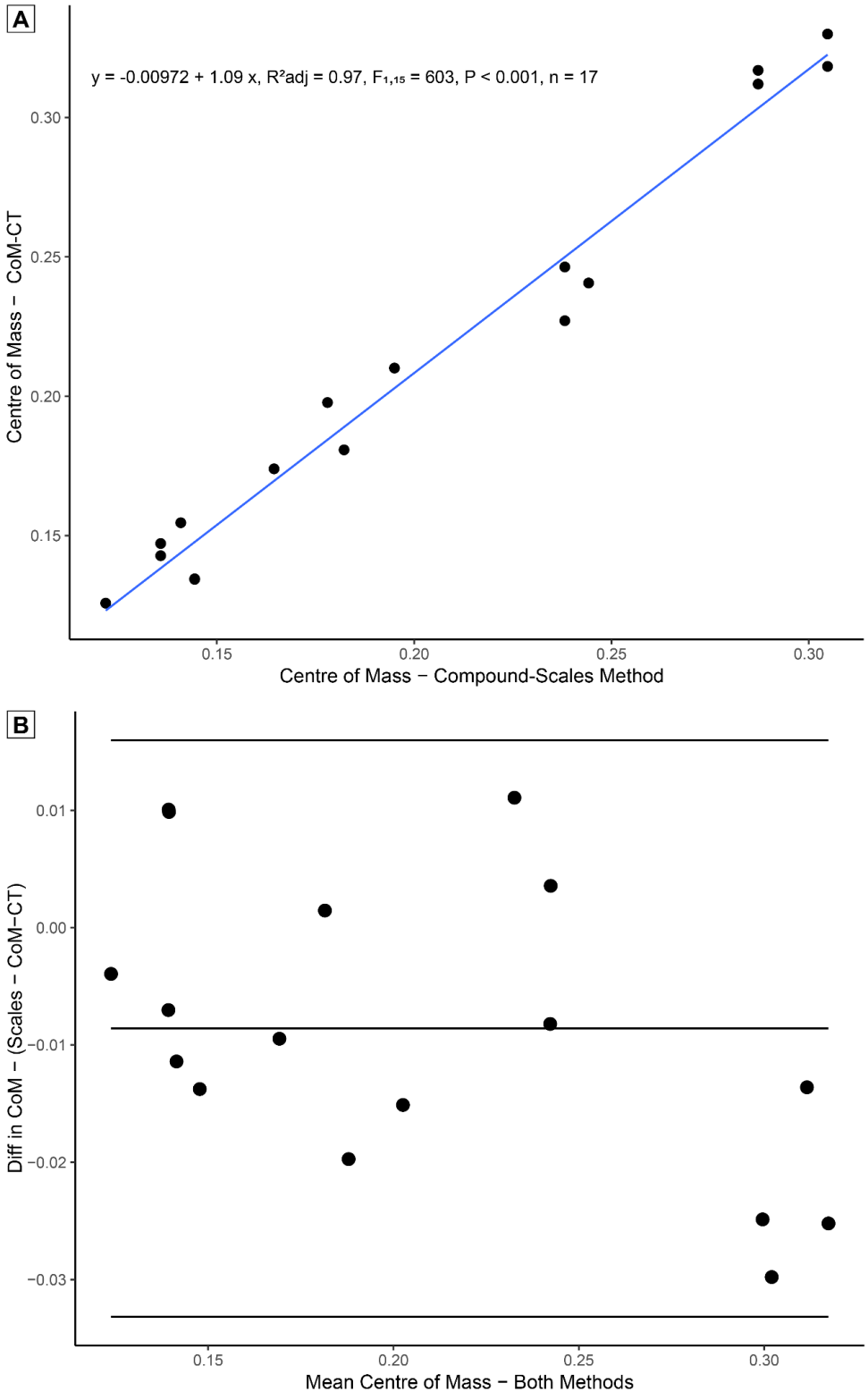

Figure 2.3. Comparison of centre of mass (CoM) estimates obtained using the compound-scales method and from computed tomography with variable, linearly regressed material density (CoM-CT). A) Linear regression evidences a strong positive linear relationship with a slope close to 1. B) Bland-Altman Plot showing small mean bias and narrow limits of agreement.

2.4.1.2 Interspecific Sample – Using COV-CT to test the influence of variation in internal anatomy on mass distribution

The aim of this analysis was to test the influence of variation in internal anatomy on mandible mass distribution. This was achieved by comparing centre of mass estimates derived from the homogenous density computed tomography method (CoV-CT) and centre of mass estimates derived from CoM-CT.

Linear regression (Figure 4. A) show a positive, almost perfectly linear relationship ($y = 0.000198 + 0.964x$, adjusted $R^2adj = 0.99$) between centre of mass estimated by CoV-CT and CoM-CT. The slope (0.964) is slightly less than unity, and the small positive intercept suggests a minor systematic bias, with the homogeneous density method yielding marginally lower CoM values at higher magnitudes. Nonetheless, the very high adjusted R^2 (0.99) confirms that the two methods are nearly equivalent in how they estimate CoM across the measured range.

The Bland-Altman plot (Figure 4. B) illustrates agreement between the two methods. The mean bias (central line) is small and positive, showing that, on average, the CoV-CT derived values are slightly higher than those from estimated by the CoM-CT method.

Overall, these results demonstrate that the two methods yield highly comparable and statistically interchangeable CoM estimates, with only negligible systematic differences. The interchangeability of both methods suggests variation in the internal anatomy of the mandible, in terms of mineralised tissues, has little influence on its mass distribution.

The scatter of points around the mean bias is narrow, and nearly all observations lie within the limits of agreement, indicating very high consistency between methods. No clear proportional bias is apparent, although there is a single outlier at a higher CoM value (~0.04 difference).

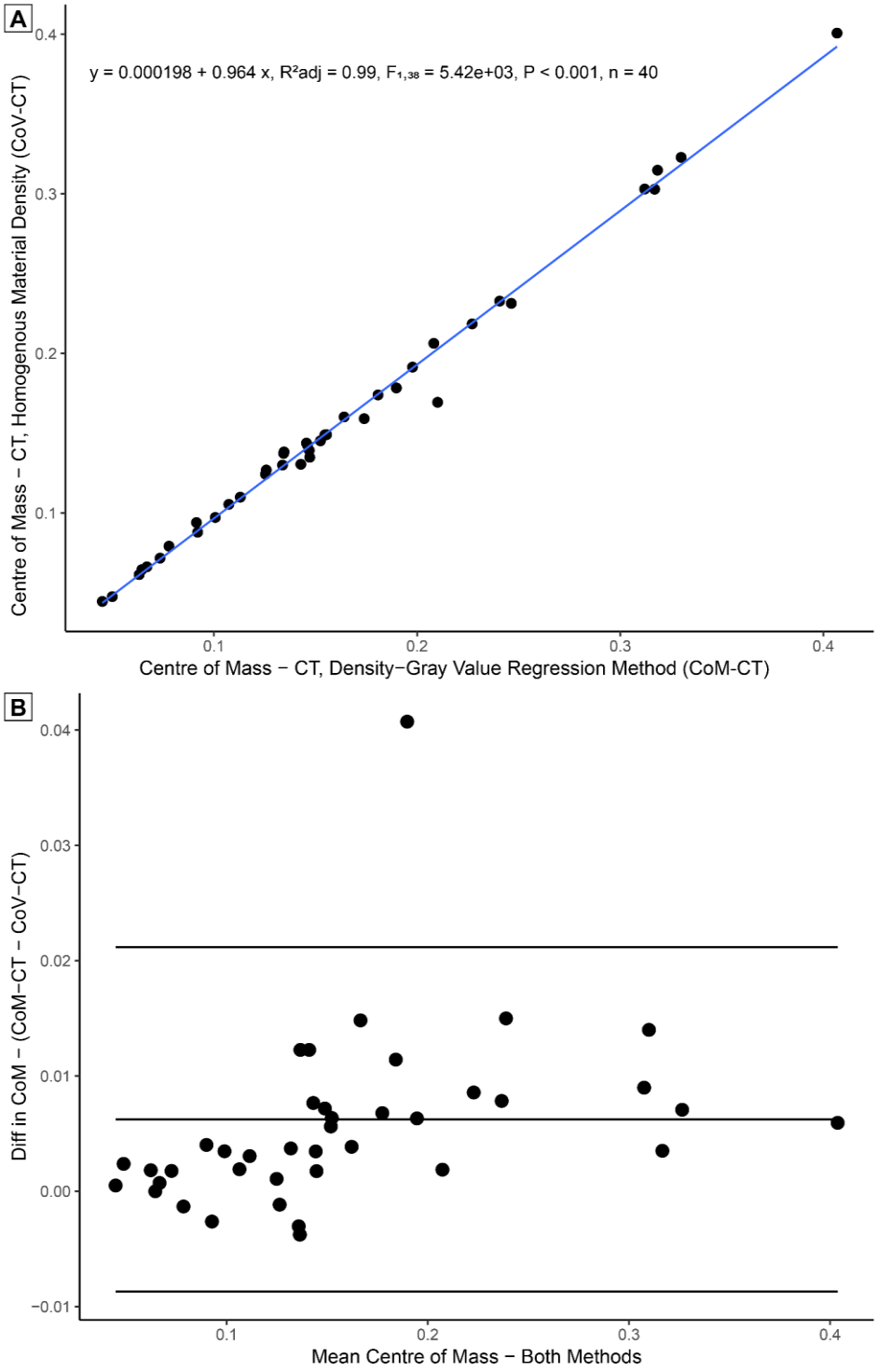

Figure 2.4. Comparison of centre of mass estimates obtained using the computed tomography with variable, linearly regressed material density method (CoM-CT) and the homogenous density computed tomography method (CoV-CT). A) Linear regression evidences a strong positive linear relationship with a slope close to 1, and adjusted R^2 very close to 1 (0.99). B) Bland-Altman Plot showing small positive mean bias and narrow limits of agreement.

2.4.1.3 Interspecific Sample – Using CoM-Surface to test the influence of internal architecture on mass distribution

The aim of this analysis was to test the influence of the internal architecture of the mandible on its mass distribution. This was achieved by comparing centre of mass estimates derived from the surface model method (CoM-Surface) and centre of mass estimates derived from CoM-CT.

Linear regression (Figure 5. A) show a positive, almost perfectly linear relationship ($y = 0.0118 + 0.92x$, adjusted $R^2adj = 0.98$) between centre of mass estimated by CoM-Surface and CoM-CT.

However, the slope (0.92) is slightly below unity, and the small positive intercept (0.0118) suggest a systematic underestimation of CoM by the surface model method at higher values. Despite this small proportional bias, the high coefficient of determination (adjusted $R^2 = 0.98$) indicates that both methods are scaling very similarly.

The Bland-Altman plot (Figure 5. B) illustrates general agreement between the two methods, albeit with some outliers. The mean bias (central line) is approximately zero, indicating minimal overall systematic difference between surface- and CoM-CT derived estimates. Most data points fall well within the limits of agreement (outer lines), which are narrow relative to the overall range of CoM values, confirming agreement between the two methods. No clear proportional trend is visible, though a few data points deviate at higher means. Agreement between these two methods suggests the internal architecture of the mandible does not have significant influence on the position of its centre of mass. However, the outlier datapoints suggest this may not be necessary the case for species with unusually large medullary cores and mandibular canals which would present as air-filled voids in CT scan images.

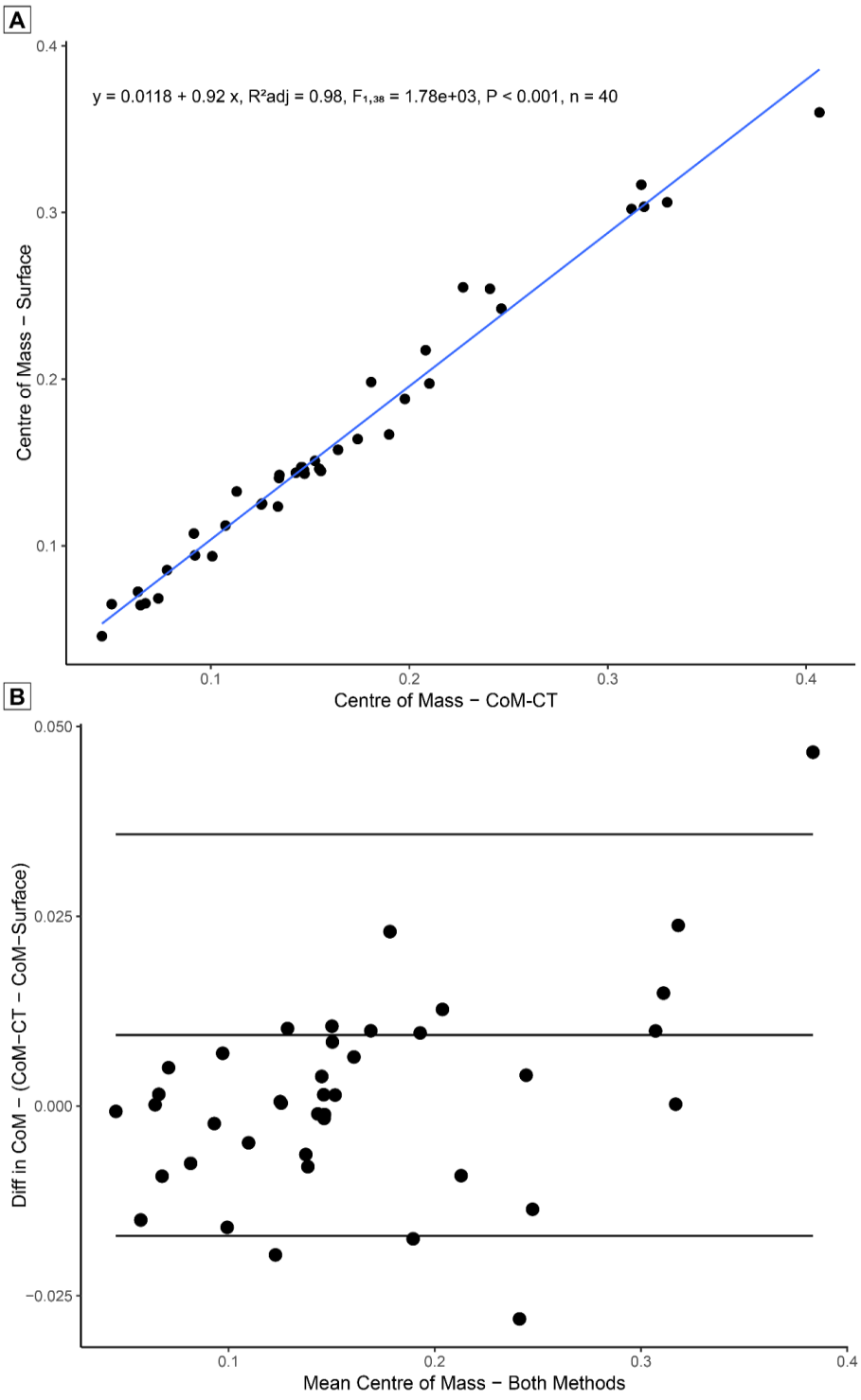

Figure 2.5. Comparison of centre of mass estimates obtained using the computed tomography with variable, linearly regressed material density method (CoM-CT) and surface model method (CoM-Surface). A) shows a strong positive relationship between CoM values estimated by both methods. B) Bland–Altman plot showing a near-zero mean bias and narrow limits of agreement.

2.4.1.4 Interspecific Sample – Jaw Length as a Proxy for Centre of Mass

The aim of this analysis was to investigate if jaw length would serve as a practical proxy for centre of mass in the ungulate mandible.

The regression (Figure 6) evidences a positive linear relationship (y = –0.0272 + 0.501x, adjusted R^2adj = 0.88) between jaw length and CoM. The slope of 0.5 suggests CoM position increases at approximately half the rate of jaw length.

This result suggests jaw length alone is not a suitable proxy for CoM as the slope (0.5) and negative intercept (-0.0272) show jaw length is not proportional to CoM. However, as the linear fit is strong (adjusted R^2adj = 0.88) jaw length could be used as a first-order predictor for CoM.

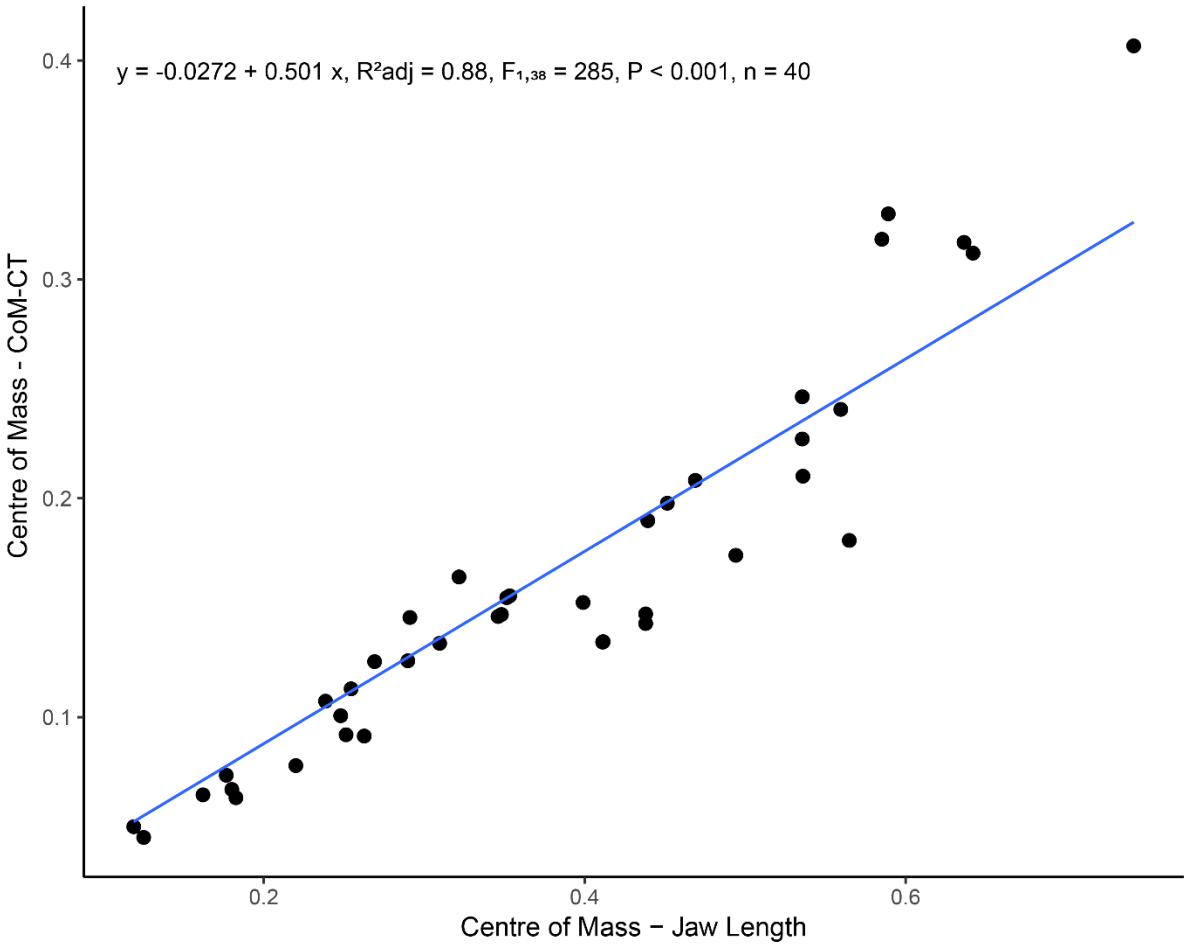

Figure 2.6. Linear regression plot illustrating the scaling relationship between mandibular CoM (CoM–CT) and jaw length.

2.4.2 Results 2 – *Diceros bicornis* Ontogenetic Sample

2.4.1.2 Ontogenetic Sample – Using COV-CT to test the influence of variation in internal anatomy on mass distribution

The aim of this analysis was to test the influence of variation in internal anatomy on mandible mass distribution in an ontogenetic intraspecific sample, as scaling during development is fundamentally different to interspecific scaling. This was achieved by comparing centre of mass estimates derived from CoV-CT and CoM-CT for the *Diceros bicornis* ontogenetic sample (Table 2).

The linear regression (Figure 7. A) evidences a very strong positive linear relationship ($y = 0.00261 + 0.948x$, adjusted $R^2adj = 0.93$). The slope (0.948) is close to, but slightly less, than unity, and near-zero intercept suggests essentially no proportional bias.

The Bland-Altman plot (Figure 7. B) illustrates agreement between the two CT-based methods. The mean bias is close to zero and the scatter around the mean is nearly uniform and small, with the exception of one outlier outside the limits of agreement.

The agreement of the CoV-CT and CoM-CT estimates indicates that, in the ontogenetic sample variation in internal anatomy, meaning the variation in mineralised tissue density, does not substantially influence mandibular mass distribution.

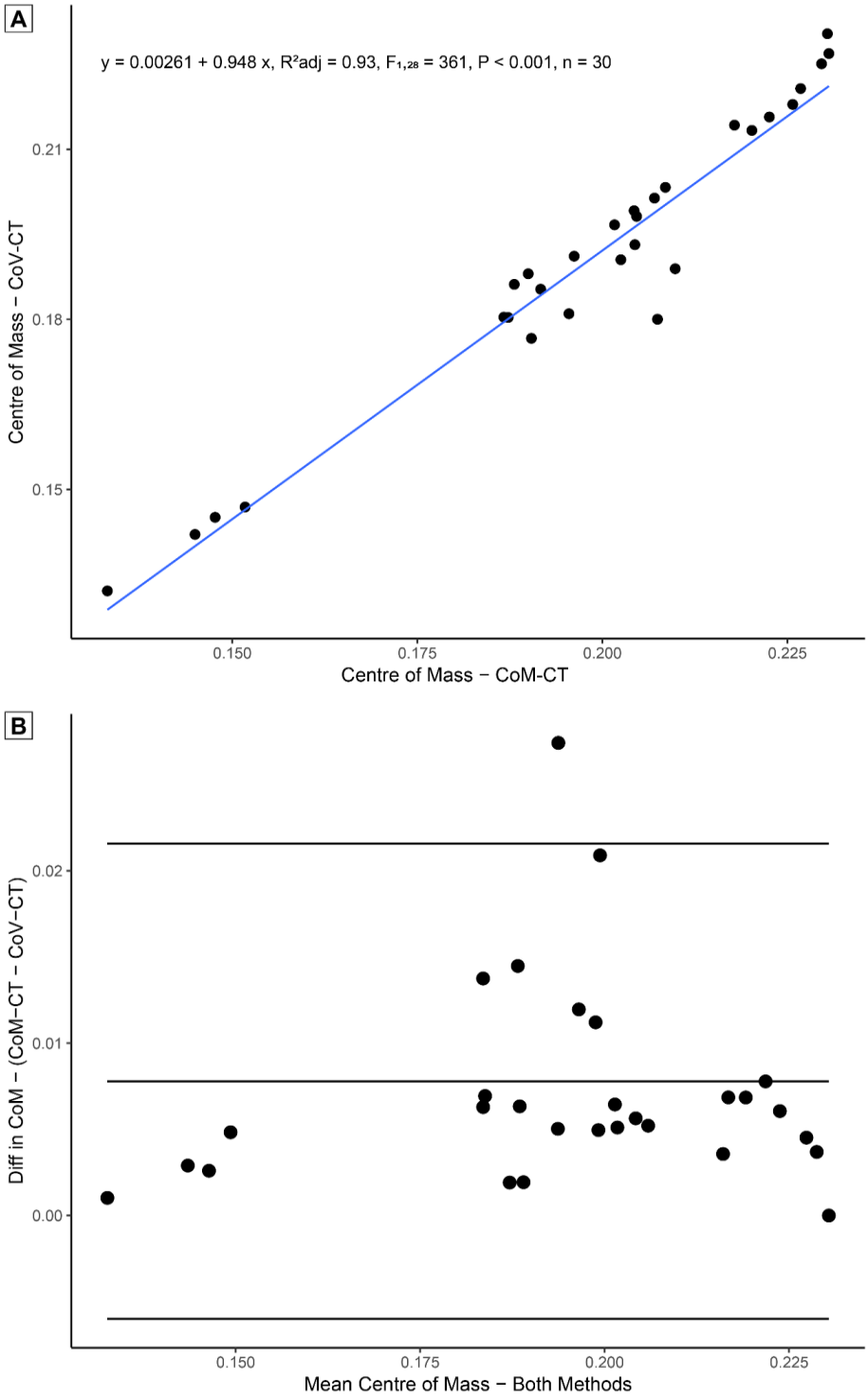

Figure 2.7. Comparison of centre of mass estimates for the ontogenetic sample obtained using the computed tomography with variable, linearly regressed material density method (CoM-CT) and the homogenous density computed tomography method (CoV-CT). A) Linear regressionevidences a strong positive linear relationship with slope close to 1, and adjusted R^2 close to 1 (0.95). B) Bland-Altman Plot showing near zero mean bias and narrow limits of agreement.

2.4.2.2 Ontogenetic Sample – Using CoM-Surface to test the influence of internal architecture on mass distribution

The CoM-Surface method estimates CoM from surface models which do not account for air filled voids in the osteological specimen which are evident in CT-based methods. The aim of this analysis was to test the influence of variation in internal architecture, meaning the size and distribution of these voids, on mandible mass distribution in an ontogenetic intraspecific sample. This was achieved by comparing CoM estimates derived from CoM-Surface and CoM-CT using linear regression and Bland-Altman analysis.

The linear regression (Figure 8. A) evidences a very strong positive linear relationship (y = -0.017 + 0.853x, adjusted R^2adj = 0.67), although the moderate adjusted R^2 (0.67) indicates this is not a particularly well-fitted relationship. The slope (0.853), being less than 1, reveals a proportional bias. CoM-Surface tends to estimate lower CoM values than CoM-CT.

The Bland-Altman plot (Figure 7. B) evidences no agreement between the two CT-based methods. The mean bias is positive, the scatter of differences is wide relative to the total range of CoM values, and several points fall near the limits of agreement, suggesting substantial variability between methods.

While CoM-Surface and CoM-CT are positively associated, they are not interchangeable. Taken together, these results confirm that the internal architecture of the mandible in this ontogenetic intraspecific sample plays an influential role in determining mandibular mass distribution.

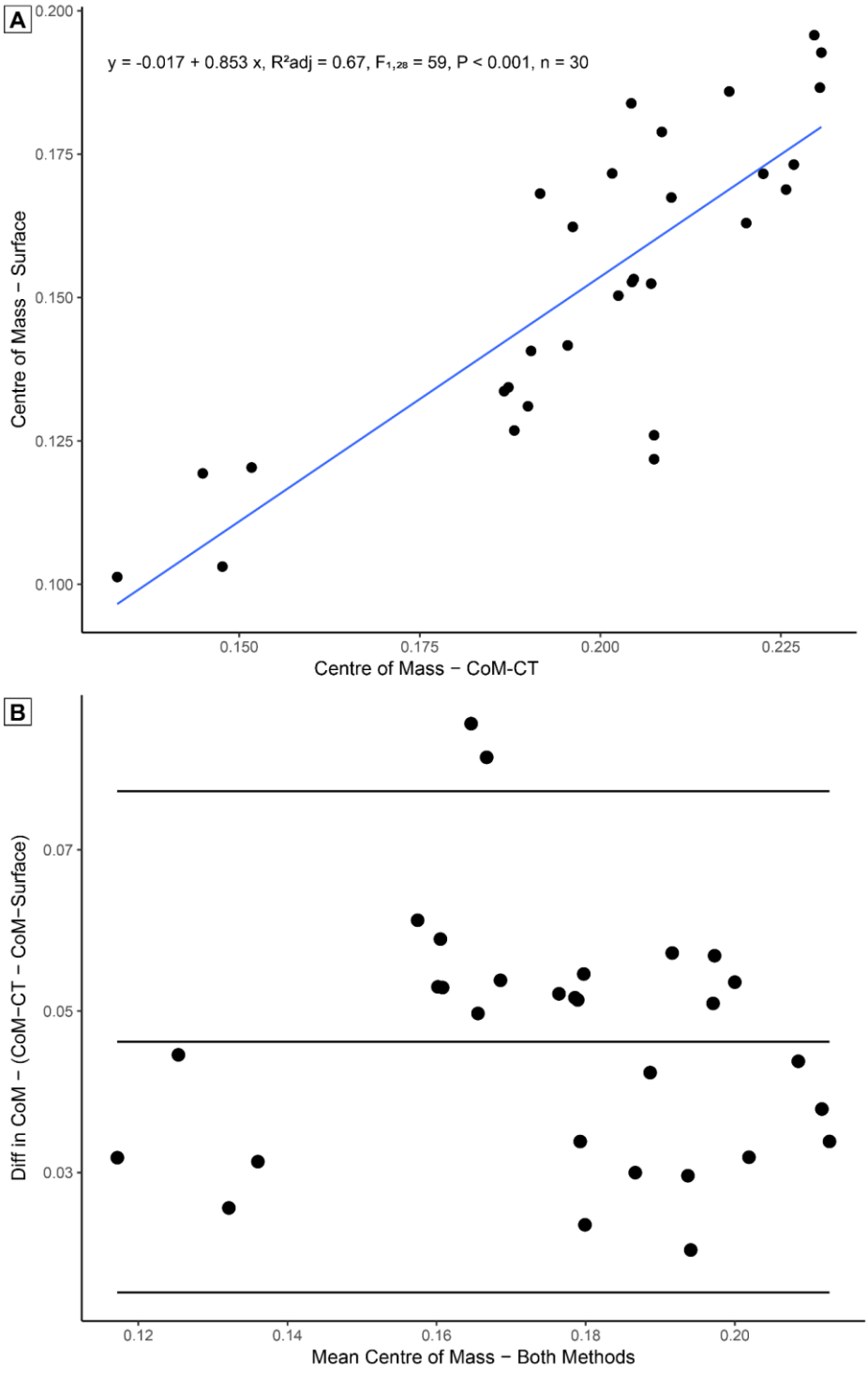

Figure 2.8. Comparison of centre of mass estimates obtained for the ontogenetic sample using CoM-CT and CoM-Surface. A) shows a strong positive relationship between CoM values estimated by both methods. B) Bland–Altman plot showing a near-zero mean bias and narrow limits of agreement.

2.4.2.3 Ontogenetic Sample – Jaw Length as a Proxy for Centre of Mass

Jaw length was investigated as a potential practical proxy for CoM in the ontogenetic intraspecific sample by linearly regressing CoM-CT derived CoM estimates against jaw length (Figure 9). The regression equation ($y = 0.062 + 0.358x$) and adjusted R^2 (0.84) demonstrate a strong and statistically significant positive relationship. However, as the slope (0.358) is substantially below 1, jaw length alone cannot be used as a CoM.

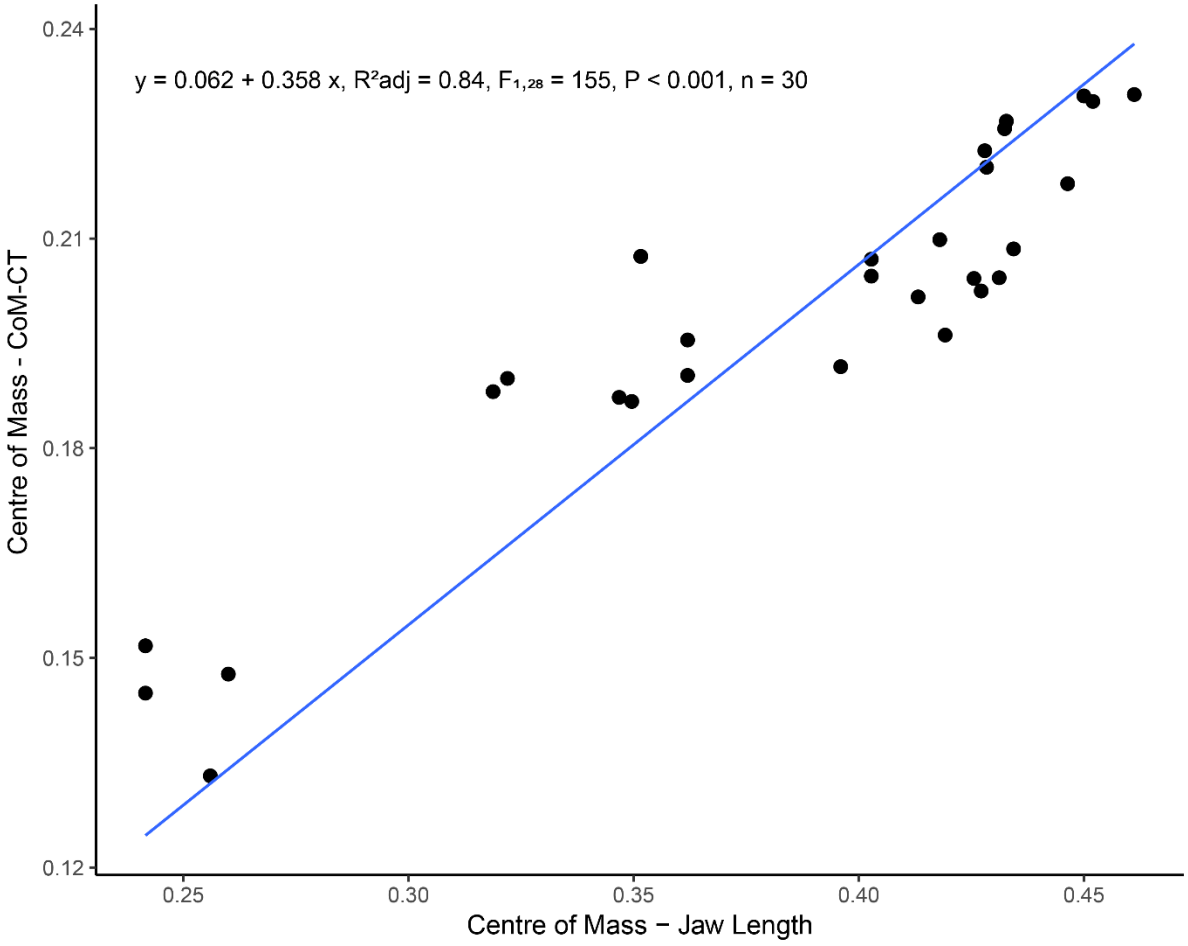

Figure 2.9. Linear regression plot illustrating the scaling relationship between mandibular CoM (CoM–CT) and jaw length in the ontogenetic intraspecific sample.

2.5 Discussion

This study investigated the determinants of mass distribution in the mammalian mandible in two case studies: 1) an interspecific sample of adult individuals (Table 2.1), and 2) an intraspecific ontogenetic sample of the black rhinoceros*, Diceros bicornis* (Table 2.2). Several methodological approaches for estimating centre of mass (CoM) from mineralised tissues were evaluated.

2.5.1 Validation of CoM-CT Methodology

Before hypothesis testing, the accuracy of the CoM-CT method for estimating centre of mass was validated against an establish standard, the compound-scales method (Clemente 2014; Macaulay et al, 2017). Whether CoM-CT, which uses voxel grayscale as a proxy for material density, produces estimates of CoM consistent with those derived from the compound-scales method was tested using linear regression and Bland-Altman Analysis. A strong, statistically significant linear relationship was observed between CoM-CT and compound-scales estimates ($y = –0.00972 + 1.09x$, adjusted $R^2 = 0.97$, $F_{1,,15} = 603$, $P < 0.001$, $n = 17$), with a slope close to unity and a near-zero intercept. This result indicated minor proportional bias, where higher compound-scales estimates correspond to slightly progressive larger CoM-CT estimates; CoM-CT estimates for larger mandibles are marginally more anteriorly located than compound-scales estimates for the same specimen. However, the adjusted R^2 (0.97), demonstrates an extremely high goodness-of-fit with only 3% of the variation left unexplained. Bland-Altman analysis found a very small, near-zero mean bias with narrow limits of agreement, demonstrating that the differences between the methods were minimal and randomly distributed across the measured range. This suggests interchangeability of the estimates derived from the two methods, allowing aggregate datasets to be formed from the combination of datasets derived from either method.

These results confirm that CoM-CT accurately replicates the CoM estimated from physical measurements. The CoM–CT approach can therefore be considered a valid method for estimating mandibular mass distribution. Computed tomography methods have benefits over more traditional methods as they are non-destructive, non-invasive, and do not require access to the physical specimen. CT-scan data can be shared between researchers more easily and more cheaply than physical visits, do not necessarily require visits to museums and other research institutions, can be shared on publicly accessible online data repositories. This open

accessibly of data offers researchers the opportunity to expand their datasets, invites collaboration with international research teams, and democratises research.

2.5.2 Addressing Hypothesis 1 – the influence of hard tissue anatomy

To test whether variation in the amount, density, and distribution of mineralised hard tissue (i.e., enamel, dentine, bone) meaningfully affects mandibular mass distribution, CoM estimates from the variable density computed tomography method (CoM-CT) were compared with those derived from a computed tomography method which assumed homogeneous density (CoV-CT). The objective was to determine whether voxel-specific material densities derived from computed tomography scans significantly alter estimates of CoM position compared with methods that assume a homogeneous density throughout the mandible.

Using linear regression and Bland-Altman analysis, CoM estimates from both methods were found to be statistically indistinguishable in both the interspecific sample (Table 1) and intraspecific ontogenetic sample (Table 2). CoM-CT and CoV-CT derived CoM estimates are interchangeable, indicating close proximity of the mass centres and geometrics centres of the mandible along its longitudinal axis.

Therefore, the variation of hard tissue anatomy in the mandible does not meaningfully alter the longitudinal mass distribution of the mandible. Consequently, future studies concerned with coarse-scale mechanical parameters can reliably use homogeneous density computed tomography metrics or other methods of estimating geometric centres without substantial loss of accuracy compared with specific voxel density methods such as CoM-CT.

2.5.3 Addressing Hypothesis 2 – the influence of internal architecture

Comparison of CT-derived (Com-CT) and surface-derived (CoM-Surface) CoM estimates showed that the internal architecture of the mandible contributes relatively little to CoM position in interspecific comparisons of adult individuals. The high adjusted R^2 (0.92) and narrow limits of agreement indicate that mass distribution along the long axis is largely determined by external geometry rather than being meaningfully influenced by the dimensions and distribution of internal cavities.

In contrast, the poorer fit of the linear regression (adjusted $R^2 = 0.853$) and agreement in the intraspecific ontogenetic series indicates that developmental changes in the size and

distribution of internal cavities do influence mass distribution as individuals grow. Early ontogenetic stages likely exhibit proportionally larger cavities and less development of cortical bone, as well as smaller teeth with thinner enamel, than in adult individuals, leading to a greater influence of internal architecture on mass distribution.

2.5.4 Addressing Hypothesis 3 – Jaw Length as a Proxy for Centre of Mass

Past studies have suggested jaw length may be used as a proxy for centre of mass in pigs (Zhang et al., 2001), humans (Zhang et al., 2002), and primates (Ross et al., 2017). Testing this hypothesis in a more morphologically diverse range of mandibles, such as the ungulate-grade mandible, offers wider applicability of this proxy in mammal studies.

Linear regression of CoM-CT estimates of CoM against jaw length evidence positive linear scaling but with slopes below 1 in both the interspecific (slope = 0.501) and intraspecific ontogenetic samples (slope = 0.358). These positive linear relationships indicate that with increasing jaw length, the CoM moves anteriorly, or distally from the TMJ, in in absolute terms. However, the regressions slopes, being below 1, suggest that longer jaw and proportionally more posterior, or proximal to the TMJ, CoM positions.

These linear relationships also indicate jaw length can predict CoM position with fairly high precision, the slopes and residual variation mean it should not be used as a strict proxy. Instead, if jaw length is to be used as a predictor of CoM position, it should be treated as a calibrated estimator specific to the study sample rather than a direct substitute. The regression equation ($\hat{y} = -0.0272 + 0.501 \times$ jaw length) should be applied to generate predicted CoM values, as this accounts for the intercept and negatively allometric slope. The predictive accuracy of this model should be quantified using appropriate error metrics such as the root mean square error (RMSE) or mean absolute error (MAE), and uncertainty should be expressed through 95% confidence intervals. Agreement between measured and predicted CoM values could then be evaluated using Bland-Altman analysis to determine whether the regression provides sufficiently precise estimates for biological interpretation.

2.5.5 Functional and Evolutionary Implications

The external morphology of the mandible alone can be used to provide accurate and precise estimations of CoM. The evolutionary and adaptive pressures which have influenced mandibular morphology (i.e., dietary specialisation, mechanical advantage, adductor muscle

morphology, and efficiency, particularly in terms of relative mechanical performance) likely converge on anatomies that allow for sufficient rigidity and resistance to bending, dentition, and mechanics while minimising moments of inertia. The posterior bias of CoM in large species likely reflects an adaptive response to the high muscular torques generated by powerful muscles required for prolonged chewing of fibrous plant material and high bite force required for crushing (e..g, Suids).

2.5.6 Methodological Implications

Establishing that surface models provide statistically interchangeable CoM estimates to CoM-CT methods in adult specimens has practical implications. It allows researchers to use freely available 3D surface scans, dramatically expanding comparative sample sizes and enabling inclusion of museum specimens or fossil mandibles where internal anatomy is unavailable, such as casts or specimens too large to be practically CT scanned. The CoM-CT method also provides a framework for integrating high resolution mass distribution data where fine-scale precision would be beneficial, such as finite-element analysis (FEA) or dynamic modelling of mastication.

2.5.7 Limitations and Future Work

Although this study demonstrates good consistency across the evaluated methods, several limitations remain. The interspecific sample was intentionally biased towards adult ungulate-grade mammals. While a functionally and morphologically sample compared to previous studies which focused on pigs, humans, and primates, inclusion of taxa with markedly different mandibular morphologies (e.g., Carnivora, Cingulata) may yield different scaling relationships. Ontogenetic effects, such as changes in the dimensions and distributions of internal cavities, require further exploration to understand how growth and functional transitions (e.g., weaning) influence mass changes in mass distribution. Additionally, log-transformed allometric analyses should be applied to confirm scaling exponents statistically and the potential influence of phylogenetic constraints should be addressed statistically (i.e., Phylogenetic Generalised Least Squares (PGLS)).

2.5.8 Concluding Statement

This study demonstrates that the external morphology of the mandible is the principal determinant of its mass distribution, while internal tissue and architecture variation and have relatively minor effects. The scaling of CoM with jaw length highlights predictable biomechanical optimisation across mammals and offers a practical, efficient, and inexpensive method for rough estimations of mandibular mass properties from simple linear measures of external morphology. These findings not only validate computed tomography-based methods for estimating mass distribution and centres of mass but also provide new insight into how mammalian mandibles have evolved to balance the competing demands of structural performance and mechanical performance. The consistent scaling of centre of mass position and the posterior bias of mass distribution across taxa suggest that mandibular form is evolutionarily constrained by the need to minimise rotational inertia and muscular effort during feeding, while preserving the strength and stiffness required for effective bite generation. This balance reflects an adaptive optimisation which may be fundamental to the functional evolution of the mammal mandible.

3. Biological and Mechanical Implications of Mandibular Mass Distribution in Ungulate-Grade Mammals (Orders Artiodactyla, Perissodactyla, Proboscidea)

3.1 Introduction

3.1.1 Conceptual Context and Short Summary

Efforts have been made to understand the influence of limb mass distribution on the mechanics of locomotion; however, limited research has examined the effects of mandibular mass distribution on mastication. Using a reliable, non-destructive method for estimating the mass distribution of the mineralised tissues of the mandible and deriving mass properties from computed tomography, this chapter investigates the relationship between these mass properties, mandibular anatomy, and masticatory mechanics. The analysis focuses on how mandible size scales with centre of mass and rotational inertia, how these variables covary with jaw adductor muscle force and lever arm configuration, and how these traits in species with differing dietary and digestive strategies have been modified to accommodate the mechanical demands of various mass distributions. The results indicate that mandible mass and centre of mass scale isometrically, while rotational inertia exhibits weak positive allometry relative to mandible length. The area of the masseter insertion scales isometrically with mandibular rotational inertia, indicating that the masseter is functionally adapted to the inertial properties of the mineralised mandibular tissues, even without considering the contribution of soft tissues that would increase total masticatory mass in vivo. Furthermore, the findings suggest that body size, diet, and digestive strategy collectively constrain the morphology of the ungulate-grade mandible.

3.1.1 The Mammalian Masticatory System

Mammals have a unique masticatory apparatus, and while chewing is not exclusive to mammals, it is one of their most distinctive characteristics (Herring, 1993). As such, any investigation of mammalian mastication presents a singular challenge, one that is critical to

understanding the evolution and diversity of the clade. Mammalian masticatory systems are characterised by a three-boned middle ear and a mandible composed of a single bone, the dentary, which articulates with the temporal bone at the temporomandibular joint (Crompton and Park, 1978). Distinguishing functional features of the masticatory system include occluding teeth, a reorganised jaw musculature and joint, a secondary palate, and a muscular system for food transport involving the tongue and pharynx. Teeth are the most common mammalian fossils, and variation in dental form and jaw musculature in extant species reflects adaptive evolution. Greater understanding of teeth and mastication contributes directly to the study of mammalian evolution.

3.1.1.2 Dentition

In most mammals, the dentition is divided into incisors, canines, premolars, and molars, although considerable variation exists due to dietary and functional specialisation. In elephants, tusks are modified incisors, while hippopotamus tusks are lower canines, and their large, interlocking incisors prevent lateral jaw movement (Avedik and Clauss, 2023). The African rhinoceroses (i.e., *Ceratotherium simum* and *Diceros bicornis*) lack both canines and incisors, instead using prehensile lips to collect grasses or browse. Elephants represent a more extreme condition, having only a pair of large molars and relying on the trunk to grasp and transport food. These specialisations are expected to influence mandibular mass distribution: hippopotamuses likely display an anterior bias, whereas rhinos and elephants, lacking anterior teeth and their associated mass, probably exhibit a more posterior distribution.

Teeth make a major contribution to mandibular mass distribution. They consist of three mineralised tissues – cementum, dentine (1.79–2.12g/cm^3), and enamel (2.61–2.77g/cm^3) – which are denser than cortical bone (1.60–2.00g/cm^3). The amount of enamel present in the teeth varies with diet and dental morphology, implying that dietary differences influence mass distribution. In mammals, the crowns of molars, and often premolars, act as shearing surfaces that break down food material during occlusion. The diverse morphology of the molar reflects both the phylogeny and diet of the species. Among ungulate-grade mammals, bunodont molars with rounded cusps occur in suids and are associated with omnivory (in this study, categorised within the “generalist” dietary category). Lophodont molars, characterised by ridges of enamel running along or across the molar row, occur in many herbivores, with loxodonty representing an extreme form in elephants. Ruminant artiodactyls, such as cervids and bovids, as well as the psuedoruminant camelids, possess selenodont molars, where cusps form crescent-shaped

ridges. Aside from the shape of the molar crown, the height of the tooth is also varied among ungulates. Hypsodont molars with high crowns and extended enamel resist wear from abrasive diets rich in grasses containing phytoliths and incidental exogenous grit. Many mixed feeders are also hypsodont, but some, depending on their diet or habitat, retain brachydonty like specialised browsers, or exhibit an intermediate condition known as mesodonty (Damuth and Janis, 2011). The degree of hypsodonty correlates with both diet and food intake; for example, equids consume greater food volumes than similarly sized ruminants and exhibit higher hypsodonty indices. High hypsodonty is expected to shift mass distribution toward the molar row due to the density of enamel.

During occlusion, opposing shearing surfaces must align precisely, requiring the mandible to move anteroposteriorly, transversely, pitch and roll, or in a combination of these movements. The size and shape of these shearing surfaces and the pattern of the movements vary considerably and reflect the type of food chewed. The orientation of the lines of action and positions of the jaw adductor musculature facilitates the ability of the jaw to move in these complex patterns. The masseter, inserting laterally on the mandible, is responsible for horizontal movement and pitch, and the temporalis, inserting on the coronoid process, produces upward, backward, and inward movement. Differential contractions of parts or all these muscles enable transverse motion, which is especially pronounced in herbivores that grind food rather than crush it.

3.1.1.1 Leverage Mechanics and Adductor Musculature

The lines of action of the jaw muscles forces converge above the molars and can be balanced so that the temporomandibular joint is not load-bearing; when the jaw is closed but not chewing, the opposing forces balance, producing zero net torque.

As a result, mammals can generate very high occlusal forces without generating large normal reaction forces at the jaw joint. The forces of chewing are not only resisted by the teeth and the temporomandibular joint, but the bones also distort during function and move relative to each other at the sutures. Concentrating bone mass near the molars may therefore assist in resisting strain, while also contributing to a posterior mass distribution. Many traditional mechanical analyses of the jaw have focused on the estimation of occlusal force. However, since herbivory generally requires low absolute bite force relative to body size when compared with carnivory or omnivory (Wroe et al., 2005; Christiansen and Wroe, 2007), this study considers the

physiological cross-sectional area of the masseter as a proxy for food-processing capacity, as a larger muscle experiences less fatigue per chewing cycle.

Muscle fatigue is influenced by fibre type composition. Type 1 fibres are slow-twitch and fatigue-resistant; Type 2b fibres are fast-twitch, glycolytic, and fatigue-prone; and Type 2a fibres are intermediate (Salmons, 2009). A reduction in Type 2b fibres and an increase in oxidative capacity can occur during an individual's lifetime, leading to greater fatigue resistance but reduced muscle volume (Pullen, 1977). Assuming a consistent distribution of fibre types across ungulate-grade taxa, a larger masseter would be expected to show reduced fatigue. The jaw-closer muscles, including the masseter, are largely composed of Type 1 fibres in ruminants (Picard et al., 1994; Basit, Tariq, and Siccardi, 2023), suggesting a relationship between continuous mastication and slow, fatigue-resistant fibres. If other ungulate-grade taxa share this composition, then a larger masseter would exhibit slower fatigue due to greater total force capacity and energy reserves. Larger muscles contain more fibres working in parallel, reducing strain on individual fibres and slowing fatigue given adequate oxygen supply. They also store more glycogen, which is consumed more slowly at moderate activity levels (Vøllestad, Tabata, and Medbø, 1992)

Herring (1993) argues that it is more important for mammal jaws to be effective, rather than efficient. This chapter seeks to investigate whether there is substantial evidence for mechanical efficiency in terms of how mass is distributed. Two species with equal mandible length and mandible mass but differing mass distributions will differ in efficiency. A more posterior mass distribution, with centre of mass closer to the temporomandibular joint, experiences lower rotational inertia and reduced resistance to angular motion. Although this represents a complex mechanical problem, this study focuses on select anatomical and mechanical parameters to explore mandibular mass distribution. If the assumption that the ungulate masseter is predominantly composed of Type 1 fibres holds, then it is proposed that the masseter exhibits negative allometric scaling with mandibular rotational inertia. Among similarly sized species, a smaller masseter associated with a more posterior mass distribution would indicate improved masticatory efficiency.

3.1.2 Browsing–Grazer Continuum in Ungulata and Proboscidea

Browsing, a diet consisting of woody and herbaceous plants, and grazing, a diet characterised by consumption of grasses, are distinctly different feeding behaviours.

Browsing, defined as the consumption of woody and herbaceous vegetation, and grazing, defined as feeding primarily on grasses, represent distinct dietary behaviours. Among ungulates, these diets are associated with differing morphologies, foraging strategies, body sizes, and physiological characteristics, and therefore likely with different mandibular mass distributions. The orders Artiodactyla and Perissodactyla, collectively referred to as the Ungulata, differ in their morphophysiological adaptations to diet. Perissodactyls, or odd-toed ungulates, are hindgut fermenters, as are extant elephants, while many artiodactyls, including camelids and members of the suborder Ruminantia (Families Tragulidae, Moschidae, Cervidae, Antilocapridae, Giraffidae, Bovidae), are foregut fermenters. Ruminants are typically characterised by a four-chambered stomach, the absence of upper incisors, a pronounced diastema, and lower canines modified to resemble incisors.

At comparable body size, foregut fermenters tend to be more gracile than hindgut fermenters, process less food daily, possess smaller jaw adductor muscles, and have a shallower mandibular angle. As a result, they exhibit more selective feeding behaviour due to slower digestion. Proboscideans, though not part of the Ungulata, are “ungulate-grade” hindgut fermenters, like perissodactyls. Of the ten known proboscidean families, only three, dating from the Miocene to the present, show grazing adaptations such as lophodont or hypsodont molars. The remaining families possess bunodont or bilophodont cheek teeth, indicative of browsing, and perhaps differing jaw movements during mastication.

At equivalent body size, hindgut fermenters are expected to exhibit heavier mandibles and more posterior centres of mass than foregut fermenters. This pattern results from the high degree of hypsodonty that concentrates mass at the molar row and the accumulation of bone at the bite point, necessary to resist the cumulative strain from repetitive chewing cycles. Such mechanical loading can produce microdamage and trigger remodelling even below mechanostate thresholds and may mechanically “fine tune” the mandible increasing its mechanical efficiency (Martin et al., 2015).

Several other craniodental features also differentiate browsers and grazers in response to the distinct mechanical requirements of processing grasses and browse. Grasses are more fibrous, more abrasive due to higher silica content, and lower in nutrient density than browse. Consequently, grazers generally possess larger masseters, deeper mandibular angles, and broader anterior jaws, adaptations that facilitate higher intake rates. Browsers and mixed feeders, in contrast, are more selective and benefit from narrower jaws and proportionally longer diastemata. These adaptations are expected to influence mandibular mass distribution

directly. A broader and deeper mandibular angle provides greater surface area for masseter insertion and increases posterior mandibular mass. A long, narrow diastema extends the mandible without significantly increasing its overall mass.

Ruminants have evolved a foregut-fermenting digestive system that enables efficient mastication relative to body size, as fermentation reduces particle size and enhances nutrient absorption. Incisors are used only during ingestion, not during rumination, making them more susceptible to wear in environments with high exogenous grit, which is subsequently washed away during rumination (Valerio et al., 2022; Healy, 1965). The dental pad, or incisor pad, present in ruminants and camelids, compensates for the absence of upper incisors and assists in gathering foliage. Bovids use the lower incisors to press vegetation against the dental pad, tearing plant material prior to chewing (Clauss et al., 2003). In cervids, the pad similarly facilitates browsing (Hofmann, 1989), while in camelids, it assists in the processing of fibrous vegetation. The strain generated. During ingestion, the lower incisors press against the dental pad to shear or tear vegetation, generating torque and mechanical stress at the incisor roots. These stresses can damage the supporting tissues, increasing tooth mobility and inducing bone resorption (Northey and Hawley, 1975). The resorbed bone may be replaced through osteoblastic activity and mineralisation, altering bone density and structure in response to functional demands (Hadjidakis and Androulakis, 2006).

Dense or highly mineralised bone would be advantageous for transmitting incisal bite forces; however, because this action occurs less frequently and over a smaller area than molar chewing, the contribution of additional bone mass in the anterior mandible would be minor compared to the posterior region. Consequently, the presence of a pronounced, but lightly built, diastema is expected to produce a more relatively posteriorly positioned centre of mass, as mandibular length increases without a proportional increase in anterior mass.

3.1.3 Scaling – Interspecific and Intraspecific Ontogenetic

Interspecific scaling and intraspecific ontogenetic scaling represent key concepts in evolutionary biology. Relevant aspects to this study, include the definition of traits, changes in body size, and the maintenance or alteration of function during ontogeny or between species. Understanding the distinct effects of ontogenetic and interspecific scaling is essential for determining whether covariation and scaling of anatomical or mechanical traits result solely from size differences or reflect functional adaptation at different growth stages.

Throughout mammalian evolution, changes in body size have been accompanied by corresponding changes in physiology, including the scaling of organs, including the teeth. Molar teeth exhibit relatively invariant shape scaling with body size, showing a strong linear relationship that allows molar dimensions to be used as proxies for estimating the body masses of extinct species (Damuth and MacFadden, 1990; Copes and Schwartz, 2010). In ungulates, the size and scaling of the teeth, particularly molar volume, are linked to dietary demands, body size, and the mechanical demands of food processing (Damuth and Janis, 2011).

However, the scaling of teeth, which significantly influence mandibular mass distribution, does not occur uniformly across taxa. In suid artiodactyls and ceratomorph perissodactyls, the area of the postcanine teeth scales isometrically with body weight (Prothero and Sereno, 1982) but exhibits positive allometry relative to skull size (Fortelius, 1985). In contrast, tooth width and surface area display slight negative allometry with both body and skull size in selenodont artiodactyls (Fortelius, 1985). Although there is no strong evidence for allometry in ungulates generally, deviations from isometry may occur at lower taxonomic levels in either positive or negative directions. Fortelius (1985) proposed that if geometric similarity corresponds to functional similarity through size-related change, departures from isometry at lower levels may not necessarily indicate functional significance.

While total postcanine tooth volume may not scale allometrically overall, it correlates with the total amount of food consumed daily when comparing different clades. Grazing equids, which are hindgut fermenters, possess greater dental volume than grazing ruminant artiodactyls of comparable body size (Janis, 1988). Hindgut fermenters also tend to exhibit longer molar rows than foregut fermenters because more mastication is required early in the digestive process (Raia et al., 2010). This pattern likely corresponds to a higher proportion of mandibular mass concentrated around the molar row. In ungulate mammals, both individual and total postcanine tooth volume, as well as individual molar crown height, scale isometrically with body weight and correlate with dietary type (Janis, 1988). Nonetheless, some authors have identified a conceptual difficulty with isometric scaling in dental metrics (Fortelius, 1985; Janis, 1988), as most physiological processes, including ingestion rate (Kleiber, 1932; McMahon, 1973; Peters, 1983).

During ontogeny, mammals experience marked changes in dental anatomy from the deciduous (milk) stage through weaning and into adulthood, typically with the development of a single set of permanent teeth. Most mammals are diphyodont, producing two sets of teeth during their lifetime. Exceptions include taxa with continuous tooth replacement, or polyphyodonty, such as

manatees, kangaroos, and elephants. Elephants represent a unique case, producing six sets of molars that are replaced sequentially throughout life (Schiffmann et al., 2019). Each stage facilitates the dietary needs and functional demands of that life stage. The process of tooth development, eruption, and replacement is integral to how mammals, particularly ungulates and other ecologically similar herbivores, adapt to their environment throughout life (Lucas, 2004).

The deciduous teeth typically erupt during early infancy and assist in the transition from milk feeding to the consumption of soft plant material. These teeth are smaller and less robust than permanent teeth, as they are not required to resist the mechanical forces associated with processing fibrous or abrasive vegetation. This functional shift likely alters mandibular mass distribution, as adult dentition and the bone supporting the molar row are adapted to withstand greater mechanical loads. In herbivores, deciduous molars and premolars are underdeveloped, reflecting the limited chewing activity required before weaning. Weaning represents the transitional phase during which the diet shifts from milk to solid food and coincides with the eruption of permanent teeth (Smith, 1991), which support the increased mechanical demands of mastication. As individuals approach adulthood, the full complement of permanent teeth is typically present. After the transition from weaning to solid feeding, subsequent developmental changes are minor, limited to refinement of feeding patterns, morphology, and muscle function (Herring, 1985). These observations suggest that changes in mandibular mass distribution after the establishment of adult feeding are less significant than those associated with the functional transition from milk to solid food.

3.1.4 Chewing Cycles – Frequency, Period, and Scaling

Chew cycle frequency, defined as the number of chewing cycles completed per unit time, represents an important parameter of masticatory mechanical performance. When two species possess comparable masticatory structures and total daily chewing time but differ in mandibular mass distribution and rotational inertia, the species with the higher chewing frequency will expend more energy to achieve an equivalent caloric intake.

Chew cycle frequency is limited by the maximum force of the muscle and exhibits negative allometric scaling with body mass. In large animals, the upper limit of chewing frequency scales with body mass$^{1/3}$, as determined by jaw length, the elastic modulus of the food, and occlusal surface area scaled isometrically with body mass. In small animals, the upper limit is a constant frequency (8Hz). however, the lower limit scales with body mass$^{1/6}$ (Virot et al., 2017).

More specifically, empirical data indicate that chewing frequency is inversely proportional to body mass$^{-0.128}$ and the period of a single chewing cycle is proportional to jaw length$^{0.383}$ (Ravosa et al., 2010). Druzinsky (1993) proposed that, because chewing frequency does not scale with metabolic rate, it is determined by the mass and length of components of the masticatory apparatus, making it directly relevant to studies of mandibular mass distribution. As with mastication, locomotor stride frequency scales inversely with body size (Heglund et al., 1974; Biewener and Taylor, 1986; Heglund and Taylor, 1988), reflecting common biomechanical constraints on cyclic movements.

Smaller mammals exhibit higher chewing frequencies than larger species (Hiraiwa, 1978; Fortelius, 1985; Druzinsky, 1993; Gerstner and Gerstein, 2008; Ross et al., 2009a). Consequently, smaller animals experience a greater number of loading cycles per unit time and load the mandible at faster rates, potentially influencing bone fatigue and strength (Ravosa et al., 2010). Peak strain magnitude, a proxy for bite force, correlates primarily with loading rate rather than with loading duration within the power stroke (Ross et al., 2007a; Ravosa et al., 2010). In larger mammals, bite forces exceeding those required to process food may therefore relate more to the volume of tough material consumed than to its material toughness. Previous studies have also demonstrated that jaw adductor lever arms and muscle physiological cross-sectional area scale negatively with dentary mass, thereby constraining chewing rate to decrease with increasing body size (Druzinsky, 1993; Reilly, 1995; Richard and Wainwright, 1995; Wainwright and Richard, 1995).

Taken together, previous research indicates that bite force, jaw adductor lever arm geometry, and mandibular mass distribution are interrelated determinants of masticatory performance, providing a rationale for analysing their covariation. These parameters provide a quantitative framework for examining how the mechanical constraints of mastication scale with body size and morphology in ungulate-grade mammals. Investigating how these variables co-vary offers insight into the mechanical cost of chewing and the scaling of chew cycle frequency, thereby linking mandibular mass distribution to both functional efficiency and masticatory energy expenditure.

3.2 Hypotheses

3.2.1 Hypothesis 1

Hypothesis 1A: With increasing mandible length there is a posterior shift in mass distribution, indicated by a more posterior centre of mass than would be expected by isometry.

Hypothesis 1B: This posterior shift proportionally decreases the rotation inertia of the mandible which *in theory* would reduce the energetic cost of chewing.

3.2.3 Hypothesis 2

The jaw adductor musculature, particularly the masseter, is adapted to contend with the mechanical demands of moving a heavy jaw through many daily chewing cycles. This functional role is likely augmented by *increased mechanical efficiency, in terms of mechanical advantage of the jaw lever arm arrangement, especially in large taxa with anteriorly heavy mandible*s. This adaptation is expected to be expressed as a negatively allometric relationship between masseteric insertion area and rotational inertia, and as higher mechanical advantage of the masseter in large species with anteriorly heavy mandibles.

3.2.4 Hypothesis 3

If mandibular mass distribution reflects dietary specialisation, *browsers and grazers should exhibit distinct ratios of rotational inertia to mandible length*. This ratio serves as a coarse proxy for the mechanical cost of mastication, as it represents the muscular torque required to move the mandible per unit length. If this ratio proves efficacious in identifying feeding guild in extant ungulates, it may therefore be used to infer the feeding ecology of extinct species.

3.3 Materials and Methods

3.3.1 Materials

The analyses in this study employed the same adult interspecific sample of Artiodactyls, Perissodactyls, and Proboscideans (Table 2.1) and the same intraspecific ontogenetic series of *Diceros bicornis* (Table 2.1) used in the preceding chapter. No additional specimens were included in either sample, and all specimen identifiers, scanning details, and data sources are provided in Table 2.1 and Table 2.2.

3.3.1.1 Adult Interspecific Sample

The adult interspecific consisted of a selection of 40 specimens, incorporating 32 species of functionally diverse terrestrial mammalian herbivores and generalist omnivores (Suids) belonging to the Orders Artiodactyla, Perissodactyla, and Proboscidea. The primary specimen selection criterion was to maximise the taxonomic, morphological, and ecological diversity of species within practical limits. Specimens obtained from online repositories and those previously scanned at the University of York (Table 2.1), were often limited to a single hemi-mandible (e.g., *Bos taurus*, *Cephalophus* sp.), had unusable areas on a single hemi-mandible due to noise or operator error (e.g., *Elephas maximus*), or contained metal inserts from repair or mounting that were not apparent during selection (e.g., *Damaliscus jimela*, *Dicerorhinus sumatrensis*, *Mazama americana*). To standardise this sample, complete mandibles were digitally separated into paired hemi-mandibles. This approach also minimised unquantifiable error from mandibular asymmetry and increased the effective sample size, which was advantageous for large specimens that were difficult and costly to scan (e.g., *Hippopotamus amphibius*, *Loxodonta africana*).

3.3.1.2 Intraspecific Ontogenetic Sample

The second sample consisted of an intraspecific sample consisting of 15 individual black rhinoceros, *Diceros bicornis*, across four ontogenetic stages ranging from neonates to old adults (Table 2). In keeping with the process undertaken for the interspecific sample, each complete mandible was divided into paired hemi-mandibles.

3.3.2 Data Collection

All mandibular mass distribution data were calculated using the CoM-CT method described in Chapter 2, *Determinants of Mandibular Mass Distribution and Assessing Methods for Estimation of Mass Properties*. This method applies a linear regression of computed tomography (CT) grayscale values against known material densities for each component of the mandible to assign an average density to each voxel. Given the known voxel volume, voxel mass can then be calculated directly.

The Fiji distribution of the open-source software ImageJ (Schindelin et al., 2012) and the macro plugin *Macro-code-slice-count.ijm* were used to extract voxel grayscale data. The plugin outputs a spreadsheet listing each grayscale value (0–255) and the number of voxels

corresponding to that value in every CT slice. Voxels with low grayscale values, representing air and residual soft tissue, were excluded to reduce artefacts caused by partial volume averaging at bone–air boundaries. Higher grayscale values, representing mineralised tissue, were exported to a CSV file for calculation of voxel density and mass. Voxel mass values were summed for each slice and plotted as a distribution along the long axis of the mandible.

A standardised orientation was defined for all specimens using the mandibular long axis. The reference plane included the occlusal surface of the most anterior dentition—typically the incisors—or the superior surface of the mandibular symphysis in taxa lacking anterior teeth (e.g., *Elephas*, *Loxodonta*, *Ceratotherium*, *Diceros*) and the occlusal surface of the most posterior molar, aligned parallel to the horizontal. The centre of mass was calculated as the point dividing the mandible into two sections of equal mass. The mandible was modelled as a two-dimensional object rotating about a cylindrical axis located at the temporomandibular joint (TMJ). The centre of mass was expressed as a linear displacement from the TMJ along the long axis of the mandible, with the vertical component set to zero to reflect the assumed horizontal alignment. Although the standardised horizontal orientation employed here does not account for habitual head posture, this methodology provides a standardised basis for comparison among taxa with mandibles of different morphologies and dental formula and can be adjusted in future analyses if required.

Because voxel grayscale values serve only as proxies for material density, the linear regressions used to estimate density values do not exhibit perfect fits, and each derived variable represents an estimate rather than an absolute measurement. Consequently, the results of this study are interpreted comparatively, focusing on general patterns and deviations between taxa rather than on precise numerical outputs. Inferences are based on relative relationships among metrics, particularly where proxies, such as masseteric insertion area as a stand-in for muscle force, were employed in place of direct measurements.

4.3.3 Rotational Inertia

The resistance of the mandible to angular motion, or rotational inertia, was calculated by modelling the mandible as a two-dimensional object undergoing unidirectional rotation about an axis positioned at the temporomandibular joint (TMJ). Although this model represents a simplification relative to the multidirectional jaw movements that occur during feeding in ungulates and proboscideans, it was adopted because it permits estimation of rotational inertia

with the mandible held close and the teeth are in occlusion, and can be readily adjusted to incorporate species-specific habitual head postures. Rotational inertia, *I*, was calculated by:

$$(1)\ I = mr^2\ (kg.m^2)$$

Rotational inertia was calculated for the interspecific sample at four functionally relevant positions along the mandible. The first was the centre of mass, representing the resistance to angular motion that must be counteracted by muscular torque to maintain jaw closure. The second and third were the most posterior and anterior points of the molar row, used to assess the mechanical effort associated with mastication, which is presumed to be particularly relevant in grazing taxa. The fourth position was the anterior extremity of the mandible, defined as the most anterior point of the dentition or, in species lacking canines or incisors, the superior surface of the mandibular symphysis.

3.3.4 Area of Masseteric Insertion

Surface-rendered three-dimensional models were generated for each CT scan in the adult interspecific sample using the 3D Viewer plugin in Fiji (Schmid et al., 2010). The area of masseteric insertion was measured in the scan-based engineering and design software *Geomagic Design X* (Version 2023.2.0). Muscle attachment scars were delineated along the lateral surface of the ramus and angular process using the *Select By Area* tool, and surface area was calculated through the *Compute Area* function within the *Analysis Tools* menu.

The measured areas likely represent an overestimation of the true muscular attachment due to the tendonous attachment exaggerating the extent of the muscle and the polygonal construction of the model. As this overestimation is consistent across specimens and scales with total surface area, the measurements remain appropriate for comparative analyses.

In this study, the masseteric insertion area was used as a proxy for muscular force, based on the assumption that the physiological cross-sectional area (PCSA) of the masseter and its attachment area are proportionally related. This assumption follows the principle that, when all other factors are equivalent (e.g., neural control, muscle fibre type, and leverage), larger muscles generate greater force. PCSA, defined as the largest cross-sectional area of a muscle perpendicular to its fibre direction, is a strong predictor of muscle force (Rockenfeller et al., 2024). Although enthesis morphology has been shown not to correlate directly with activity type or intensity (Rabey et al., 2015), the masseteric insertion area has been applied as a comparative proxy for muscle force in ungulates in a comparative context (Zhou et al., 2019).

3.3.5 Mechanical Advantage – Lever Mechanics

Mechanical advantages of the masseter and temporalis muscles were calculated from three-dimensional measurements taken in *Blender* (Version 3.1; Blender Foundation, 2022), using the default *Measure* tool available in the toolbar, and calculated in *Microsoft Excel* (Version 16.0), following the lever-mechanics approach of Morales-García, Säilä, and Janis (2020), and in this study, are treated as proxies for the mechanical efficiency of the jaw lever system.

3.3.6 Statistical Analyses

To evaluate the statistical significance of linear relationships among the measured variables, several regression models were applied to account for the differing assumptions inherent in each method. Ordinary Least Squares (OLS) regression assumes that the independent variable is measured without error, whereas Reduced Major Axis (RMA) regression assumes that measurement error is present in both the independent and dependent variables. Employing both models allowed potential error in the independent variable to be considered during analysis.

Phylogenetic Generalized Least Squares (PGLS), which estimates expected covariance and assumes closely related species produced similar residuals from the OLS line of best fit, was employed to account for the non-independence of data due to shared phylogenetic history. A phylogenetic tree for the adult interspecific sample was generated using the R package *U.Phylomaker* (Jin and Qian, 2022) as a subtree of the consensus mammalian megatree published by Upham et al. (2019) (Figure 3.1). This tree was subsequently used for PGLS analysis in the R package *phylotools* (Revell, 2012).

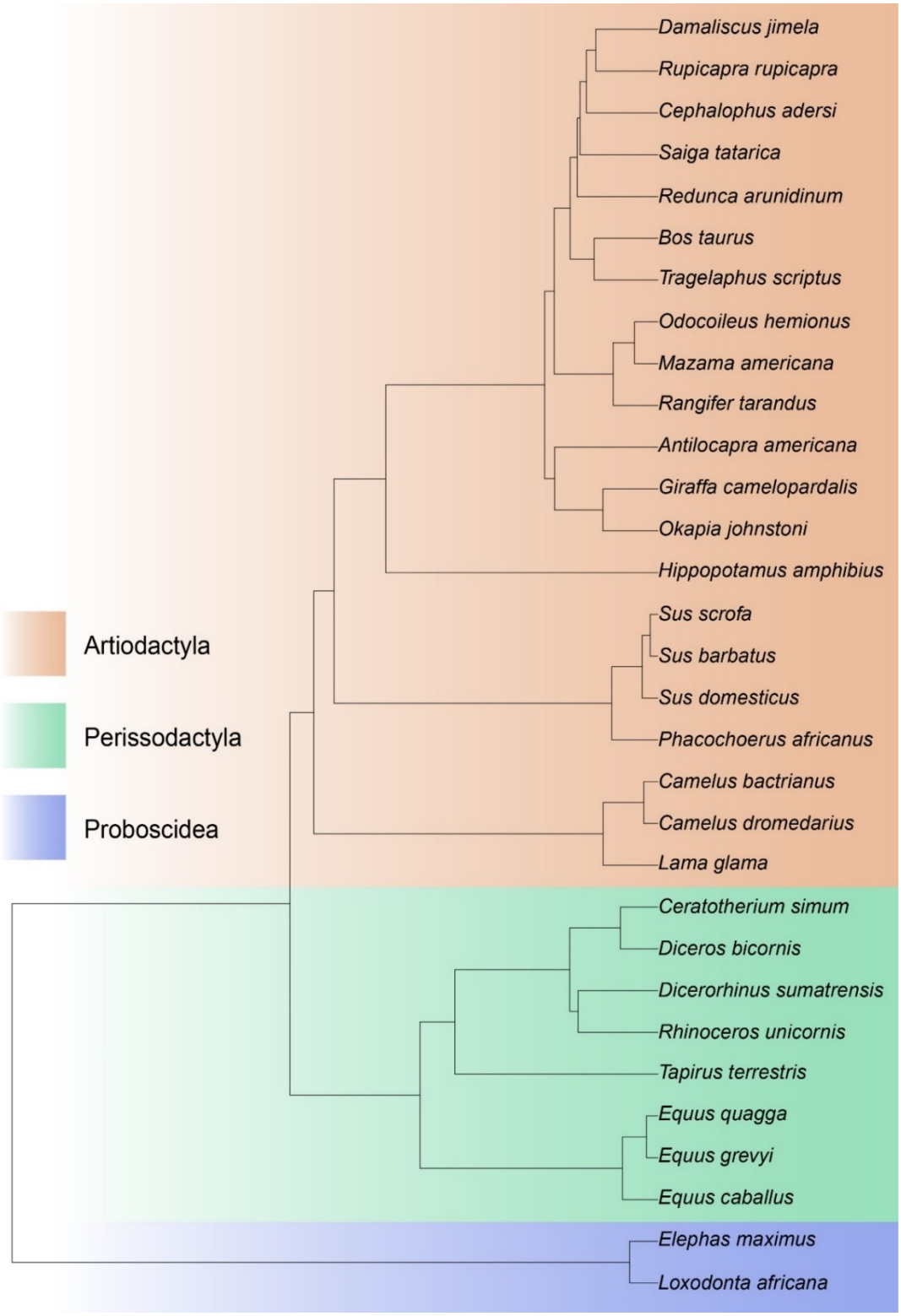

Figure 3.1. Phylogenetic tree of the adult interspecific sample taxa used in Phylogenetic Generalised Least Squares (PGLS) regression analyses. The tree was generated using the R package *U.Phylomaker* (Jin and Qian, 2022) as a subtree of the consensus mammalian megatree published by Upham et al. (2019). Taxa are colour-coded by order: Artiodactyla (orange), Perissodactyla (green), and Proboscidea (blue).

3.4 Results

3.4.1 Addressing Hypothesis 1 – Scaling of Mass Properties

The scaling relationship between mandible length and mandible mass was investigated in both the interspecific adult and intraspecific ontogenetic samples. A summary table of the linear regression statistics is provided for ease of comparison (Table 3.1).

In the interspecific sample, mass scales with positive allometry with respect to length (OLS slope = 3.95, 95% confidence interval: 3.42-4.47. RMA slope = 4.25, 95% confidence interval: 3.77-4.81. Isometry slope = 3) (Figure 3.2). The PGLS regression produced a slightly shallower slope than both the OLS and RMA models, falling marginally below the OLS 95% confidence interval, indicating that phylogenetic clustering contributed to a portion of the positive allometric signal, particular at large size.

In the intraspecific ontogenetic sample, mass also scaled with positive allometry relative to length but at a higher rate than in the interspecific sample (OLS slope = 4.67, 95% confidence interval: 4.33–5.00; RMA slope = 4.75, 95% confidence interval: 4.42–5.10; isometric expectation = 3) (Figure 3.2). These results demonstrate that positive allometry is evident at both interspecific and intraspecific scales, with the intraspecific dataset exhibiting a steeper allometric gradient.

Table 3.1. Linear regression statistics for the scaling relationship between mandible length and mandible mass.

Dataset	Regression Model	Slope	95% Confidence Interval	Isometric Expectation	Interpretation
Interspecific (adult)	OLS	3.95	3.42–4.47	3.00	Positive allometry
	RMA	4.25	3.77–4.81	3.00	Positive allometry
	PGLS	Shallower than OLS, below CI	---	3.00	Indicates phylogenetic clustering
Intraspecific (ontogenetic)	OLS	4.67	4.33–5.00	3.00	Strong positive allometry
	RMA	4.75	4.42–5.10	3.00	Strong positive allometry

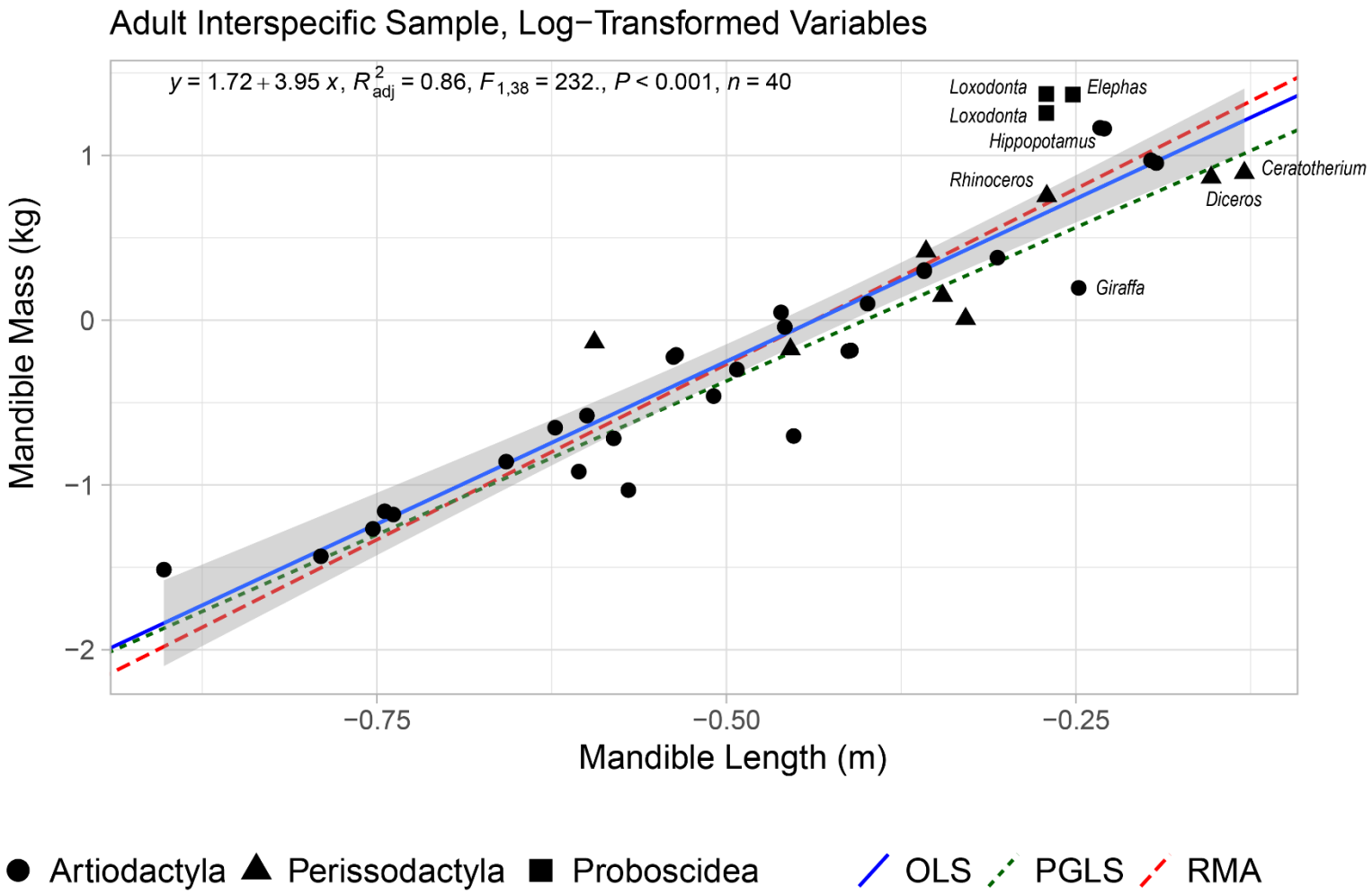

Figure 3.2. Linear regression analysis of mandible length (m) against estimated mandible mass (kg) for the adult interspecific sample.

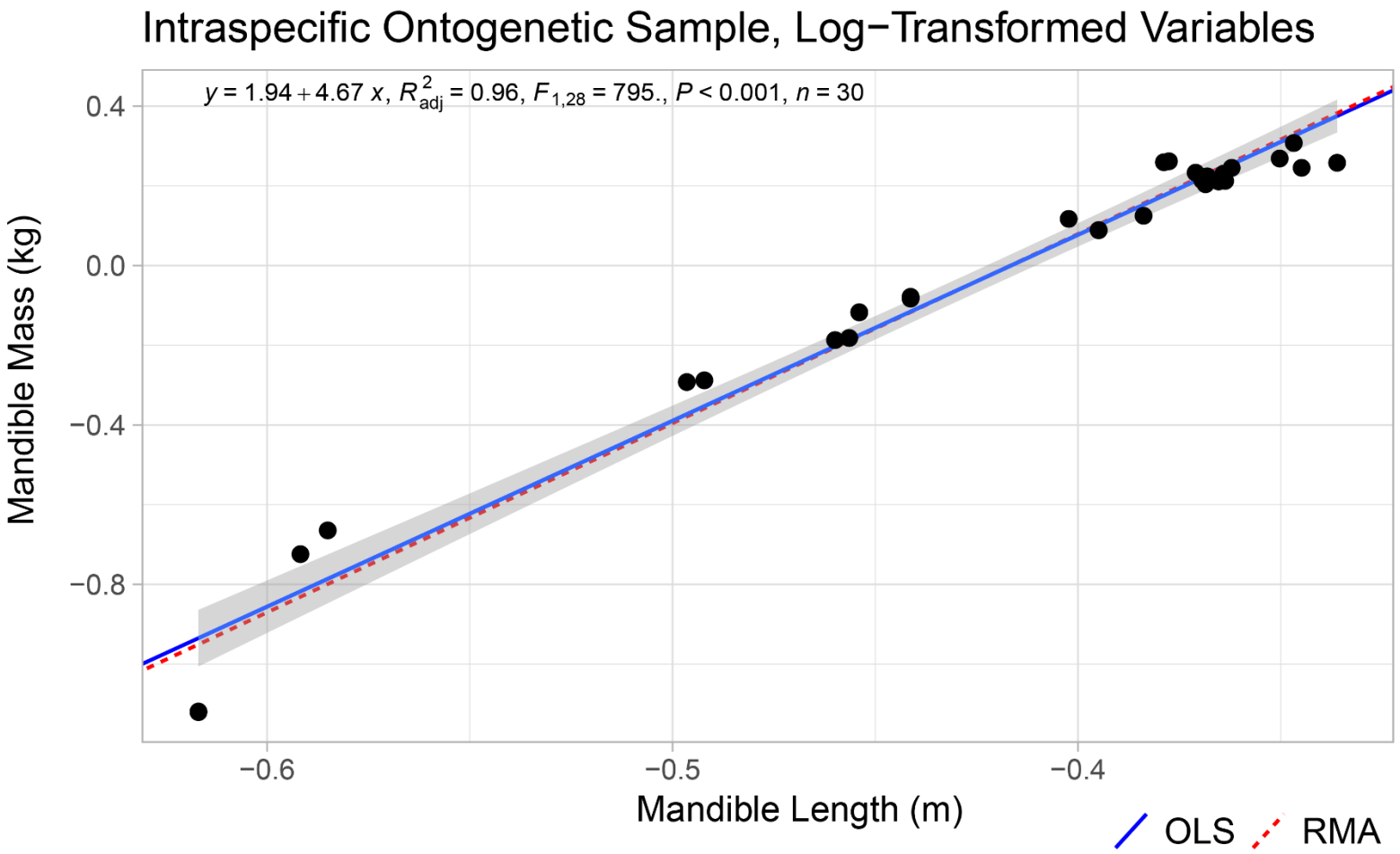

Figure 3.3. Linear regression analysis of mandible length (m) against estimated mandible mass (kg) for the intraspecific ontogenetic sample.

The distribution of OLS residuals from the regression of mandible mass against mandible length in the adult interspecific sample (Figure 3.4) demonstrates most taxa cluster close to the regression line, indicating a strong fit. However, several species display notable positive and negative residuals. The most positive residuals belong to *Loxodonta* and *Elephas*, following by *Hippopotamus*, indicating proportionally heavy mandibles. The most negative residuals belong to browsing artiodactyls characterised by slender, lightly built mandibles with pronounced diastema, such as *Giraffa*.

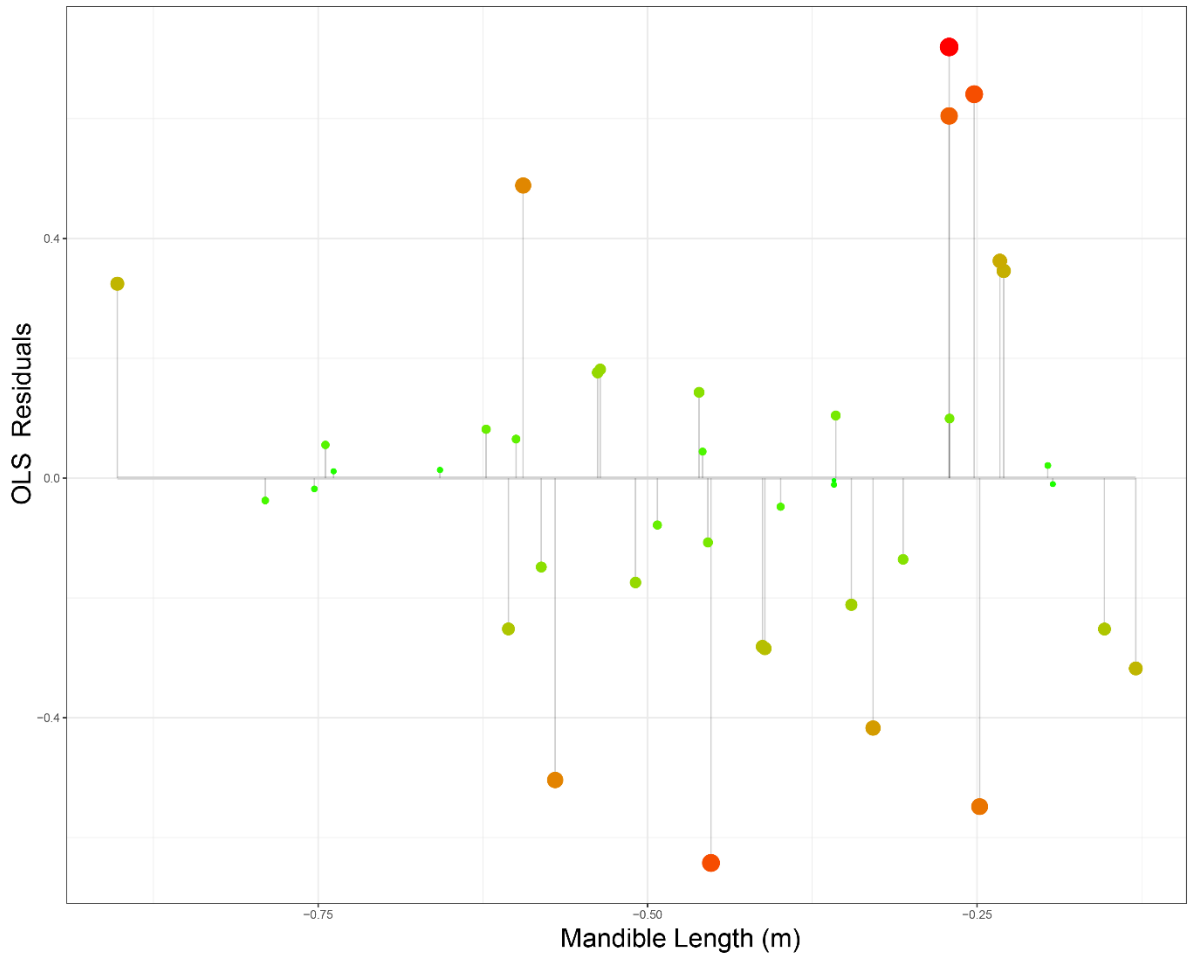

Figure 3.4 Residuals from the Ordinary Least Squares (OLS) regression of mandible mass on mandible length in the adult interspecific sample. The size of the residual is directly represented by the length of the vertical line from the point to the regression line. Point colour and size is mapped to residual size; small residuals are represented as small green point, progressing through yellow and orange to red, for increasingly large residuals.

Next, the scaling of centre of mass displacement as a function of mandible length was evaluated in both the interspecific adult and intraspecific ontogenetic samples; the regression

statistics are summarised below (Table 3.2). Centre of mass exhibits positively allometric linear relationship with mandible length (R^2_{adj} = 0.93; OLS slope = 1.13, 95% confidence interval: 1.03-1.23. RMA slope = 1.17, 95% confidence interval: 1.07-1.27. Isometry slope = 1) in the adult interspecific sample (Figure 3.5) and negative allometry in the intraspecific ontogenetic sample (R^2_{adj} = 0.93. OLS slope = 0.68, 95% confidence interval: 0.58-0.79. RMA slope = 0.73, 95% confidence interval: 0.64-0.85) (Figure 3.6). The PGLS regressions falls within the OLS 95% confidence internal, indicating little-to-no phylogenetic influence on the weak positive allometric scaling trend in the adult interspecific sample.

Table 3.2. Linear regression statistics for the scaling relationship between mandible length and centre of mass.

Dataset	Regression Model	Slope	95% Confidence Interval	Isometric Expectation	Interpretation
Interspecific (adult)	OLS	1.13	1.03–1.23	1.00	Weak positive allometry
	RMA	1.17	1.07–1.27	1.00	Weak-to-moderate positive allometry
	PGLS	Shallower than OLS, within CI	---	1.00	Indicates small phylogenetic influence
Intraspecific (ontogenetic)	OLS	0.68	0.58–0.79	1.00	Negative allometry
	RMA	0.73	0.64–0.85	1.00	Negative allometry

Loxodonta and *Elephas* exhibit very small residuals, clustering close to the regression line, while *Hippopotamus* and *Ceratotherium* show positive residuals. Taxa demonstrating negative residuals (Figure 3.7), indicating more posterior than expected centres of mass, are characterised by long diastema despite a diversity of body size and diets (e.g., *Okapia*, *Giraffa* - browsers; *Camelus* - generalist herbivore; *Rhinoceros* - grazer).

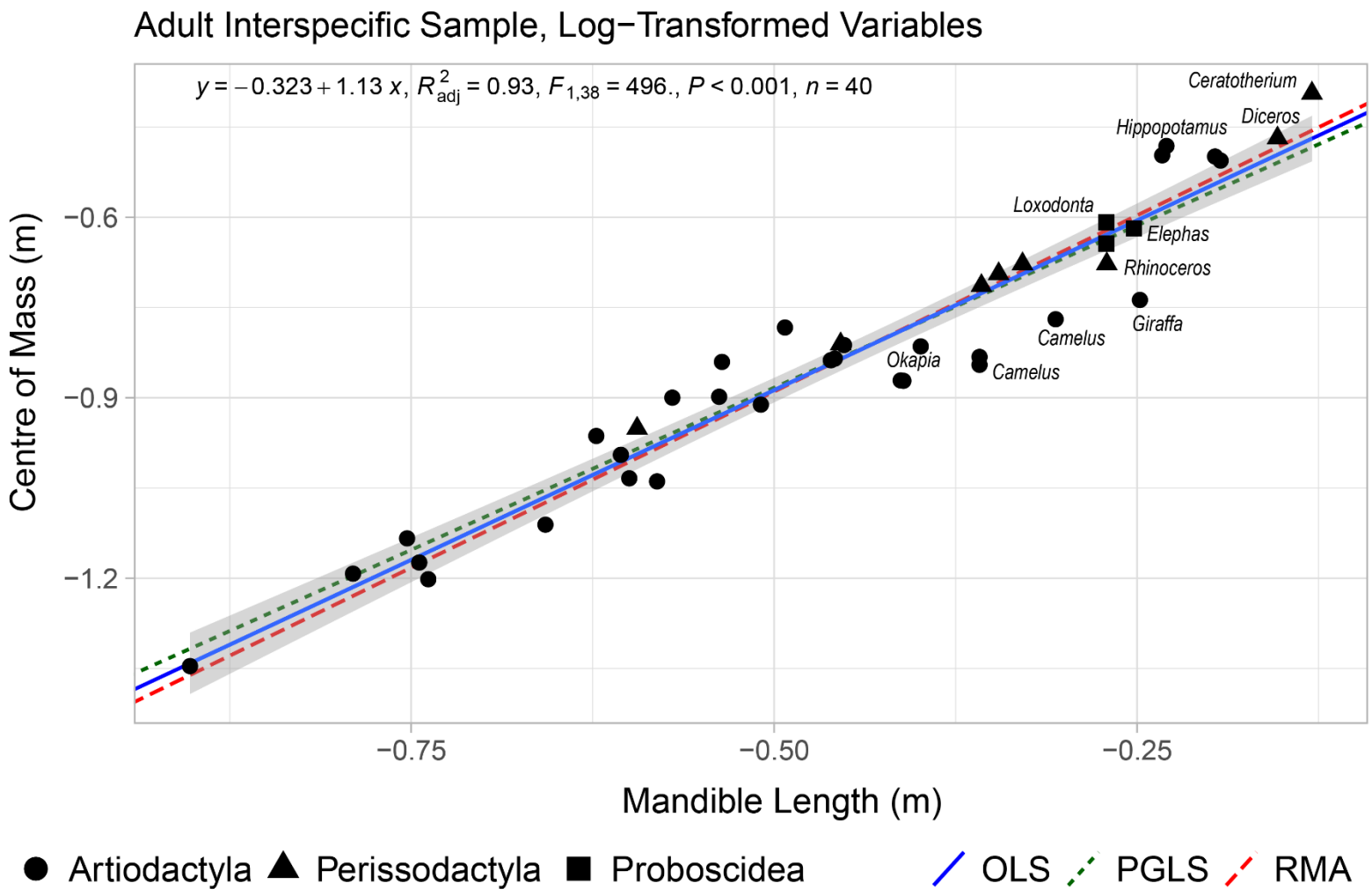

Figure 3.5. Linear regression analysis of mandible length (m) against centre of mass (m) for the adult interspecific sample.

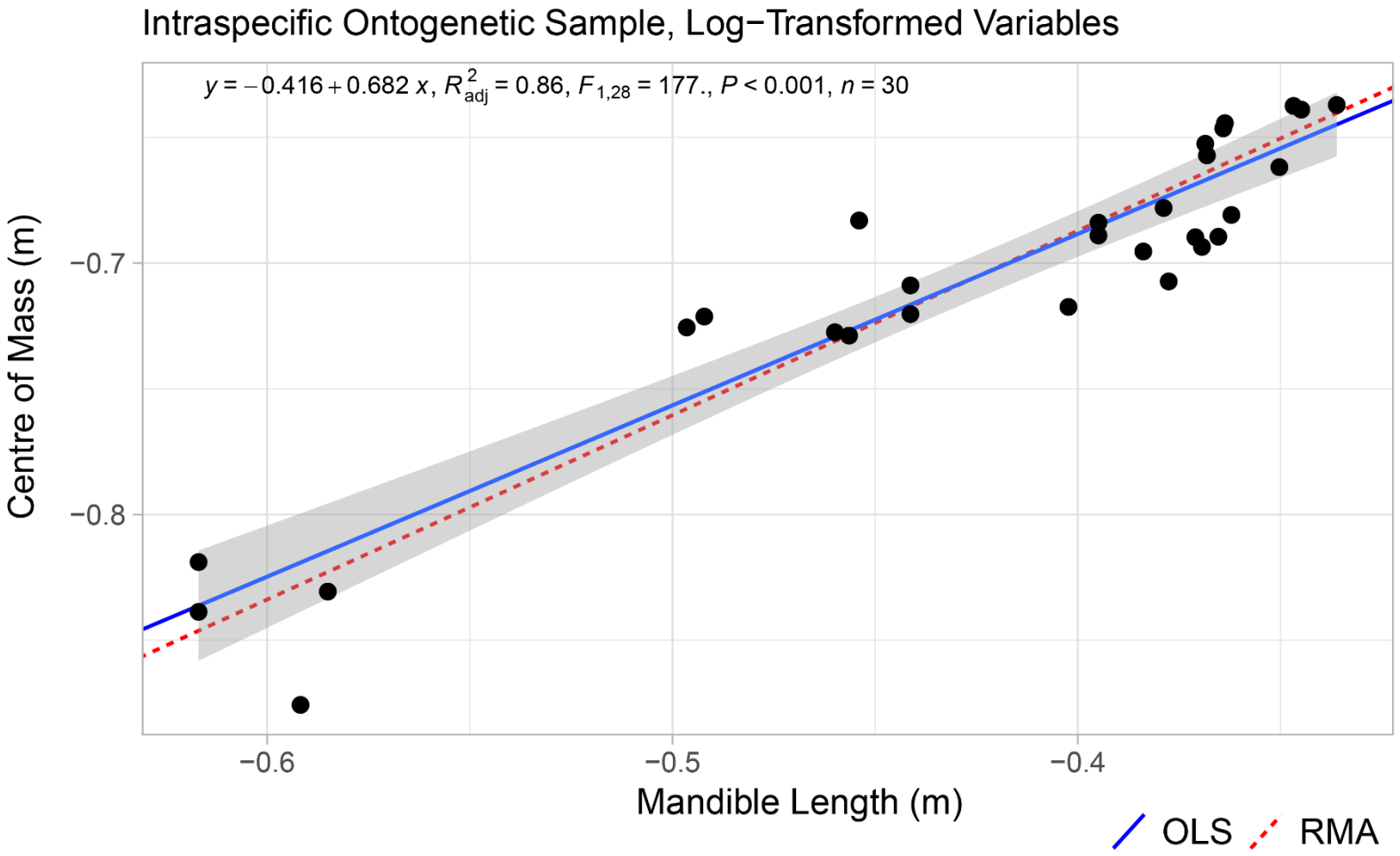

Figure 3.6. Linear regression analysis of mandible length (m) against centre of mass (m) for the intraspecific ontogenetic sample.

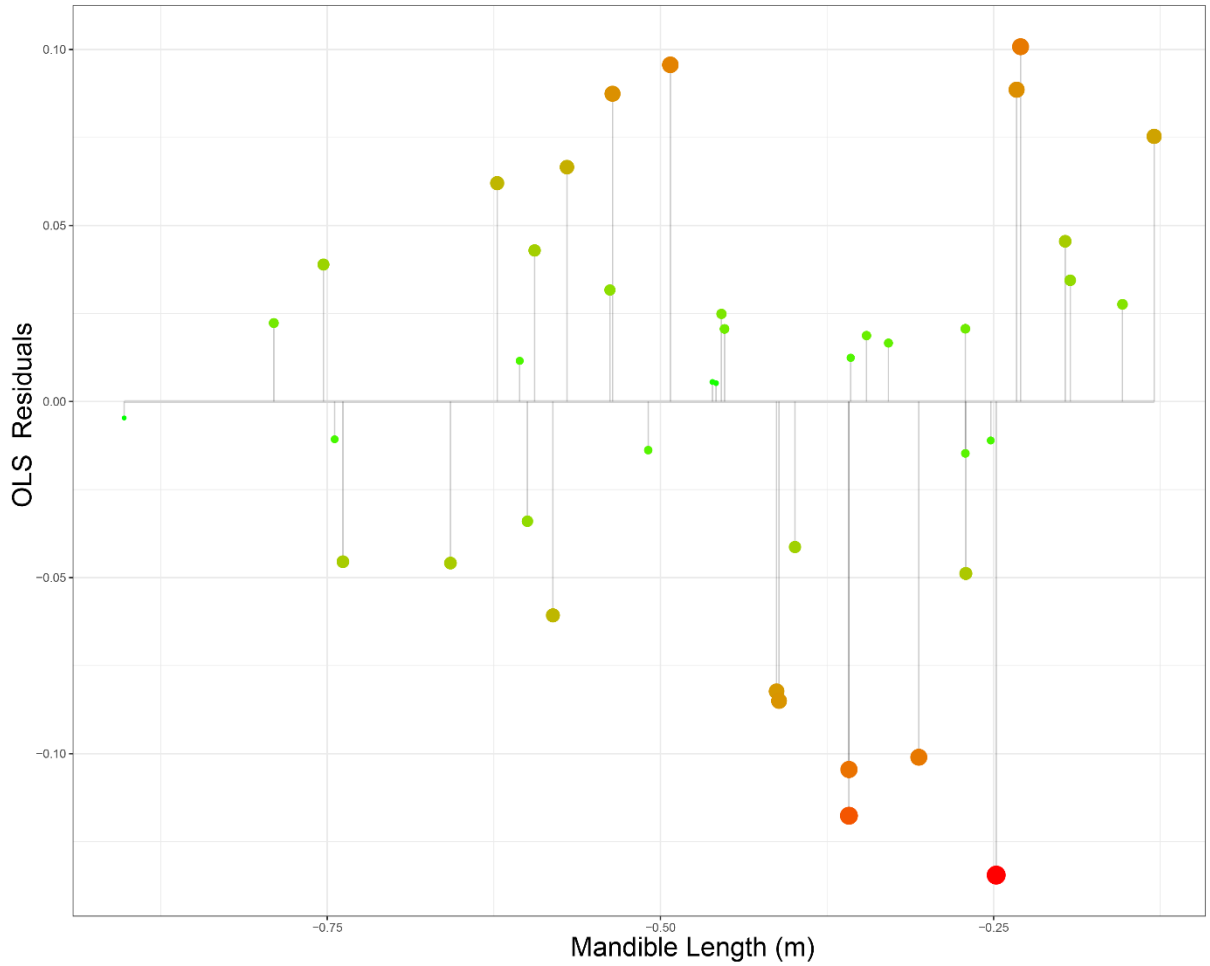

Figure 3.7 Residuals from the Ordinary Least Squares (OLS) regression of centre of mass as a function of mandible length in the adult interspecific sample. The size of the residual is directly represented by the length of the vertical line from the point to the regression line. Point colour and size is mapped to residual size; small residuals are represented as small green point, progressing through yellow and orange to red, for increasingly large residuals.

In the interspecific sample, rotational inertia scales with positive allometry with respect to mandible length (OLS slope = 6.2; 95% confidence interval: 5.60-6.8. RMA slope = 6.47; 95% confidence interval: 5.89-7.09; isometry slope = 5) (Figure 3.8). All three large-bodied rhinos fall within the OLS confidence interval. *Rhinoceros* exhibits marginally higher rotational inertia than expected for its mandible length than *Ceratotherium* and *Diceros* despite these taxa having a longer jaw and more anterior mass distribution. *Hippopotamus* demonstrates the highest rotational inertia in the dataset, despite having the second heaviest mandibles, due to a

disproportionally anterior centre of mass. Deivations from the linear scaling trend likely represent adaptations for feeding strategy. The greatest negative residuals belong to *Giraffa*, a highly specialised browser with a long, narrow, and lightly built mandible, while the highest residuals belong to the mixed feeding Loxodonta and Elephas, and Hippopotamus, a specialist grazer with a robust mandible and prominent anterior teeth (Figure 3.9).

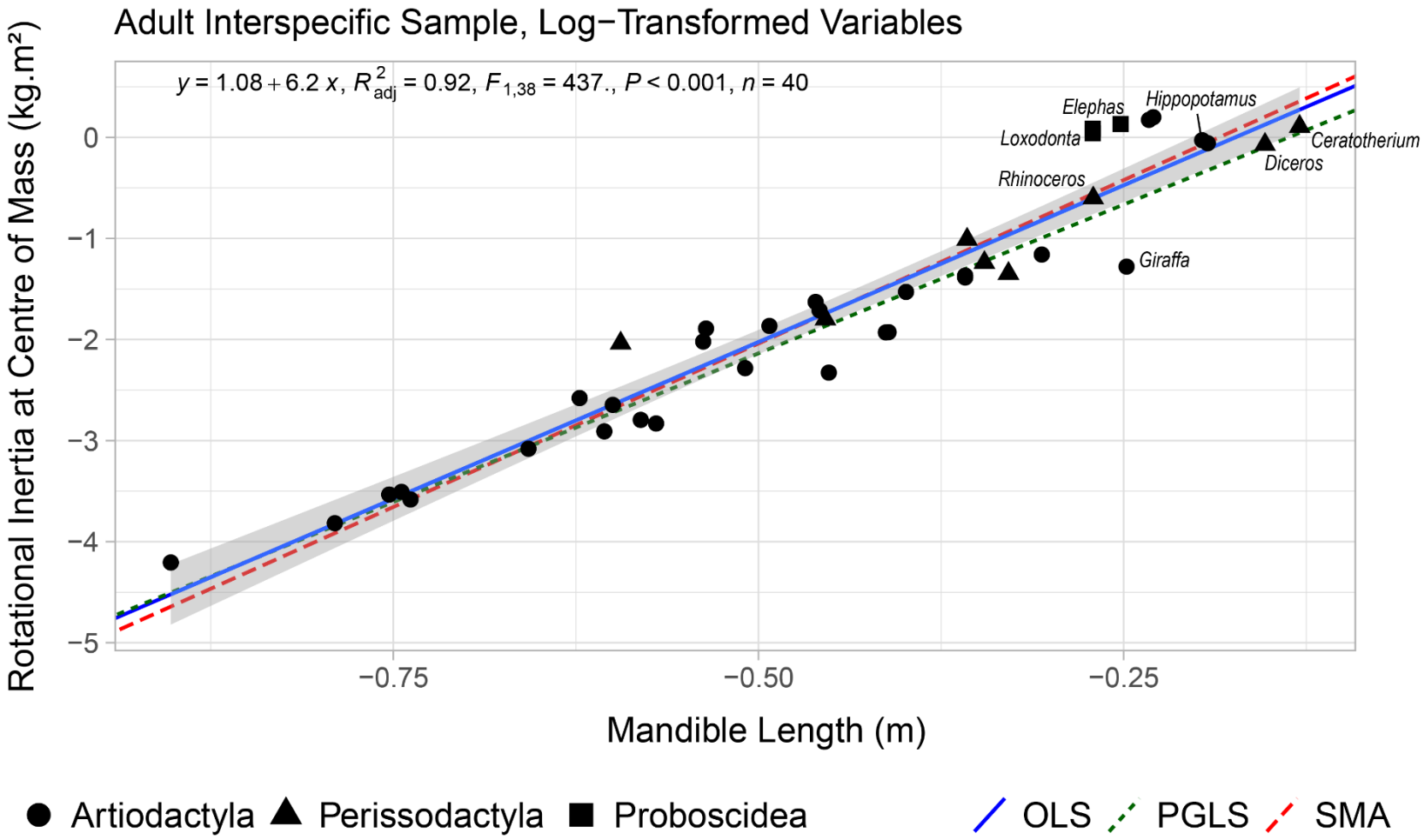

Figure 3.8. Linear regression analysis of mandible length (m) against rotational inertia (kg.m^2) for the adult interspecific sample.

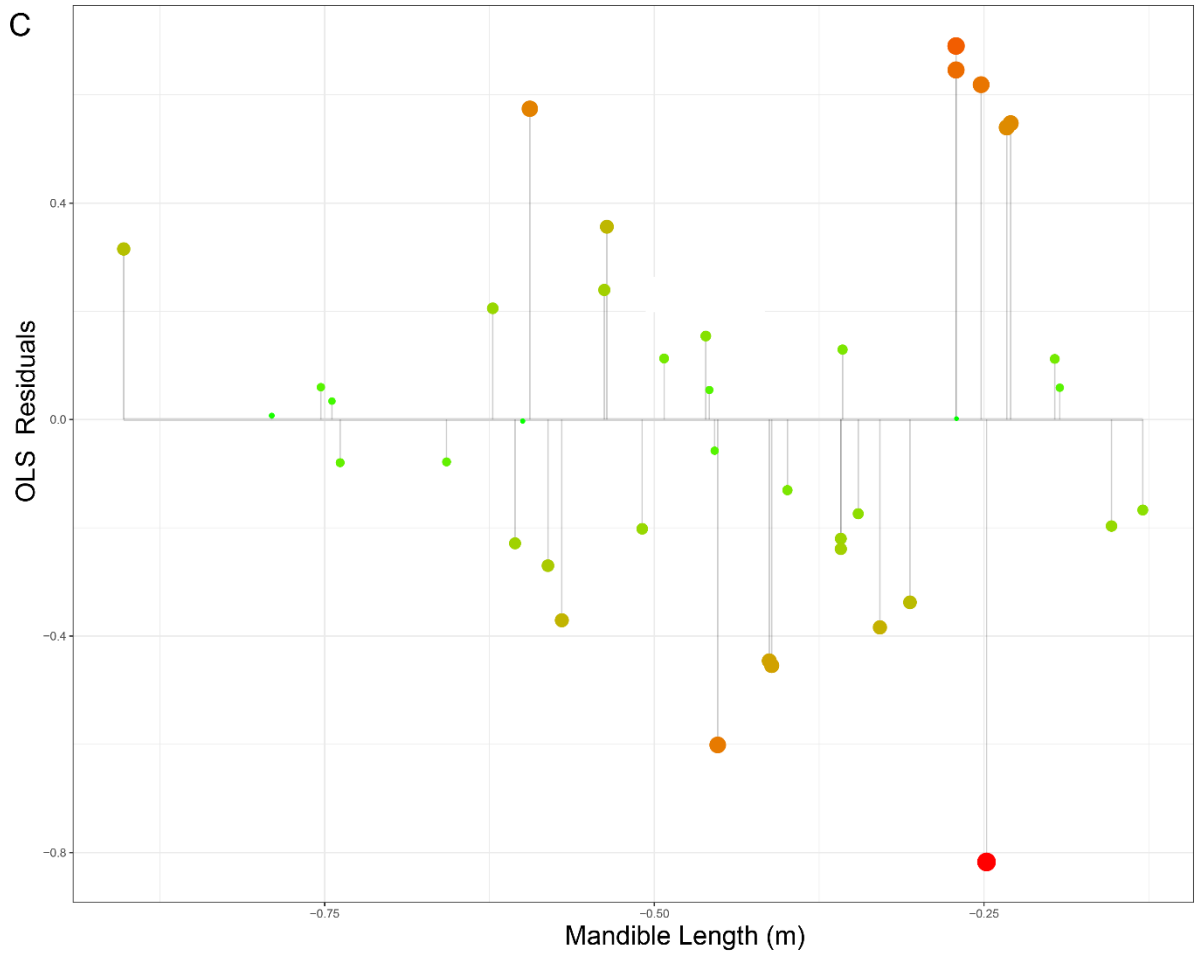

Figure 3.9. Residuals from the Ordinary Least Squares (OLS) regression of rotational inertia as a function of mandible length in the adult interspecific sample. The size of the residual is directly represented by the length of the vertical line from the point to the regression line. Point colour and size is mapped to residual size; small residuals are represented as small green point, progressing through yellow and orange to red, for increasingly large residuals.

The covariation of mandible length and rotational inertia was further investigated at three locations on the mandible assumed to be anatomically and mechanically relevant in addition to the centre of mass (Figure 3.10 A). The posterior (Figure 3.10 B). and anterior (Figure 3.10 C) extent of the molar row relate to the mechanical effort needed during chewing, crushing, and grinding tough plant material with the molars and premolars; rotational inertia at the symphysis (Figure 3.10 D) and anterior extent of the incisors is mechanically relevant during food selection, especially in the case of diastema-bearing selective browsers and mixed feeders.

Despite the presumed functional importance of these locations with respect to the role of mass distribution in masticatory mechanics, there is little difference in the scaling experienced (OLS slope = 6.2; 5.93; 6.14; 5.96) and a similar goodness of fit (R^2_{adj} = 0.92; 0.90; 0.92; 0.93) at each of the four locations as indicated by the OLS regression (Figure 3.10). As the PGLS regression differs least from the OLS and RMA models when comparing length and rotational inertia at the centre of mass, it seems therefore likely that this metric is most representative of adaptation to the inertial demand of the mandible. Additionally, the PGLS regression differs most distinctly from the other models when analysing the covariation of inertia at the posterior of the molar row with mandible length. This suggests a stronger phylogenetic constraint over the relative locations of the temporomandibular joint and the posterior extent of the molar row.

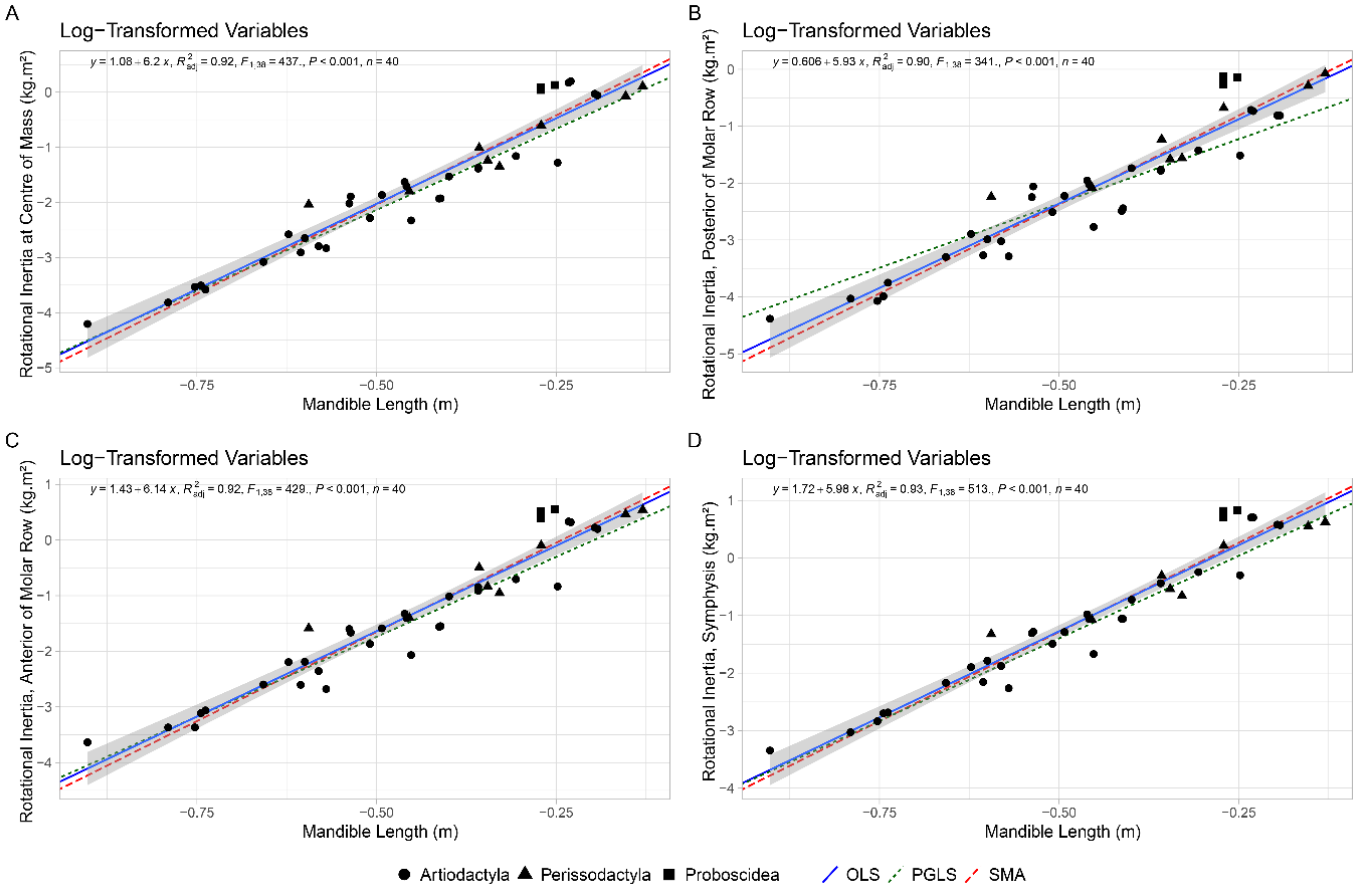

Figure 3.10. Linear regression analysis of log-transformed rotational inertia (kg m^2) as a function of mandible length (m) against at the A) centre of mass, B) the most posterior point of the molar row, C) the most anterior point of the molar row, and D) the most anterior point of the mandible, either symphysis, incisors, or canines.

3.4.2 Addressing Hypothesis 2 – Scaling of Masseteric Insertion Area and Mechanical Advantage

Linear regression analysis of the relationship between rotational inertia and the area of masseteric insertion in the adult interspecific sample (Figure 3.11) evidences a strong, significant positive relationship (R^2adj = 0.94, $F_{1,38}$ = 636, P < 0.001, n = 40), indicating that the area of the masseteric insertion increases predictably with increasing rotational inertia.

The OLS regression (slope 0.40; 95% confidence interval: 0.37–0.44) illustrates isometric scaling (isometry slope = 0.40), with agrees with the RMA regression model (slope = 0.42; 95% confidence interval: 0.38–0.45). The PGLS slope falls within the OLS confidence internal. Consistency between the three regression models shows both measurement error and phylogenetic non-independence do not influence the scaling relationship in a statistically significant way.

While the distribution of residuals is approximately symmetrical around zero, indicating that the OLS model provides a good fit to the data with bias, there are some deviations (Figure 3.12). Nonetheless, the lack of evident directional skew or heteroscedasticity indicates that variance is consistent across the range of rotational inertia, supporting the validity of the regression assumptions. Typically, at low rotational inertia, artiodactyls evidence a smaller than predict masseteric insertion area, and at moderate rotational inertia there is both positive and negative around the regression line, with most perissodactyls showing positive residuals. Larger-bodied taxa, including *Hippopotamus amphibius*, *Ceratotherium simum*, *Diceros bicornis*, *Loxodonta africana*, and *Elephas maximus*, plot toward the upper end of the distribution in the top-right quadrant, consistent with larger masseteric attachment areas associated with greater mandibular inertia. *Rhinoceros unicornis*, *Elephas maximus*, and *Loxodonta africana*, fall within the 95% confidence interval of the OLS regression, while *Hippopotamus amphibius* lies within or slightly below it. Both *Ceratotherium simum* and *Diceros bicornis* fall below the interval, showing relatively smaller masseteric insertion areas for their rotational inertia.

Overall, the results indicate that the size of the masseteric insertion scales proportionally with rotational inertia across ungulate-grade mammals. This near-isometric relationship suggests that increases in mandibular mass and inertia are matched by proportional increases in the potentially force generating capacity of the masseter muscle, maintaining functional mechanical efficiency across a broad range of body sizes, functional demands, and mandible morphologies.

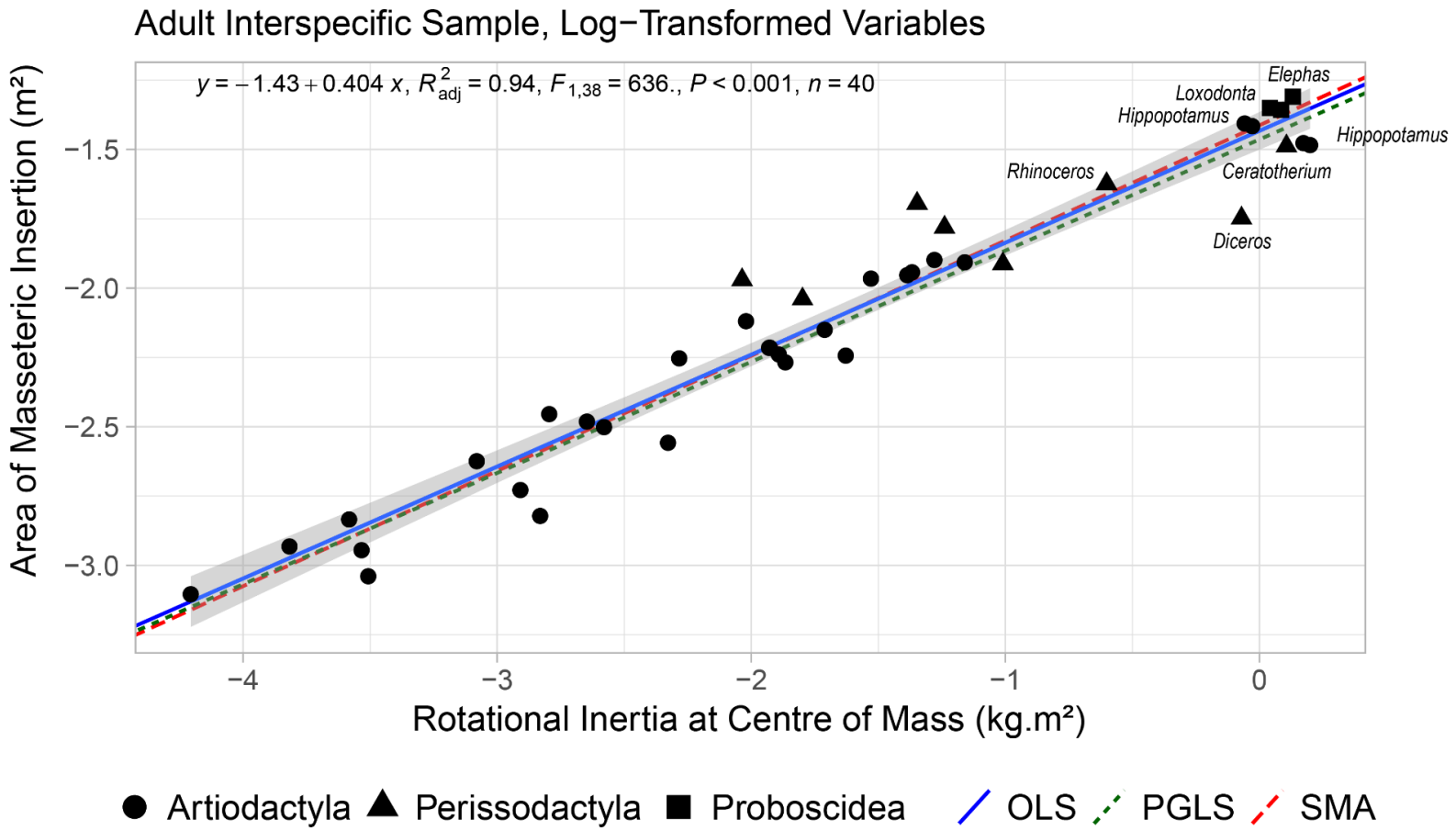

Figure 3.11. Linear regression analysis of area of masseteric insertion (m^2) as a function of rotational inertia ($kg.m^2$) for the adult interspecific sample.

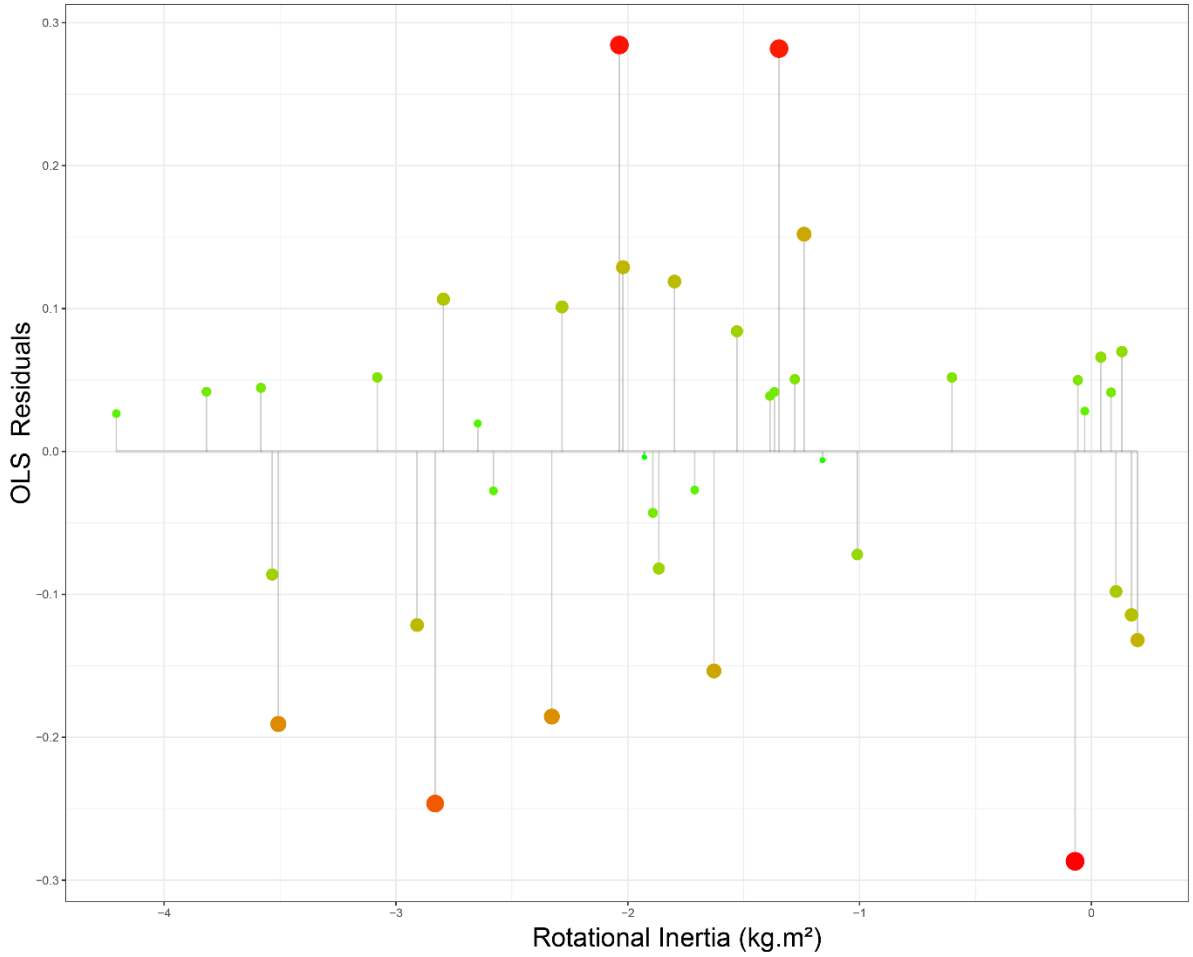

Figure 3.12. Residuals from the Ordinary Least Squares (OLS) regression of masseteric insertion area as a function of rotational inertia in the adult interspecific sample. The size of the residual is directly represented by the length of the vertical line from the point to the regression line. Point colour and size is mapped to residual size; small residuals are represented as small green point, progressing through yellow and orange to red, for increasingly large residuals.

The relationship between rotational inertia and the mechanical advantage of the masseter in the adult interspecific sample (Figure 3.13) shows no statistically significant relationship (OLS slope = 0.02, R^2adj = 0.06, $F_{1,36}$ = 3.49, P = 0.070, n = 38), indicating that variation in rotational inertia does not strongly predict changes in masseter mechanical advantage across taxa.

The regression slope is positive but shallow, and the wide confidence interval (grey shading) reflects a high degree of variability among species. This suggests that while a weak positive trend may exist the relationship is not consistent within this dataset.

The distribution of points reveals considerable interspecific variation. There is consideration interspecific variation in the relationship between mechanical advantage of the masseter and mandibular rotational inertia, as indicated by the varied distribution of datapoints. Large-bodied taxa such as *Loxodonta*, *Elephas*, and *Hippopotamus* plot towards the upper right of the graph, showing relatively high values for both rotational inertia and mechanical advantage. In contrast, *Diceros* and *Ceratotherium* lie below the regression line, indicating lower mechanical advantage for their high rotational inertia. Smaller, browsing, artiodactyls, including *Odocoileus*, *Mazama*, and *Rangifer*, cluster towards the lower left, exhibiting both low rotational inertia and low mechanical advantage. Sus and Equus, despite differing mandibular morphologies and diet, both exhibit moderation rotational inertia and high mechanical advantage.

Taken together, these results suggest that mechanical advantage of the masseter does not scale predictably with rotational inertia in ungulate-grade mammals. The weak linear trend observed likely reflects functional variability in feeding mechanics and mandibular morphology rather than a consistent biomechanical scaling relationship.

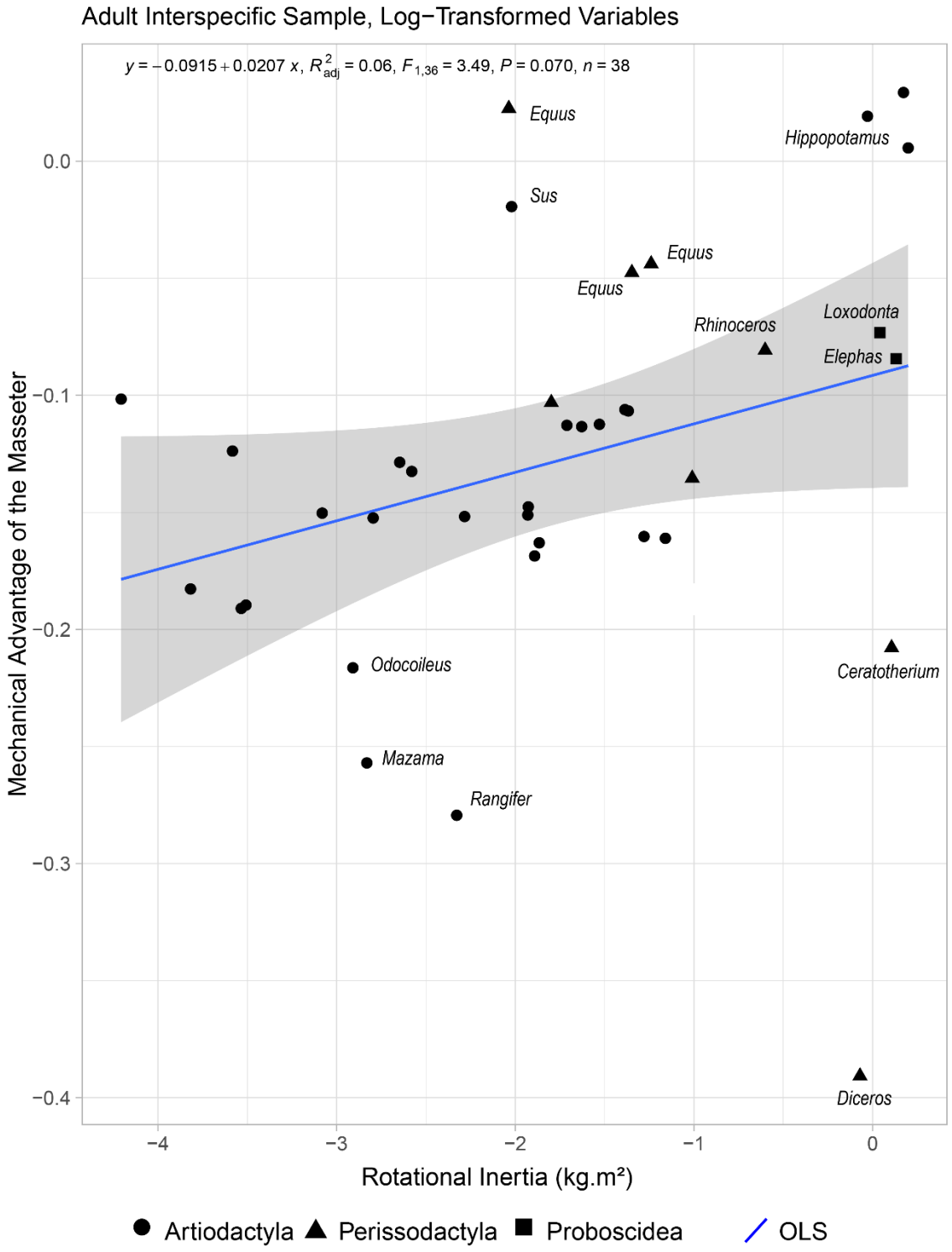

Figure 3.13. Linear regression analysis of mechanical advantage of the masseter as a function of rotational inertia (kg.m^2) for the adult interspecific sample.

Linear regression of the mechanical advantage of the temporalis on rotational inertia evidences a weak negative linear relationship that approaches, but does not quite achieve, statistical significance (OLS slope = -0.05, R^2adj = 0.08, $F_{1,36}$ = 4.08, P = 0.051, n = 38) (Figure 3.14). The broad confidence interval surrounding the OLS regression line reflects high variability among taxa, indicating that the relationship is not consistent across the sample.

Larg-bodied taxaxa such as *Loxodonta* and *Elephas* plot in the upper-right quadrant above the confidence band, displaying disproportionally high mechanical advantage despite their large rotational inertia, while *Ceratotherium* and *Diceros* exhibit the opposite pattern, with low mechanical advantage at high rotational inertia values. *Sus* and *Phacochoerus*, place in the low-middle of the plot, indicating moderate rotational inertia and low mechanical advantage of the temporalis. Lama, Camelus, Tapirus, and Giraffa each exhibit mechanical advantage values higher than would be expected from the linear trend.

Collectively, these data indicate a very weak negative scaling relationship between rotational inertia and temporalis mechanical advantage, suggesting that increased mandibular mass and resistance to angular motion are not consistently compensated t by greater leverage of the temporalis muscle across ungulate-grade mammals.

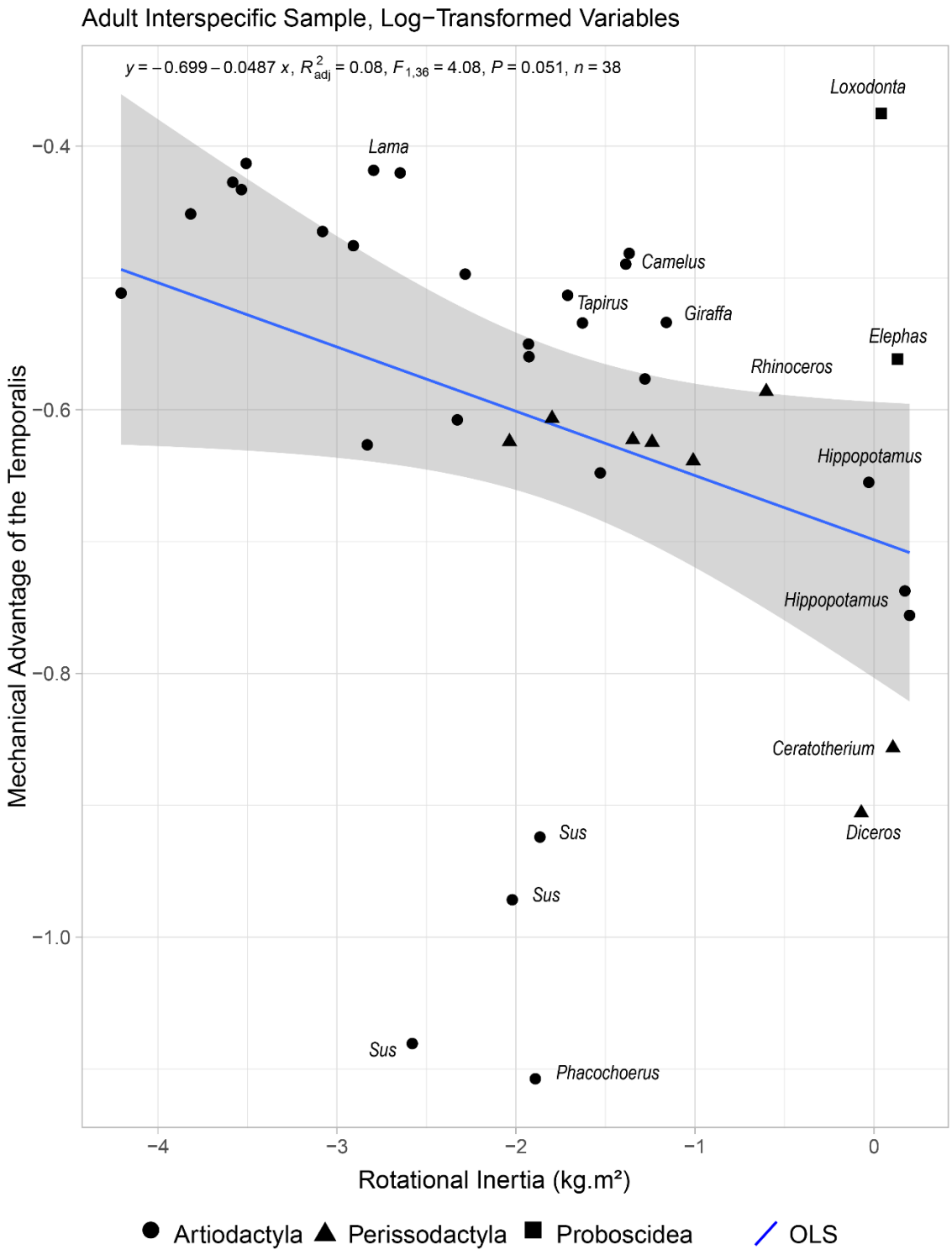

Figure 3.14. Linear regression analysis of mechanical advantage of the temporalis as a function of rotational inertia (kg.m^2) for the adult interspecific sample.

3.4.4 Addressing Hypothesis 3 – Ratio of Rotational Inertia to Mandible Length

The ratio of rotational inertia to mandible length was examined as a potential functional metric to determine whether browsers and grazers could be differentiated based on characteristic mandibular mass distributions or based on covariation between mass properties and mandible size. This ratio serves as an approximate measure of the mechanical cost of mandibular motion, representing the muscular torque required to rotate the mandible per unit length. Body size exerted a strong influence, and no extant browsers approach the size of the largest species in the dataset, which are all grazers and mixed feeders aside from the browsing *Diceros bicornis*.

When ranked in ascending order, the ratio did not scale linearly but formed three distinct subsets (Figure 3.15). These subsets correspond broadly to differences in body size, dietary category, digestive strategy, and mandible morphology.

Group 3 (low ratios, ≤ –1.6) is comprised of smaller-bodied artiodactyls, including foregut-fermenting grazers (*Redunca*, *Lama*), browsers (*Rangifer*, *Rupicapra*, *Mazama*), mixed feeders (*Antilocapra*, *Saiga*, *Tragelaphus*), and the frugivore *Cephalophus*. These taxa exhibit slender and relatively lightly built mandibles consistent with low rotational inertia.

Group 2 (intermediate ratios, –1.6 to –0.3) consists of mid-sized species representing a mixture of digestive and dietary strategies. This group includes hindgut- and foregut-fermenting grazers (*Equus*, *Bos*), browsers (*Tapirus*), and generalists with basal ungulate mandibular morphologies (*Camelus*) and mandibles adapted for generalist omnivory (Sus). These taxa occupy an intermediate mechanical range, reflecting moderate mechanical costs of mastication and a diversity of feeding and digestive strategies

Group 1 (high ratios, ≥ –0.3) includes the largest-bodied taxa, consisting of hindgut-fermenting (*Ceratotherium*) and foregut-fermenting grazers (*Hippopotamus*), hindgut-fermenting mixed feeders (Elephas, Loxodonta) and the hindgut-fermenting browser (*Diceros, Dicerorhinus)*. These species exhibit the highest relative mechanical cost of mandibular rotation, associated with large mandibular mass and anteriorly positioned centres of mass. Despite the functional and morphological disparity between the rhinoceroses, elephantids, and *Hippopotamus*, each of these taxa rotational inertia to mandible length ratios converge on similar values.

Figure 3.15. Rank-ordered distribution of the ratio between rotational inertia and mandible length for the extant interspecific sample.

3.5 Discussion

3.5.1 Overview and Research Context

At the outset of this study, empirical data on mandibular mass distribution and its functional implications for mastication were limited. The primary objective was to investigate how mass properties of the mandible scale and covary with mechanically relevant anatomical features, specifically, the jaw adductor musculature and lever arm configurations. The study further aimed to assess how ungulate-grade mammals have adapted to the mechanical and energetic challenges imposed by a heavy mandible, and whether these relationships distinguish species with differing habitual diets and digestive strategies.

This study provides new quantitative evidence for the scaling relationships among mandibular mass, length, centre of mass, rotational inertia, and muscle architecture across a broad sample of extant ungulate-grade mammals. The results demonstrate that mandibular form and function are primarily governed by mechanical scaling principles rather than by phylogenetic affinity or dietary category.

3.5.2 Hypothesis 1 - Scaling of Mandibular Mass and Centre of Mass

3.5.2.1 Interspecific and Ontogenetic Scaling

Both the adult interspecific and intraspecific ontogenetic samples exhibit near-isometric scaling between mandibular length and mass. In the interspecific dataset, the centre of mass also scales isometrically with length, contradicting the hypothesis that larger taxa exhibit posteriorly shifted mass distributions to reduce rotational inertia. Within the ontogenetic series of *Diceros bicornis*, however, the centre of mass scales with negative allometry, suggesting that mass properties vary at different rates during growth. This pattern may represent developmental adjustment within species rather than broad adaptive differentiation across taxa.

3.5.2.2 Deviations from Isometric Scaling

Among the largest taxa (i.e., *Loxodonta*, *Elephas*, *Hippopotamus*, and *Ceratotherium*) distinct scaling relationships are evident. *Hippopotamus amphibius* and *Ceratotherium simum* both possess more anteriorly distributed mass than predicted by isometry, while elephants, though morphologically shortened (brachygnathic), fall within the isometric confidence interval. Rotational inertia measured at the centre of mass scales with positive allometry (OLS slope =

6.2; RMA slope = 6.47; isometric expectation = 5). The long, anteriorly weighted mandible of Hippopotamus, with its large incisors and canines, indicates that reduction of rotational inertia was not the dominant selective pressure.

Overall, these results falsify the hypothesis that mandibular enlargement in herbivorous mammals is accompanied by posterior mass displacement to reduce mechanical cost. Weak positive allometry of rotational inertia indicates that larger species may, in fact, experience increased angular resistance. Each lineage appears to employ distinct adaptive strategies to manage this constraint. Although elephants, hippos, and rhinos exhibit comparable absolute inertia, elephants achieve this with heavier but posteriorly balanced mandibles, suggesting partial mechanical optimisation.

3.5.3 Hypothesis 2 - Functional Role of the Masseter and Mechanical Advantage

The strong positive relationship between rotational inertia and masseteric insertion area supports the prediction that the masseter is adapted to meet the mechanical demands of moving a heavy mandible. The near-isometric scaling between these variables (OLS slope = 0.40; RMA slope = 0.42; R^2adj = 0.94) indicates that increases in mandibular inertia are matched by proportional increases in potential muscle force. This relationship is robust to both measurement error and phylogenetic non-independence.

Although the proxy used, masseteric insertion area, does not account for internal fibre architecture or muscle directionality, its strong predictive fit supports its validity as a comparative measure. However, as masseter growth is negatively allometric with respect to body size, its force-generating capacity does not increase as rapidly as inertia in the largest taxa, implying that other compensatory mechanisms may exist.

Weak correlations were found between rotational inertia and the mechanical advantages of the masseter (MAM) and temporalis (MAT). Neither trend was statistically strong. However, taxa with high rotational inertia show notable contrasts: Hippopotamus exhibits high MAM, while *Diceros* and *Ceratotherium* show low MAM and MAT, implying different biomechanical solutions to the same mechanical challenge. *Loxodonta* and *Elephas* fall within the 95% confidence interval for MAM regression, indicating consistency with the general scaling trend.

3.5.4 Hypothesis 3 - Mandibular Mass Distribution and Dietary Adaptation

3.5.4.1 Ratio of Rotational Inertia to Length

The ratio of rotational inertia to mandible length was evaluated as a measure of mechanical cost per unit length. When ranked by ascending value, three distinct subsets emerged. Subset 1 includes large-bodied grazers (*Hippopotamus*, *Elephas*, *Loxodonta*) and browsing rhinos (*Diceros*, *Dicerorhinus*). Subset 2 includes mid-sized taxa with across herbivorous or generalist feeding behaviours, such as *Giraffa*, *Okapia*, *Equus*, *Camelus*, and *Sus*. Subset 3 includes small-bodied, foregut-fermenting artiodactyls with grazing, browsing, mixed feeding, and frugivorous diets.

These groupings do not correspond neatly to traditional dietary categories but instead reflect a composite influence of body size, digestive strategy, and feeding behaviour. Similar ratio values across ecologically and morphologically distinct species (*Equus*, *Camelus*, *Giraffa*) suggest that this metric captures shared biomechanical constraints associated with a fundamental biomechanical constraint of the morphology and mechanical performance of the ungulate

3.5.4.2 Feeding Efficiency and Functional Continuum

Large-bodied grazers and mixed feeders display high ratios, reflecting elevated mechanical costs of mandibular motion associated with bulk feeding. In contrast, small-bodied ruminants show low ratios consistent with reduced energetic requirements. The results support a mechanical continuum from volume-feeding to selective-browsing strategies rather than distinct categorical divisions.

3.5.4.3 *Hippopotamus amphibius*

Hippopotamus is an exception to the general pattern. Its large, anteriorly heavy mandible produces extremely high rotational inertia, yet its foregut fermentation system and low metabolic rate reduce dependence on efficient mastication. This suggests that the high mechanical cost is tolerated due to compensatory physiological adaptations, and the secondary functions (i.e., competitive and defensive behaviours) enabled by the mandibular tusks that strongly influence its anterior mass distribution.

3.5.5 Evolutionary and Functional Implications

3.5.5.1 Posterior Mass Shift and Proboscidean Evolution

The assumption that herbivore mandibles evolved toward reduced energetic cost through posteriorly weighted mass distributions is supported only in proboscideans. Extant elephants exhibit shortened, posteriorly heavy mandibles compared to their longirostrine ancestors, reflecting evolutionary reduction in inertia through mandible shortening. In contrast, artiodactyls and perissodactyls show isometric scaling of centre of mass with length, suggesting no systematic posterior shift.

3.5.5.2 Functional Diversity Among Ungulate-Grade Mammals

Proboscideans display conservative morphology and limited dietary diversity, while artiodactyls and perissodactyls exhibit broader functional and ecological variation. The diastema, prominent in many ungulates, provides an alternative strategy for reducing anterior mass while maintaining feeding selectivity. Increased masseteric leverage and enlarged insertion areas also act as compensatory adaptations in taxa with anteriorly distributed mass.

3.5.7 Limitations and Future Research Directions

The simplified two-dimensional rotational model represents a necessary approximation but does not capture the full three-dimensional dynamics of mandibular motion. It also omits instantaneous centres of rotation and the effects of soft-tissue mass, elasticity, and neuromuscular control.

Future studies should expand upon these findings through:

1. Three-dimensional dynamic modelling of mandibular motion, incorporating multiple rotational axes and more realistic representations of masticatory mechanics.
2. Soft-tissue reconstruction using imaging and comparative anatomy to estimate total masticatory mass and improve predictions of force generation.
3. Integration with finite element and musculoskeletal modelling to test stress distribution and strain energy under loading.
4. Broader taxonomic and ontogenetic sampling, especially of extinct taxa, to evaluate the temporal evolution of mandibular mass distribution.

5. Comparative analyses linking mandibular energetics to metabolic rate and feeding behaviour to explore how mechanical efficiency influences ecology.

Such approaches would refine understanding of how mechanical constraints shape mammalian feeding evolution and provide context for interpreting morphological disparity in fossil species.

3.5.8 Concluding Statement

This study demonstrates that mandibular scaling and mass distribution among ungulate-grade mammals are governed primarily by biomechanical constraints rather than by phylogenetic or dietary factors. Increases in mandibular mass and inertia are accompanied by proportional increases in adductor muscle area, maintaining mechanical balance across a wide size range. Deviations from isometric scaling represent lineage-specific responses to feeding mode, digestion, and energy demands.

The results support the interpretation that functional optimisation through biomechanical constraint has been a stronger determinant of mandibular evolution than phylogenetic heritage. This study establishes a framework for linking mandibular form, function, and energetics in both extant and extinct mammalian herbivores and provides a baseline for future work integrating biomechanics, ecology, and evolutionary morphology.

4: Habitual Head Posture and Associated Behaviours as Adaptations to Mitigate the Mechanical Effects of Mandible Mass Distribution

4.1 Introduction

4.1.1. Head Posture – Terminology, Functional Significance, and Methodologies

Head posture, meaning the angle of the head relative to the horizontal, is an important consideration when studying the dietary habits, biology, and evolution of herbivorous mammals. Ungulate-grade mammals display a diverse array of body sizes, a greater variety of documented head postures (Kohler, 1993), and a wider range of expected inner ear orientations (Solounias, 2007), a measure which has often been used as a proxy for head posture (Benoit et al. 2020; Hullar, 2006; Ven Der Klaauw, 1948), and more varied degrees of adaptation to head-butting than any other mammal group.

Throughout the literature, the terminology used to describe head posture while at rest, and not engaging in any behaviour involving head movement, has varied. For instance, Zeuner (1934) defined the "usual" head posture of an animal as the normal position of the head while the animal is standing or walking and not engaging in any other activity, and that while maintaining this position the nuchal ligament and neck muscles should not be contracted. More recently, Benoit et al. (2020) used both "neutral head posture", defined as the angle between the main axis of the head and the horizontal when the animal is at rest, its attention is not attracted by a target, and it is not engaged in foraging, drinking, or any other behaviour involving head movement, and "cranial orientation", when reconstructing head posture from the plane of the lateral semicircular canal of the inner ear. Despite differences in terminology, both "usual" and "neutral" head posture describe head posture while at rest. In this chapter, the terminology used by previous authors is retained when referring to their work, while the term "head posture" is used when referring to original work, with clarification provided when referring to other postural contexts, such as when discussing alert postures or reconstructed cranial orientations. The following discussion briefly examines the biological and behavioural factors influencing head posture in ungulate-grade herbivores

4.1.2 Functional Significance of Head Posture

4.1.2.1 Thermoregulation

Head posture is relevant to the evolution of thermoregulation and the origin of endothermy. The blood pressure required to reach the head directly depends on head posture, the elevation of the head, and thermophysiology. In general, greater head and neck inclination, and consequently higher head elevation, necessitate higher blood pressure to ensure perfusion of the brain. As species with low metabolism have a lower blood pressure than species with a high metabolism, they cannot generate sufficient blood pressure to supply blood to the brain in an elevated head position (Seymour, 2016).

4.1.2.2 Behavioural Contexts

Head posture varies both between and within species, shifting throughout the day to support different activities; typically lowered during resting, feeding, and foraging, and elevated in alert postures to enhance environmental awareness. Head posture during these activities underlies variations in behaviour between species, such as spatial navigation and locomotion dynamics, predator vigilance, browsing versus grazing dietary strategies, and head-butting.

4.1.2.2.1 Head-butting

It has been suggested that modifications of the skull and musculature for shock absorption, result in a direct relationship between head posture and head-butting behaviour (Benoit et al. 2017; Sakagami and Kawabe, 2020; Schaffer and Reed, 1972). In contrast, the plane of the lateral semicircular canal (LSC) was found to be more inclined in head-butting species than in non-head-butting species (46° and 33°, respectively), indicating that the LSC, rather than head posture, is functionally adapted to head-butting. Although head-butting species exhibit structural specialisations supporting this behaviour, current evidence suggests that head posture itself is not correlated with head-butting (Benoit et al., 2020), possibly due to the limited proportion of time spent in this posture compared with that used for resting, feeding, or locomotion. Consequently, head-butting behaviour is excluded from the scope of this analysis.

4.1.2.2.2 Locomotion

During locomotion, ungulates “nod” their heads while walking as a method of reducing energy expenditure. Although moving the head-neck unit requires muscular work, the timing of the

vertical displacements of the head-neck unit is consistent with minimising energy expenditure in an inverted pendulum walking gait (Löscher et al., 2016). In this way, the animal maximises its field of view and enables a high degree of vigilance during locomotion by holding the head in an elevated position in a highly energy-efficient manner.

4.1.2.2.3 Alert postures and vigilance

Many published accounts of head posture in mammals do not readily distinguish between "at rest" and "alert" postures (Vidal, Graf, and Berthoz, 1986; Hullar, 2006; Marugán-Lobón, Chiappe and Farke, 2013; Courtier et al., 2017). Benoit et al (2020) notes species achieve alert posture in different ways. Rhinoceroses raise their snouts when engaging in alert posture, the opposite of their feeding and foraging posture wherein the head is inclined downward (Owen-Smith, 1973). Lagomorphs and felids rest in an alert posture by simultaneously dorsiflexing at the cervico-dorsal junction and ventriflexing at the cranio-cervical junction to retract the head and achieve a horizontal orientation (Stevens, 2013; Graf et al., 1995). In ungulates, the neck is generally extended and the head raised, resulting in a higher and more horizontal position than that observed at rest, which serves to improve the field of vision (Estes, 2012).

4.1.2.2.4 Feeding behaviour

Head posture has been associated with feeding behaviour in herbivorous species. For instance, browsers are expected to hold their head higher than grazers. Owen-Smith (1988) reported that white rhinoceroses (*Ceratotherium simum*) spend approximately 49% of daylight hours and 50% of the night foraging, indicating that feeding activities occupy a substantial proportion of their lifetime. As feeding and foraging constitute a major component of an herbivore's life, variation in feeding height is likely to influence the habitual head posture adopted by a species and, consequently, the orientation of the mandible.

4.1.2.3 Biomechanical cost of mastication

Head posture and mandible orientation, defined as the angle of the jaw relative to the horizontal, are not identical but exhibit a strong correlation when the jaw is closed; a more anteriorly inclined head implies a similarly inclined mandible. As data on mandible orientation are scarce, available measurements of head posture provide the best current proxy. In the resting, jaw-closed position, the mandibular and maxillary molars are in occlusion, gape is

minimal, and the head angle approximates the minimum anterior inclination of the mandible, at which mandibular rotational inertia is at its maximum. Conversely, when gape is maximal, the anterior inclination of the mandible is greatest, and rotational inertia is at its minimum.

4.1.3 Methods of measuring head posture

4.1.3.1 Direct observations versus reconstruction from inner-ear proxy

A variety of methods has been employed to measure head posture, including field observations, open-access photographic repositories, published photographic records, and estimations derived from the orientation of the lateral semicircular canal (LSC) using X-ray imaging, computed tomography, or dissection. The diversity of these approaches, combined with the typically limited scope of individual studies, has made it difficult to establish and substantiate broad inferences regarding the relationship between the LSC plane and head posture.

Benoit et al (2020) conducted a methodologically homogenous, broad-scale interspecific analysis of the LSC-head posture relationship by documenting head posture in perissodactyls, artiodactyls, and paenungulates using photographs of zoo animals taken in lateral view. This study evaluated the long-standing assumption that the plane of the LSC is parallel to the horizontal when the head is at rest, an assumption frequently used in reconstructions of head posture in extinct taxa. This assumption is based on the functional significance of the orientation of the semi-circular canal of the inner ear as a determinant of how rotational movement of the head is detected and identified (Coutier et al, 2017).

The assumption that the plane of the LSC lies parallel to the horizontal when the head is at rest has been used, likely erroneously according to Benoit et al. (2020), to reconstruct head posture and diet in extinct species of herbivores (Sereno et al., 2007; Benoit et al., 2017). For example, the woolly rhinoceros (*Coelodonta antiquitatis*) has been interpreted as a grazer with a low usual head posture (Kurtén, 2017; Zeuner, 1934), comparable to the downward-oriented head of the extant white rhinoceros (*Ceratotherium simum*) (Schellhorn, 2018). This method has not been limited to mammals, Taylor et al. (2009) applied the same assumptions about the plane of the LSC to multiple sauropod genera, using extant birds and crocodilians as analogues. Sereno et al. (2007) used the LSC plane to estimate the usual head posture of the Cretaceous sauropod *Nigersaurus taqueti* as inclined 67° anteriorly downward, consistent with a low-level browsing feeding strategy.

4.1.3.2 Strengths and pitfalls of established methods

Whether the orientation of the LSC represents the usual or neutral head posture or instead reflects other behavioural positions such as those adopted during resting, locomotion, or feeding, cannot be conclusively determined due to the absence of quantitative behavioural data derived from direct observation.

A review of dietary preference and feeding height in extant rhinoceroses (Schellhorn, 2018) suggests that a relationship may exist among LSC orientation, occipital morphology, feeding strategy, and usual head posture. However, the most recent study incorporating direct behavioural observation (Benoit et al., 2020) reported no significant relationship between LSC orientation and head posture. Instead, the plane of the LSC was found to be significantly correlated with head-butting behaviour and useful in distinguishing between browsing and grazing taxa.

The orientation of the plane of the LSC has been employed to reconstruct usual head posture, with one of its advantages being its applicability to both extinct and extant species through CT scanning of museum specimens. Nevertheless, it cannot be used to estimate precise head posture angles. In extant taxa, direct observation remains a more reliable means of obtaining accurate measurements

4.1.3.3 Correlations with body size, phylogeny, morphology and feeding, and mandible mass distribution

4.1.3.3.1 Body size

Benoit et al. (2020) reported that species with body masses below 100 kg exhibit an average neutral head posture of 30° and a reconstructed cranial orientation of 39°, whereas species exceeding 100 kg display an average neutral head posture of 37° and a reconstructed cranial orientation of 40°. These findings indicate an effect of body mass on head posture, as proposed by Köhler (1993), but not on cranial orientation reconstructed from the plane of the LSC. Köhler (1993) argued that basal ruminants were small-bodied, short-limbed forms inhabiting closed environments. As ruminants adapted to open habitats, morphological changes associated with increased vigilance and intraspecific combat occurred, including limb elongation and the evolution of horns and antlers. Medium- and large-bodied species subsequently tended to maintain the head at or below the level of the withers. Thus, larger species, particularly those occupying open habitats, generally exhibit a lower head posture angle. However, no clear difference in LSC orientation is evident between size groups (39° and 40°, respectively

4.1.3.3.2 Phylogeny

Benoit et al. (2020) found that, when corrected for phylogenetic effects using phylogenetic generalized least squares (PGLS), the influence of body mass on head posture and cranial orientation was no longer significant. For example, within Tylopoda, the neutral head posture of the mixed-feeding *Camelus bactrianus* (450–700 kg), the browsing *Camelus dromedarius* (300–650 kg), the mixed-feeding *Lama* (113–250 kg), and the grazing *Vicugna* (45–55 kg) (Niehaus, 2022) is nearly horizontal. Based on body mass alone, neutral head postures of approximately 37° for *Camelus* and *Lama* and 30° for *Vicugna* would be expected. Similarly, members of the Suoidea, which exhibit an average neutral head posture of 46, also deviate from the trend as predicted by body mass. The grazing *Phacochoerus* (73-85kg) and the browsing *Catagonus* (35kg), incline their head at 46-53° and 46° respectively, while body mass predictions near 30°. These results suggest that the most reliable approach for reconstructing the head posture of fossil species is through phylogenetic regression based on extant relatives, rather than reliance on LSC orientation, body mass, or assumed dietary habits. The majority of proboscidean diversity prior to the end-Miocene displayed craniodental features consistent with browsing and omnivory. Following the expansion of grasslands and increased aridity during the End Miocene Thermal Maximum, proboscideans broadly adopted grazing diets, while Plio-Pleistocene and extant representatives retained comparatively conservative morphologies. Extant proboscideans, which are relatively brachygnathic yet possess massive mandibles, are likely outliers relative to the proportionally longer-jawed artiodactyls and perissodactyls examined in this study.

4.1.3.3.3 Feeding

Dietary strategy, specifically browsing and grazing, and head-butting behaviour are significantly correlated with the orientation of the lateral semicircular canal (LSC) but not with actual head posture. Although, browsers generally maintain a higher head position than grazers (Schellhorn, 2018). Anatomical and behavioural factors, including occipital morphology, the presence and size of cranial appendages or tusk-like lower incisors, and feeding height, influence usual head posture. A backward-inclined occiput is associated with a downward inclined head, typical of grazers, whereas a forward-inclined occiput corresponds to the more horizontal head posture observed in browsing rhinoceroses. The morphology of the inner ear provides additional information for interpreting head postures related to feeding strategies.

On average, browsers exhibit a less anteriorly inclined neutral head posture (26°) than mixed feeders (32°) and grazers (36°), supporting the notion that feeding strategy and feeding height influence neutral head posture. As grazers maintain a low head position while feeding on grasses and browsers reach for foliage at higher levels, and given that herbivores devote substantial time to acquiring low-energy food (Estes, 2012; Walker, 2023; Benoit et al., 2020), it is expected that the skull, neck musculature, and vestibular apparatus would evolve to reflect these behavioural differences, which would be expressed even in resting posture (Sereno et al., 2007; Schellhorn, 2018; Coutier et al., 2017). Accordingly, a progressively more anteriorly inclined neutral head posture is expected across the gradient from browsers to mixed feeders and grazers (Sereno et al., 2007; Schellhorn, 2018). Schellhorn (2018) was the first to compare reconstructed cranial orientation and actual head posture in Rhinocerotidae and identified results consistent with this trend. Similarly, Benoit et al. (2020) found a more inclined reconstructed cranial orientation in the grazing white rhinoceros (*Ceratotherium simum*, 38°) than in the mixed-feeding *Rhinoceros* (34°) and the browsing *Dicerorhinus* and *Diceros* (31°).

In contrast, the Cervidae exhibit relatively consistent head posture, maintaining the head within approximately 10° of an average neutral posture of 20°, regardless of diet, and browser and grazers are not distinguishable based on neutral head posture (30° and 28°, respectively). This suggests that head posture is not a useful tool for reconstructing diet in at least some clades.

4.1.3.3.4 And perhaps the mass distribution of the mandible

As described in Chapter 3, the closer the centre of mass (CoM) of the mandible lies along the horizontal axis to the temporomandibular joint (TMJ) for a given mandibular mass, the lower the rotational inertia that must be overcome by the jaw adductor musculature during chewing or while maintaining jaw closure in a resting or neutral posture. A downward anterior inclination of the head decreases the horizontal distance between the CoM and the TMJ, thereby reducing effective mandibular rotational inertia. The greater the angle of inclination, the greater the reduction of rotational inertia.

It is proposed that distinctions in head posture among grazers, mixed feeders, and browsers become more pronounced, and therefore more detectable, in large-bodied taxa such as rhinocerotids, but not in smaller-bodied groups such as cervids. This pattern may result from the substantially greater mandibular rotational inertia in larger species, the corresponding increase in energetic expenditure during mastication, and the greater volume of low-energy food required to sustain large body mass. Consequently, as mandibular size increases, the

resulting rotational inertia resisting mandibular movement during mastication also increases, requiring greater muscular effort to maintain jaw closure. This effect is partially offset by anterior tilting of the head during rest, active feeding, and in neutral posture.

A more anteriorly inclined neutral head posture, and therefore proportionally greater reduction in rotational inertia, is therefore expected in species with heavy mandibles and anteriorly skewed mass distributions, such as *Hippopotamus amphibius*, *Ceratotherium simum*, and *Diceros bicornis*.

4.2 Hypotheses

4.2.1 Hypotheses 1

Accounting for *in vivo* head posture will not alter the direction of relationships among mandibular mass properties and anatomical features (i.e., mandible length, masseteric insertion area) but will alter their scaling rate relative to horizontally oriented models.

Prediction 1: Mandibular centre of mass estimated from (1) a model assuming a horizontal mandible and (2) a model adjusted for in vivo head posture is expected to exhibit positive linear relationships with mandible length in both cases; however, the scaling rate is expected to be lower in the head posture adjusted model.

Prediction 2: Mandibular rotational inertia estimated from (1) a model assuming a horizontal mandible and (2) a model adjusted for in vivo head posture is expected to exhibit positive linear relationships with mandible length in both cases; however, the scaling rate is expected to be lower in the head posture adjusted model.

Prediction 3: Masseteric insertion area will exhibit a positive linear relationship with rotational inertia estimated from (1) a model assuming a horizontal mandible and (2) a model adjusted for in vivo head posture; however, because rotational inertia is reduced, the scaling rate is expected to be higher in the head posture adjusted model.

4.2.2 Hypotheses 2

Accounting for in-vivo head posture will better explain the relationships between jaw anatomy (i.e., mandible length, masseteric insertion area) and its mass properties, in terms of a stronger

linear association as indicated by correlation coefficients, than the previously used horizontally orientated model.

This will be tested by calculating and comparing correlation coefficients for variable pairs (i.e., mandible length and centre of mass; mandible length and rotational inertia; rotational inertia and masseteric insertion area) using centre of mass and rotational inertia values for both orientations.

In Chapter 3, no clear linear relationship was identified between the mechanical advantage of the masseter (MAM) or temporalis (MAT) and mandibular rotational inertia, despite the expectation that the mechanical advantage of the adductor musculature would correlate with mandibular rotational inertia. It is proposed that, even if head posture adjusted rotational inertia more accurately represents the resistance acting against the adductor musculature, it will remain weakly associated with both MAM and MAT.

Prediction 1: A pairwise comparison of correlation coefficients will show the head postured adjusted metrics (centre of mass, rotational inertia) will be more highly correlated with the anatomical metrics (mandible length, masseter insertion area) than those from the original horizontally orientated dataset.

Prediction 2: No significant correlation is expected between (1) mechanical advantage of the masseter and (2) mechanical advantage of the temporalis with rotational inertia calculated from either orientation.

4.2.3 Hypotheses 3

The reduction in mandibular rotational inertia achieved through head posture adjustment is primarily associated with mandible size, rather than taxonomic or dietary grouping.

If habitual head posture evolved partly to minimise the muscular and energetic work of mastication, then larger mandibles, which exhibit greater, and more distally distributed mass, would benefit most from anteriorly inclined postures that reduce effective rotational inertia.

Prediction 1: The absolute and proportional reduction in centre of mass distance and mandibular rotational inertia due to head posture angle increases with increasing mandible length across all taxonomic groups and feeding ecologies.

Prediction 2: After accounting for mandible length, residual variation in these reductions will not differ significantly among taxonomic or dietary groups.

4.3 Materials and Methods

4.3.1 Adult Interspecific Sample

This study employs a, 31 specimen subsample of the adult interspecific sample of Artiodactyls, Perissodactyls, and Proboscideans as in Chapter 2 and Chapter 3, for which head posture data were available (Table 4.1.).

Table 4.1. Adult interspecific sample species representing 31 specimens across 23 species. Neutral head posture adapted from Benoit et al. (2020, Table 1). Specimens not included in mechanical advantage of masseter and temporalis datasets (n = 2) due to scanning artifacts at the coronoid and mandibular condyle (*).

Museum abbreviations: 1) zmh - Zoologisches Museum Hamburg, University of Hamburg, Hamburg, Germany. 2) zmb - Museum für Naturkunde, Berlin, Germany. 3) usn:mamn - National Museum of Natural History, Smithsonian Institution, Division of Mammals. 4) TMM - Texas Memorial Museum, Austin, Texas, USA). 5) NMS – National Museum of Scotland; RDVS, Royal (Dick) School of Veterinary Studies, Edinburgh, United Kingdom.

Specimen No.	**Species**	**Scanner Type**	**Scanning Facility - Institute**	**Equipment Used**	**Software Versions**	**Original Voxel Size (mm)**	**Final Voxel Size (mm)**	**Voltage (kVp)**	**Neutral Posture Angle (°)**
zmh-s:2552	*Ceratotherium simum*	Clinical CT	Universitätsklinikum Hamburg Eppendorf (UKE)	Philips Brilliance 64 CT Scanner	N/A	0.6510	2.9686	120.0	57
zmh-s:9379	*Diceros bicornis*	Clinical CT	Oregon Imaging Centers	Philips Brilliance 64 CT Scanner	N/A	0.9777	2.8107	120.0	35
NMS. Z.2009.152*	*Rhinoceros unicornis*	Clinical CT	Small Animal Hospital, Royal (Dick) School of Veterinary Studies, University of Edinburgh	Siemens SOMATOM Definition AS	Syngo CT VA48A	0.6000	2.1440	120.0	17
zmb:70335	*Equus quagga (burchelli)*	Clinical CT	Oregon Imaging Centers	Philips Brilliance 64 CT Scanner	N/A	1.0000	1.0178	140.0	47
York Specimen (UoY -CT-001)*	*Equus caballus*	Clinical CT	The York Hospital, Wigginton Road	Siemens SOMATOM Definition AS+	Syngo CT VA48A	1.0000	1.8060	120.0	59

Specimen No.	**Species**	**Scanner Type**	**Scanning Facility - Institute**	**Equipment Used**	**Software Versions**	**Original Voxel Size (mm)**	**Final Voxel Size (mm)**	**Voltage (kVp)**	**Neutral Posture Angle (°)**
York Specimen (UoY-CT-002)*	*Equus caballus*	Clinical CT	The York Hospital, Wigginton Road	Siemens SOMATOM Definition AS+	Syngo CT VA48A	1.0000	1.4056	120.0	59
TMM-M-16 (left)	*Tapirus terrestris*	Custom CT Scanner	High-Resolution X-ray Computed Tomography Facility, University of Texas at Austin	North Star Imaging NSI Custom Build	N/A	0.2996	1.3925	210.0	23
TMM-M-16 (right	*Tapirus terrestris*	Custom CT Scanner	High-Resolution X-ray Computed Tomography Facility, University of Texas at Austin	North Star Imaging NSI Custom Build	N/A	0.2996	1.3925	210.0	23
York Specimen (UoY -CT-004)	*Bos taurus*	Clinical CT	The York Hospital, Wigginton Road	Siemens SOMATOM Definition AS+	Syngo CT VA48A	1.0000	1.5960	120.0	36
kupri:z928	*Cephalophus* sp.	Clinical CT	Primate Research Institute, Kyoto University	---	---	0.4000	0.5008	---	38
usnm:mammals:367429	*Redunca arundinum*	Custom CT Scanner	High-Resolution X-ray Computed Tomography Facility, University of Texas at Austin	North Star Imaging NSI Custom Build	N/A	0.3427	0.8801	190.0	23
usnm:mammals:291836	*Rupicapra rupicapra*	Custom CT Scanner	High-Resolution X-ray Computed Tomography Facility, University of Texas at Austin	North Star Imaging NSI Custom Build	N/A	0.2420	0.6486	190.0	36

Specimen No.	Species	Scanner Type	Scanning Facility - Institute	Equipment Used	Software Versions	Original Voxel Size (mm)	Final Voxel Size (mm)	Voltage (kVp)	Neutral Posture Angle (°)
usnm:mammals:164562	*Tragelaphus scriptus*	Custom CT Scanner	High-Resolution X-ray Computed Tomography Facility, University of Texas at Austin	North Star Imaging NSI Custom Build	N/A	0.2420	0.7066	190.0	25
TMM M-454	*Sus scrofa*	Clinical CT	High-Resolution X-ray Computed Tomography Facility, University of Texas at Austin	Varian Medical Systems, ACTIS CT scanner with FeinFocus X-ray source	N/A	0.4500	0.9540	N/A	47
usnm:mammals:145297	*Sus barbatus*	Custom CT Scanner	High-Resolution X-ray Computed Tomography Facility, University of Texas at Austin	North Star Imaging NSI Custom Build	N/A	0.2244	1.3051	200.0	55
usnm:mammals:a36000	*Phacochoerus africanus*	Custom CT Scanner	High-Resolution X-ray Computed Tomography Facility, University of Texas at Austin	North Star Imaging NSI Custom Build	N/A	0.3308	1.1644	220.0	46
York Specimen (UoY-CT-006)	*Camelus sp*	Clinical CT	The York Hospital, Wigginton Road	Siemens SOMATOM Definition AS+	Syngo CT VA48A	1.0000	1.9768	120.0	-1
NMS.Z.2009.72.1 (left)	*Camelus bactrianus*	Clinical CT	Small Animal Hospital, Royal (Dick) School of Veterinary Studies, University of Edinburgh	Siemens SOMATOM Definition AS	Syngo CT VA48A	0.6000	1.7520	120.0	2

Specimen No.	Species	Scanner Type	Scanning Facility - Institute	Equipment Used	Software Versions	Original Voxel Size (mm)	Final Voxel Size (mm)	Voltage (kVp)	Neutral Posture Angle (°)
NMS.Z.2009.72.1 (right)	*Camelus bactrianus*	Clinical CT	Small Animal Hospital, Royal (Dick) School of Veterinary Studies, University of Edinburgh	Siemens SOMATOM Definition AS	Syngo CT VA48A	0.6000	1.7520	120.0	59
NMS.Z.2008.35 (left)*	*Hippopotamus amphibius*	Clinical CT	Small Animal Hospital, Royal (Dick) School of Veterinary Studies, University of Edinburgh	Siemens SOMATOM Definition AS	Syngo CT VA48A	0.6000	2.3408	120.0	59
NMS.Z.2008.35 (right)	*Hippopotamus amphibius*	Clinical CT	Small Animal Hospital, Royal (Dick) School of Veterinary Studies, University of Edinburgh	Siemens SOMATOM Definition AS	Syngo CT VA48A	0.6000	2.3408	120.0	59
Unregistered (left)	*Hippopotamus amphibius*	Clinical CT	Small Animal Hospital, Royal (Dick) School of Veterinary Studies, University of Edinburgh	Siemens SOMATOM Definition AS	Syngo CT VA48A	0.6000	2.5680	120.0	59
Unregistered (right)	*Hippopotamus amphibius*	Clinical CT	Small Animal Hospital, Royal (Dick) School of Veterinary Studies, University of Edinburgh	Siemens SOMATOM Definition AS	Syngo CT VA48A	0.6000	2.5680	120.0	59
usnm:mammals:246649	*Rangifer tarandus*	Custom CT Scanner	High-Resolution X-ray Computed Tomography Facility, University of Texas at Austin	North Star Imaging NSI Custom Build	N/A	0.2433	1.4131	190.0	35

Specimen No.	Species	Scanner Type	Scanning Facility - Institute	Equipment Used	Software Versions	Original Voxel Size (mm)	Final Voxel Size (mm)	Voltage (kVp)	Neutral Posture Angle (°)
York Specimen (UoY-CT-007)	*Giraffa sp*	Clinical CT	The York Hospital, Wigginton Road	Siemens SOMATOM Definition AS+	Syngo CT VA48A	1.0000	2.2596	120.0	24
NMS.GH3.21 (left)	*Okapia johnstoni*	Clinical CT	Small Animal Hospital, Royal (Dick) School of Veterinary Studies, University of Edinburgh	Siemens SOMATOM Definition AS	Syngo CT VA48A	0.6000	1.6448	120.0	19
NMS.GH3.21 (right)	*Okapia johnstoni*	Clinical CT	Small Animal Hospital, Royal (Dick) School of Veterinary Studies, University of Edinburgh	Siemens SOMATOM Definition AS	Syngo CT VA48A	0.6000	1.6448	120.0	19
usnm:mammals:282308	*Antilocapra americana*	Custom CT Scanner	High-Resolution X-ray Computed Tomography Facility, University of Texas at Austin	North Star Imaging NSI Custom Build	N/A	0.3118	1.0763	190.0	36
NMS.Z.2001.147 (left)	*Elephas maximus*	Clinical CT	Small Animal Hospital, Royal (Dick) School of Veterinary Studies, University of Edinburgh	Siemens SOMATOM Definition AS	Syngo CT VA48A	0.6000	2.2384	120.0	39
NMS.Z.2013.148.1 (left)	*Loxodonta africana*	Clinical CT	Small Animal Hospital, Royal (Dick) School of Veterinary Studies, University of Edinburgh	Siemens SOMATOM Definition AS	Syngo CT VA48A	0.6000	2.2384	120.0	48
NMS.Z.2013.148.1 (right)*	*Loxodonta africana*	Clinical CT	Small Animal Hospital, Royal (Dick) School of Veterinary Studies, University of Edinburgh	Siemens SOMATOM Definition AS	Syngo CT VA48A	0.6000	2.2384	120.0	48

4.3.2 Linear Regression Analyses

The same set of linear regression analyses were completed in this study, as in the previous chapter, Chapter 3 - *Biological and Mechanical Implications of Mandibular Mass Distribution in Terrestrial Mammalian Herbivores (Orders Artiodactyla, Perissodactyla, Proboscidea)*. As masseteric insertion area, and mechanical advantage of the masseter and the temporalis are not affected by the head posture adjustment process, these data were carried over from Chapter 3.

Linear relationships between the measured variables (i.e., mandible length and centre of mass; mandible length and rotational inertia; rotational inertia and masseteric insertion area; rotational inertia and mechanical advantage of the masseter, and the temporalis) were tested for statistical significance using both Ordinary Least Squares (OLS) Reduced Major Axis (RMA) regression. OLS regression assumes the independent variable is measured without error while RMA regression accounts for measurement error in both independent and dependent variables. Linear regressions were performed for each pair of variables for centre of mass and rotational inertia estimated from each specimen twice; for both a horizontal mandible orientation, and for a head posture adjusted orientation.

4.3.3 Head Posture Adjusted Centre of Mass

The position of the centre of mass (CoM) along the longitudinal axis of the mandible was estimated for the adult interspecific sample of ungulate-grade mammals (Table 4.1) under two conditions; a horizontal orientation and a head posture adjusted orientation (Figure 4.1). In the first case, the mandible was oriented horizontally, consistent with the standardised orientation employed in the preceding two chapters. In this orientation, the *z*-axis was defined as parallel to a plane passing through the occlusal surface of the most anterior dentition, typically the incisors, or the superior surface of the mandibular symphysis in species lacking anterior teeth, and the most posterior molar, typically M3. The *x*-axis was defined as the plane bounding the posterior surface of the condylar processes and perpendicular to the *z*-axis. For this orientation, the CoM was estimated directly using the CoM-CT method described in Chapter 2 and applied in Chapter 3. This orientation was performed in the *Fiji* (Version 1.54p) variant of ImageJ (Schindelin et al., 2012) using the plugin *TransformJ* (Meijering et al., 2001).

In the second case, the head-posture-adjusted CoM was estimated indirectly. The CoM position of each specimen was adjusted for neutral head posture by applying a rotation matrix to rotate the horizontally oriented CoM coordinates through the angle θ. The rotation matrix,

$$(1)\ R(\theta) = \begin{bmatrix} cos\theta & -sin\theta \\ sin\theta & cos\theta \end{bmatrix},$$

rotates points on the *xy* plane through an angle *θ* about the origin of a two-dimensional Cartesian coordinate system. For a point (x,y), the new coordinates after rotation are given by,

$$(2)\begin{bmatrix} x' \\ y' \end{bmatrix} = \begin{bmatrix} cos\theta & -sin\theta \\ sin\theta & cos\theta \end{bmatrix}\begin{bmatrix} x \\ y \end{bmatrix}.$$

Therefore, the new coordinates (x',y') after rotation are given by,

$$(3)\ x' = xcos\theta - ysin\theta, \text{ and } y' = xsin\theta + ycos\theta.$$

In this study, the x-coordinate represents the perpendicular distance from the vertical plane containing the centre of mass to the vertical plane containing the TMJ, therefore, y = 0, as there is no vertical displacement. As such, the new centre of mass distance after rotation, is given by

$$(4)\ x' = xcos\theta,$$

where x is the horizontally oriented centre of mass, and *θ* is the angle of inclination during neutral head posture.

The adjustment calculations were performed in *Microsoft Excel*, using neutral head posture angles sourced from Benoit et al. (2020, Table 1). First, the horizontally orientated CoM values and head posture angles were imported for each specimen. Head posture angles reported in degrees were converted to radians as required for trigonometric functions in *Excel* using the function =RADIANS(). Head posture adjusted CoM was calculated from (1) where *x* is the horizontally oriented centre of mass, and *θ* is the angle of inclination of the mandible during neutral head posture. Rotational inertia, *I*, was then calculated for both orientations by

$$(5)\ I = mr^2\ (kg.m^2),$$

where *m* represents mandible mass and *r* is the centre of mass distance for, firstly, the horizontal centre of mass, and secondly, the head posture adjusted centre of mass. A comparison of the original horizontal orientation and the head posture adjusted orientation is present

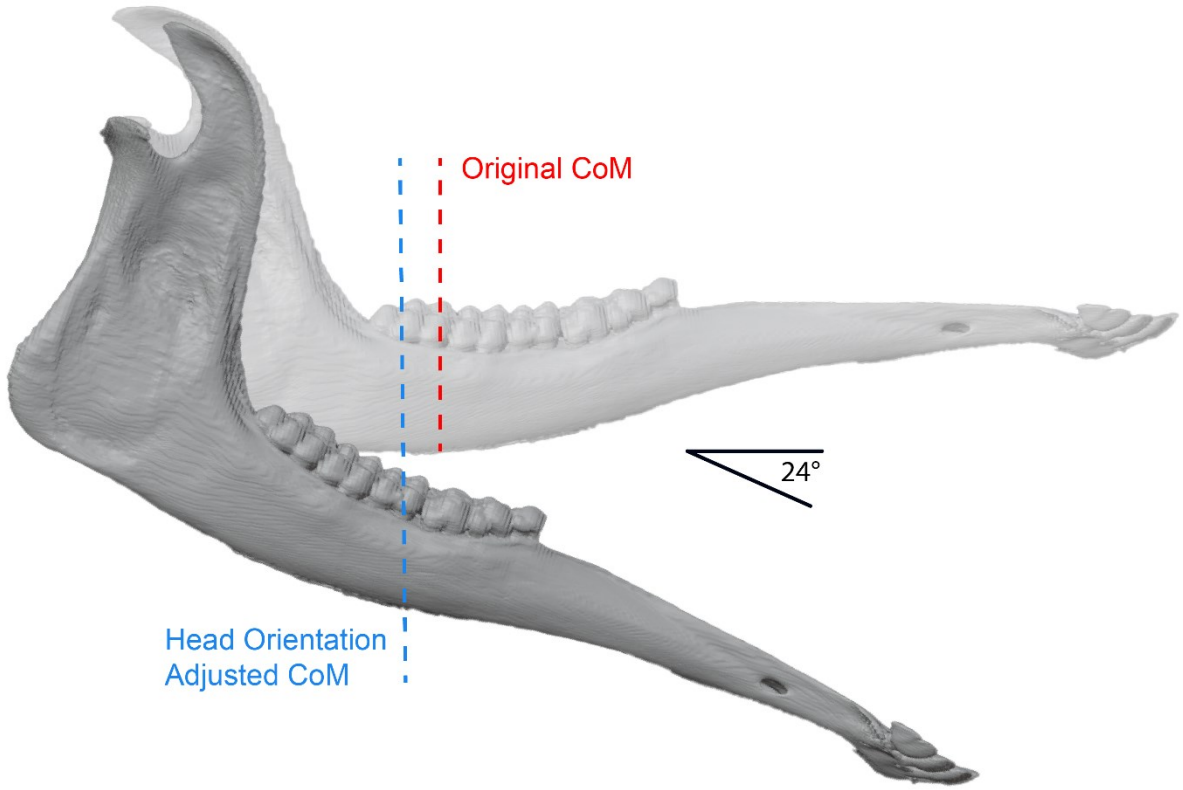

Figure 4.1. Comparison of mandible orientation used for estimating centre of mass: the original horizontal orientation and the anteriorly inclined orientation adjusted to reflect neutral head posture. Example shown using the mandible of *Giraffa* sp., rotated 24° anteriorly downward from horizontal, corresponding to the head posture reported by Benoit et al. (2020, Table 1).

4.3.4 Correlation Coefficients for Pairwise Comparisons

Correlation coefficients were calculated in base R (R Core Team, 2021). The procedure used to determine the appropriate correlation test depended on the distribution of the data. Normality was first assessed visually using histograms and statistically using the Shapiro-Wilk test. In the case that the Shapiro-Wilk test indicated marginal normality, the Anderson-Darling test was additionally applied to provide clarity through further assessment of normality. If normality was confirmed, the Breusch-Pagan test was used to evaluate heteroscedasticity. When data were both normally distributed and homoscedastic, Pearson's correlation coefficient was calculated; otherwise, Spearman's rank correlation coefficient was used.

4.4 Results

4.4.1 Results 1 – Centre of Mass

The horizontally oriented centre of mass data followed a normal distribution (Shapiro–Wilk: W = 0.96012, $p = 0.2938$) and exhibited homoscedasticity (Breusch–Pagan: BP = 1.604, df = 1, $p = 0.2053$). Accordingly, Pearson's correlation coefficient was calculated, indicating a strong positive linear association between centre of mass and mandible length ($t = 17.425$, df = 29, $p < 2.2 \times 10^{-16}$, $r \approx 0.955$). The original centre of mass scaled isometrically or with weak positive allometry relative to mandible length, with a high goodness-of-fit (R^2adj = 0.91). Ordinary Least Squares (OLS) regression produced a slope of 1.10 (95% CI: 0.97–1.22), while Reduced Major Axis (RMA) regression yielded a slope of 1.15 (95% CI: 1.03–1.29), both encompassing the isometric expectation of 1 (Figure 4.2).

After head posture adjustment, centre of mass values again satisfied assumptions of normality (Shapiro–Wilk: W = 0.95094, $p = 0.1657$) and homoscedasticity (Breusch–Pagan: BP = 0.25598, df = 1, $p = 0.6129$). Pearson's correlation confirmed a strong positive linear relationship ($t = 15.835$, df = 29, $p = 8.24 \times 10^{-16}$, $r \approx 0.947$), consistent with the original data. The adjusted centre of mass maintained a linear scaling relationship with mandible length and exhibited a high goodness-of-fit (R^2adj = 0.90). However, the relationship demonstrated isometric to weak negative allometric scaling. OLS regression yielded a slope of 0.94 (95% CI: 0.82–1.07), and RMA regression yielded a slope of 1.00 (95% CI: 0.88–1.13), both overlapping the isometric slope of 1 (Figure 4.2). A summary of normality and homoscedasticity test results, regression statistics, and correlation coefficients is provided in for comparison (Table 4.2).

Both correlations were high, with the horizontally oriented data explaining slightly more of the variance (approximately 1.5%) than the head posture–adjusted data, suggesting a marginally stronger association between mandible length and the unadjusted centre of mass. Linear regression models for both datasets showed comparable goodness-of-fit (0.91 vs 0.90), with the horizontally oriented data scaling isometrically or with weak positive allometry, and the adjusted data scaling isometrically or with weak negative allometry.

Table 4.2. Statistical summary of original horizontally oriented and head posture adjusted centre of mass data against mandible length. Correlation coefficients calculated across all in individuals in the full interspecific sample (31 specimens, 23 species). The original horizontal orientation refers to the standardised mandible orientation used in Chapters 2&3.

	Original Horizontal Orientation	**Adjusted Head Posture Orientation**
Normality	W = 0.9601, p = 0.2938	W = 0.9509, p = 0.1657
Homoscedasticity	BP = 1.604, df = 1, p = 0.2053	BP = 0.25598, df = 1, p = 0.6129
Pearson's r	t=17.425, df = 29, p < 2.2e-16, r ≈ 0.955	t=15.835, df = 29, p = 8.24e-16, r ≈ 0.947
Adj. R^2	0.91	0.90
OLS slope	1.10 (95 % CI: 0.97–1.22)	0.94 (95 % CI: 0.82–1.07)
RMA slope	1.15 (95 % CI: 1.03–1.29)	1.00 (95 % CI: 0.88–1.13)
Allometry	Isometry or weak **positive** allometry	Isometry or weak **negative** allometry

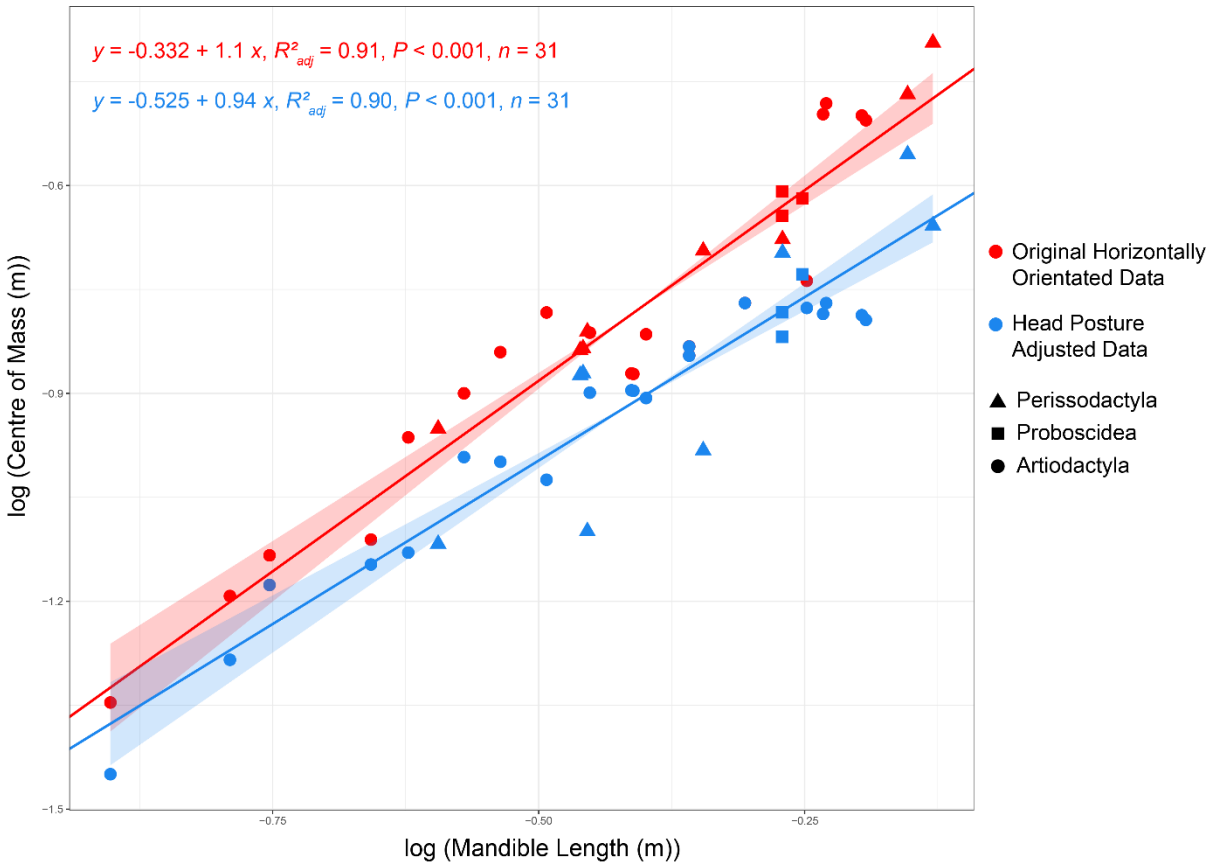

Figure 4.2. Relationship between log-transformed mandible length and log-transformed centre of mass for the original horizontally oriented and head-posture-adjusted datasets as evidenced by Ordinary Least Squares (OLS) regression. Red symbols and regression line represent the original horizontally oriented data; blue symbols and regression line represent the head-posture-adjusted data. Shaded areas indicate 95% confidence intervals. Shapes denote taxonomic groups: triangles = Perissodactyla, squares = Proboscidea, and circles = Artiodactyla.

4.4.2 Results 2 – Mandibular Rotational Inertia

Horizontally orientated mandibular rotational inertia measurements exhibited marginal deviation from normality (Shapiro-Wilk: W = 0.93135, p = 0.04773). An Anderson-Darling test (A = 0.67286, p = 0.0713) similarly failed to provide strong evidence against normality, though the test statistic suggested pronounced deviations in the tails. Visual inspection of the histogram (Figure 4.3) revealed a left-skewed and potentially bimodal distribution. Consequently, the data were treated as non-normal and analysed using Spearman's rank correlation, which demonstrated a very strong monotonic association with mandible length (S = 387.08, p = 1.79×10^{-13}, $\rho \approx 0.92$).

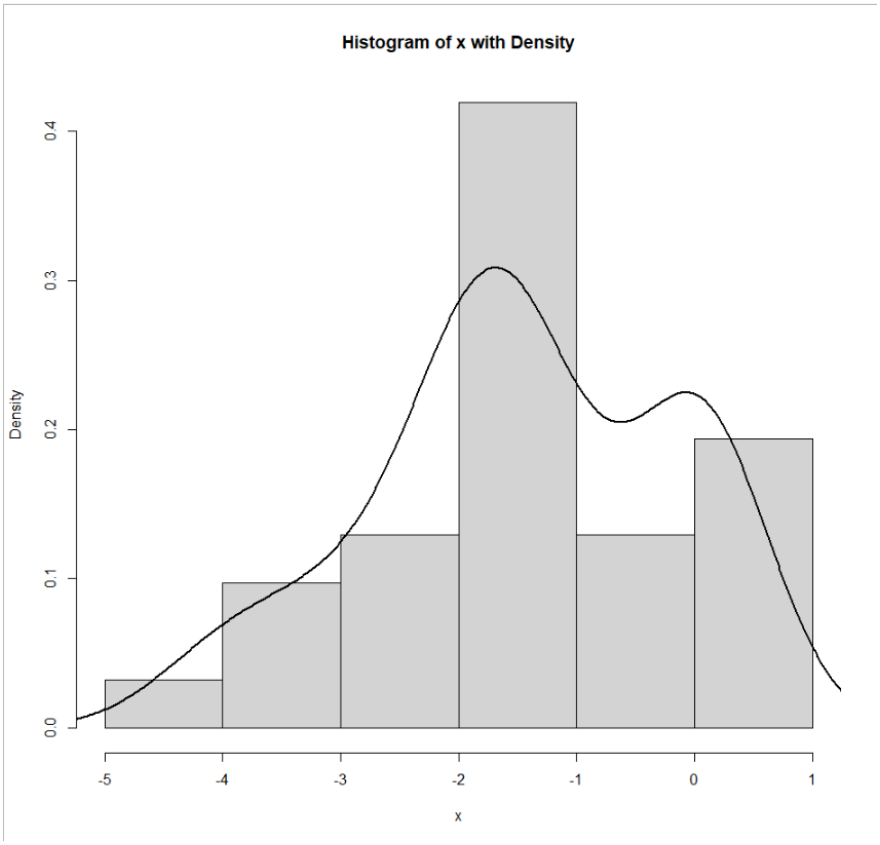

Figure 4.3. Histogram showing the distribution of original horizontally orientated rotational inertia with an overlaid kernel density curve.

Following adjustment, rotational inertia again presented conflicting normality assessments: Shapiro-Wilk ($W = 0.9451$, $p = 0.114$) and Anderson-Darling ($A = 0.48536$, $p = 0.2108$) tests did not reject normality, yet the histogram (Figure 4.4) displayed moderate left skewness and possible bimodality, which may be due to the small sample size ($n = 31$). To allow for direct comparison with horizontally orientated centre of mass normality was not assumed, and Spearman's rank correlation was calculated, confirming a very strong monotonic relationship with mandible length ($S = 439.09$, $p = 1.039 \times 10^{-12}$, $\rho \approx 0.91$).

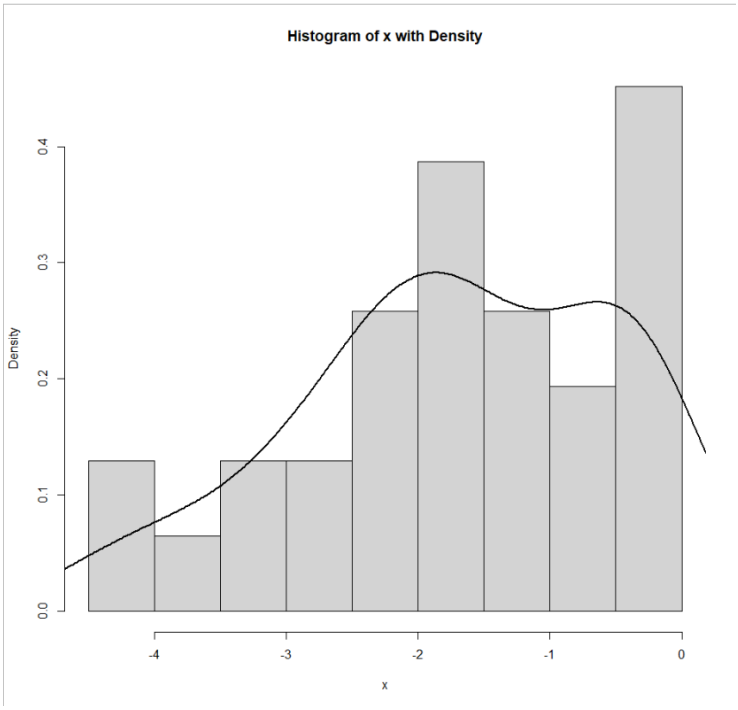

Figure 4.4. Histogram showing the distribution of head posture adjusted rotational inertia with an overlaid kernel density curve.

Linear regression analysis of the relationship between mandible length and horizontally orientated rotational inertia indicated a very strong linear relationship (R^2_{adj} = 0.91). OLS regression yielded a slope of 6.14 (95 % CI: 5.39–6.89), while RMA regression produced a slope of 6.45 (95 % CI: 5.75–7.25), both exceeding the isometric expectation of 5 (Figure 4.5) indicating positive allometry.

The adjusted dataset maintained a very strong linear relationship (R^2_{adj} = 0.92). OLS regression yielded a slope of 5.83 (95 % CI: 5.17–6.49), while RMA regression produced a slope of 6.08 (95 % CI: 5.46–6.78) (Figure 4.5), again indicating positive allometry but at a marginally lower scaling rate than in the horizontally orientated dataset. A summary table of normality and homoscedasticity test results, regression statistics, and correlation coefficients is presented below for ease of comparison (Table 4.3).

In both datasets, rotational inertia exhibits positive allometric scaling with mandible length. This indicates rotational inertia scales disproportionally with mandible length despite the compensatory effects of an anterior downward head tilt in neutral posture.

The difference between rank correlation coefficient is negligible in practical terms as both associations are equally strong. Both the original rotational data and the head posture adjusted

data show very strong positive rank-order associations with mandible length (Spearman $\rho = 0.922$ vs. 0.911). The absolute difference ($\Delta\rho = 0.011$) is trivial, and a bootstrap comparison produces a 95 % confidence interval that includes zero, indicating the two relationships do not significantly differ in strength. Again, this suggests head posture, and therefore the orientation of the jaw relative to the horizontal, is not strongly influencing musculoskeletal adaptation in the masticatory system.

Table 4.3. Statistical summary of original horizontally oriented and head posture adjusted rotational inertia against mandible length. Correlation coefficients calculated across all in individuals in the full interspecific sample (31 specimens, 23 species). The original horizontal orientation refers to the standardised mandible orientation used in Chapters 2&3.

	Original Horizontal Orientation	**Adjusted Head Posture Orientation**
Normality (Shapiro–Wilk)	W = 0.93135, p = 0.04773 (marginally non-normal)	W = 0.94510, p = 0.11400 (no evidence against normality)
Anderson–Darling	A = 0.67286, p = 0.07130 (no strong rejection, but tail deviations)	A = 0.48536, p = 0.21080 (no evidence against normality)
Histogram	Non-normal; left skew; possible bimodality	Non-normal histogram; left skew; possible bimodality (despite test statistics)
Correlation (Spearman's ρ)	S = 387.08, p = 1.79×10^{-13}, ρ ≈ 0.92 (very strong monotonic)	S = 439.09, p = 1.04×10^{-12}, ρ ≈ 0.91 (very strong monotonic)
Adjusted R^2	0.91	0.92
OLS slope	6.14 (95 % CI: 5.39 – 6.89)	5.83 (95 % CI: 5.17 – 6.49)
RMA slope	6.45 (95 % CI: 5.75 – 7.25)	6.08 (95 % CI: 5.46 – 6.78)
Isometry slope	5.00	5.00
Allometry	Positive allometry (slopes > isometric expectation)	Positive allometry (slopes > isometric expectation)

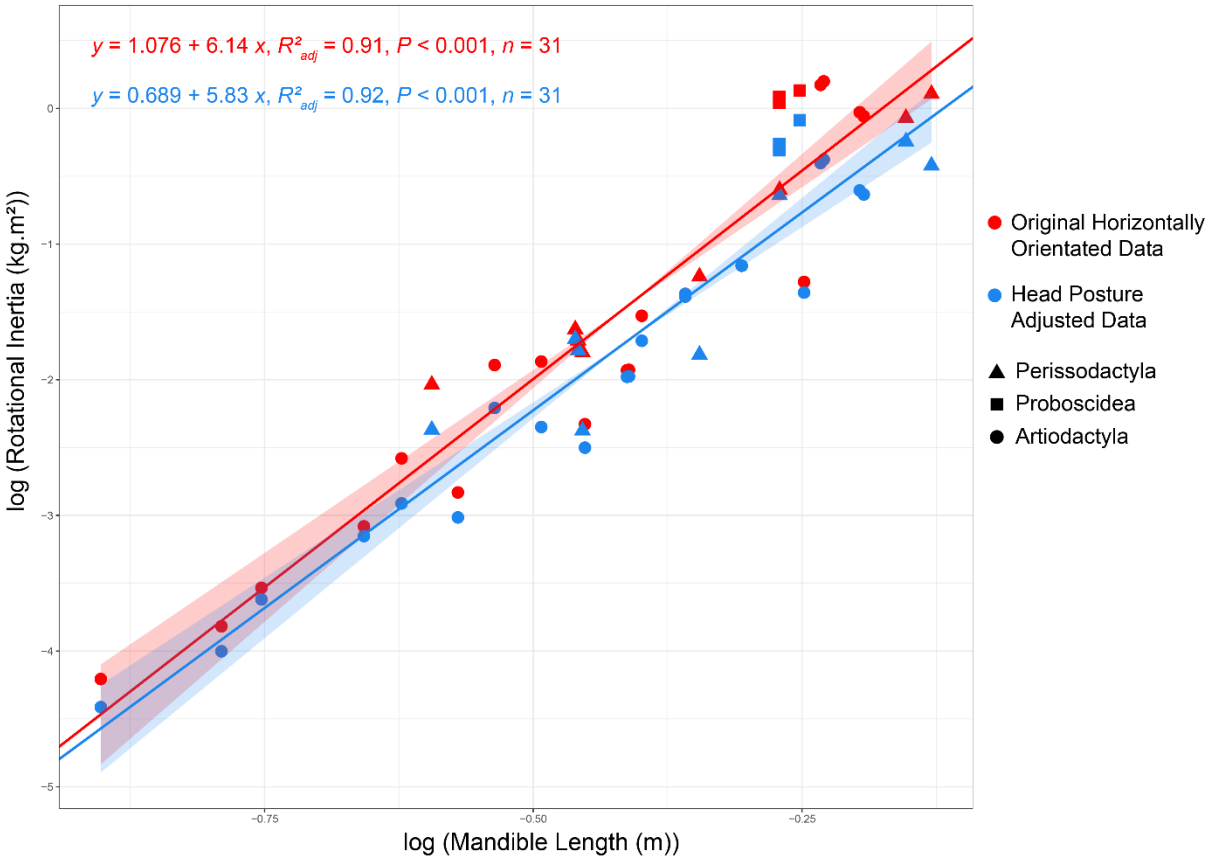

Figure 4.5. Relationship between log-transformed mandible length and log-transformed rotational inertia for the original horizontally oriented and head posture adjusted datasets as evidenced by Ordinary Least Squares (OLS) regression. Red symbols and regression line represent the original horizontally oriented data; blue symbols and regression line represent the head-posture-adjusted data. Shaded areas indicate 95% confidence intervals. Shapes denote taxonomic groups: triangles = Perissodactyla, squares = Proboscidea, and circles = Artiodactyla.

4.4.3 Results 3 – Masseter Insertion Area

The scaling of masseter insertion area relative to mandibular rotational inertia was examined by comparing the strength of their correlations and by performing linear regression of masseter insertion area on mandibular rotational inertia for both the original and head posture–adjusted datasets.

Masseter insertion area measurements met the assumptions required for parametric analysis, displaying normality (Shapiro-Wilk: W = 0.94464, p = 0.1109; Anderson-Darling: A = 0.47822, p = 0.2197) and homoscedasticity (Breusch–Pagan: BP = 3.7354×10^{-5}, df = 1, p = 0.9951).

Pearson's correlation between masseter insertion area and the original mandibular rotational inertia indicated a strong positive linear association ($t = 17.425$, df = 29, $p < 2.2 \times 10^{-16}$, $r \approx 0.97$). Linear regression analysis showed a highly linear scaling relationship (R^2adj = 0.95). Both Ordinary Least Squares (OLS) regression (slope = 0.40; 95% CI: 0.36–0.44) and Reduced Major Axis (RMA) regression (slope = 0.41; 95% CI: 0.38–0.45) corresponded closely to the isometric expectation of 0.4 (Figure 4.6).

When adjusted mandibular rotational inertia was evaluated, Pearson's correlation remained strong ($t = 17.921$, df = 29, $p < 2.2 \times 10^{-16}$, $r \approx 0.96$). Linear regression again indicated a robust linear relationship (R^2adj = 0.92), slightly lower than that observed in the original dataset. OLS regression yielded a slope of 0.41 (95% CI: 0.37–0.47), and RMA regression produced a slope of 0.44 (95% CI: 0.39–0.49), both consistent with isometry (Figure 4.6).

Correlations were high in both datasets, with only a small difference in variance explained (1.9%) in favour of the original data. This may suggest that masseter insertion area is more closely associated with the original, horizontally oriented rotational inertia values than with the head posture–adjusted values. However, given the small difference, this interpretation is weakly supported and may benefit from further analysis. A summary of normality and homoscedasticity tests, regression statistics, and correlation coefficients is presented in Table 4.4 for ease of comparison.

Table 4.4. Statistical summary of original horizontally oriented and head posture adjusted rotational inertia against mandible length. Correlation coefficients calculated across all in individuals in the full interspecific sample (31 specimens, 23 species). The original horizontal orientation refers to the standardised mandible orientation used in Chapters 2&3.

	Original Horizontal Orientation	**Adjusted Head Posture Orientation**
Pearson's *r*	$t = 17.425$, $df = 29$, $p < 2.2 \times 10^{-16}$; $r \approx 0.97$	$t = 17.921$, $df = 29$, $p < 2.2 \times 10^{-16}$; $r \approx 0.96$
Adjusted R^2	0.95	0.92
OLS slope	0.40 (95 % CI: 0.36 – 0.44)	0.41 (95 % CI: 0.37 – 0.47)
RMA slope	0.41 (95 % CI: 0.38 – 0.45)	0.44 (95 % CI: 0.39 – 0.49)
Isometry slope	0.40	0.40
Allometry classification	Isometric scaling (slope ≈ isometry)	Isometric scaling (slope ≈ isometry)

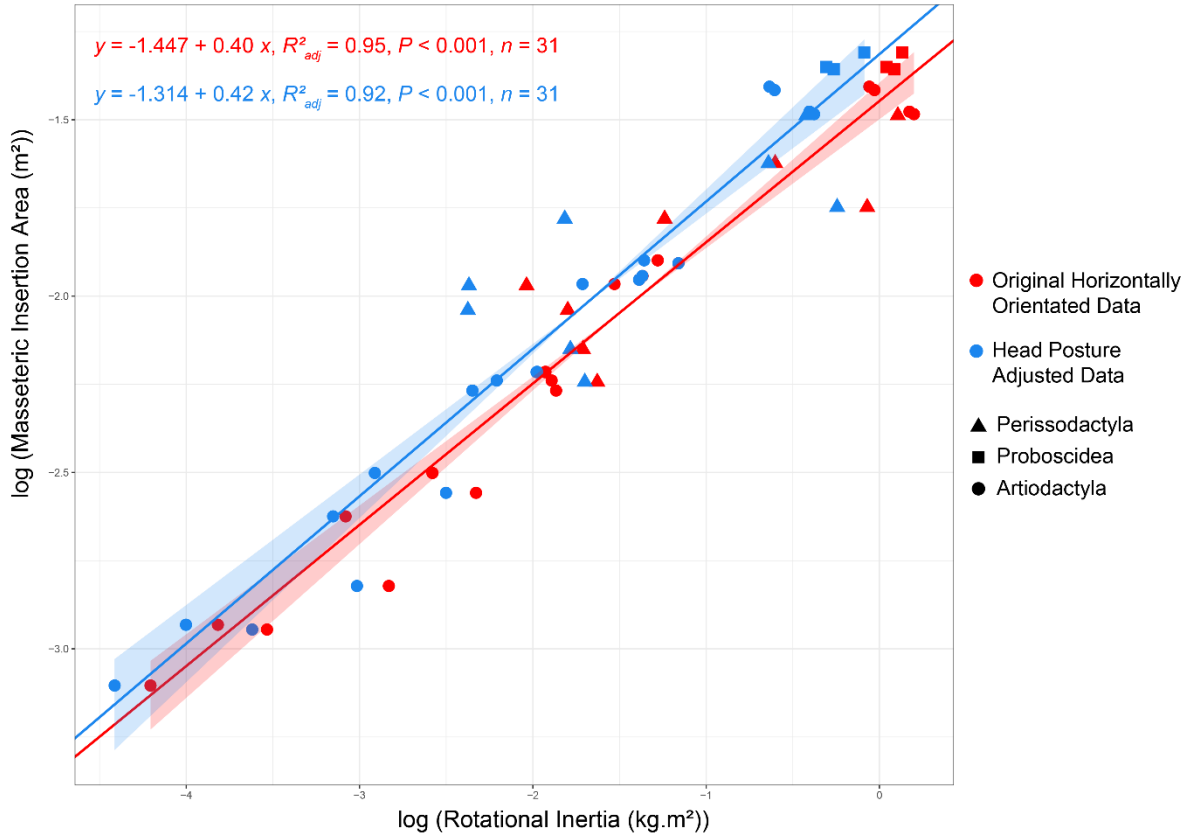

Figure 4.6. Relationship between log-transformed masseter insertion area and log-transformed rotational inertia for the original horizontally oriented and head posture adjusted datasets as evidenced by Ordinary Least Squares (OLS) regression. Red symbols and regression line represent the original horizontally oriented data; blue symbols and regression line represent the head-posture-adjusted data. Shaded areas indicate 95% confidence intervals. Shapes denote taxonomic groups: triangles = Perissodactyla, squares = Proboscidea, and circles = Artiodactyla.

4.4.4 Results 4 – Mechanical Advantage of the Masseter

The mechanical advantage of the masseter (MAM) data conformed to normality (Shapiro-Wilk: W = 0.94398, p = 0.1275; Anderson–Darling: A = 0.56339, p = 0.132) but did not meet the assumption of homoscedasticity (Breusch-Pagan: BP = 5.3308, df = 1, p = 0.02095).

Spearman's rank correlation between original horizontally orientated mandibular rotational inertia and MAM indicated a statistically significant, moderate positive monotonic association (S = 2344, p = 0.02323, ρ ≈ 0.423). In contrast, linear regression revealed only a weak relationship. One-tailed Pearson's correlation approached, but did not reach, significance (p =

0.07), and only 8% of the variance in MAM was explained by rotational inertia (R^2adj = 0.08). OLS and RMA regressions yielded shallow slopes (OLS slope = 0.02, 95% CI: -0.0072 to 0.0488; RMA slope = 0.02, 95% CI: -0.0072 to 0.0491), with confidence intervals encompassing zero, indicating the absence of a reliable linear trend (Figure 4.7).

Following adjustment for head posture, Spearman's rank correlation between rotational inertia and MAM remained positive but was no longer statistically significant (S = 2696, p = 0.0753, ρ ≈ 0.336), likely reflecting reduced statistical power associated with the smaller sample size (n = 29). The reduced sample resulted from noise and scanning artefacts that obscured the condylar and coronoid processes, preventing accurate measurement of muscle lever arms. Linear regression analysis also failed to identify a significant relationship: the one-tailed Pearson's test yielded p = 0.12, and R^2adj decreased to 0.05, indicating that rotational inertia explained only 5% of the variation in MAM. Both OLS and RMA regressions again produced nearly identical, shallow slopes (OLS slope = 0.02, 95% CI: -0.01248 to 0.04739; RMA slope = 0.02, 95% CI: -0.01255 to 0.04770), with confidence intervals spanning zero, further supporting the absence of a meaningful linear association (Figure 4.7). A summary table of normality and homoscedasticity test, regression statistics, and correlation coefficients is presented below for ease of comparison (Table 4.5).

Overall, there is no strong evidence that MAM scales with rotational inertia, suggesting it does not influence the morphology of the mandible for species with longer and heavier mandibles to have greater mechanical advantage. Neither original horizontally orientated nor the head posture adjusted rotational explains variation in the mechanical advantage of the masseter to a substantially greater degree than the other. There is no strong evidence that MAM scales with rotational inertia, suggesting it does not influence the morphology of the mandible for species with longer and heavier mandibles to have greater mechanical advantage.

Table 4.5. Statistical summary of mechanical advantage of the masseter against original horizontally oriented and head posture adjusted rotational inertia. Correlation coefficients calculated across all in individuals in the full interspecific sample (31 specimens, 23 species). The original horizontal orientation is so named as it is the standardised mandible orientation used in Chapters 2&3.

Feature	**Original Horizontal Orientation**	**Adjusted Head Posture Orientation**
Spearman's ρ	S = 2344, p = 0.02323; ρ ≈ 0.423 (moderate, significant)	S = 2696, p = 0.0753; ρ ≈ 0.336 (moderate, not significant)
Adjusted R^2 (linear)	0.08	0.05
Parametric linear p-value (one-tailed)	p = 0.07 (weak, not significant)	p = 0.12 (not significant)
OLS slope	0.02 (95 % CI: –0.0072 – 0.0488)	0.02 (95 % CI: –0.01248 – 0.04739)
RMA slope	0.02 (95 % CI: –0.0072 – 0.0491)	0.02 (95 % CI: –0.01255 – 0.04770)
Allometry classification / Significance Notes	Effect size very small; CIs include zero (no clear allometry)	Effect size very small; CIs include zero (no clear allometry)

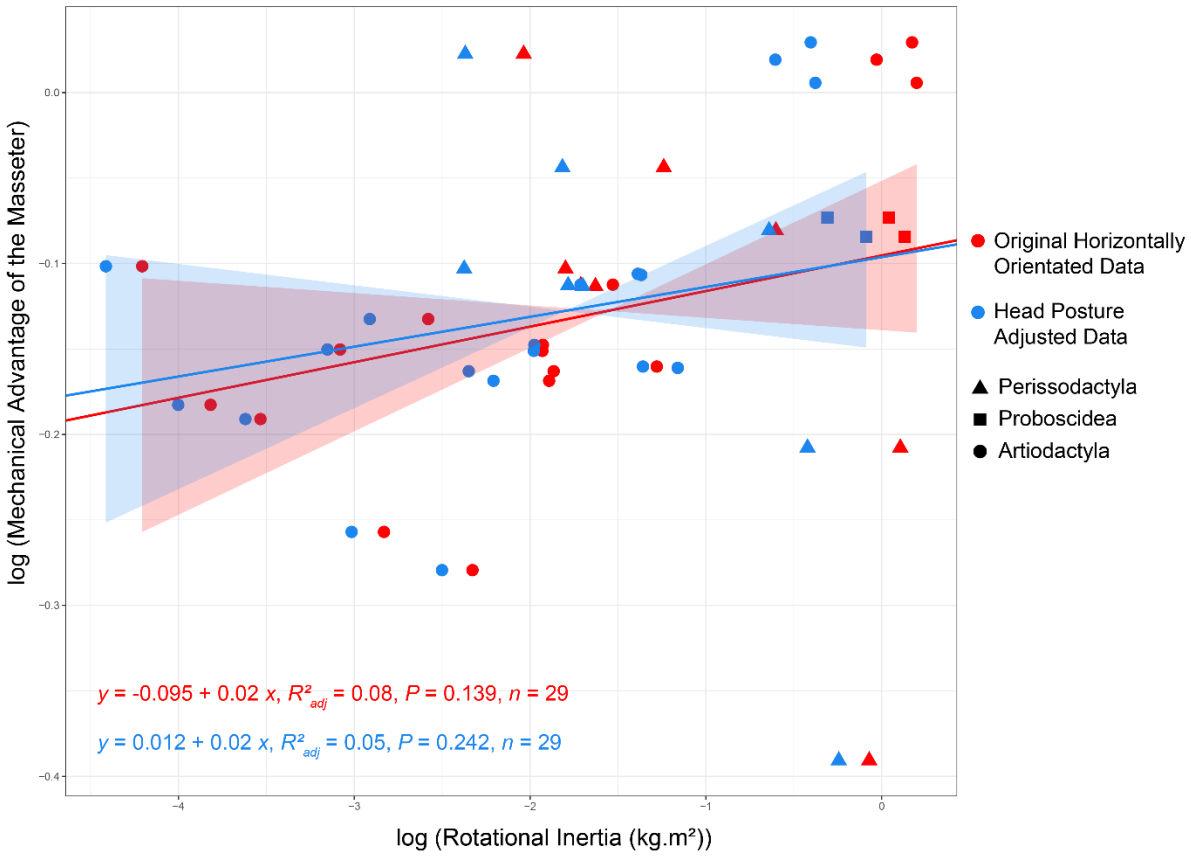

Figure 4.7. Relationship between log-transformed mechanical advantage of the masseter and log-transformed rotational inertia for the original horizontally oriented and head posture adjusted datasets as evidenced by Ordinary Least Squares (OLS) regression. Red symbols and regression line represent the original horizontally oriented data; blue symbols and regression line represent the head-posture-adjusted data. Shaded areas indicate 95% confidence intervals. Shapes denote taxonomic groups: triangles = Perissodactyla, squares = Proboscidea, and circles = Artiodactyla.

4.4.5 Results 5 – Mechanical Advantage of the Temporalis

The mechanical advantage of the temporalis (MAT) data are not normally distributed (W = 0.68311, p-value = 1.215e-06; A = 2.6773, p-value = 6.246e-07) nor homoscedastic (BP = 7.453, df = 1, p-value = 0.006333).

Spearman's rank correlation between original mandibular rotational inertia and the mechanical advantage of the temporalis (MAT) revealed a moderate negative monotonic relationship (S = 5756, p = 0.02502, ρ ≈ -0.418). Linear regression further indicated a statistically significant but relatively weak negative association (one-tailed p = 0.024; two-tailed p = 0.048) and rotational

inertia accounted for only 14% of the variance in MAT (R^2_{adj} = 0.14). Both OLS and RMA regressions produced slopes of -0.83 (OLS: 95% CI: -0.17862 to -0.00009; RMA: 95% CI: -0.18931 to -0.00137), neither confidence interval encompassing zero, although the marginal nature of the effect warrants caution, if the intervals are rounded to two decimal places, they would include zero, negating formal significance (Figure 4.8).

In the head posture adjusted dataset, Spearman's rank correlation revealed a moderate negative monotonic relationship between mandibular rotational inertia and temporalis mechanical advantage (MAT) (S = 5 546, p = 0.0516, ρ ≈ -0.366). Linear regression analysis likewise indicated a weak negative association, accounting for just 10% of the variance in MAT (R^2_{adj} = 0.10) and achieving marginal significance when directionality was specified (one-tailed p = 0.044; two-tailed p = 0.088). Both OLS and RMA regressions yielded similarly shallow slopes (OLS: slope = -0.82, 95 % CI: -0.1753 to 0.0130; RMA: slope = -0.87, 95 % CI: -0.1898 to 0.0135), with confidence intervals that narrowly encompass zero (Figure 4.8). To facilitate easier comparisons of the statistical results between orientations, a summary stable has been provided (Table 4.6).

Species exhibiting greater mandibular rotational inertia thus tend to have lower temporalis mechanical advantage, yet this relationship is only marginally significant or may have no formal significance. The limited sample size (n = 29) likely constrained statistical power; future investigations should expand taxonomic breadth, include a wider array of mandible morphologies and dietary strategies, and increase sample size to more definitively quantify the links between mandible mass properties and both masseter and temporalis mechanical advantage.

Table 4.6. Statistical summary of mechanical advantage of the temporalis against original horizontally oriented and head posture adjusted rotational inertia. Correlation coefficients calculated across all in individuals in the full interspecific sample (31 specimens, 23 species). The original horizontal orientation is so named as it is the standardised mandible orientation used in Chapters 2&3.

Feature	**Original Horizontal Orientation**	**Adjusted Head Posture Orientation**
Spearman's ρ	S = 5756, p = 0.02502; ρ ≈ –0.418 (moderate, significant)	S = 5546, p = 0.05161; ρ ≈ –0.366 (moderate, not significant)
Adjusted R^2	0.14	0.10
Parametric p-values	one-tailed p = 0.024; two-tailed p = 0.048	one-tailed p = 0.044; two-tailed p = 0.088
OLS slope	–0.83 (95 % CI: –0.17862 to –0.00009)	–0.82 (95 % CI: –0.17531 to 0.01303)
RMA slope	–0.83 (95 % CI: –0.18931 to –0.00137)	–0.87 (95 % CI: –0.18984 to 0.01345)
Allometry classification / Significance Notes	Slopes' CIs exclude 0 (marginally significant; note rounding to two decimals may include 0)	Slopes' CIs marginally include 0 (marginal significance; small sample size limits power)

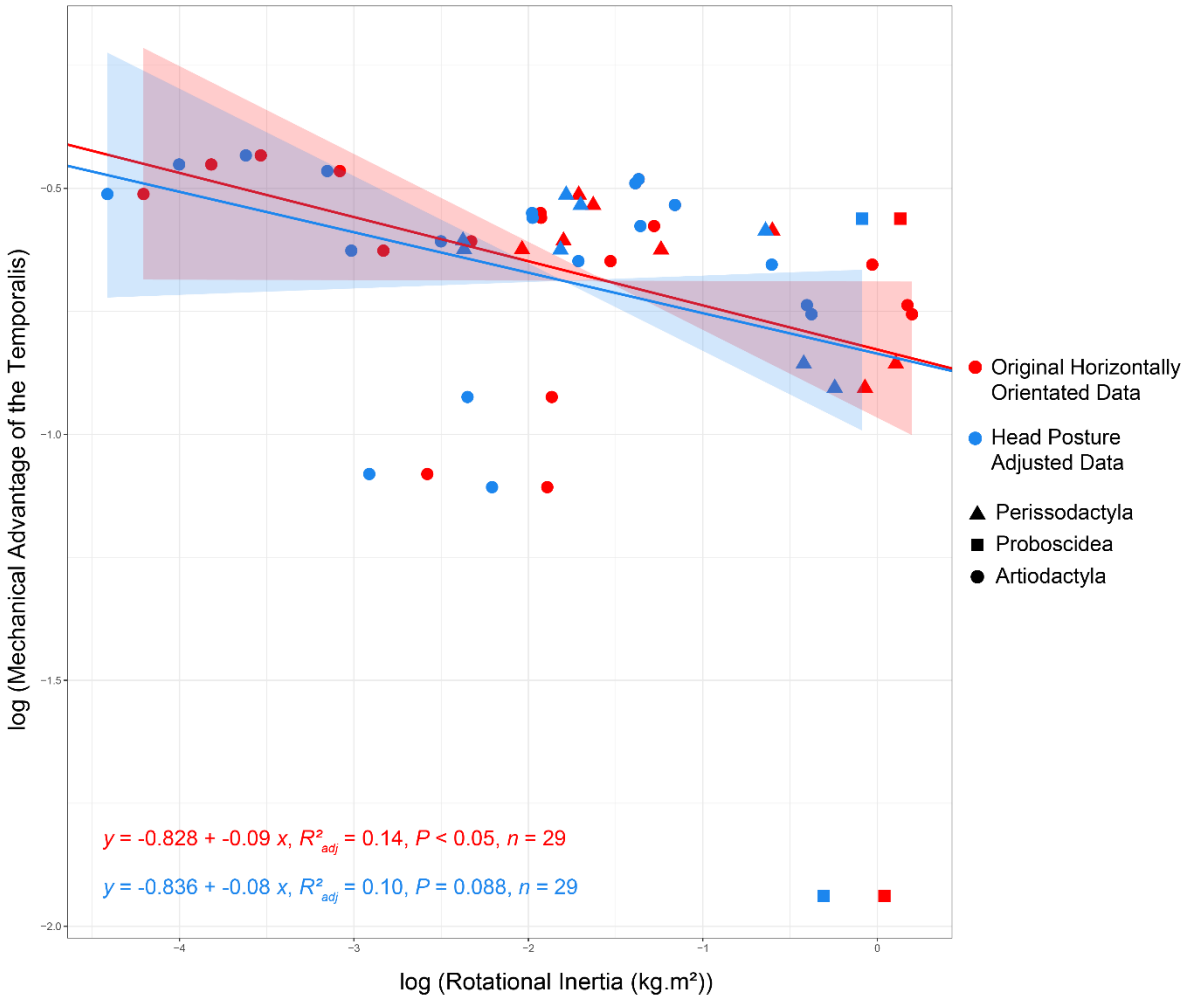

Figure 4.8. Relationship between log-transformed mechanical advantage of the temporalis and log-transformed rotational inertia for the original horizontally oriented and head posture adjusted datasets as evidenced by Ordinary Least Squares (OLS) regression. Red symbols and regression line represent the original horizontally oriented data; blue symbols and regression line represent the head-posture-adjusted data. Shaded areas indicate 95% confidence intervals. Shapes denote taxonomic groups: triangles = Perissodactyla, squares = Proboscidea, and circles = Artiodactyla.

4.5.6 Results 6 – Changes in Centre of Mass

The relationship between mandible length and the change in centre of mass (CoM) distance between the original horizontally oriented and head posture–adjusted datasets was examined by assessing both absolute (Figure 4.9) and proportional (Figure 4.10) differences. Data points were grouped by taxonomic affiliation (Artiodactyla, Perissodactyla, Proboscidea) and labelled with feeding ecology (grazer, browser, mixed feeder, frugivore).

The absolute change in CoM distance increased approximately linearly with mandible length (Figure 4.9), although substantial scatter was observed, largely attributable to differences in feeding ecology. As expected, long-mandibled grazers, whether artiodactyl or perissodactyl, exhibited the largest absolute shifts (approximately 0.15 m), reflecting greater anterior displacement of the CoM when the head was inclined downward from the horizontal. In contrast, the single frugivore specimen clustered with short-mandibled taxa of all feeding types at the lower end of the range, while browsers with intermediate or long mandibles consistently exhibited smaller shifts than predicted by the regression. Generalist feeders spanned short to intermediate mandible lengths but deviated widely both above and below the fitted line. Mixed-feeding proboscideans were largely contained within the 95% confidence interval of the OLS regression.

These patterns indicate that broad dietary classifications account for only part of the variation in posture-related CoM shifts. For instance, grazing perissodactyls occurred at both the high and low extremes of the distribution, and several artiodactyl generalists also deviated in both directions. Such variation suggests that finer-scale morphological and behavioural traits, beyond categorical labels such as grazer, browser, or generalist, influence how mandible length and feeding strategy interact to determine changes in CoM. Feeding ecology therefore appears to exert a stronger influence on posture-related shifts in CoM than either mandible length or taxonomy alone. Further investigation incorporating more detailed ecological and functional classifications may better capture these relationships.

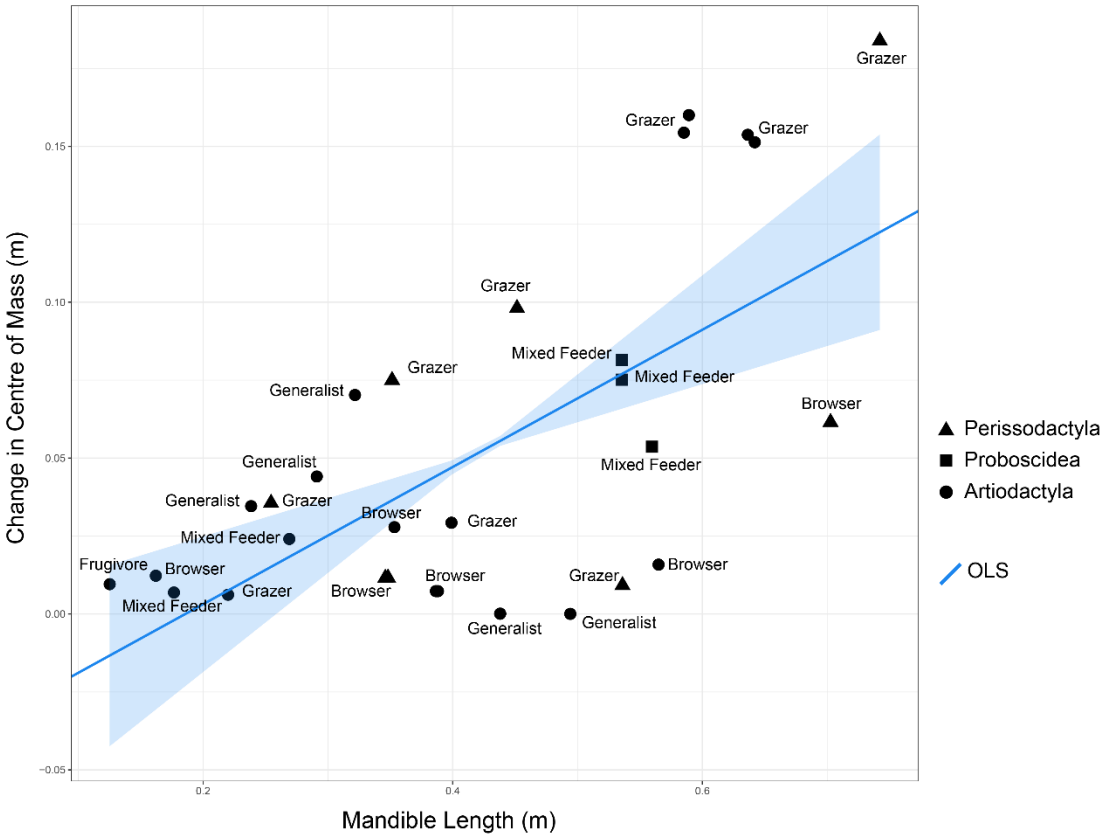

Figure 4.9. Relationship between mandible length and absolute change in centre of mass following adjustment for neutral head posture (n = 29). The blue line represents the ordinary least squares (OLS) regression with a 95% confidence interval (shaded area). Points represent the shift in centre of mass after adjustment for each species (Change in Centre of Mass = Horizontally Orientated CoM – Adjusted CoM). Points are differentiated by taxonomic group (triangles = Perissodactyla, squares = Proboscidea, circles = Artiodactyla) and labelled by feeding ecology (i.e., grazer, browser, mixed feeder, generalist, frugivore).

Proportional change in centre of mass (expressed as a percentage of the original horizontal COM) increases with mandible length (Figure 4.10), though wide confidence intervals demonstrate a high degree of uncertainty and mirror the pattern observed in the absolute COM-shift plot (Fig. 9). This trend is more strongly modulated by feeding ecology and taxonomy than by mandible length alone. Grazers cluster in the upper-central and upper-right regions, exhibiting the largest proportional shifts, likely due to a combination of elongate mandibles and habitual head-down posture. Mixed feeders adhere most closely to the overall scaling trend, reflecting an intermediate head posture between grazing and browsing. Browsers show smaller proportional changes, especially at intermediate mandible lengths, while generalists are widely

scattered (from minimal to large shifts) implying that this broad category masks underlying functional and morphological diversity. The single frugivore, possessing the shortest mandible, falls within the confidence interval, but sample limitations (n = 1) preclude broader inference for frugivores.

At the clade level, both artiodactyl and perissodactyl grazers display the highest relative COM shifts, underscoring the overriding influence of diet and feeding strategy over phylogeny. Artiodactyls span the greatest range of mandible lengths and proportional COM changes, highlighting their morphological and ecological diversity. The brachygnathic mixed-feeding proboscideans also conform closely to the linear trend, reinforcing the link between mandible morphology, feeding ecology, and head posture induced CoM displacement.

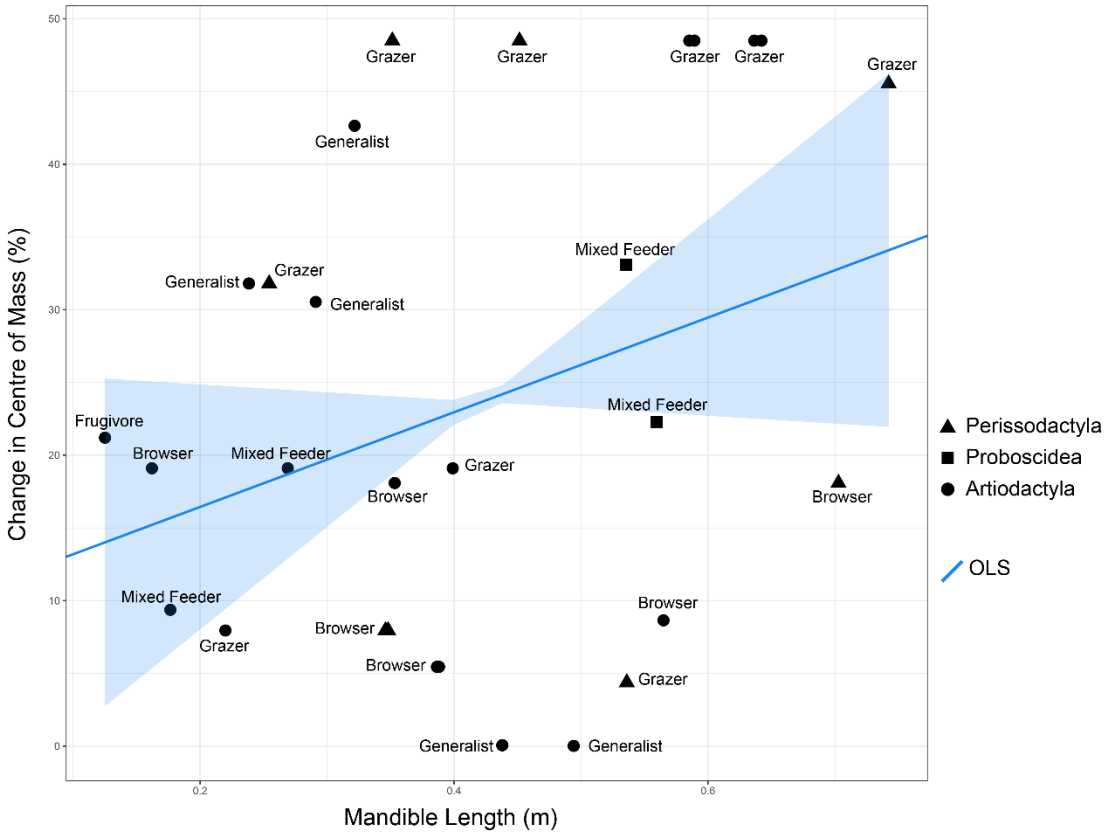

Figure 4.10. Relationship between mandible length and absolute change in centre of mass following adjustment for neutral head posture (n = 29). The blue line represents the ordinary least squares (OLS) regression with a 95% confidence interval (shaded area). Points represent the shift in centre of mass after adjustment as a proportion of the horizontal centre of mass value (Proportional Change in Centre of Mass = ((Horizontally Orientated CoM – Adjusted CoM) / Horizontally Orientated CoM)*100). Points are differentiated by taxonomic group (triangles = Perissodactyla, squares = Proboscidea, circles = Artiodactyla) and labelled by feeding ecology (i.e., grazer, browser, mixed feeder, generalist, frugivore).

4.5.7 Results 7 – Changes in Rotational Inertia

The relationship between mandible length and the change in mandibular rotational inertia between the original horizontally oriented and head posture–adjusted datasets was examined by assessing both absolute (Figure 4.11) and proportional (Figure 4.12) differences. Data points were grouped by taxonomic affiliation (Artiodactyla, Perissodactyla, Proboscidea) and feeding ecology (grazer, browser, mixed feeder, frugivore, generalist).

Short- to medium-mandibled artiodactyls and perissodactyls (mandible length ≈ 0.2–0.5 m) clustered near Δ(rotational inertia) = 0, indicating that smaller browsers, frugivores, generalists, and grazers experience negligible change in rotational inertia due to head posture adjustment. In contrast, mixed-feeding proboscideans (mandible length ≈ 0.55 m) exhibited reductions of approximately 0.5–0.7 kg·m^2, considerably greater than any artiodactyl or perissodactyl of similar jaw length. Their massive mandibles, and correspondingly high rotational inertia, result in greater absolute reductions even with moderate downward head inclination and a proportionally short mandible. These taxa plot above both the ordinary least squares (OLS) regression and exponential trend lines, suggesting they experience greater than predicted reductions in rotational inertia for their mandible length.

Grazers predominantly occupy the upper right region of the plots, consistent with their long mandibles and downward head orientation adapted for ground-level grazing. The longest-jawed grazers (i.e., *Hippopotamus amphibius*, *Ceratotherium simum*) exhibit the greatest absolute reductions in rotational inertia, reflecting their large, elongate mandibles, anteriorly positioned centres of mass, and head-down feeding posture. Among browsers, *Diceros bicornis* (the black rhinoceros) displays the greatest change in rotational inertia (≈ 0.3 kg·m^2), though this remains markedly lower than that of the grazing *Ceratotherium simum*, the taxa most similar to *Diceros* in terms of mandible morphology and taxonomic affinity.

Overall, neither the linear nor the exponential model fully captures the observed trend. The linear OLS regression describes the general increase in rotational inertia change at shorter to intermediate mandible lengths but underestimates the large reductions observed in the biggest grazers and mixed feeders while overestimating reductions in *Diceros bicornis*. The exponential model remains close to zero for small mandibles, consistent with minimal changes in inertia, and rises sharply beyond approximately 0.5 m, more closely reflecting the pronounced reductions in the largest taxa. However, it overestimates the change observed in the browsing *Diceros bicornis* and fails to capture the unusually high reduction exhibited by the grazing *Hippopotamus amphibius*, which possesses a markedly anteriorly positioned mandible.

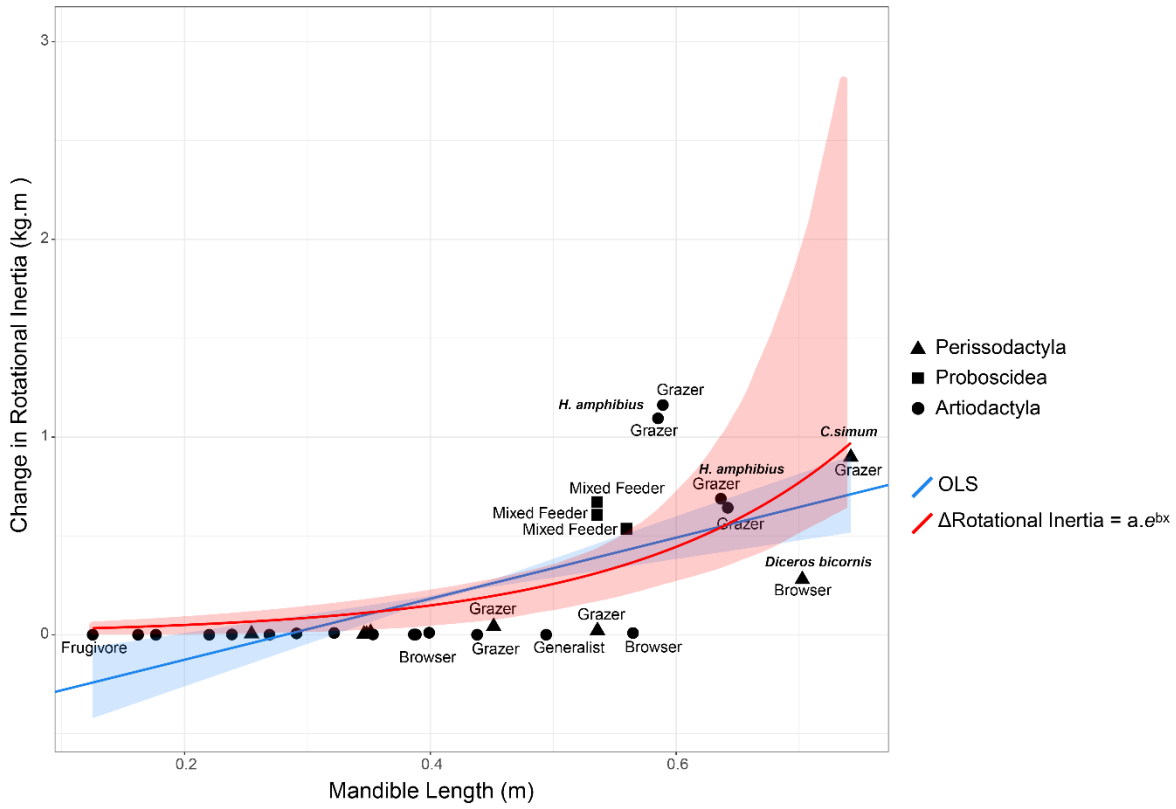

Figure 4.11. Linear regression plot of the change in rotational inertia (kg.m^2), for each species between the original horizontally orientated dataset and the head posture adjusted dataset, on mandible length (m).

Proportional change in rotational inertia (%) exhibits a modest positive trend with mandible length (m), as evidenced by the OLS regression, but this relationship is not tight nor uniform; feeding ecology and phylogeny introduce substantial scatter around that trend (Figure 4.12).

The grazers, which dominate the upper-right and upper-centre, exhibit the greatest change, several exceeding 70%, consistent with their elongate mandibles and pronounced head-down posture. Mixed-feeding proboscideans also incur large reductions, clustering within or just above the OLS confidence band. Browsers, in contrast, cluster near the lower end of the reduction axis; their typically near-horizontal head posture produces minimal change in rotational inertia.

Mixed feeders occupy the mid-range of both mandible length and inertia reduction, closely hugging the regression line. Generalists, however, are scattered across the full spectrum, from almost no reduction to some of the highest, demonstrating that this broad category masks underlying functional and morphological diversity.

While the overall positive slope confirms that longer mandibles tend to benefit more from an anteriorly downward head posture, the wide dispersion, especially the grazers with unexpectedly low reductions and generalists with unexpectedly high ones, emphasizes that feeding ecology and taxon-specific traits exert a stronger influence on inertia correction than mandible length alone. Similarly to the analysis of proportional change in centre of mass, these results underscore the importance of moving beyond coarse dietary classifications (e.g., generalist) and instead utilising higher resolution categorisations to capture the nuanced relationship between mandible form, head posture, and masticatory mechanics in herbivorous mammals.

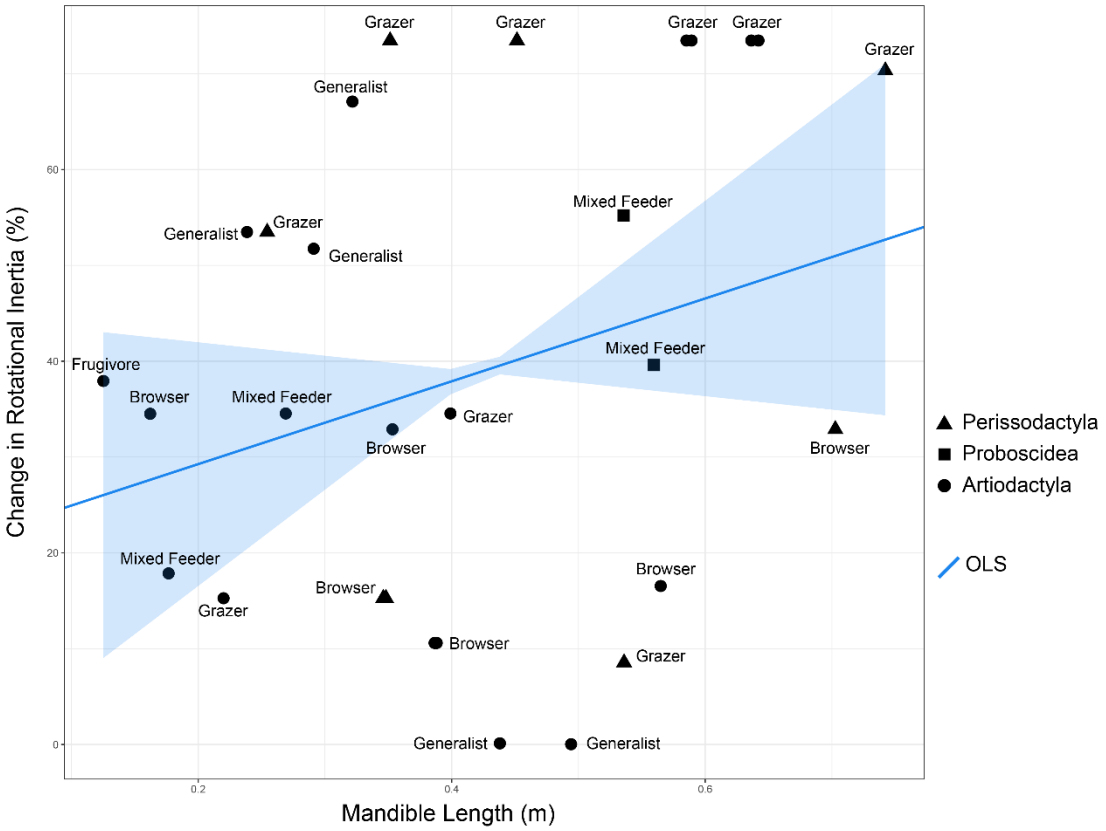

Figure 4.12. Relationship between mandible length and absolute change in rotational inertia following adjustment for neutral head posture (n = 29). The blue line represents the ordinary least squares (OLS) regression with a 95% confidence interval (shaded area). Points represent the shift in centre of mass after adjustment as a proportion of the horizontal centre of mass value (Proportional Change in Centre of Mass = ((Horizontally Orientated CoM – Adjusted CoM) / Horizontally Orientated CoM)*100). Points are differentiated by taxonomic group (triangles = Perissodactyla, squares = Proboscidea, circles = Artiodactyla) and labelled by feeding ecology (i.e., grazer, browser, mixed feeder, generalist, frugivore).

The final figure (Figure 4.13) illustrates the absolute reduction in mandibular rotational inertia for each specimen through a pairwise comparison of values before and after adjustment for head posture. Each pair of points represents a single specimen plotted against mandible length, with symbols denoting taxonomic group and feeding ecology.

A clear size dependent trend is evident: mandibular rotational inertia remains low up to a mandible length of approximately 0.45 m, beyond which a sharp increase occurs. This increase is more gradual in the head posture adjusted dataset. In the original horizontally oriented data, rotational inertia rises from near zero in small-mandibled taxa of all feeding ecologies to approximately 1.1–1.3 $kg \cdot m^2$ in mixed-feeding proboscideans and 1.5–1.8 $kg \cdot m^2$ in large grazers. In contrast, after adjustment for head posture, mixed-feeding proboscideans reach 0.5–0.8 $kg \cdot m^2$, while large grazers do not exceed 0.3–0.4 $kg \cdot m^2$. The largest browser, *Diceros bicornis*, exhibits a value of approximately 0.6 $kg \cdot m^2$, exceeding that of the largest grazers.

These results indicate that the original horizontally aligned model does not accurately reflect the rotational inertia experienced in vivo. Adjusting for head posture substantially improves the physiological relevance of the estimates and is therefore essential for studies examining the scaling of adductor musculature with mandibular mass properties. Head posture adjustment compresses the overall range of rotational inertia, particularly in large grazing taxa, reducing inertia by approximately 70–80% in the largest artiodactyl and perissodactyl species and by 50–60% in proboscideans. By contrast, small taxa, regardless of feeding ecology, show negligible change.

This pattern highlights that the mechanical advantage derived from shifting the mandibular centre of mass closer to the temporomandibular joint is minimal in small mandibles but substantial, and taxon-specific, in large jaws. Grazers, particularly *Hippopotamus amphibius* and *Ceratotherium simum*, exhibit the greatest inertial reduction and thus derive the greatest functional benefit.

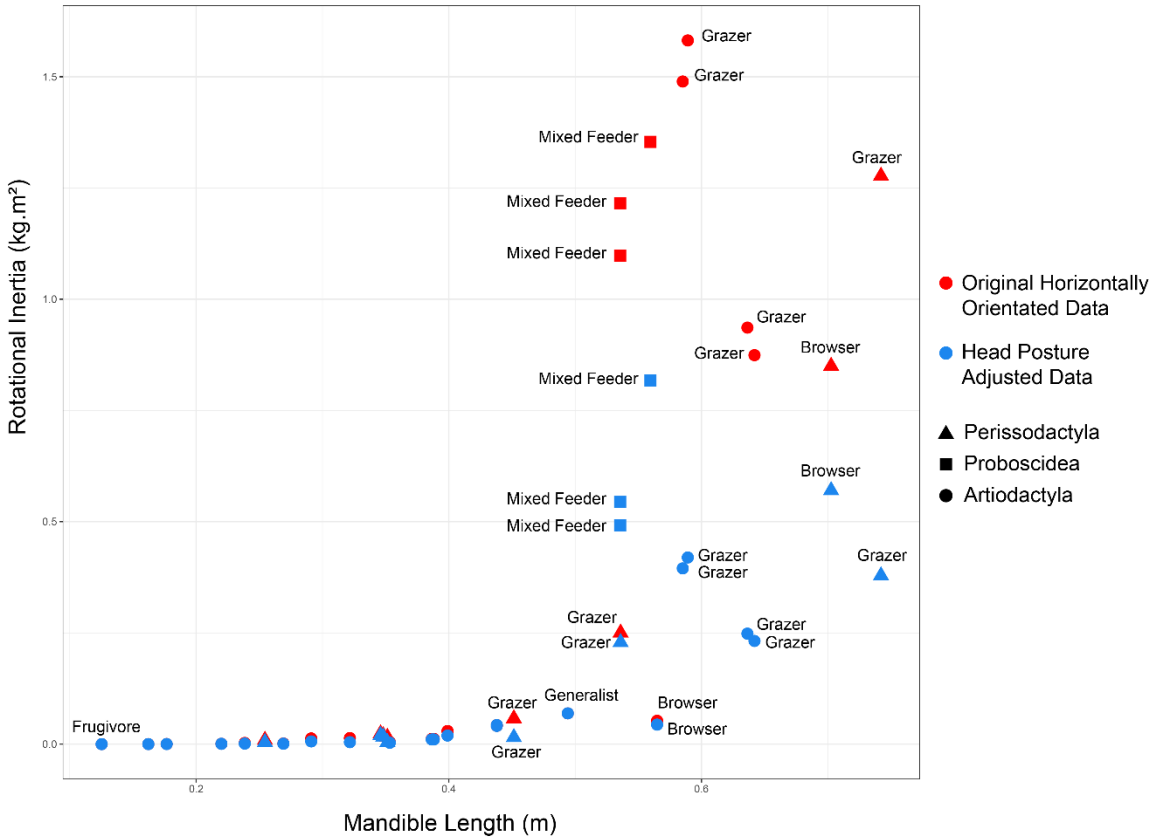

Figure 4.13. Pairwise comparison of mandibular rotational inertia before and after adjustment for neutral head posture, plotted against mandible length. Each specimen is represented by a pair of points: red markers indicate the original horizontally oriented data, and blue markers indicate the head posture adjusted data. Taxonomic groups are differentiated by symbol (triangles = Perissodactyla, squares = Proboscidea, circles = Artiodactyla) and labelled by feeding ecology.

4.5 Discussion

Chapter 3 examined the scaling and covariation of mandibular mass properties with anatomical and mechanical features in ungulate-grade mammals. That analysis employed a standardised horizontal orientation for all specimens, which does not necessarily reflect the habitual head posture maintained during life. The present chapter extended that work by assessing whether variation in head posture, and therefore mandibular orientation, influences effective mandibular mass properties and their scaling with mandible length, masseteric insertion area, and the mechanical advantage of the masseter and temporalis.

It was hypothesised that the anterior downward inclination typical of herbivorous head posture would reduce the effective rotational inertia of the mandible, thereby providing a more realistic estimate of the resistance to angular motion encountered during mastication and jaw closure. This study therefore compared results derived from a subset of the adult interspecific sample employed in Chapter 3, for which head posture data exists in the literature, in two contexts: (1) mandible orientation matches the original horizontal orientation, and (2) mandible orientation was adjusted to account for observed head posture.

4.5.1 Influence of Head Posture on Scaling Relationships

The first hypothesis stated that accounting for in vivo head posture will not alter the direction of relationships among mandibular mass properties and anatomical features (i.e., mandible length, masseteric insertion area) but will alter their scaling rate relative to horizontally oriented models.

The first two predictions of this hypothesis, that mandibular centre of mass and mandibular rotational inertia, and estimated from (1) a model assuming a horizontal mandible and (2) a model adjusted for in vivo head posture are expected to exhibit positive linear relationships with mandible length in both cases, but with lower scaling rates in the head posture adjusted model are supported by this study.

Both the OLS and RMA linear regression of the original data suggest isometric scaling or a tendency towards weak positive allometry, while for the adjusted data, isometric or weak negative allometric scaling is evident. While it cannot be said that an entirely different scaling regime is evident, as the scaling of both datasets is indistinguishable from isometry, the adjusted centre of mass scaling is shallower, with a slope that tends towards negative allometry, rather than the tendency towards positive allometric scaling in the original dataset. Similarly, both the original and adjusted rotational inertia data scale with positive allometry with respect to mandible length, albeit the adjusted rotational inertia scales with a marginally shallower slope. The overall scaling relationships did not change by accounting for head posture when calculating centre of mass and rotational inertia. Both isometric (Mandible Length vs CoM) and positive allometric (Mandible Length vs Rotational Inertia) linear scaling relationships were maintained, though with shallower, but not significantly so, slopes in the adjusted dataset.

The third prediction, that masseteric insertion area will exhibit a positive linear relationship with rotational inertia estimated from (1) a model assuming a horizontal mandible and (2) a model

adjusted for in vivo head posture; however, because rotational inertia is reduced, the scaling rate is expected to be higher in the head posture adjusted model, is not supported by the findings of this study. Both the original and adjusted data scale with positive allometry with respect to mandibular rotational inertia, although the adjusted slope (OLS: 0.40; RMA: 0.41) is marginally higher than the original slope (OLS: 0.41; RMA: 0.44), both are well within their confidence intervals and have no tendency towards positive allometry. This suggests that while mandibular rotational inertia and masseteric insertion area are highly correlated, this correlation does not necessarily imply a causative functional relationship.

4.5.2 Comparative Strength of Mass Property-Anatomy Correlations

The second hypothesis presented in this chapter stated that accounting for in-vivo head posture will better explain the relationships between jaw anatomy (i.e., mandible length, masseteric insertion area) and its mass properties, in terms of a stronger linear association as indicated by correlation coefficients, than the previously used horizontally orientated model

The first prediction, that pairwise comparison of correlation coefficients will show the head postured adjusted metrics (centre of mass, rotational inertia) will be more highly correlated with the anatomical metrics (mandible length, masseter insertion area) than those from the original horizontally orientated dataset, is refuted.

Both the original and adjusted centre of mass data show very strong positive linear associations with mandible length, though the original data marginally surpasses the adjusted data (Pearson's r – Original: 0.955, Adjusted: 0.947; Variance Explained – Original 91%, Adjusted 90%). In practical terms, both datasets perform essentially identically, and the slight difference may be explained by the smaller sample size of the adjusted dataset.

Both the original and adjusted rotational inertia data show extremely tight monotonic and linear scaling with mandible length. The strength of the monotonic association is slightly higher in the original data (Original: 0.92, Adjusted: 0.91), while slightly more of the variance in the linear relationship is explained by the adjusted data (Original: 91%, Adjusted: 92%). These associations are equally strong and practically indistinguishable.

While the masseter attachment area demonstrates isometric scaling with rotational inertia, the original horizontally orientated data has a marginally closer linear fit (Pearson's r – Original: 0.97, Adjusted: 0.96; Variance Explained – Original 95%, Adjusted 92%). Once again, in practical

terms, the association between both the original and adjusted data with the masseter insertion area is virtually identical.

The second prediction, that no significant correlation is expected between (1) mechanical advantage of the masseter and (2) mechanical advantage of the temporalis with rotational inertia calculated from either orientation, is also not supported by this study.

Horizontally orientated rotational inertia show a small but statistically significant monotonic association with MAM while the adjusted data show a weaker, non-significant association (Spearman's ρ – Original: 0.423, Adjusted: 0.336). Similarly, the linear models evidence equally poor relationships (Variance Explained – Original 8%, Adjusted 5%), both with slopes indicating no linear scaling relationships (OLS and RMA slopes ≈ 0.02 with 95 % CIs including zero). Taken together, the original data captures any subtle relationship with rotational inertia and MAM slightly better than the adjusted data, but neither dataset provides evidence for any substantial relationship.

The original horizontally orientated rotational inertia data exhibits a moderate negative monotonic relationship with MAT while the relationship between the adjusted data and MAT is a weaker, non-significant monotonic relationship (Spearman's ρ – Original: -0.418, Adjusted: -0.336). The linear models evidence a similar poor fit, with the original data explaining moderately more of the variance than the adjusted (Variance Explained – Original 14%, Adjusted 10%), and a marginally significant negative relationship in the original data with a confidence interval that barely excludes 0, and a non-significant negative relationship for the adjusted data with the confidence interval including 0 (OLS/RMA – Original: -0.83/-0.83, Adjusted: -0.82/-0.87). While both datasets hint at a weak negative scaling of MAT with rotational inertia, the original slightly more so than the adjusted, the evidence is not robust.

Overall, this hypothesis is not supported by the findings of these analyses. There is no evidence to suggest that adjusting mass property calculations to account for in vivo head postures appreciably affect how these metrics scale with mandibular anatomy. As such, future studies may reduce the data collection and processing time by not having to collect and account for head posture, and therefore mandible orientation, and by validating the use of a standard orientation of the mandible during calculation, allowing for a more streamlined and easily automated data collection. In biological terms, the implication is therefore that head posture does not influence adaptation towards a particular mechanical arrangement, or vice versa; moreover, it seems both features are the consequence of adaptation towards a particular diet and feeding strategy.

4.5.3 Influence of Size and Feeding Ecology

The third hypothesis stated the reduction in mandibular rotational inertia achieved through head posture adjustment is primarily associated with mandible size, rather than taxonomic or dietary grouping.

The first prediction underlying this hypothesis, the absolute and proportional reduction in centre of mass distance and mandibular rotational inertia due to head posture angle increases with increasing mandible length across all taxonomic groups and feeding ecologies, is supported. However, the second prediction, that residual variation in these reductions will not differ significantly among taxonomic or dietary groups, is not supported.

While the reduction in rotational inertia is primarily associated with mandible size, there are substantial nonlinearities associated with dietary diversity. Further investigation the future is warranted to provide clarity.

The analysis of the absolute and proportional change in mass properties from a horizontal orientation to the in vivo head posture of the taxon reveals that accounting for head posture profoundly alters our understanding of how mandible form impacts both the centre of mass and rotational inertia across large herbivores. These comparisons demonstrate consistent positive relationships between mandible length and both absolute and proportional changes, yet with pronounced nonlinearities and strong modulation owing to differences in feeding ecology and taxonomic grouping; artiodactyls and perissodactyls differ from proboscideans, and grazers experience the most substantial reductions, followed by mixed feeders, and finally browsers. Generalist was found to be too broad of a category for meaningful interpretations to be made.

These findings highlight the necessity of incorporating head posture into functional morphology studies of ungulate-grade, and particular herbivorous, mastication. Ignoring the compensatory effect of head posture would overlook the fact that downward-angled head positions can mitigate up to 70-80% of the mechanical penalty imposed by heavy, elongate mandibles. Conversely, small mandibles derive negligible benefit, indicating an ecological threshold (approximately 0.45 m) beyond which head posture becomes mechanically important.

4.5.4 Conclusions and Implications for Future Work

Calculating the centre of mass and rotational inertia while accounting for habitual head posture produces marginal differences in scaling rates. However, the original horizontally oriented dataset exhibits slightly stronger correlations with mandible length and masseteric insertion

area than the head posture adjusted dataset. Neither the mechanical advantage of the masseter nor that of the temporalis demonstrates a significant linear relationship with mandibular rotational inertia. These results suggest that adaptation of the adductor musculature is not strongly influenced by the force required to overcome mandibular rotational inertia, whether in the habitual resting posture or in a horizontal orientation.

As this study included only the mineralised components of the mandible, the calculated rotational inertia values are lower than would be expected if the mass of soft tissues (e.g., adductor muscles, tongue, mylohyoid) were considered. This limitation reflects methodological constraints, available facilities, and sample size considerations. Future research incorporating detailed soft tissue data through dissection or virtual modelling would improve the accuracy of these estimates, although such approaches would likely require smaller sample sizes.

Despite the limited predictive difference between datasets, the findings demonstrate that a downward head posture substantially reduces rotational inertia in long and heavy mandibles. The magnitude of this reduction varies among ecological groups: it is greatest in grazers, moderate in mixed feeders, and least in browsers. Given that large herbivores spend a significant proportion of their time feeding and chewing, even modest reductions in rotational inertia could yield considerable cumulative energy savings.

Although head posture and associated mandibular orientation do not appear to be primary determinants of mandibular or masticatory morphology, they may act as one element within a broader suite of taxonomic, anatomical, and ecological adaptations influencing feeding mechanics.

This study is limited by a small sample size (n = 31), the inclusion of only one frugivorous taxon, and reliance on two-dimensional measurements of mass properties. Future investigations should employ three-dimensional musculoskeletal models that incorporate soft tissue anatomy and expand taxonomic and ecological coverage, particularly among frugivores, browsers, and mixed feeders. Expanding the representation of large-bodied taxa remains constrained by the limited number of extant species; however, this study includes the largest living browsers (*Diceros bicornis*, *Giraffa* sp.), mixed feeders, and two of the three extant proboscideans (*Elephas maximus*, *Loxodonta africana*), as well as major grazing taxa (*Ceratotherium simum*, *Rhinoceros unicornis*, *Hippopotamus amphibius*).

In summary, incorporating habitual head posture refines estimates of mandibular mass properties but does not substantially alter their scaling with anatomical or mechanical metrics.

The compensatory effect of an anteriorly downward head posture provides meaningful energetic advantages in large grazing taxa, yet appears to operate as part of a broader complex of morphofunctional and ecological adaptations rather than as an independent driver of mandible morphology.

5: Mandibular Mass Distribution in Cenozoic Megafaunal Ungulate-Grade Mammals

5.1 Introduction

5.1.1 Conceptual Context

The mechanics of the mandible are central to understanding the feeding biology of large terrestrial herbivores. The distribution of mass within the mandible influences its rotational inertia, which in turn affects the energetic costs of mastication and the functional demands placed on the masticatory musculature. This chapter builds on the methodological and comparative findings of the previous three chapters. Chapter 2, *Determinants of the Mass Distribution of Mineralised Tissues in the Mammal Mandible and Assessing Methods for Estimation of Mass Properties*, established that mass property estimates derived from surface scans are as reliable as those obtained using computed tomography or the compound scales method, thereby enabling analyses of specimens which were otherwise inaccessible, either due to size restrictions in conventional scanners, administrative or practical considerations surrounding the transportation of specimens, or were only available in museums as casts of the osteological specimen. Chapter 3, *Biological and Mechanical Implications of Mandibular Mass Distribution in Terrestrial Mammalian Herbivores (Orders Artiodactyla, Perissodactyla, Proboscidea*), examined scaling relationships between mandibular mass properties and masticatory anatomy in extant ungulate-grade herbivores, identifying both isometric and allometric patterns that relate to diet and body size. Chapter 4, *Habitual Head Posture and Associated Behaviours as Adaptations to Mitigate the Mechanical Effects of Mandible Mass Distribution,* extended this analysis by accounting for habitual head posture, showing that relatively small changes in mandible orientation can reduce the mechanical costs of mastication in large-bodied taxa. While these findings establish a framework for analysing mandibular mechanics, they also highlight key limitations. The reliance on extant species constrains the scope of inference, as living herbivores represent only a narrow subset of the morphological, ecological, and phylogenetic diversity of their clades. This chapter addresses these limitations by incorporating fossil taxa in order to evaluate whether the scaling trends observed in modern species reflect general biomechanical principles or are artefacts of restricted sampling.

5.1.2 Limitation of Extant Samples

Although previous chapters established scaling relationships between mandibular mass properties, masticatory anatomy, and body size in extant herbivorous mammals, these findings remain limited by the scope of the available sample. Modern terrestrial herbivores represent only a narrow phylogenetic distribution, being largely restricted to artiodactyls, perissodactyls, and proboscideans, and therefore capture only a fraction of the morphological and ecological diversity once present among large herbivores. Extinct relatives of these clades exhibited far more extreme mandibular morphologies and a wider range of dietary strategies, often at body sizes without modern analogues such as the mandibular-tusked proboscideans such as *Gomphotherium*, *Zygolophodon*, and *Deinotherium*, the giant browsing rhinocerotoid *Paraceratherium*, and specialised grazing proboscideans such as *Mammuthus*.

A major limitation of the previous dataset lies in the range and distribution of body size. Among extant taxa there is a pronounced gap between species that reach a maximum body mass of approximately 1,400kg, such as *Giraffa camelopardalis* (mean = 1,174kg) (Hall-Martin et al., 1977), and much larger giants that can exceed several tonnes. These include *Rhinoceros unicornis* (Indian rhinoceros; mean = 1,600–2,200kg, maximum = 4,000kg) (Laurie et al., 1983), *Diceros bicornis* (black rhinoceros; mean = 1,400kg, maximum = 2,896kg) (Mallet et al., 2020), *Ceratotherium simum* (white rhinoceros; mean = 2,000–300kg, maximum = 3,600kg) (Owen-Smith, 1988), *Hippopotamus amphibius* (common hippopotamus; mean = 1,480kg, maximum = 2,660kg) (Martínez-Navarro et al., 2010), *Elephas maximus* (Asian elephant; mean = 3,000–7,000 kg) (Larramendi, 2016), and *Loxodonta africana* (African bush elephant; mean = 5,200–6,900kg, maximum = 10,400kg) (Larramendi, 2016). Recent extinct relatives of these taxa extend this pattern of gigantism further. For instance, *Hippopotamus antiquus*, may have reached twice the mass of the extant common hippopotamus and likely differed in diet a with preference for aquatic vegetation (Adams, Candy, and Schreve, 2022).

To address this issue, the present study incorporates fossil taxa to expand the range of body size, mandibular morphology, and dietary strategies represented in the analysis. This approach allows for a more comprehensive test of whether extant patterns reflect general principles of mastication mechanics in large terrestrial herbivores or are biased by limited phylogenetic and morphological sampling.

5.1.3 Expanding Morphological, Functional, and Phylogenetic Diversity

To test whether the scaling patterns identified in extant ungulate-grade mammals represent universal biomechanical constraints or are restricted to particular placental lineages, this study incorporates extinct representatives of the extant ungulate-grade mammal clades (Artiodactyla, Perissodactyla, Proboscidea), several extinct ungulate-grade orders (Dinocerata, Notoungulata, Litopterna, Pyrotheria, Embrithopoda) a small number of phylogenetically distant but ecologically analogous taxa (Cingulata, Pilosa, Diprotodontia) (Figure 5.1). These additions broaden the phylogenetic scope of the dataset while maintaining focus on large-bodied terrestrial herbivores with broadly comparable feeding strategies.

5.1.3.1 Ungulata

The term ungulate has a long and often contentious history in mammalogy, traditionally referring to hoof-bearing mammals. The formerly used taxon Ungulata referred to a monophyletic clade which encompassed all hooved mammals, including the artiodactyls, perissodacyls, as well as the paenungulates (i.e., proboscideans, hyracoids, and sirenians), as well as various extinct orders (Janis, 2008).

Modern phylogenetic analyses have revealed that this clade is no monophyletic but instead a polyphyletic grade defined by shared ecomorphology rather than common ancestry (Janis, 2008; Gheerbrand and Tassy, 2009; Asher, Bennet, and Lehmann, 2009). As such, the term ungulate is best understood as an ecomorphological term rather than a formal phylogenetic clade. This thesis uses the term “ungulate-grade”, with the qualifier “-grade”, added to acknowledge that this grouping is ecomorphological rather than phylogenetic, rather the more traditional polyphyletic usage of “ungulate”.

Phylogenetic, the extant ungulates are constrained to the Artiodactyla and Perissodactyla. Beyond these orders, a number of extant and extinct lineages are traditionally referred to as ungulates. These include the Afrotherian clades Proboscidea, Hyracoidea, and the extinct Embrithopoda (Gheerbrant, 2009; Gheerbrant and Tassy, 2009). However, molecular and morphological phylogenetic analyses have demonstrated their ecomorphological similarities to the true ungulates are due to convergent evolution rather than due to common descent (Gheerbrant, 2009; Janis, 2008; Asher, Bennet, and Lehman, 2009).

The South American Native Ungulates, including the orders Notoungulata, Litopterna, and Pyrotheria, represent another potentially independent radiation of ungulate-grade animals,

though the taxonomic affinities of the notoungulates and pyrotheres remains contentious. These groups occupied herbivorous niches equivalent to those of true ungulates, evolving a similar suite of locomotor and dental adaptations (Cassini et al., 2017; Püschel et al., 2022). Phylogenomic and palaeoproteomic analyses have recently placed Notoungulata and Litopterna within Laurasiatheria, most closely related to Perissodactyla (Buckley, 2015; Welker et al., 2015) or along with Pyrotheria forming a sister-clade to Artiodactyla (de Muzion et al., 2015). Regardless of their exact taxonomic affinity, these orders demonstrate typical ungulate-grade traits such (i) limb elongation and reduction of distal digits for cursorial movement, (ii) development of hooves for stability and energy-efficient locomotion, and (iii) specialised dentition with complex occlusal surfaces for grinding vegetation (Janis, 2008; Fortelius, 1985; Schultz et al., 2020); Casini et al., 2017.

The Dinocerata, also known as uintatheres, were a lineage of large-bodied herbivores that occupied North American and Asian ecosystem during the early and middle Eocene (Burger, 2015; Schoch and Lucas, 1985). Characterised by massive, graviportal post-cranial skeletons adapted for supporting large body mass, elongate skulls with bony protuberances, and deep bodied, robust mandible with broad and heavily fuses symphysis (Shoch and Lucas, 1985; Burger, 2015), these animals were morphologically and, likely ecologically, comparable to large rhinocerotids. The combination of large attachment areas for masticatory musculature, a structural robust and rigid mandible, and bilophodont dentition (Shoch and Lucas, 1985) suggest uintathere processed fibrous vegetation similarly to true ungulates and meridiungulates reinforcing the notion that these are ecologically and morphofunctionally analogous groups.

The Embrithopoda were an order of large-bodies herbivores that superficially resembled rhinocerotids known from the Eocene and Oligocene of Africa and Asia, though the biogeography of their origins is uncertain (Erdal, Antoine, and Sen, 2016; Gheerant, Schmitt, and Kocsis, 2018). Although most species are known from dental remains, *Arsinioitherium ziletti*, perhaps the most well-known representative, evidences convergent evolution towards an ungulate-grade morphology. Embrithopods are now recognised as relatives of the proboscideans within Afrotheria, but share many of the postcranial skeletal and dental adaptations typical of true ungulates such as rigid mandible and complex (Gheerbrant, 2009; Gheerbrand and Tassy, 2009)

5.1.3.2 Diprotodontia

The extinct marsupial *Diprotodon* is included as an outgroup representative of giant herbivores outside Placentalia. As the largest known marsupial, with body mass estimates of up to 3,500kg, *Diprotodon* converged with placental grazers in both size and mandibular anatomy but exhibited mechanically distinct mastication. As in most grazers, *Diprotodon* had a prominent masseter, but likely had a large temporalis compared to its lateral pterygoid which would have limited transverse movement of the mandible, suggesting a crushing rather than grinding bite at the molars. The masseteric insertion is large, attaching to the entire postero-ventral surface of the angle of the mandible and the lateral surface of the horizontal ramus, and lies anterior to the orbits, allowing for a high degree of control of the incisors. Like other diprotodontids, the molar teeth are bilophodont and the single pair of lower incisors are rootless and grow continuously during life. Based on interpretations of isotype analyses (Gröcke, 2017) and tooth morphology, *Diprotodon* likely had a mixed feeding diet, capable of changing its diet to align with the environment conditions. Being the most phylogenetically distant taxon in the data set with a functionally distinct but morphologically comparable masticatory apparatus to from the ungulate-grade placentals, *Diprotodon* provides an outgroup useful in investigating if the scaling relationships between mass properties and functional metrics are ubiquitous, or if a different mandible morphology results in an appreciably different functional arrangement (Sharp, 2014). Its inclusion provides a test of whether scaling relationships in mandibular mass properties are conserved across deep evolutionary divergences or whether distinct morphologies, such as those found in marsupials, produce fundamentally different relationships between mandibular mass properties and masticatory function.

5.1.3.3 Xenarthra – Cingulata and Pilosa

Xenarthrans, another distinct superorder within Eutheria, comprising orders such as Cingulata (armadillos) and Pilosa (anteaters and sloths), provide an additional set of ecological and morphological contrasts. Genera such as *Glyptodon*, *Megatherium*, and *Scelidotherium* represent large-bodied herbivores that differ markedly from ungulate-grade mammals in dentition and mandibular construction. Their enamel-less, osteodentine hypselodont teeth and distinctive jaw mechanics (Bargo et al., 2000) offer a test of whether the trends observed in ungulate-grade taxa are general features of mammalian herbivores or are contingent on specific dental and mandibular anatomies.

Megatherium (3,700–4,000kg) and *Scelidotherium* (850kg), giant ground sloths dating from Early Pliocene to the Late Pleistocene, exhibited mandible morphologies and feeding strategies distinct from true ungulates. Both genera possessed deep, robust jaws with fused symphyses, though *Scelidotherium* was more the more gracile of the two, that provided rigidity and broad areas for the attachment of powerful jaw adductor muscles, particularly the masseter and temporalis. While ungulates typically exhibit heterodonty and transverse jaw movements that enable efficient grinding of fibrous vegetation, *Megatherium* and *Scelidotherium* were adapted primarily for vertical shearing and crushing, with limited lateral movement of the mandible.

Glyptodon, a genus of large-bodied, quadrupedal, and herbivorous armadillo species (400–2,000kg) originated in the Pliocene, approximately 3.2Ma, and died out at the end Pleistocene, approximately 11kya. Glyptodont dentition is among the most extreme examples of hypsodonty known in terrestrial mammals. The post-Miocene glyptodontines were bulk feeders, as in they consume the entire plant rather than simply leaves or stem. Due to their body form, with the head close to the ground and fused cervical vertebrae, glyptodontines would obligately have foraged close to the ground. This, along with their extremely hypsodont molars, indicates a heavy grazing diet. Their craniomandibular joint limited lateral jaw movement, though large osteodentine ridges would have been effective in grinding food material (Bargo et al, 2009.), and the mandible is robust, designed to withstand significant forces during mastication (Casini et al. 2012), suggesting a diet composed of tough vegetation. The TMJ is located well above the tooth row, with the highest ratio of TMJ-height-to-skull-length recorded in mammals. Glyptodonts, despite have some analogous features with ungulates, also differ by their unique evolutionary adaptations, such as its unusual dental morphology and lack of enamel, and unusual mechanical set up of the TMJ and leverages.

By including these outgroup taxa, the analysis can assess whether observed mass property scaling patterns are restricted to ungulate-grade placentals or represent broader, more foundational features of mammalian herbivory.

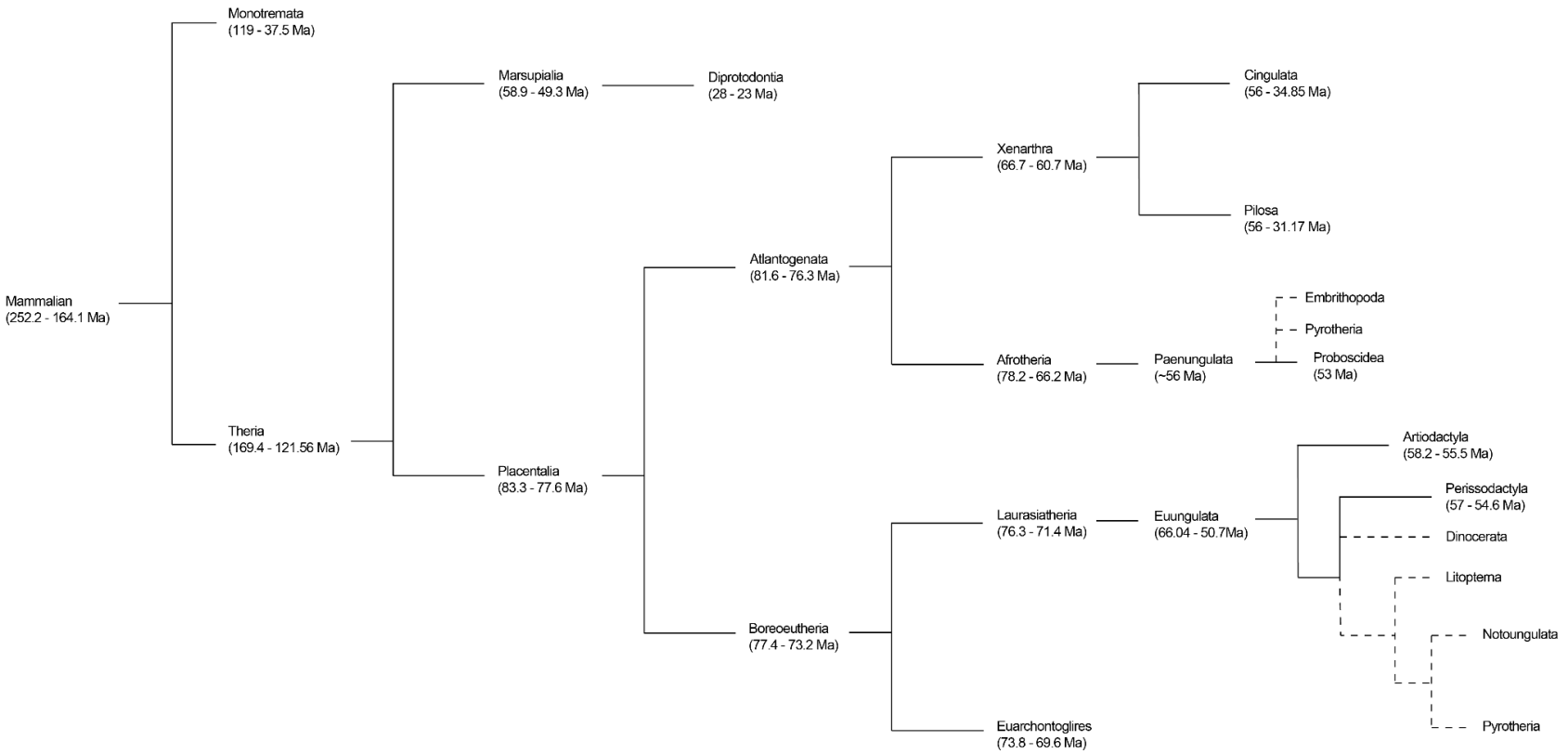

Figure 5.1. Cladogram of order-level taxonomy with divergence times for total dataset. Dashed lines represent phylogenetic relationships which are currently unresolved or contentious. Major clades and divergence times are taken from Álvarez-Carretero et al. (2021). The taxonomic affinities of Dinocerata (Shoch and Lucas, 1985; Burger, 2015). Embrithopoda within Paenungulata from Gheerbrandt, Schmitt, and Kocsis (2018).Notoungulata, Pyrotheria, Litopterna affinities with Artiodactyla and Perissodactyla from de Muizon et al. (2015), Welker et al. (2015), and Buckley (2015).

5.1.4 Clade-specific case studies: Rhinocerotoidea and Proboscidea

Rhinocerotoids and proboscideans are emphasised in this study because they exemplify both the extremes of body size and the loss of diversity through extinction. Each clade today is reduced to a handful of species, yet their fossil record demonstrates much greater disparity in mandible form and function. Analysing these groups provides a means to test whether extant taxa share mechanical traits that distinguish them from their extinct relatives, and whether scaling patterns observed in earlier chapters are evident across their full evolutionary and morphological diversity.

5.1.4.1 Rhinocerotoidea

The extant rhinoceroses represent only a small remnant of a once highly diverse radiation. Today, five species remain, divided among three lineages (the African rhinos *Ceratotherium* and *Diceros*; the Asian genera *Rhinoceros* and *Dicerorhinus*; and the Sumatran rhino as the sole survivor of its tribe). These species span a range of ecologies, from specialised grazers to selective browsers, and they inhabit contrasting environments across Africa and Asia. Their survival indicates ecological flexibility, yet their mandibles represent only a fraction of the functional disparity that characterised rhinocerotoids in the past.

Arising during the Palaeocene, fossil rhinocerotoids demonstrate far greater extremes in body size, morphology, and dietary specialisation than their extant relatives. The gigantic *Paraceratherium* reached body masses more than 9,000kg, making it one of the largest terrestrial mammals known. Other lineages, such as the elasmotheres, evolved hypsodont dentition and grazing adaptations, while *Teleoceras* and related taxa exhibited short, robust limbed morphologies no longer present in living species. Many of these lineages disappeared during intervals of environmental change, particularly following the Middle Miocene Climatic Optimum and the Late Pleistocene megafaunal extinctions.

The phylogeny of the superfamily Rhinocerotoidea (Figure 5.2) illustrates the past diversity of this clade throughout the Cenozoic (Prothero, 2005; Kosintsev et al., 2019; Bai et al., 2020; Liu et al., 2021; Deng et al., 2021). Members of the Paracerathiinae, such as the browsing *Paraceratherium bugtiense,* with an estimated body mass of 9,112kg, is well in excess of any extant rhinocerotoid, while others such as the recently described *Dzungariotherium* sp. may have weighed as much as 20,558kg, which makes it a contender for the largest terrestrial mammal of all time and is only rivalled by the largest proboscideans (e.g., *Palaeoloxodon namadicus*). The subfamily Aceratheriinae is represented here by *Teleoceras* and *Chilotherium*.

Teleoceras aepysoma and *Teleoceras fossiger* (Prothero, 2005) and *Chilotherium schosseri* (Cerdeno, 1998) are similar in size to the extant *Diceros bicornis* and *Ceratotherium simum* but are differentiated by their shorter statue and lack of nasal or frontal horns.

The family Rhinocerotidae encompasses the subfamilies Elasmotheriinae and Rhinocerotinae, to which all extant rhinoceroses, as well as many extinct species, belong. *Subhyracodon*, a relatively small-bodied (approximately 100kg) hornless rhinocerotid from the Oligocene (Mead and Wall, 1998), is considered a basal member of *Elasmotheriinae* by Kosintsev et al. (2019). *Elasmotherium,* the last surviving member of the Elasmotheriinae, was the largest known rhinocerotoid apart from the Paraceratheres with an estimated body mass of 3,500–5,000kg for *Elasmotherium sibiricum* (Zhegallo et al, 2005; Kosintsev et al., 2019),). The hypsodont molars of *E. sibiricum* have a molar mesowear score similar to *Ceratotherium simum* suggesting a pure grazing diet (Rivals et al., 2020). The last common ancestor of the Rhinocerotinae has been suggested to have lived ~16 Mya, with the *Rhinoceros* lineage first diverging in the middle-to-late Miocene and being more closely related to the clade containing *Coelodonta*, *Stephanorhinus*, *Dicerorhinus*, and *Dihoplus*, than to the African rhinoceroses, Ceratotherium and *Diceros*. *Rhinoceros unicornis,* the Indian rhinoceros, and *Rhinoceros sondaicus*, the Javan rhinoceros, are the only extant members of their genus.

Dicerorhinus sumatrensis, the Sumatran rhinoceros, a browser feeds primarily on leaves and saplings (Nardelli, 2014), is the smallest extant rhinoceros, with an average body mass between 500-1,000kg. *Dihoplus*, an extinct genus, lived from the Late Miocene into the Pliocene, likely fed primarily on browse (Hullot et al., 2022; Pandolfi et al., 2020). Body mass estimates have been reported for some species; 2,122kg for *Dihoplus schleiermacheri* and 1,100kg for *D. pikermiensis* (Mallet et al., 2022). *Stephanorhinus etruscus* was a browser (Rivals and Lister, 2016; Ballatore and Breda, 2013) while *S. hemitoechus* was likely a grazer-dominated mixed feeder (Rivals and Lister, 2016). *Coelodonta antiquitatis*, more commonly known as the woolly rhinoceros, was comparable in size to *Ceratotherium simum* (~1,500-2,900kg) (Mallet et al., 2022; Ma, Wang, and Deng, 2024), inhabited open spaces and mesowear analysis suggests a usually strict grazing diet with seasonal inclusion of browse (Rivals and Lister, 2016).

Ceratotherium neumayri has gone through a contentious history of taxonomic assignment. First being assigned to the genus *Atelodus*, then to both *Diceros* and *Ceratotherium*, and suggested as the ancestor of both genera, before finally being reassigned to *Miodiceros*. Having lived during the late Miocene, immediately following the Middle Miocene Climatic Optimum, this species, comparable in size to *Ceratotherium simum*, seems to represent a transitional stage in

rhinocerotid adaptation from closed forest to more open habitats evidenced by dental microwear analysis which indicates a mixed feeding diet.

This expansive rhinocerotoid diversity in the fossil record provides a critical opportunity to assess whether mandibular mass properties and their influence on the mechanics of the mandible played an influential role in the survival and extinction of functionally and morphologically distinct lineages.

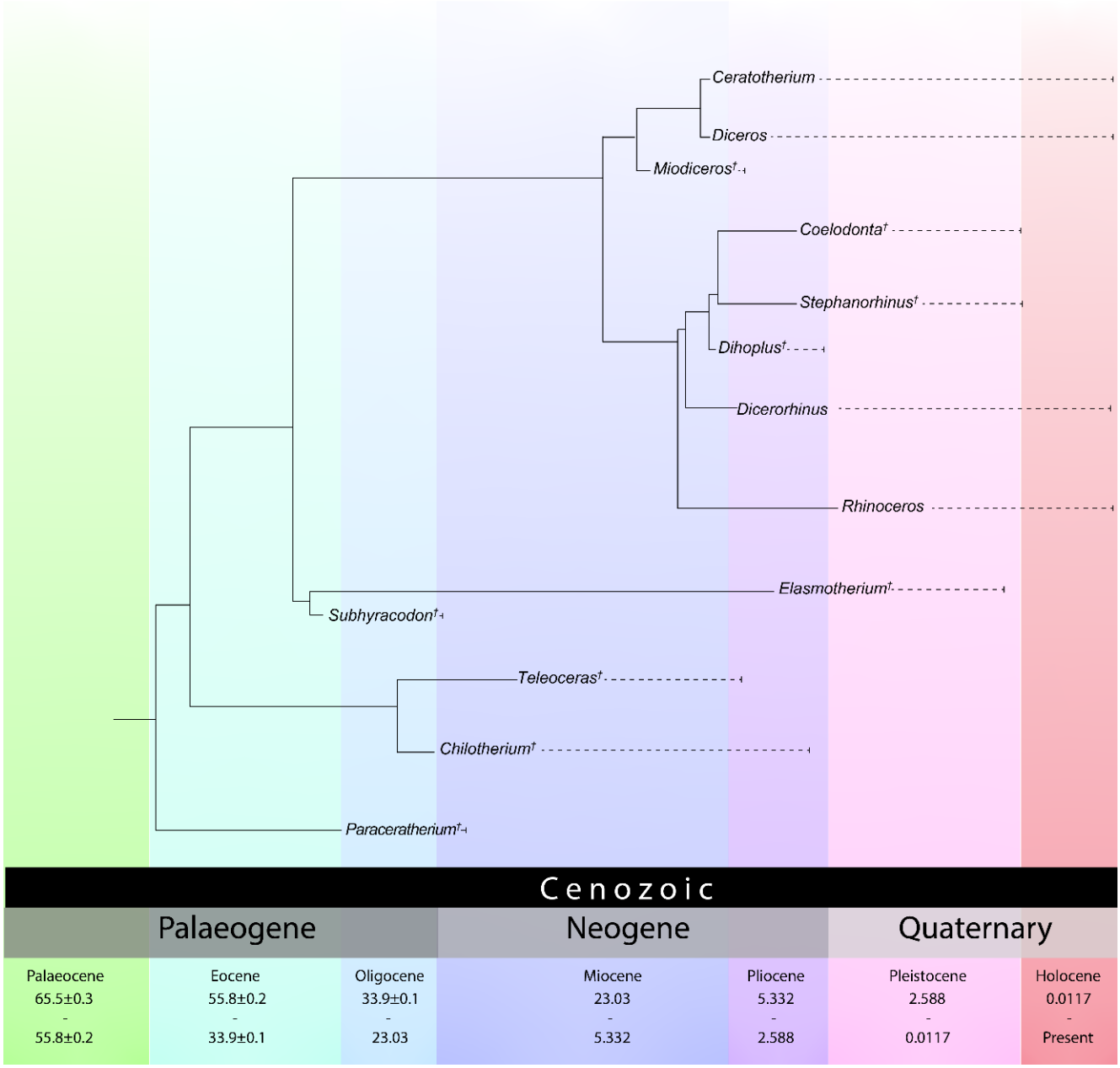

Figure 5.2. Cladogram of the perissodactyl superfamily Rhinocerotoidea genera included in this study with approximate divergence and extinction times.

5.1.4.2 Proboscidea

Modern elephants (*Loxodonta* and *Elephas*) are relictual survivors of a clade that once exhibited broad taxonomic and ecological diversity. Whereas extant species are all large-bodied mixed feeders, extinct proboscideans encompassed a broad spectrum of diets and mandibular morphologies. Early forms such as *Moeritherium* were small-bodied and semi-aquatic, while deinotheres possessed downturned mandibular tusks and maintained browsing ecologies into the Pleistocene (Sanders, 2023). The gomphotheres displayed elongate jaws with both upper and lower tusks, while mammoths evolved into specialised grazers with extreme hypsodonty.

This diversity highlights how proboscidean mandibles have adapted in response to ecological opportunity and environmental change. Many lineages with specialised mandibular anatomies became extinct, leaving only the more generalist-feeding elephants today. By including fossil proboscideans alongside living taxa, this study can investigate whether mandibular mass properties reveal functional differences that contributed to the survival of the few extant species. The proboscidean phylogeny (Shoshani, 1998; Baleka et al., 2022) presented here (Figure 5.3) similarly illustrates that the two surviving genera, *Elephas* and *Loxodonta*, represent only a small fraction of this once diverse clade.

Moeritherium, a basal Proboscidean known from the Eocene-Early Oligocene Fayum deposits, likely had a semi-aquatic lifestyle, inhabited freshwater swamps and riparian environments, and fed on aquatic vegetation (Liu et al., 2008; 2008; Raafat et al., 2024). This genus differed from later proboscideans in lacking a proboscis, possessing elongate incisors but no tusks, and its small statue, standing only 70cm at the shoulder and weighing only 235kg (Larramendi, 2016).

The Deinotheriidae, represented here by Early-Middle Miocene *Prodeinotherium* (4,000kg) and Mid Miocene–Early Pleistocene *Deinotherium,* with body masses potentially reaching 12–13,00kg (Christiansen, 2004; Larramendi, 2016) were short-trunked, browsing, mandibular tusked animals which more closely resembled extant elephants than other early proboscideans except for their skulls and mandibles. Both *Moeritherium* and the Deinotheres belong to the early suborder Plesielephantiformes.

The Mammutidae derived from the ancestors of modern elephants during the Oligocene. An early member of this lineage, *Palaeomastodon* (~2,500kg), an ancestor of the later mastodons (*Mammut*) and among the earliest of the Elephantiformes but closely resembled early gomphotheres than later mastodons.

Zygolophodon, a Miocene mammutid or "true mastodon", had a longirostrine mandible with a long, narrow symphysis, both upper and lower tusks (Von Koenigswald et al., 2023) and low-crowned bunodont molar indicative of a browsing diet (Geer et al., 2016). No detailed body mass estimations have been done for *Zygolophodon* but it was certainly larger than *Palaeomastodon* though not as large as more derived mammutids or modern elephants. *Mammut*, like other mammutids, had zygodont dentition well suited for browsing and which distinguishing them from the Elephantidae but unlike many of its ancestors did not have mandibular tusks and a shortened mandibular symphysis. Mastodons had a notably inflexible diet evidenced by coprolites (Newsrom and Mihlbachler, 2006) which may have prevented them from migrating to South America and inhibited their survival during turnover to grasslands from closed forests. The mastodon postcranial skeleton was much more robustly built than those of elephantids; *Mastodon borsoni* may have weighed as much as 16,000kg, and smaller species like *M. americanum* likely weighted around 11,000kg, being comparable in shoulder height to extant elephants (Larramendi, 2016).

The Gomphotheriidae are a paraphyletic group considered ancestral to Elephantidae. The proboscideans had bunodont molars, and the ancestral condition for this family was and elongate mandibular symphysis and tusks (e.g., *Gomphotherium angustidens*), however, later species developed shorted jaws, described as brevirostine, and lost their lower tusks. A convergent condition which in Elephantidae and Mammutidae. Perhaps the most famous genus, *Gomphotherium,* is composed of at least 10 species. Most were comparable in size to the extant *Elephas,* though one species, *G. steinheimense*, is estimated to have been larger with a body mass of ~7,000 kg.

The taxonomic position of *Stegodon* has been debated, at various time being resolved with Elephantidae and within its own family Stegodontidae with *Stegolophodon*, and again more recently within Elephantinae as the sister-taxon to *Loxodonta*. *Stegodon insignis*, from the Late Pliocene, were likely mixed feeders based on isotopic evidence (Suraprasit et al., 2019), while microwear analysis suggests *S. orientalis* and *S. huananensis* known from the Pleistocene of China and southeast Asia were browsers (Zhang et al., 2017). *Stegodon* species varied in size from dwarf species from Flores, *S. sondaari* and *S. florensis* (~570 kg) (Geer et al., 2016) to *S. zdanskyi* (~12,500 kg) (Larramendi, 2016).

Mammuthus, the mammoths, comprise at least ten species of specialist grazing proboscideans and are most closely related to *Elephas* than any other genera. As with *Stegodon*, the mammoths encompass a considerable size range from dwarf taxa such as *M. lamarmorai* (~550

kg) to *perhaps the largest bodied species of mammoth, M. trogontherii* (10,400–14,300 kg) (Larramendi, 2016).

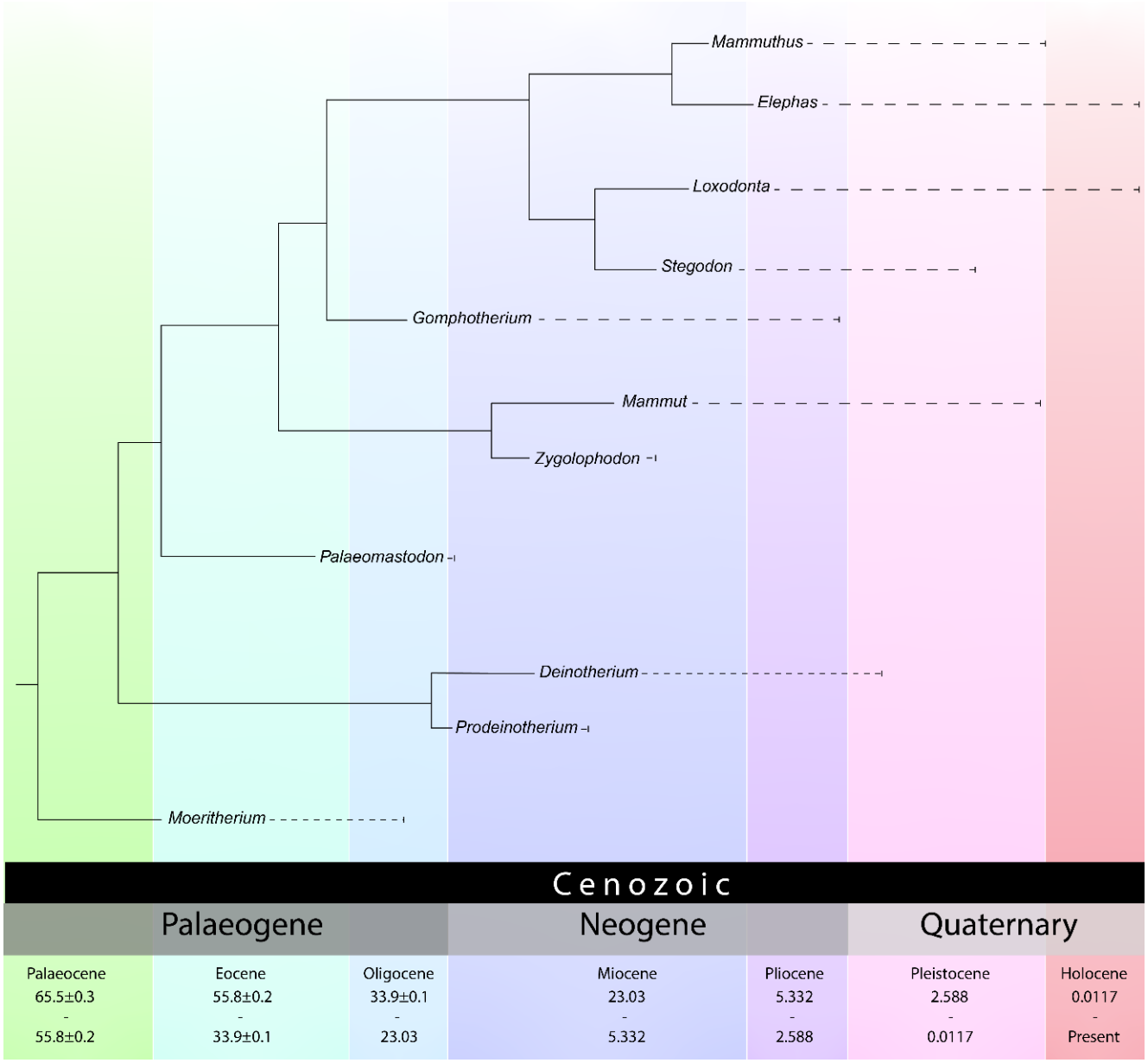

Figure 5.3. Cladogram of the afrotherian order Proboscidea genera included in this study with approximate divergence and extinction times.

5.1.5 Aims and Objectives

The limited size, morphological, and dietary diversity of extant ungulate-grade mammals only a narrow remnant of their former range. Modern datasets based solely on living taxa therefore

provide an incomplete picture of the diversity in mandibular form, function, and ecology that once characterised this grouping. Consequently, the linear scaling relationships observed between mandibular length, centre of mass, rotational inertia, and masseteric insertion area in extant species may not capture the full spectrum of functional and biomechanical variation expressed throughout their evolutionary history.

Incorporating fossil taxa that span a broader phylogenetic and temporal range is essential for bridging these gaps by extending the representation of body size, mandibular morphological disparity, and dietary strategy. Such integration also enables tests of whether the scaling trends identified in living species reflect underlying biomechanical principles or arise from restricted sampling. Although dietary categorisations have remained broadly consistent, several clades now represented by only a few surviving species, such as Proboscidea and Rhinocerotoidea, once occupied feeding niches with no direct modern analogues. To further expand the comparative framework, this study also includes ecologically analogous marsupials and xenarthrans, providing a wider context for evaluating mandibular form and function across primarily herbivorous lineages.

Accordingly, this chapter has four main aims:

1. To expand the size and morphological range of the interspecific data presented in previous chapters by including extinct species beyond the limits of extant samples.
2. To test whether observed scaling relationships represent fundamental mechanical constraints or are the result of sampling bias.
3. To investigate the mechanical cost of mastication in species with extreme mandible morphologies, and to assess if particular costs are associated dietary specialisation and extinction risk.
4. To assess how functional diversity, specifically co-variation of mandibular mass properties and biomechanical traits, has influenced adaptability and survivability in large ungulate-grade mammals.
5. To determine whether extant members of once more diverse clades share patterns of mandibular mass distribution that may have contributed to their survival relative to extinct relatives.

5.2 Hypotheses

5.2.1 Hypothesis 1: Linear scaling rates of anatomical, biomechanical, and mass property metrics observed in extant ungulate-grade taxa will be conserved across analysis of extant-only and combined extinct and extant population samples.

It is hypothesised that the linear scaling relationships among mandibular length, mass properties, and masseteric dimensions reflect a fundamental mechanical model of mastication in ungulate-grade herbivores. These relationships are expected to persist across both extant and extinct species, despite variation in body size, morphology, and phylogenetic affiliation. This would imply these relationships are fundamental to ungulate-grade taxa and not the result of sampling bias in a reduced extant-only sample. Linear regression of log-log transformed anatomical, biomechanical, and mass property variables will be used to determine allometric relationships, while PGLS regression will be used to investigate phylogenetic constraint.

Prediction**:** OLS and RMA regression analysis will evidence similar overall scaling in the total sample (extant and extinct taxa) as in the extant interspecific sample alone. PGLS regression will fall within the confidence interval of the OLS linear regression, evidencing a non-significant phylogenetic constraint.

5.2.2 Hypothesis 2: Extinct species without modern analogues will exhibit the highest ratios of rotational inertia to mandible length in an ecologically, morphologically, and phylogenetically diverse sample.

The ratio of mandibular rotational inertia to mandible length provides a coarse proxy for the mechanical cost of mastication. High ratios represent more substantial costs per unit of functional length, while low ratios represent low costs per unit of functional length. Morphological configurations that reduce this ratio, such as a posteriorly positioned centre of mass, a long but lightweight diastema, or a shortened symphysis, minimise the energy required for jaw movement, whereas thickened symphyses and large anterior tusks substantially increase mechanical cost, but may facilitate functions other mastication despite the high mechanical cost.

Among proboscideans, species such as *Palaeomastodon*, *Gomphotherium*, *Zygolophodon*, *Prodeinotherium*, and *Deinotherium* represent the most extreme mandible morphologies. Their elongate symphyses and mandibular tusks add substantial anterior mass, likely shifting the

centre of mass anteriorly, increasing rotational inertia despite their specialised browsing adaptations. Subsequent reductions in mandible length and increased reliance on the trunk for food acquisition are interpreted as functional optimisations that lowered energetic expenditure and enhanced ecological resilience (Shoshani and Tassy, 2005; Gheerbrant and Tassy, 2009; Li et al., 2024), and highlights the crucial role of open-land adaptation in megaherbivores for survival in modern ecosystems (Janis, 1982; 2008).

Building on the findings of *Chapter 3* concerning mandibular mass distribution in terrestrial herbivores, this study will examine how the ratio of rotational inertia to mandible length varies across extinct and extant ungulate-grade mammals. It is hypothesised that the most extreme mandibular morphologies, particularly in giant browsing proboscideans, will yield inertia-to-length ratios exceeding those of living taxa, reflecting their highly specialised morphology, the associated energetic costs of mastication, and poor ecological resistance.

Prediction: Species with extreme mandible morphology, such as the longirostrine, browsing proboscideans, will exhibit ratio values exceeding the upper limit of extant species, and exceeding the ratio observed in similarly sized grazing and mixed feeding species. In this way, this ratio may inform on the relationship between mandible anatomy, function, and mastication energetics, and serve as a measure of specialisation towards dietary niche and ecological resistance.

5.2.3 Hypothesis 3: Covariation of mandibular mechanics, mass properties, and dietary specialisation reflects a suite of adaptive traits promoting functional performance and survival, rather than being primarily determined by phylogenetic affinity or dietary category.

During the Miocene, megaherbivorous mammals exhibited high taxonomic and ecological diversity. However, following the Middle Miocene Thermal Maximum, global cooling, aridification, and the expansion of grasslands reduced the habitats that supported specialised browsing taxa, particularly among giant-sized species (Blanco et al., 2025). Consequently, the diversity of ungulate-grade mammals declined, driven by climatic change and intensified competition for increasingly scarce resources. This contraction was accompanied by a reduction in mandibular morphological disparity, most notably among browsing rhinocerotoids and proboscideans.

It is hypothesised that this decline in diversity is reflected in the co-variation of mandible length, mandibular mass properties (i.e., centre of mass and rotational inertia) and mechanical traits (i.e., masseteric insertion area, masseter and temporalis mechanical advantage), and dietary strategy. Specifically, it is suggested that particular combinations of these traits represent adaptive suites which facilitated survival under increasingly resource-limited conditions. This hypothesis will be tested in three comparative samples using k-means clustering of principal components: (1) a broad, total dataset, sample of ungulate-grade mammals, (2) a focused subset of rhinocerotoids, and (3) a focused subset of proboscideans.

Prediction 1: PCA and k-means clustering analysis of mass property, mechanical, anatomical and dietary traits will cluster species by extant or extinct status rather than phylogenetic affinity or dietary category, in the broad interspecific ungulate-grade sample.

Prediction 2: PCA and k-means clustering analysis of mass property, mechanical, anatomical and dietary traits will cluster species by extant or extinct status rather than phylogenetic affinity or dietary category, in clade specific samples of proboscideans and rhinocertoids.

5.3 Materials and Methods

5.3.1 Materials

Mandibular mass property data calculated using the CoM-CT method in Chapter 3 were combined with new measurements obtained for specimens scanned at the Natural History Museum, London, using the CoM-Surface method described in Chapter 2. Additional models were sourced from publicly available repositories, including *MorphoSource* and *Sketchfab* (Table 5.1). A subset of this sample for which phylogenetic information was available was selected for inclusion in the Phylogenetic Generalised Least Squares (PGLS) analysis. This subset, spanning four taxonomic orders (Artiodactyla, Perissodactyla, Pilosa, and Proboscidea), is represented as a cladogram (Figure 5.4)

Mandibles of extinct species were digitised using an *Artec Eva* structured-light 3D scanner to generate high-resolution surface models. Bone density values were derived from CT-scanned mandibles of extant taxa and were found to be normally distributed across specimens regardless of size or taxonomy. The mean bone density was applied as a uniform value to surface-scan models, allowing estimation of mandibular mass and rotational inertia in fossil taxa.

All mandibles were aligned to a standardised long-axis orientation, and the position of the centre of mass (CoM) was expressed as a linear displacement from the temporomandibular joint (TMJ). Each mandible was modelled as a two-dimensional structure rotating about the TMJ. Although this represents a simplification of masticatory kinematics, the approach ensures consistency and comparability across taxa.

Table 5.1. Taxa list for combined extant and extinct interspecific sample. * denotes specimens without masseter insertion area data.

Institutional Abbreviations: (Museum abbreviations: 1) zmh - Zoologisches Museum Hamburg, University of Hamburg, Hamburg, Germany. 2) zmb - Museum für Naturkunde, Berlin, Germany. 3) usn:m - National Museum of Natural History, Smithsonian Institution, Division of Mammals, Washington D.C, USA. 4) TMM - Texas Memorial Museum, Austin, Texas, USA. 5) Ulg - Université de Liège, Liège, Belgium. 6) ism - Illinois State Museum, Springfield, Illinois, USA. 6) GPIH - Geologisch-Paläontologisches Institut und Museum, University of Hamburg, Hamburg, Germany. 7) etmnh – East Tennessee State University Museum of Natural History, Gray, Tennesee, USA. 8) uomnh – University of Oregon Museum of Natural and Cultural History, Eugene, Oregon, USA. 9) wsc – Western Science Centre, Hemet, California, USA. 10) omsi – Oregon Museum of Science and Industry, Portland, Oregon, USA. 11) kupri - Primate Research Institute, Kyoto University, Inuyama, Aichi Prefecture, Japan.

Family	**Genus, species**	**Specimen / Registration No.**	**Status**	**Modality / Scanner Type**	**Scanning Facility - Institute**	**Equipment Used**
Order - Artiodactyla						
Anthracotheriidae	*Brachyodus onoideus†*	Ulg:M:50000a	Extinct	Laser Scanner	Evolution and Diversity Dynamics Lab, University of Liège, Liège, Belgium.	Creaform Handyscan 300
Antilocapridae	*Antilocapra americana*	usnm:mammals:282308	Extant	Custom CT Scanner	High-Resolution X-ray Computed Tomography Facility, University of Texas at Austin, Austin, USA.	North Star Imaging NSI Custom Build
Bovidae	*Bos taurus*	York Specimen (UoY -CT-003)	Extant	Clinical CT	The York Hospital, Wigginton Road, York, United Kingdom.	Siemens SOMATOM Definition AS+
Bovidae	*Bos taurus*	York Specimen (UoY -CT-004)	Extant	Clinical CT	The York Hospital, Wigginton Road, York, United Kingdom.	Siemens SOMATOM Definition AS+
Bovidae	*Cephalophus sp.*	kupri:z928	Extant	Clinical CT	Primate Research Institute, Kyoto University	---

Bovidae	*Damaliscus lunatus jimela*	usnm:mammals:199074	Extant	Custom CT Scanner	High-Resolution X-ray Computed Tomography Facility, University of Texas at Austin, Austin, USA.	North Star Imaging NSI Custom Build
Bovidae	*Redunca arundinum*	usnm:mammals:367429	Extant	Custom CT Scanner	High-Resolution X-ray Computed Tomography Facility, University of Texas at Austin, Austin, USA.	North Star Imaging NSI Custom Build
Bovidae	*Rupicapra rupicapra*	usnm:mammals:291836	Extant	Custom CT Scanner	High-Resolution X-ray Computed Tomography Facility, University of Texas at Austin, Austin, USA.	North Star Imaging NSI Custom Build
Bovidae	*Saiga tatarica*	usnm:mammals:336264	Extant	Clinical CT	High-Resolution X-ray Computed Tomography Facility, University of Texas at Austin, Austin, USA.	Varian Medical Systems (Bio-Imaging Research, Inc) ACTIS CT scanner with FeinFocus X-ray source
Bovidae	*Tragelaphus scriptus*	usnm:mammals:164562	Extant	Custom CT Scanner	High-Resolution X-ray Computed Tomography Facility, University of Texas at Austin, Austin, USA.	North Star Imaging NSI Custom Build
Camelidae	*Lama glama*	TMM M-2052	Extant	Custom CT Scanner	High-Resolution X-ray Computed Tomography Facility, University of Texas at Austin, Austin, USA.	North Star Imaging NSI Custom Build

Camelidae	*Lama glama*	usnm:mammals:278681	Extant	Custom CT Scanner	High-Resolution X-ray Computed Tomography Facility, University of Texas at Austin, Austin, USA.	North Star Imaging NSI Custom Build
Camelidae	*Camelus sp*	York Specimen (UoY-CT-006)	Extant	Clinical CT	The York Hospital, Wigginton Road, York, United Kingdom.	Siemens SOMATOM Definition AS+
Camelidae	*Camelus bactrianus*	Z.2009.72.1 (left)	Extant	Clinical CT	Small Animal Hospital, Royal (Dick) School of Veterinary Studies, University of Edinburgh, United Kingdom	Siemens SOMATOM Definition AS
Camelidae	*Camelus bactrianus*	Z.2009.72.1 (right)	Extant	Clinical CT	Small Animal Hospital, Royal (Dick) School of Veterinary Studies, University of Edinburgh, United Kingdom	Siemens SOMATOM Definition AS
Cervidae	*Cervalces scotti†*	ism:geo:499313	Extinct	Laser Scanner	Illinois State Museum Imaging Lab	NextEngine 3D Laser Scanner
Cervidae	*Megaloceros giganteus†*	NHM UK M 2328	Extinct	Structured Light Scanner	Scanned for this study - Natural History Museum, London, United Kingdom.	Artec Eva
Cervidae	*Mazama americana*	usnm:mammals:374880	Extant	Custom CT Scanner	High-Resolution X-ray Computed Tomography Facility, University of Texas at Austin, Austin, USA.	North Star Imaging NSI Custom Build
Cervidae	*Odocoileus hemionus*	usnm:mammals:246649	Extant	Custom CT Scanner	High-Resolution X-ray Computed Tomography Facility, University of Texas at Austin, Austin, USA.	North Star Imaging NSI Custom Build

Cervidae	*Rangifer tarandus*	usnm:mammals:246649	Extant	Custom CT Scanner	High-Resolution X-ray Computed Tomography Facility, University of Texas at Austin, Austin, USA.	North Star Imaging NSI Custom Build
Entelodontidae	*Entelodon sp.†*	NHM UK - Unregistered	Extinct	Structured Light Scanner	Scanned for this study - Natural History Museum, London, United Kingdom.	Artec Eva
Giraffidae	*Giraffa jumae†*	NHM UK - Unregistered	Extinct	Structured Light Scanner	Scanned for this study - Natural History Museum, London, United Kingdom.	Artec Eva
Giraffidae	*Giraffa sp.*	York Specimen (UoY-CT-007)	Extant	Clinical CT	The York Hospital, Wigginton Road, York, United Kingdom.	Siemens SOMATOM Definition AS+
Giraffidae	*Okapia johnstoni*	GH3.21 (left)	Extant	Clinical CT	Small Animal Hospital, Royal (Dick) School of Veterinary Studies, University of Edinburgh, United Kingdom	Siemens SOMATOM Definition AS
Giraffidae	*Okapia johnstoni*	GH3.21 (right)	Extant	Clinical CT	Small Animal Hospital, Royal (Dick) School of Veterinary Studies, University of Edinburgh, United Kingdom	Siemens SOMATOM Definition AS
Hipoopotamidae	*Hippopotamus amphibius*	Z.2008.35 (left)	Extant	Clinical CT	Small Animal Hospital, Royal (Dick) School of Veterinary Studies, University of Edinburgh, United Kingdom	Siemens SOMATOM Definition AS

Hipoopotamidae	*Hippopotamus amphibius*	Z.2008.35 (right)	Extant	Clinical CT	Small Animal Hospital, Royal (Dick) School of Veterinary Studies, University of Edinburgh, United Kingdom	Siemens SOMATOM Definition AS
Hipoopotamidae	*Hippopotamus amphibius*	Unreg, Dick Vet Specimen (left)	Extant	Clinical CT	Small Animal Hospital, Royal (Dick) School of Veterinary Studies, University of Edinburgh, United Kingdom	Siemens SOMATOM Definition AS
Hipoopotamidae	*Hippopotamus amphibius*	Unreg, Dick Vet Specimen (right)	Extant	Clinical CT	Small Animal Hospital, Royal (Dick) School of Veterinary Studies, University of Edinburgh, United Kingdom	Siemens SOMATOM Definition AS
Hippopotamidae	*Hippopotamus antiquus*	NHMUK PV M 2521	Extinct	Structured Light Scanner	Scanned for this study - Natural History Museum, London, United Kingdom.	Artec Eva
Hippopotamidae	*Hexaprotodon sivalensis*	NHMUK – Unregistered*	Extinct	Structured Light Scanner	Scanned for this study - Natural History Museum, London, United Kingdom.	Artec Eva
Suidae	*Sus scrofa*	TMM M-454	Extant	Clinical CT	High-Resolution X-ray Computed Tomography Facility, University of Texas at Austin, Austin, USA.	Varian Medical Systems (Bio-Imaging Research, Inc) ACTIS CT scanner with FeinFocus X-ray source

Suidae	*Sus barbatus*	usnm:mammals:145297	Extant	Custom CT Scanner	High-Resolution X-ray Computed Tomography Facility, University of Texas at Austin, Austin, USA.	North Star Imaging NSI Custom Build
Suidae	*Sus domesticus*	York Specimen (UoY-CT-005)	Extant	Clinical CT	The York Hospital, Wigginton Road, York, United Kingdom.	Siemens SOMATOM Definition AS+
Suidae	*Phacochoerus africanus*	usnm:mammals:a36000	Extant	Custom CT Scanner	High-Resolution X-ray Computed Tomography Facility, University of Texas at Austin, Austin, USA.	North Star Imaging NSI Custom Build
Order - Cingulata						
Chlamyphoridae	*Glyptodon reticulatus†*	NHMUK PV OR 39478	Extinct	Structured Light Scanner	Scanned for this study - Natural History Museum, London, United Kingdom.	Artec Eva
Order - Dinocerata						
Uintatheriidae	*Uintatherium sp.†*	NHMUK - Unregistered	Extinct	Structured Light Scanner	Scanned for this study - Natural History Museum, London, United Kingdom.	Artec Eva
Order - Diprotodontia						
Diprotodontidae	*Diprotodon benetti†*	NHMUK PV OR 47855	Extinct	Structured Light Scanner	Scanned for this study - Natural History Museum, London, United Kingdom.	Artec Eva
Diprotodontidae	*Diprotodon sp.†*	NHMUK PV M 3645	Extinct	Structured Light Scanner	Scanned for this study - Natural History Museum, London, United Kingdom.	Artec Eva
Order - Embrithopoda						

Arsinoitheriidae	*Arsiniotherium zittelі†*	NHMUK PV M 104239b	Extinct	Structured Light Scanner	Scanned for this study - Natural History Museum, London, United Kingdom.	Artec Eva
Order - Litopterna						
Macraucheniidae	*Macrauchenia sp.†*	NHMUK - Unregistered	Extinct	Structured Light Scanner	Scanned for this study - Natural History Museum, London, United Kingdom.	Artec Eva
Order - Notoungulata						
Toxodontidae	*Nesodon imbricatus†*	NHMUK PV M 4656*	Extinct	Structured Light Scanner	Scanned for this study - Natural History Museum, London, United Kingdom.	Artec Eva
Toxodontidae	*Nesodon imbricatus†*	NHMUK PV M 7297*	Extinct	Structured Light Scanner	Scanned for this study - Natural History Museum, London, United Kingdom.	Artec Eva
Toxodontidae	*Toxodon platensis†*	NHMUK PV OR 19949	Extinct	Structured Light Scanner	Scanned for this study - Natural History Museum, London, United Kingdom.	Artec Eva
Toxodontidae	*Trigodon gaudryi†*	NHMUK PV M 9863	Extinct	Structured Light Scanner	Scanned for this study - Natural History Museum, London, United Kingdom.	Artec Eva
Order - Perissodactyla						
Brontotheriidae	*Megacerops sp.†*	NHM UK - Unregistered	Extinct	Structured Light Scanner	Scanned for this study - Natural History Museum, London, United Kingdom.	Artec Eva
Equidae	*Equus quagga (burchelli)*	zmb:70335	Extant	Clinical CT	Oregon Imaging Centers at University District, Eugene, OR 97401, USA.	Philips Brilliance 64 CT Scanner

Equidae	*Equus grevyi*	usnm:mammals:241009	Extant	Custom CT Scanner	High-Resolution X-ray Computed Tomography Facility, University of Texas at Austin, Austin, USA.	North Star Imaging NSI Custom Build
Equidae	*Equus caballus*	York Specimen (UoY -CT-001)	Extant	Clinical CT	The York Hospital, Wigginton Road, York, United Kingdom.	Siemens SOMATOM Definition AS+
Equidae	*Equus caballus*	York Specimen (UoY-CT-002)	Extant	Clinical CT	The York Hospital, Wigginton Road, York, United Kingdom.	Siemens SOMATOM Definition AS+
Paraceratheriidae	*Paraceratherium bugtiense†*	NHMUK PV M 12683	Extinct	Structured Light Scanner	Scanned for this study - Natural History Museum, London, United Kingdom.	Artec Eva
Rhinocerotidae	*Ceratotherium simum (*fossil*)*	NHM UK PV M 26548	Extinct	Structured Light Scanner	Scanned for this study - Natural History Museum, London, United Kingdom.	Artec Eva
Rhinocerotidae	*Chilotherium schosseri†*	GPIH:3015a	Extinct	Structured Light Scanner	NA	Artec Space Spider
Rhinocerotidae	*Coelodonta antiquitatis†*	NHM UK – Unregistered*	Extinct	Structured Light Scanner	Scanned for this study - Natural History Museum, London, United Kingdom.	Artec Eva
Rhinocerotidae	*Coelodonta antiquitatis†*	Ulg:PA:9472	Extinct	Laser Scanner	Evolution and Diversity Dynamics Lab, University of Liège, Liège, Belgium.	Creaform Handyscan 300
Rhinocerotidae	*Coelodonta antiquitatis†*	NHMUK PV OR 49661	Extinct	Structured Light Scanner	Scanned for this study - Natural History Museum, London, United Kingdom.	Artec Eva

Rhinocerotidae	*Stephanorhinus hemitoechus†*	NHMUK PV M 36620*	Extinct	Structured Light Scanner	Scanned for this study - Natural History Museum, London, United Kingdom.	Artec Eva
Rhinocerotidae	*Ceratotherium neumayri†*	NHMUK PV M 10150	Extinct	Structured Light Scanner	Scanned for this study - Natural History Museum, London, United Kingdom.	Artec Eva
Rhinocerotidae	*Dihoplus schleiermacheri†*	NHMUK PV M 2781	Extinct	Structured Light Scanner	Scanned for this study - Natural History Museum, London, United Kingdom.	Artec Eva
Rhinocerotidae	*Elasmotherium sp.†*	NHM UK - Unregistered	Extinct	Structured Light Scanner	Scanned for this study - Natural History Museum, London, United Kingdom.	Artec Eva
Rhinocerotidae	*Stephanorhinus etruscus†*	NHMUK PV OR 37341	Extinct	Structured Light Scanner	Scanned for this study - Natural History Museum, London, United Kingdom.	Artec Eva
Rhinocerotidae	*Stephanorhinus hemitoechus†*	NHMUK PV OR 45214	Extinct	Structured Light Scanner	Scanned for this study - Natural History Museum, London, United Kingdom.	Artec Eva
Rhinocerotidae	*Subhyracodon sp.†*	NHMUK PV - Unregistered	Extinct	Structured Light Scanner	Scanned for this study - Natural History Museum, London, United Kingdom.	Artec Eva
Rhinocerotidae	*Teleoceras fossiger†*	NHMUK PV M 10579	Extinct	Structured Light Scanner	Scanned for this study - Natural History Museum, London, United Kingdom.	Artec Eva
Rhinocerotidae	*Teleoceras fossiger†*	NHMUK - Unregistered	Extinct	Structured Light Scanner	Scanned for this study - Natural History Museum, London, United Kingdom.	Artec Eva

Rhinocerotidae	*Teleoceras aepysoma†*	etmnh:601	Extinct	Structured Light Scanner	East Tennessee State University Natural History Museum, Tennessee, USA.	Artec Eva
Rhinocerotidae	*Ceratotherium simum*	zmh-s:2552	Extant	Clinical CT	University Medical Center Hamburg-Eppendorf, University of Hamburg, Hamburg, Germany.	Philips Brilliance 64 CT Scanner
Rhinocerotidae	*Dicerorhinus sumatrensis*	zmh-s:8273	Extant	Clinical CT	Yxlon International	Yxlon CT Modular
Rhinocerotidae	*Diceros bicornis*	zmh-s:9379	Extant	Clinical CT	Oregon Imaging Centers at University District, Eugene, OR 97401, USA.	Philips Brilliance 64 CT Scanner
Rhinocerotidae	*Rhinoceros unicornis*	z.2009.152	Extant	Clinical CT	Small Animal Hospital, Royal (Dick) School of Veterinary Studies, University of Edinburgh, United Kingdom	Siemens SOMATOM Definition AS
Tapiridae	*Tapirus terrestris*	TMM-M-16 (right)	Extant	Custom CT Scanner	High-Resolution X-ray Computed Tomography Facility, University of Texas at Austin, Austin, USA.	North Star Imaging NSI Custom Build
Tapiridae	*Tapirus terrestris*	TMM-M-16 (left)	Extant	Custom CT Scanner	High-Resolution X-ray Computed Tomography Facility, University of Texas at Austin, Austin, USA.	North Star Imaging NSI Custom Build
Order - Pilosa						
Megatheriidae	*Megatherium americanum†*	NHMUK PV OR 19953	Extinct	Structured Light Scanner	Scanned for this study - Natural History Museum, London, United Kingdom.	Artec Eva

Scelidotheriidae	*Scelidotherium leptocephalum†*	NHMUK PV OR 37309*	Extinct	Structured Light Scanner	Scanned for this study - Natural History Museum, London, United Kingdom.	Artec Eva
Scelidotheriidae	*Scelidotherium bravardi†*	NHMUK PV OR 37649	Extinct	Structured Light Scanner	Scanned for this study - Natural History Museum, London, United Kingdom.	Artec Eva
Order - Proboscidea						
Deinotheriidae	*Deinotherium giganteum†*	Goldfuss Museum, University of Bonn - Unregistered	Extinct	Structured Light Scanner	Bonn Center for Digital Humanities, University of Bonn, Bonn, Germany.	NA
Deinotheriidae	*Prodeinotherium barvaricum†*	NHMUK PV M 19009	Extinct	Structured Light Scanner	Scanned for this study - Natural History Museum, London, United Kingdom.	Artec Eva
Elephantidae	*Mammuthus trogontherii†*	NHMUK PV OR 44974	Extinct	Structured Light Scanner	Scanned for this study - Natural History Museum, London, United Kingdom.	Artec Eva
Elephantidae	*Mammuthus trogontherii†*	NHMUK PV OR 44975	Extinct	Structured Light Scanner	Scanned for this study - Natural History Museum, London, United Kingdom.	Artec Eva
Elephantidae	*Mammuthus primigenius†*	NHMUK PV M 10190*	Extinct	Structured Light Scanner	Scanned for this study - Natural History Museum, London, United Kingdom.	Artec Eva
Elephantidae	*Mammuthus primigenius†*	NHMUK PV OR M 4008	Extinct	Structured Light Scanner	Scanned for this study - Natural History Museum, London, United Kingdom.	Artec Eva

Elephantidae	*Mammuthus primigenius†*	NHMUK PV M 10347*	Extinct	Structured Light Scanner	Scanned for this study - Natural History Museum, London, United Kingdom.	Artec Eva
Elephantidae	*Mammuthus meridionalis†*	NHMUK PV OR 37334	Extinct	Structured Light Scanner	Scanned for this study - Natural History Museum, London, United Kingdom.	Artec Eva
Elephantidae	*Elephas planifrons†*	NHMUK PV OR 16442	Extinct	Structured Light Scanner	Scanned for this study - Natural History Museum, London, United Kingdom.	Artec Eva
Elephantidae	*Elephas maximus*	Z.2001.147 (left)	Extant	Clinical CT	Small Animal Hospital, Royal (Dick) School of Veterinary Studies, University of Edinburgh, United Kingdom	Siemens SOMATOM Definition AS
Elephantidae	*Loxodonta africana*	Z.2013.148.1 (left)	Extant	Clinical CT	Small Animal Hospital, Royal (Dick) School of Veterinary Studies, University of Edinburgh, United Kingdom	Siemens SOMATOM Definition AS
Elephantidae	*Loxodonta africana*	Z.2013.148.1 (right)	Extant	Clinical CT	Small Animal Hospital, Royal (Dick) School of Veterinary Studies, University of Edinburgh, United Kingdom	Siemens SOMATOM Definition AS
Gomphotheriidae	*Gomphotherium angustidens†*	NHMUK PV OR 37243	Extinct	Structured Light Scanner	Scanned for this study - Natural History Museum, London, United Kingdom.	Artec Eva
Gomphotheriidae	*Gomphotherium angustidens†*	NHMUK PV M 13995	Extinct	Structured Light Scanner	Scanned for this study - Natural History Museum, London, United Kingdom.	Artec Eva

Mammutidae	*Mammut americanum†*	uomnh:p:10291*	Extinct	Structured Light Scanner	East Tennessee State University Natural History Museum, Tennessee, USA.	Artec Space Spider
Mammutidae	*Mammut pacificus†*	wsc:18743	Extinct	Photogrammery	NA	Panasonic Lumix DC-ZS70S
Mammutidae	*Mammut pacificus†*	wsc:19730	Extinct	Photogrammery	NA	Panasonic Lumix DC-ZS70S
Mammutidae	*Mammut americanum†*	NHMUK M 17426	Extinct	Structured Light Scanner	Scanned for this study - Natural History Museum, London, United Kingdom.	Artec Eva
Mammutidae	*Zygolophodon proavus†*	omsi:p:1946.02.1026	Extinct	Structured Light Scanner	East Tennessee State University Natural History Museum, Tennessee, USA.	Artec Eva
Moeritheriidae	*Moeritherium fayum†*	NHMUK PV M 9263	Extinct	Structured Light Scanner	Scanned for this study - Natural History Museum, London, United Kingdom.	Artec Eva
Palaeomastodontidae	*Palaeomastodon sp.†*	NHM UK - Unregistered	Extinct	Structured Light Scanner	Scanned for this study - Natural History Museum, London, United Kingdom.	Artec Eva
Stegodontidae	*Stegodon insignis†*	NHMUK PV M 3037	Extinct	Structured Light Scanner	Scanned for this study - Natural History Museum, London, United Kingdom.	Artec Eva
Order - Pyrotheria						
Pyrotheriidae	*Pyrotherium sorondoi†*	NHMUK PV M 8544	Extinct	Structured Light Scanner	Scanned for this study - Natural History Museum, London, United Kingdom.	Artec Eva

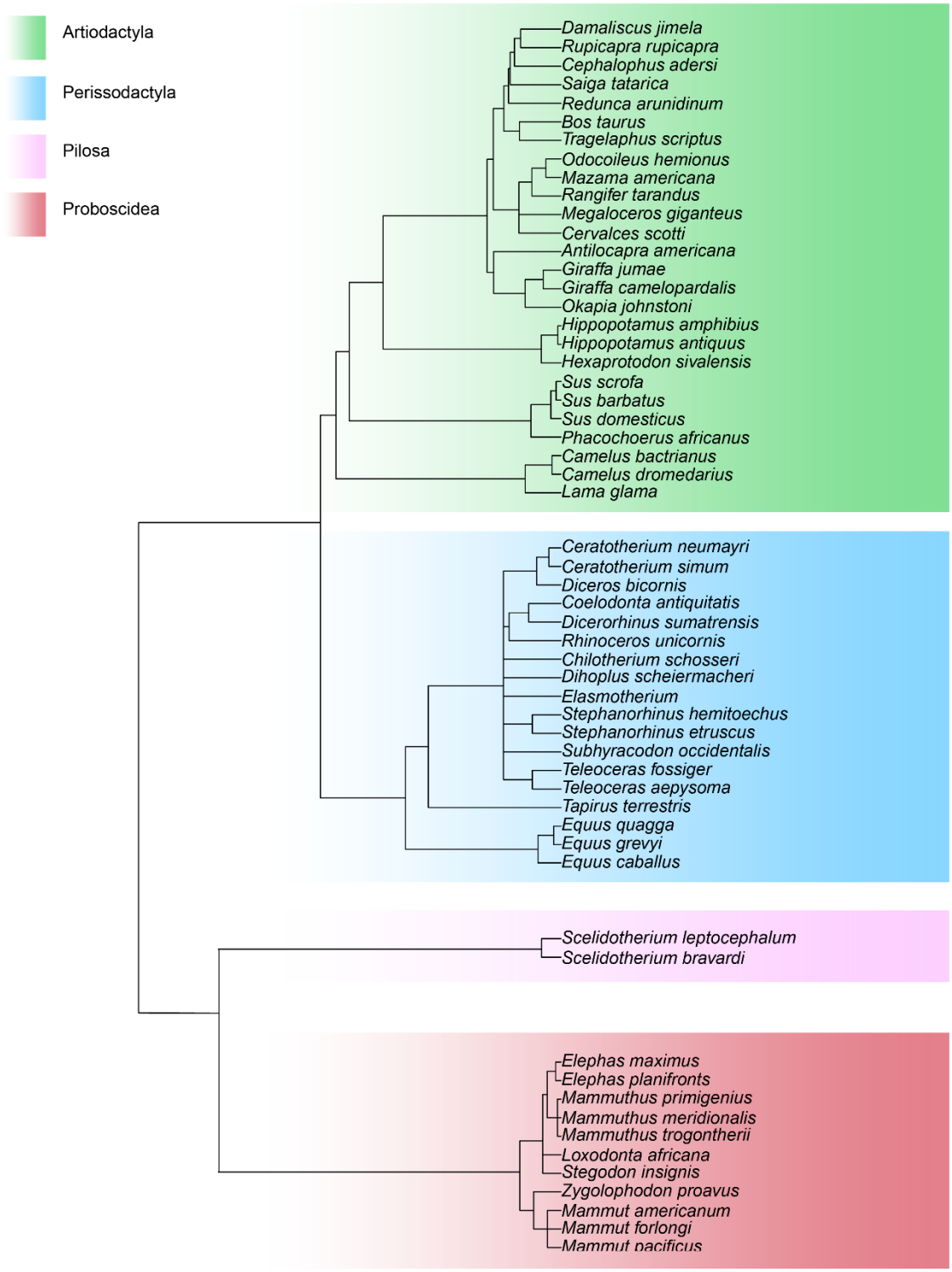

Figure 5.4. Cladogram showing hypothesised relationships among sampled taxa representing Artiodactyla, Perissodactyla, Pilosa, and Proboscidea, used for phylogenetic comparative analyses. (Shoshani, 1998; Upham, Esselstyn, and Jetz, 2019; Bai et al., 2020; Baleka et al., 2022).

5.3.2 Data Collection and Linear Regression

The analytical framework employed in this chapter follows that used in Chapters 3 and 4, *Biological and Mechanical Implications of Mandibular Mass Distribution in Terrestrial Mammalian Herbivores* and *Habitual Head Posture and Associated Behaviours as Adaptations to Mitigate the Mechanical Effects of Mandible Mass Distribution*. Linear regression analyses were performed as in the previous chapters, with the exception of the scaling of the mechanical advantages of the masseter and temporalis with respect to rotational inertia, as earlier results did not support a linear relationship between these variables.

Mandible length and centre of mass for surface-based models was measured in *Blender* (Version 3.1; Blender Foundation, 2022) following the procedure described in Chapter 2. Mean material densities were calculated for CT-scanned specimens from the interspecific sample described in Chapters 2 and 3. These densities were found to be normally distributed regardless of variation in mandible size, morphology, or taxonomy, yielding an average of 1.48g/cm^3. Because surface-based models represent volume but not mass, this mean value was applied as an ersatz density to all surface-derived models, permitting estimation of mandibular mass and rotational inertia.

All hemi-mandibles were aligned along a standardised long-axis orientation, and the position of the CoM was expressed as a linear displacement from the temporomandibular joint (TMJ). Each mandible was modelled as a two-dimensional structure rotating about the TMJ, a simplification that allows consistent comparison among taxa while acknowledging that complex three-dimensional kinematics and habitual head posture were not modelled.

Masseteric insertion areas were estimated from the surface-derived three-dimensional models using *Geomagic Design X* (Version 2023.2.0). Muscle attachment scars were delineated along the lateral surface of the ramus and angular process to define the masseteric insertion using the *Select By Area* tool, then navigating to the *Analysis Tools* menu, and selecting *Compute Area*. Mechanical advantage of the masseter and temporalis muscles were subsequently calculated from three-dimensional measurements taken in *Blender* (Version 3.1; Blender Foundation, 2022), using the default *Measure* tool available in the toolbar, and calculated in *Microsoft Excel* (Version 16.0), following the lever-mechanics approach of Morales-García, Säilä, and Janis (2020). Masseteric insertion area data could not be accurately collected for specimens which lacked definite muscle attachment scars (Table 5.1), as such these specimens were excluded from the linear aggression analysis investigating the scaling of mandible length and masseteric insertion area.

All data were log-transformed to allow for analysis of allometric scaling relationships. Both Ordinary Least Squares (OLS) and Reduced Major Axis (RMA) regressions were used to account for potential measurement error in the independent variables. Phylogenetic Generalised Least Squares (PGLS) analyses were also performed to correct for non-independence among taxa due to shared evolutionary history. A composite phylogenetic tree was constructed using the *R* package *U.PhyloMaker* (Jin and Qian, 2022), and the PGLS analysis was performed using the R package *phytools* (Revell, 2012).

5.3.3 Multivariate Analysis – Principal Component Analysis and K-means Clustering

Additionally, a multivariate approach was used to investigate patterns of covariance between mandibular morphological and biomechanical variables (i.e., mandible mass, long-axis length, absolute and proportional centre of mass, rotational inertia, area of masseter insertion, and mechanical advantage of the masseter and temporalis), and to assess if these patterns led to adaptive suites which map to dietary category. Principal component analysis (PCA) was applied for unsupervised dimensional reduction to allow the data to be visualised in a reduced space while capturing the maximum proportion of variance and to investigate which of these variables covary. Following the PCA, k-means clustering was applied to determine if natural groups in the data aligned species with their dietary categorisations from the literature.

These analyses were applied to three datasets: a broad interspecific dataset of both extant and extinct species, a rhinocerotoid-only dataset, and a proboscidean-only dataset. The inclusion of the two phylogenetically restricted datasets was intended to assess if the morphological and biomechanical variables covary more strongly, and if any alignment with dietary categorisation could be made, within a clade rather than in a broad interspecific sample. In all three datasets, I additionally investigated if extant species cluster more closely with each other than with more closely related extinct species, thereby assessing if morphofunctional adaptation within the mandible, and masticatory system more broadly, aided their survival to the present day.

Each of three datasets (i.e., the complete dataset, and proboscidean and rhinocerotoid subsets) were imported into R and prepared for analysis by first inspecting its structure, variable types, and completeness. To ensure comparability of variables measured on different scales, all numeric variables were standardised using z-score normalisation; each variable was mean-centred and divided by its standard deviation. This step prevented variables with large ranges (e.g., mandible mass, length) from having an outstated influence on the clustering results. Any

missing data were handled by listwise deletion to main consistency in the analysis; this resulted in a number of taxa being removed from the analysis.

The first three principal components were extracted and used for visualisation. PCA biplots were generated to aid interpretation and convex hulls were drawn around groups of within cluster points as a visual indication of cluster separation and overlap. Clustering was performed using the k-means algorithm which partitions the data into k groups by minimising the within-cluster sum of squares (WCSS). The optimum number of clusters, *k*, was determined by the Elbow Method. This involves plotting the total within-cluster sum of squares (WCSS) against increasing values of *k*, the number of clusters. As *k* increases, WCSS always decreases but after a certain point the rate of improvement becomes marginal. This is referred to as the elbow point and is the optimum number of clusters. In each case, the cluster assignments were overlaid on the PCA biplots and convex hulls were again used to investigate the degree of separation between groups.

Cluster quality was evaluated using both external and internal validation metrics. Purity score is an external validation metric that evaluates how well the clusters align with pre-set class labels; in this case, dietary category). The purity score is determined by assigning a label to a cluster based on which label class is most common in that cluster, counting how many data points are "correctly" classified and dividing by the total number of points. Perfect alignment is indicated by a score of 1, while a score of 0 indicates no alignment. It is important to consider that purity score always increases when using more clusters; purity score should therefore be interpreted alongside the elbow method and silhouette score. Internal validation was done using the Silhouette Score which measures how well observation is matched to its cluster by comparing the average distance to points in the same cluster with the average distance to points in the nearest neighbouring cluster. Silhouette scores range of -1 to 1; values near 1 are well-matched to its cluster, near 0 indicates the point is on the boundary between clusters and not well matched to either, values less than 0 suggest the point is likely in the wrong cluster. Average silhouette scores were calculated for k=2 to k=10 and used to support the *k* value selected using the Elbow Method. Average silhouette scores were calculated for each clustering solution and plots were generated to visualise the distribution of values within each cluster.

5.4 Results

5.4.1 Results 1 – Addressing H1: Linear scaling rates of anatomical, biomechanical, and mass property metrics observed in extant ungulate-grade taxa will be conserved across analysis of extant-only and combined extinct and extant population samples.

Firstly, the scaling relationship between mandible length and mandibular mass was examined for all taxa (Figure 5.5 A, B). In the untransformed dataset (Figure. 5.5 A), mandibular length explained 41% of the variation in mass according to the Ordinary Least Squares (OLS) regression ($F_{1,95} = 66.9$, $p < 0.001$, $R^2adj = 0.41$). The Reduced Major Axis (RMA) regression produced a steeper slope, reflecting error in both variables. Considerable vertical dispersion at greater mandible lengths indicates heteroscedasticity and limits the interpretability of raw values, suggesting that differences in scale and body size introduce non-linearity.

After log-transformation (Figure 5.5 B), the relationship between mandible length and mass became strongly linear, with both OLS ($R^2adj = 0.73$, slope = 3.62, $p < 0.001$) and RMA regressions indicating a good fit to the data. Mandibular mass scales with positive allometry relative to length, implying that larger species possess disproportionately heavier mandibles. Among major clades, Proboscidea exhibit the most positive residuals, reflecting exceptionally massive mandibles for their length, while Perissodactyla and Notoungulata also plot above the regression line, consistent with robust mandibular anatomy. In contrast, the Xenarthran orders Cingulata and Pilosa fall below the trend, indicating relatively slender, lightly built jaws.

Additionally, the relationship between mandible length and mandible mass was evaluated for extant and extinct representatives of Artiodactyla, Perissodactyla, Pilosa, and Proboscidea (Figure 5.6 A,B) using OLS, RMA, and PGLS. In the untransformed dataset (Figure 5.6 A), mandibular length explained approximately 48% of the variation in mandibular mass ($F_{1,55} = 52.2$, $p < 0.001$, $R^2adj = 0.48$). The Ordinary Least Squares (OLS) and Reduced Major Axis (RMA) regressions show similar trends, although the RMA slope is steeper, reflecting proportional error in both axes. Following log-transformation (Figure 5.6 B), the relationship between length and mass became strongly linear (OLS: $F_{1,55} = 219$, $p < 0.001$, $R^2adj = 0.80$). The slopes of the OLS, RMA, and Phylogenetic Generalised Least Squares (PGLS) regressions are nearly identical, demonstrating the robustness of the scaling relationship when accounting for both measurement error and non-independence due to phylogenetic constraint.

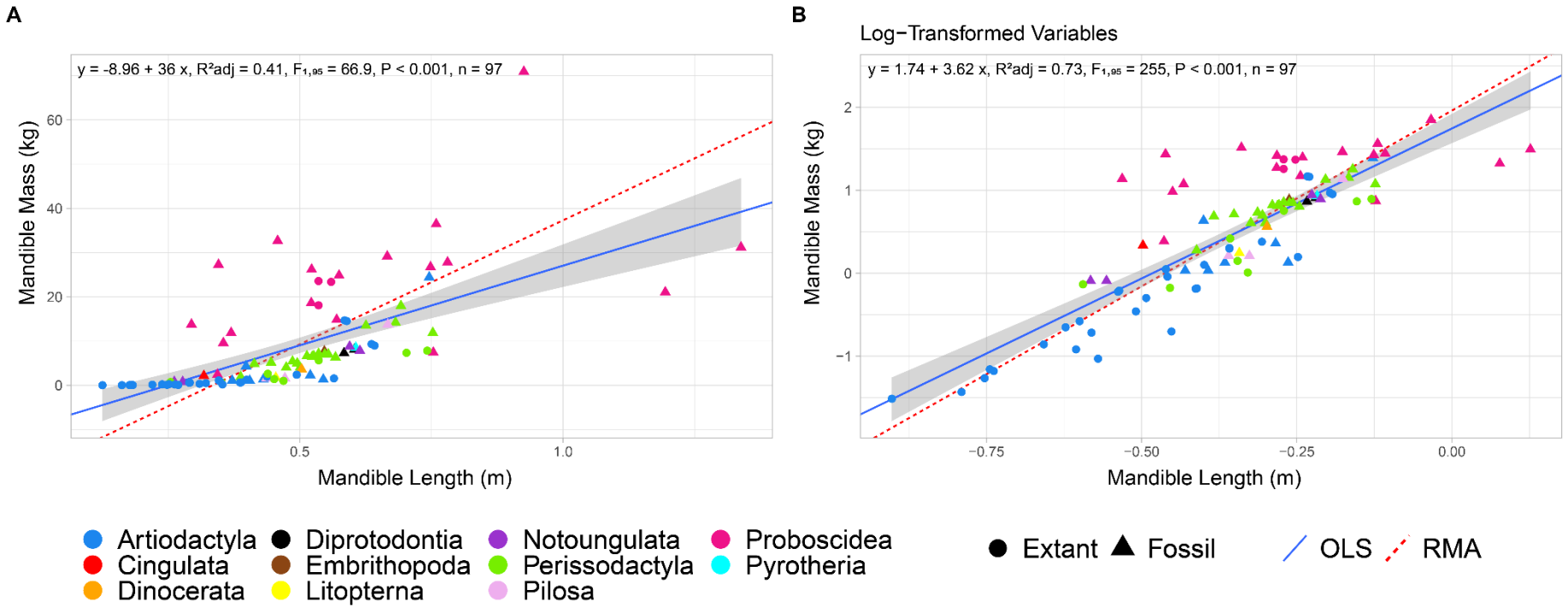

Figure 5.5. Linear regression of mandible length against mandible mass across extant and extinct mammals.

(A) Raw data showing the relationship between mandible length and mandible mass for all taxa. (B) Log-transformed data showing the linearised allometric relationship. Regression lines represent Ordinary Least Squares (OLS; solid blue line) and Reduced Major Axis (RMA; dashed red line).

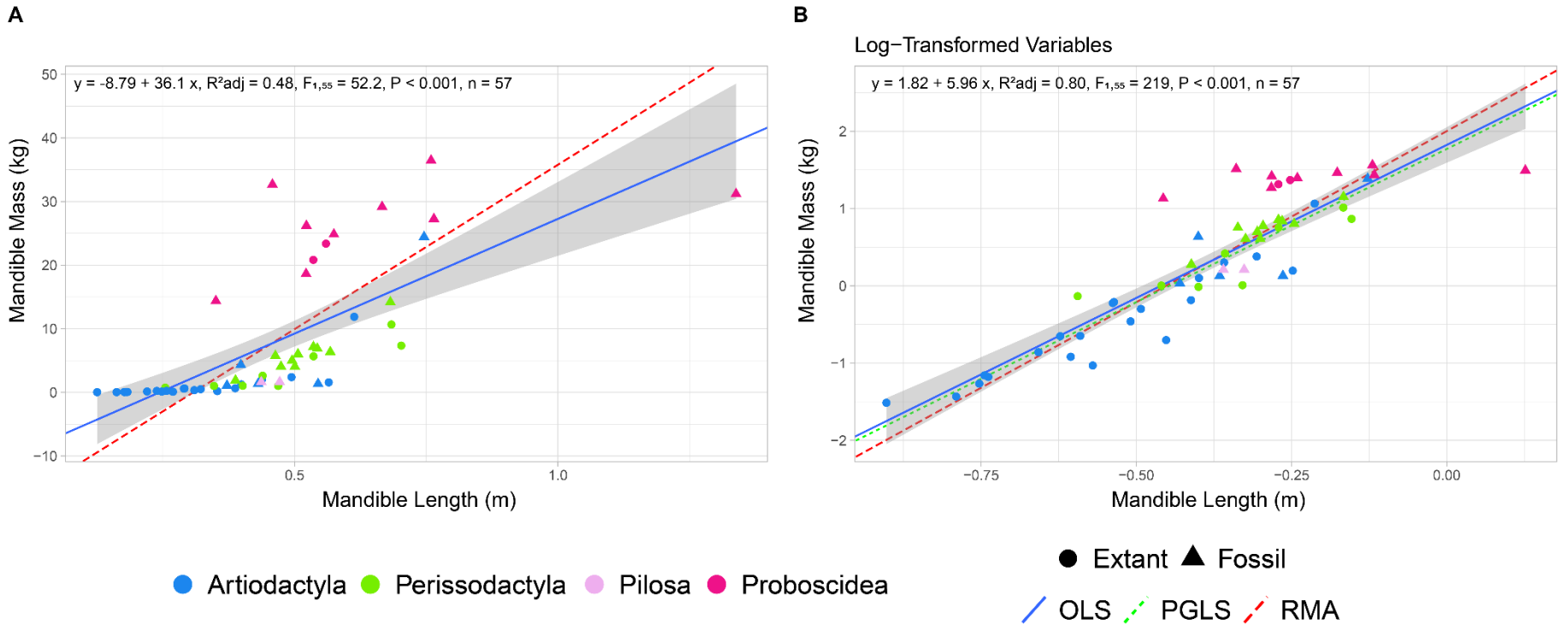

Figure 5.6. Linear regression of mandible length against mandible mass across extant and extinct members of the mammal orders Artiodactyla, Perissodactyla, Proboscidea, and Pilosa. (A) Raw data showing the relationship between mandible length and mandible mass. (B) Log-transformed data showing the linearised allometric relationship. Regression lines represent Ordinary Least Squares (OLS; solid blue), Reduced Major Axis (RMA; dashed red), and Phylogenetic Generalised Least Squares (PGLS; dotted green).

Secondly, the relationship between mandible length and centre of mass was examined across the full dataset of extant and extinct taxa (Figure 5.7A, B). The untransformed data (Figure 5.7 A) exhibit a strong linear relationship, with mandible length explaining 84% of the variation in centre of mass position ($F_{1,95}$ = 522, P < 0.001, R^2adj = 0.84). The RMA intercept is lower, and slope higher, than that of the OLS regression but still falls within the confidence interval, displaying small but not significant error, and therefore a consistent proportional relationship between mandible length and centre of mass.

When both variables were $\log_{10}$-transformed (Fig. 5.7B), the relationship strengthened slightly (R^2adj = 0.86). The OLS (slope = 1.10) and RMA (slope = 1.18) regressions both indicate weak-to-moderate positive allometric scaling, with confidence intervals that exclude zero (Table 5.2). The close correspondence between regression methods, with the RMA line falling within the OLS confidence interval, suggests that the relationship is robust and not substantially influenced by scaling or measurement error. Despite the relatively strong fit of the linear regression model to the data, there is significant scatter around the regression.

A reduced subset of taxa, for which phylogenetic data were available, was analysed using PGLS (Figure 5.8 A,B). This subset exhibited an even stronger relationship between mandible length and centre of mass (R^2adj = 0.92, P < 0.001), with near-identical slopes produced by the OLS, RMA, and PGLS regressions. The close agreement among methods demonstrates that the scaling of centre of displacement with mandible length remains stable when phylogenetic non-independence is taken into account. Collectively, these results indicate that centre of mass position scales weak-to-moderate positive allometry with mandibular length. This contrasts with the scaling relationship observed in the previously analysed sample of extant artiodactyls, perissodactyls, and proboscideans where centre of mass was found to scale with isometry or weak positive allometry (Table 5.2).

Table 5.2. Summary of linear regression statistics for extant only sample and total (extant and extinct) centre of mass data against mandible length.

	Extant (n = 40)	**Extant + Extinct (n = 97)**
Adj. R^2	0.91	0.86
OLS slope	1.10 (95 % CI: 0.97 – 1.22)	1.10 (95 % CI: 1.01 – 1.18)
RMA slope	1.15 (95 % CI: 1.03 – 1.29)	1.18 (95 % CI: 1.09 – 1.27)
Allometry	Isometry or weak **positive** allometry	Weak to moderate **positive** allometry

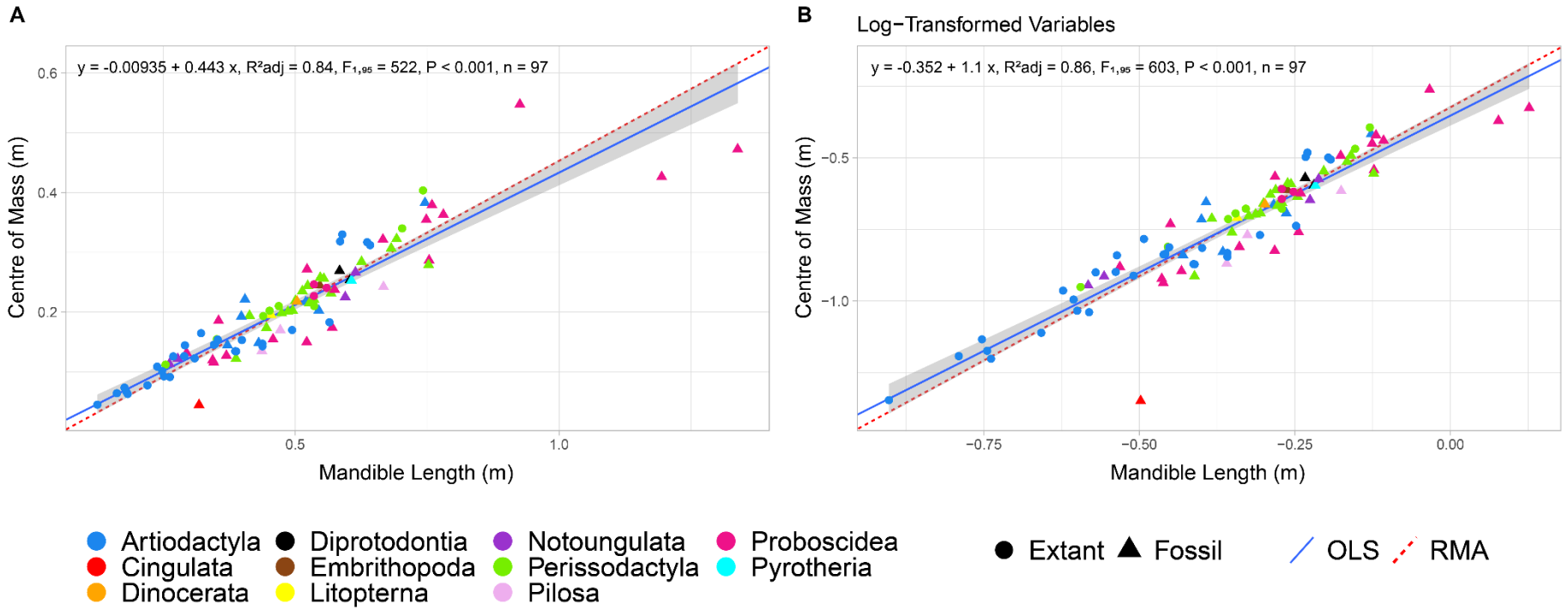

Figure 5.7. Linear regression of mandible length against centre of mass across extant and extinct mammals.

(A) Raw data showing the relationship between mandible length and centre of mass for all taxa. (B) Log-transformed data illustrating the allometric scaling relationship. Regression lines represent Ordinary Least Squares (OLS; solid blue line) and Reduced Major Axis (RMA; dashed red line).

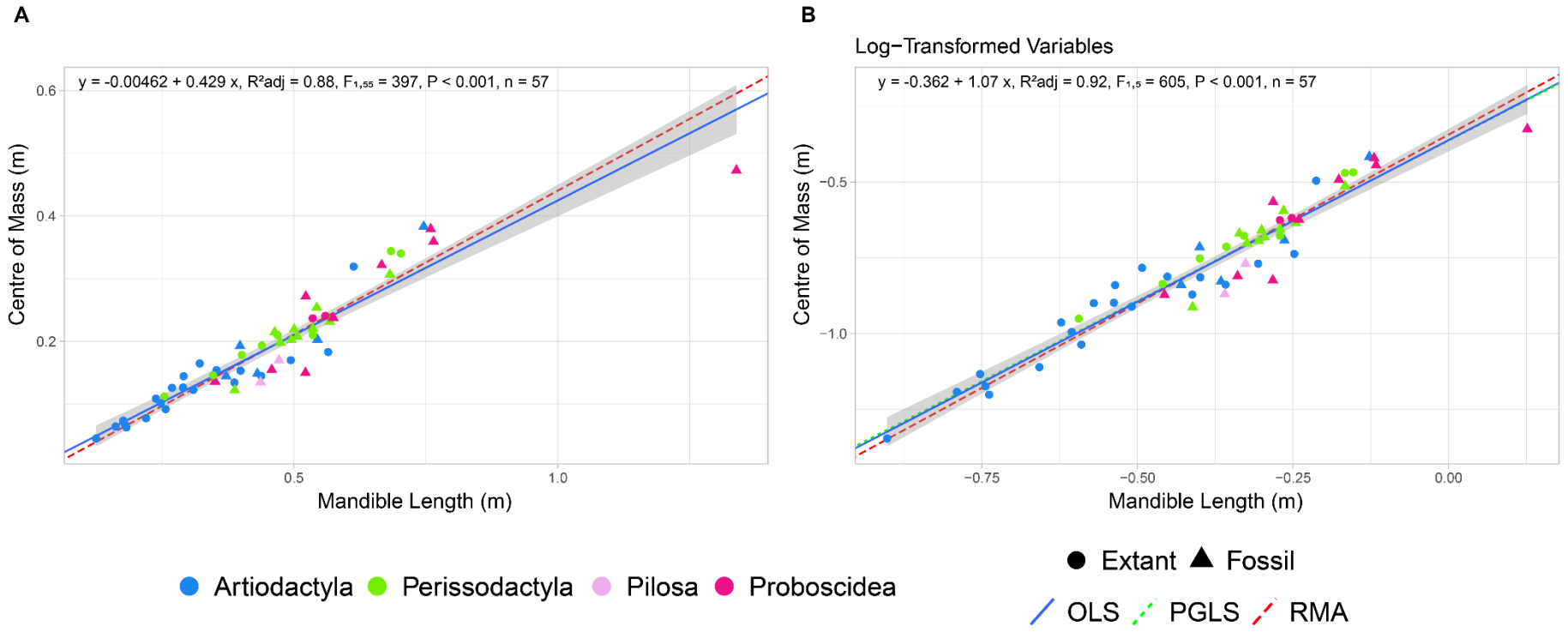

Figure 5.8. Linear regression of mandible length against centre of mass across extant and extinct members of the mammal orders Artiodactyla, Perissodactyla, Proboscidea, and Pilosa. (A) Raw data showing the relationship between mandible length and centre of mass. (B) Log-transformed data showing the allometric scaling relationship. Regression lines represent Ordinary Least Squares (OLS; solid blue), Reduced Major Axis (RMA; dashed red), and Phylogenetic Generalised Least Squares (PGLS; dotted green).

Thirdly, the relationship between mandible length and rotational inertia was investigated (Figure 5.9 A,B). For the raw data (Figure 5.9 A), mandible length explains only 31% of the variation in rotational inertia ($F_{1,95} = 44.5$, $P < 0.001$, $R^2adj = 0.31$).

After log-transformation (Figure 5.9 B), the relationship improves substantially ($R^2adj = 0.85$). However, while this indicates mandible length is a good predictor of rotational inertia across ungulate-grade mammals generally, there is substantial clade specific deviations from the regression trend. Both the OLS (slope = 5.86; 95% CI: 5.36–6.36) and RMA (slope = 6.35; 95% CI: 5.87–6.86) regressions exceed the isometric expectation (slope = 5), indicating positive allometric scaling (Table 5.4).

Compared with the extant-only sample ($R^2adj = 0.91$; OLS slope = 6.14), the combined extant and extinct sample slightly reduces explanatory power but preserves the same allometric scaling pattern (Table 5.3).

Analysis of the reduced subset for which phylogenetic data were available yielded similar results (Figure 5.10 A,B). The raw data OLS regression model demonstrates a good fit to the data ($R^2adj = 0.64$), which is strengthened following log-transformation ($R^2adj = 0.89$). The OLS and PGLS regression trends are nearly ideal, while the RMA regression line falls within the OLS confidence interval regressions are nearly identical, confirming that phylogenetic non-independence has minimal influence on the overall trend. However, again, there are clade specific deviations from the trend with pilosans and artiodactyls generally falling below the trend, perissodactyls close to the trend, and proboscideans exhibiting the most substantial residuals.

Table 5.3. Summary of linear regression statistics for extant only sample and total (extant and extinct) sample - mandible length vs rotational inertia.

	Extant	**Extant + Extinct (n = 97)**
Adjusted R^2	0.91	0.85
OLS slope	6.14 (95 % CI: 5.39 – 6.89)	5.86 (95 % CI: 5.36 – 6.36)
RMA slope	6.45 (95 % CI: 5.75 – 7.25)	6.35 (95 % CI: 5.87 – 6.86)
Isometry slope	5.00	5.00
Allometry	Positive allometry (slopes > isometric expectation)	Positive allometry (slopes > isometric expectation)

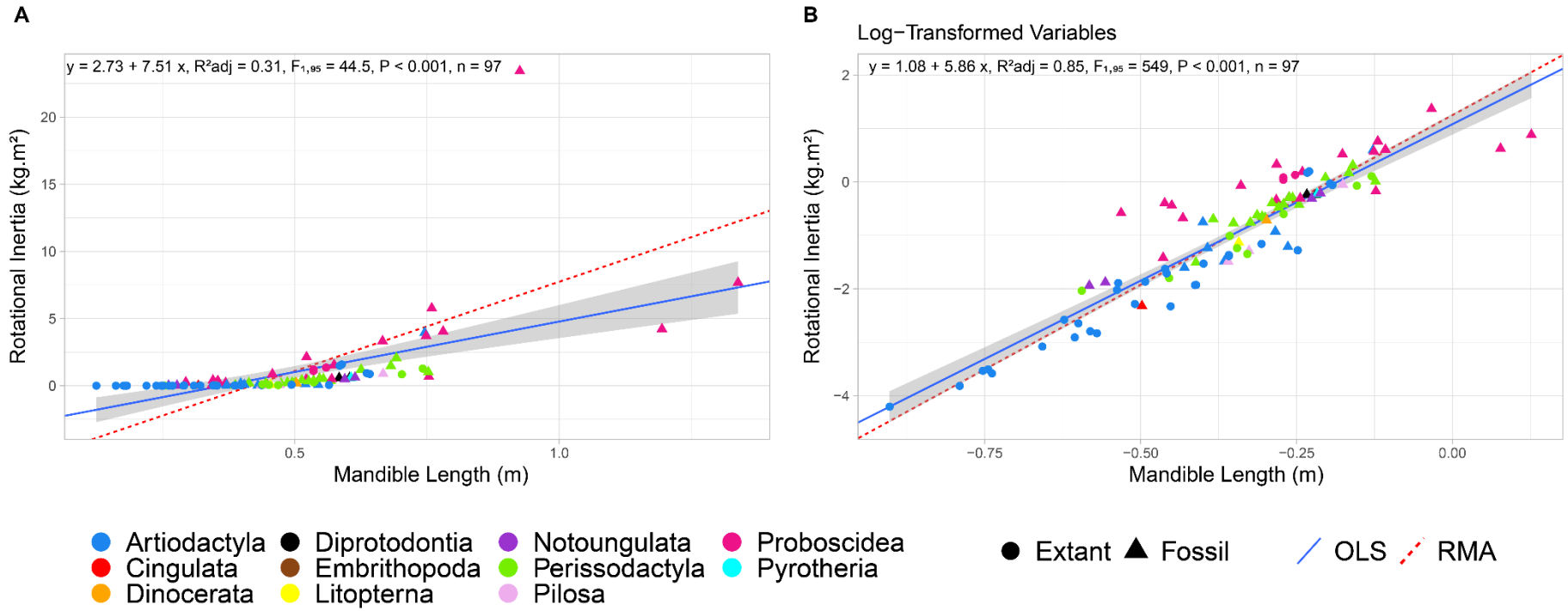

Figure 5.9. Linear regression of mandible length against rotational inertia across extant and extinct mammals.

(A) Raw data showing the relationship between mandible length and rotational inertia for all taxa. (B) Log-transformed data illustrating the allometric scaling relationship. Regression lines represent Ordinary Least Squares (OLS; solid blue line) and Reduced Major Axis (RMA; dashed red line).

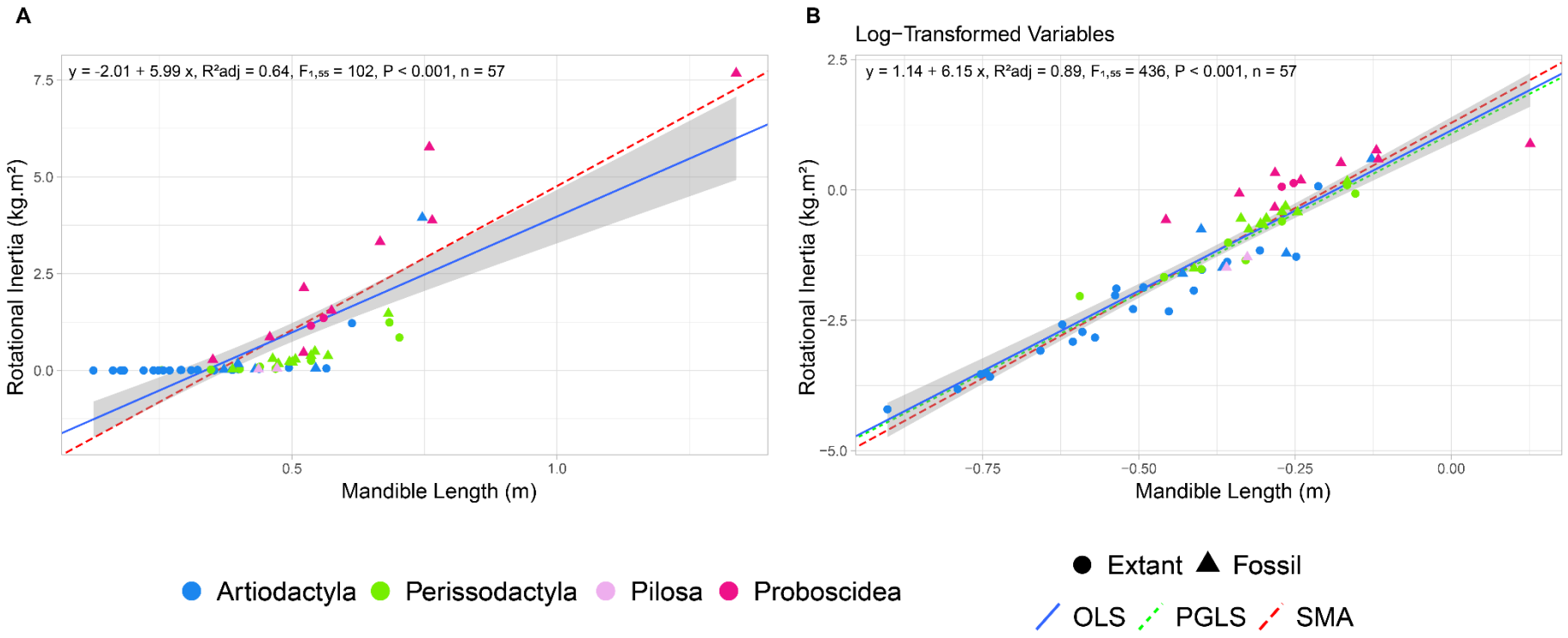

Figure 5.10. Linear regression of mandible length against rotational inertia across extant and extinct members of the mammal orders Artiodactyla, Perissodactyla, Proboscidea, and Pilosa. (A) Raw data showing the relationship between mandible length and rotational inertia. (B) Log-transformed data showing the allometric scaling relationship. Regression lines represent Ordinary Least Squares (OLS; solid blue), Reduced Major Axis (RMA; dashed red), and Phylogenetic Generalised Least Squares (PGLS; dotted green).

Finally, the relationship between rotational inertia and masseteric insertion area was examined across both the total and reduced datasets (Figure 5.11 A, B). In the untransformed data (Figure 5.11 A), a positive and moderately strong relationship is evidenced by the regression statistics (R^2adj = 0.52, $F_{1,86}$ = 95.8, P < 0.001), but visual inspection of the regression plot reveals the linear regression is highly influenced by fossil proboscideans which are distribution above the trend at moderate rotational inertia and below the trend at the higher values. However, following log-transformation, the linear relationship was substantially strengthened (Figure 5.11 B). The log-transformed data show a strong linear relationship (R^2adj = 0.86) between the two variables. In the extant-only sample, the OLS slope is 0.40 (95% CI: 0.36–0.44) and the RMA slope is 0.41 (95% CI: 0.38–0.45), with R^2adj = 0.95, evidencing a nearly perfect linear relationship. When extinct taxa are included, the slopes change only marginally: OLS = 0.39 (95% CI: 0.36–0.43), RMA = 0.42 (95% CI: 0.39–0.46). Both regressions closely match the isometric expectation (slope = 0.40) (Table 5.3), with the RMA regression within the OLS regression confidence interval, indicating that the area of masseteric insertion scales isometrically with rotational inertia across ungulate-grade mammals.

Glyptodon (Cingulata; red triangle) shows a markedly larger than expected masseteric insertion area for its rotational inertia, whereas *Diprotodon* (Diprotodontia; black triangle) exhibits the opposite condition, possessing a much smaller attachment area than predicted (Figure 5.11 B). Both taxa are phylogenetically distant from most other species in the dataset and possess highly derived mandible morphologies, suggesting that the functional mechanics of the masseter in these lineages may differ substantially from those of ungulate-grade herbivores and warrant further investigation.

Analysis of the reduced PGLS dataset reveals near-identical slopes for the OLS and RMA regression, but deviation in PGLS regression. The PGLS regression (green dashed line) exhibits a slightly higher intercept and a marginally lower slope than either the OLS or RMA models (Figure 5.12 B). As a result, at lower rotational inertia values the PGLS line lies just above the OLS fit, but at higher inertia values it falls below the lower limit of the OLS confidence interval, suggesting that when phylogenetic relationships are considered, the influence of taxa with atypically large values, particularly large-bodied fossil proboscideans, is somewhat reduced. PGLS analysis reveals OLS overestimates the true scaling relationship between rotational inertia and masseteric insertion area.

Table 5.4. Summary of linear regression statistics for extant only sample and total (extant and extinct) between rotational inertia and masseteric insertion area.

	Original Data	**Adjusted Data**
Adjusted R^2	0.95	0.86
OLS slope	0.40 (95 % CI: 0.36 – 0.44)	0.39 (95 % CI: 0.36 – 0.43)
RMA slope	0.41 (95 % CI: 0.38 – 0.45)	0.42 (95 % CI: 0.39 – 0.46)
Isometry slope	0.40	0.40
Allometry classification	Isometric scaling (slope ≈ isometry)	Isometric scaling (slope ≈ isometry)

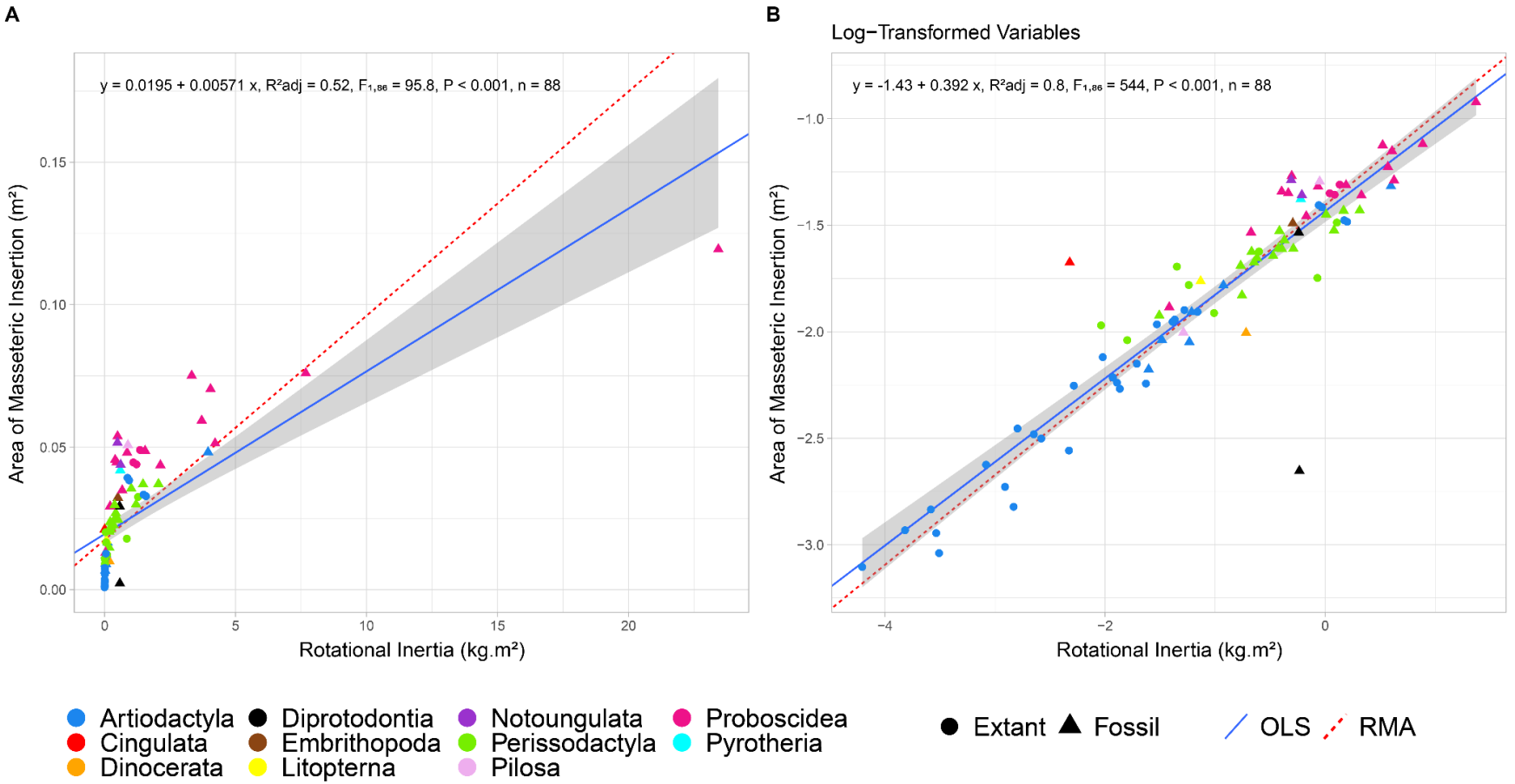

Figure 5.11. Linear regression of rotational inertia against area of masseteric insertion mass for extant and extinct mammals.

(A) Raw data showing the relationship between mandible length and centre of mass for all taxa. (B) Log-transformed data illustrating the allometric scaling relationship. Regression lines represent Ordinary Least Squares (OLS; solid blue line) and Reduced Major Axis (RMA; dashed red line).

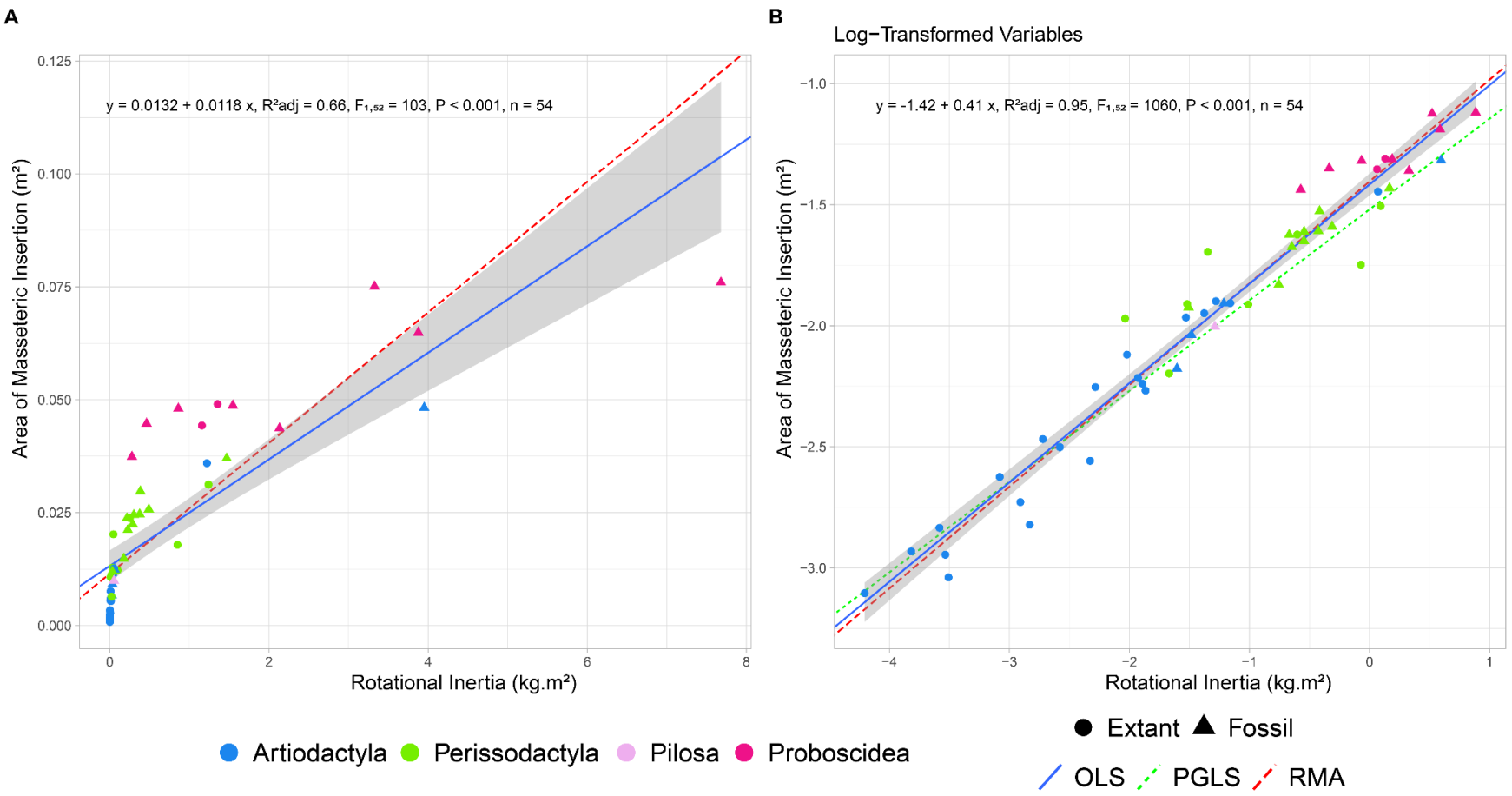

Figure 5.12. Linear regression of rotational inertia against masseteric insertion area across extant and extinct members of the mammal orders Artiodactyla, Perissodactyla, Proboscidea, and Pilosa. (A) Raw data showing the relationship between rotational inertia and masseteric insertion area. (B) Log-transformed data showing the allometric scaling relationship. Regression lines represent Ordinary Least Squares (OLS; solid blue), Reduced Major Axis (RMA; dashed red), and Phylogenetic Generalised Least Squares (PGLS; dotted green).

5.4.2 Results 2 – Addressing Hypothesis 2: Extinct species without modern analogues will exhibit the highest ratios of rotational inertia to mandible length in an ecologically, morphologically, and phylogenetically diverse sample.

Rank-ordered plots of the ratio between mandibular rotational inertia and mandible length reveal three distinct ratio bands denoted by inflexion point and distinguished by taxonomy (Figure 5.13) and dietary composition (Figure 5.14).

The low-ratio band (≤ –1.5) consists exclusively of extant artiodactyls and the extinct cingulate *Glyptodon*. Despite its large body size and graze-heavy mixed-feeding ecology, *Glyptodon* plots among small-bodied browsers and mixed feeders, continuing to represent an outlier within this group.

The mid-ratio band (–1.5 to 0) comprises a taxonomically and ecologically diverse assemblage, including artiodactyls and perissodactyls representing browsers, grazers, and mixed feeders; browsing proboscideans; and several extinct taxa such as the notoungulate *Nesodon*, the mixed-feeding pilosan *Scelidotherium*, the litoptern *Macrauchenia*, the dinoceratan *Uintatherium*, and the basal proboscidean *Moeritherium*.

The high-ratio band (≥ 0) expands considerably with the inclusion of fossil taxa. Among extant species, the highest ratios occur in *Hippopotamus amphibius* and the elephantids *Elephas maximus* and *Loxodonta africana*, though these are surpassed by extinct browsing proboscideans. Early mastodonts such as *Zygolophodon* and *Mammut* exhibit ratios of approximately 0.5–0.7, elephantids cluster around 0.8–0.9, and *Deinotherium* exceeds 1.2. The upper portion of this band is dominated by grazers and browsing taxa, while its lower range includes mixed-feeding members of Diprotodontia, Notoungulata, and Pilosa.

The wide range of feeding strategies and digestive physiologies represented within the mid- and high-ratio bands indicates substantial ecological overlap among taxa. Browsers, grazers, and mixed feeders occur across all ranges, although the only highest ratios (> 0.4) belong to artiodactyl Hippopotamids and browsing proboscideans.

The extremely high ratios observed in extinct browsing proboscideans, which possess robust and elongate symphyses and mandibular tusks, or markedly reinforced jaws, support this hypothesis.

These taxa would have incurred substantial mechanical and energetic costs in moving and stabilising their mandibles during mastication, rest, and locomotion. The predominance of extinct species among the highest ratios highlights the evolutionary consequences of such

specialisation. Taxa exhibiting extreme mandibular inertia and highly derived morphologies likely required extensive daily food intake and expended considerable energy in each chewing cycle. Combined with narrow dietary preferences and sensitivity to resource fluctuations, these mechanical and energetic constraints would have significantly increased extinction risk among high-ratio megaherbivores.

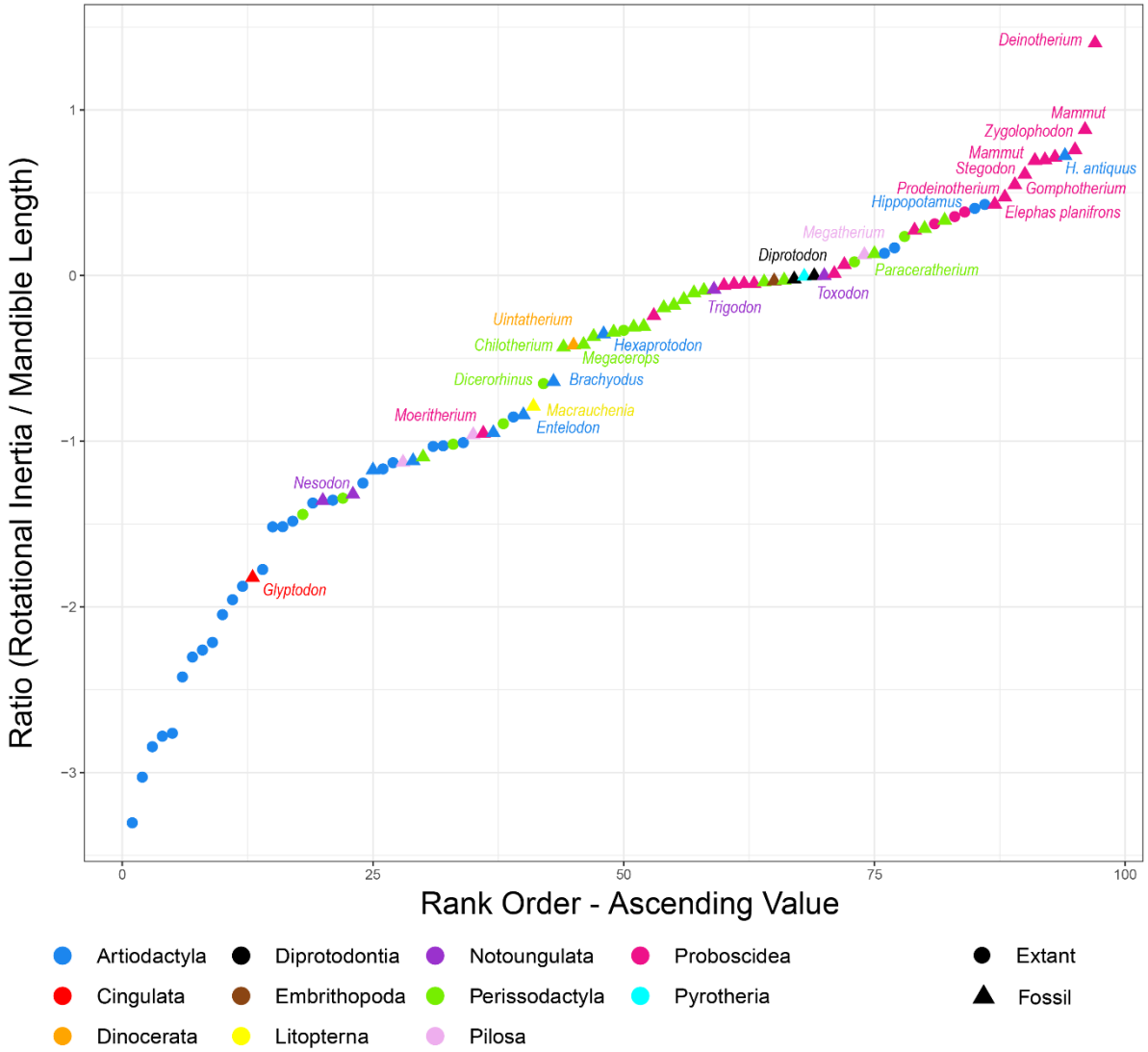

Figure 5.13. Total dataset. Ratio of rotational inertia to mandible length, plotted in order of ascending ratio value and denoted by taxonomic order.

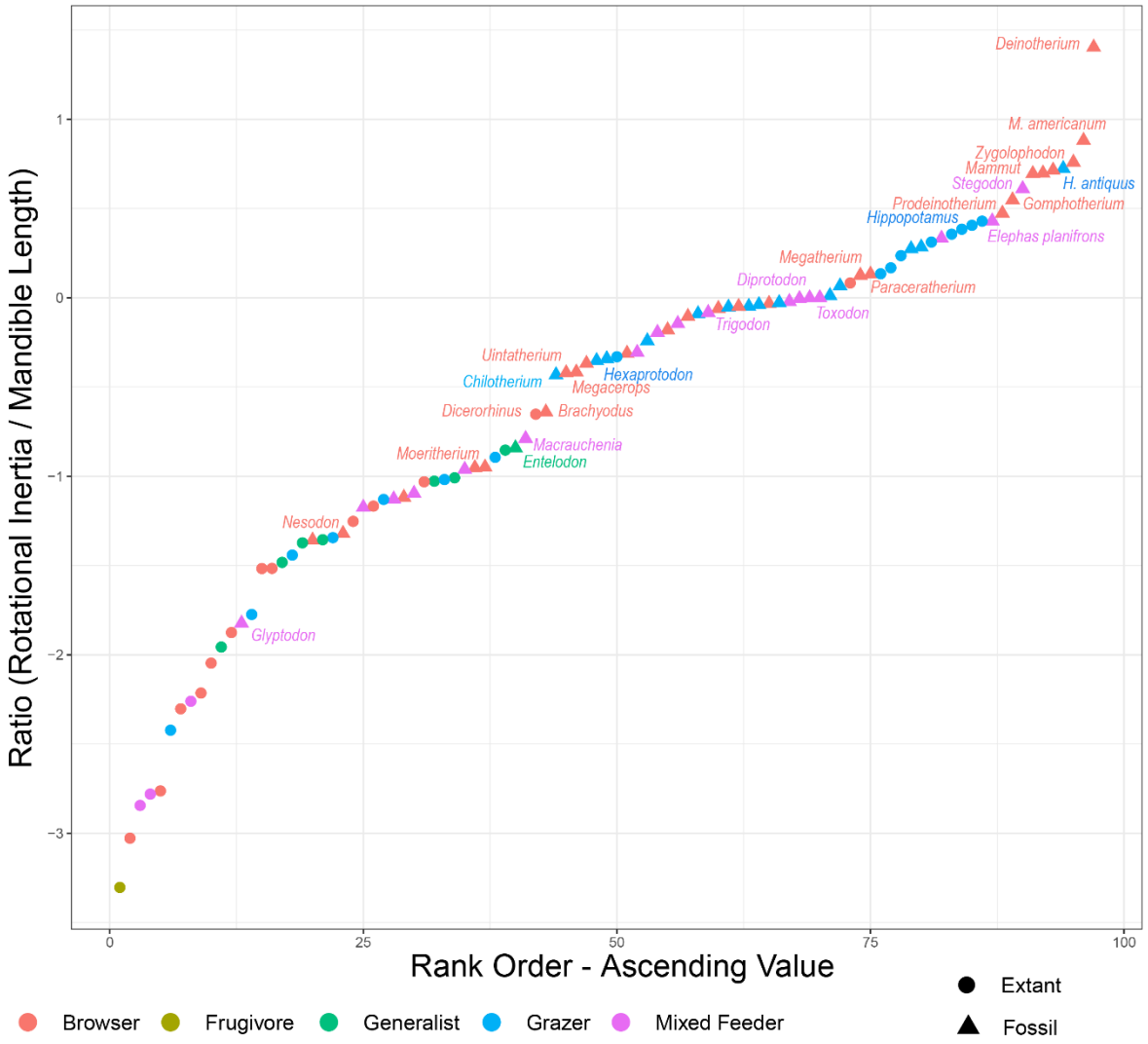

Figure 5.14. Total dataset. Ratio of rotational inertia to mandible length, plotted in order of ascending ratio value and denoted by broad dietary categorisation from the literature.

5.4.3 Results 3 – Addressing Hypothesis 3: co-variation of mandibular mechanics, mass properties, and dietary specialisation reflects a suite of adaptive traits promoting functional performance and survival, rather than being primarily determined by phylogenetic affinity or dietary category.

5.4.3.1 Results 3 – Addressing Hypothesis 3: Prediction 1: PCA and k-means clustering analysis of mass property, mechanical, anatomical and dietary traits will cluster species by extant or extinct status rather than phylogenetic affinity or dietary category, in the broad interspecific ungulate-grade sample.

For the total interspecific sample, the Elbow Method plot (Figure 5.15 A) shows a reduction in within-cluster sum of squared errors between k = 2 and k = 3. The inflection point, at k = 3, indicates diminishing returns in variance reduction beyond this value of k. However, the average Silhouette Score (Fig 15.5 B) was found to be below 0.5 for all values of k, with the highest score observed at k = 2. Silhouette scores less than 0.5 reflect weak separation between clusters, suggesting that while three clusters were a practice choice as indicated by the Elbow Methods, these data do not exhibit strong cluster structure.

The PCA biplots (PC1-PC2 (Figure 15.6 A) and PC1-PC3 (Figure 15.6 B) show overlap between the three k-means clusters. PC1, which accounts for 53.93% of total variance, is primarily associated with mandibular size and mass distribution variables, including mandible length, mass, centre of mass (CoM), and rotational inertia (Rot_I), as well as the masseteric insertion area (MIAREA), which is strongly correlated with inertia. PC2 (20.21%) and PC3 (11.99%) capture variation largely driven by the mechanical advantages of the masseter (MAM) and temporalis (MAT) muscles.

Purity scores for k = 3 (0.4074) and k = 4 (0.4321) indicate weak correspondence between the k-means clusters and dietary categories, suggesting that cluster structure is not strongly influenced by feeding ecology. Instead, clusters appear to reflect continuous gradients in mandibular form and biomechanical configuration rather than discrete ecological or phylogenetic groups.

Both Cluster 1 and Cluster 3 contain extant and extinct taxa spanning nearly the entire size range, including *Mammathus*, *Paraceratherium*, *Elasmotherium*, and *Arsiniotherium* near the upper bounds of the range, and across all taxonomic orders and dietary categories. Cluster 2 is

characterised by large-mandibled browsing, grazing, and mixed feeding taxa, with the negative aspect of PC1 dominated by extinct, longirostrine, browsing proboscideans.

This signals a decrease in total functional and morphological diversity overtime, as the extinct taxa expand the occupation of PC space substantially, and may suggest a particular suite of adaptations which facilitate efficient mastication while balancing functional capacity, structural strength, and dietary requirements were beneficial for survival. This suit of adaptations likely reflects decreased dietary specialisation, and therefore greater dietary adaptability and decreased extinction risk due to changing ecosystems.

Although extinct taxa tend to occupy regions of the PC morpho-functional space associated with high mass and rotational inertia, extant and extinct species overlap considerably along each of the PCs, indicating that these patterns result from mechanical scaling rather than categorical differences in evolutionary status. The PCA therefore shows that variation among taxa is governed chiefly by size-related and biomechanical parameters, with weak phylogenetic and ecological signal. Consequently, these results do not support the first prediction of Hypothesis 3, as species do not cluster by dietary category, phylogenetic affinity, or extinct or extant status, but instead along continuous functional and morphological gradients.

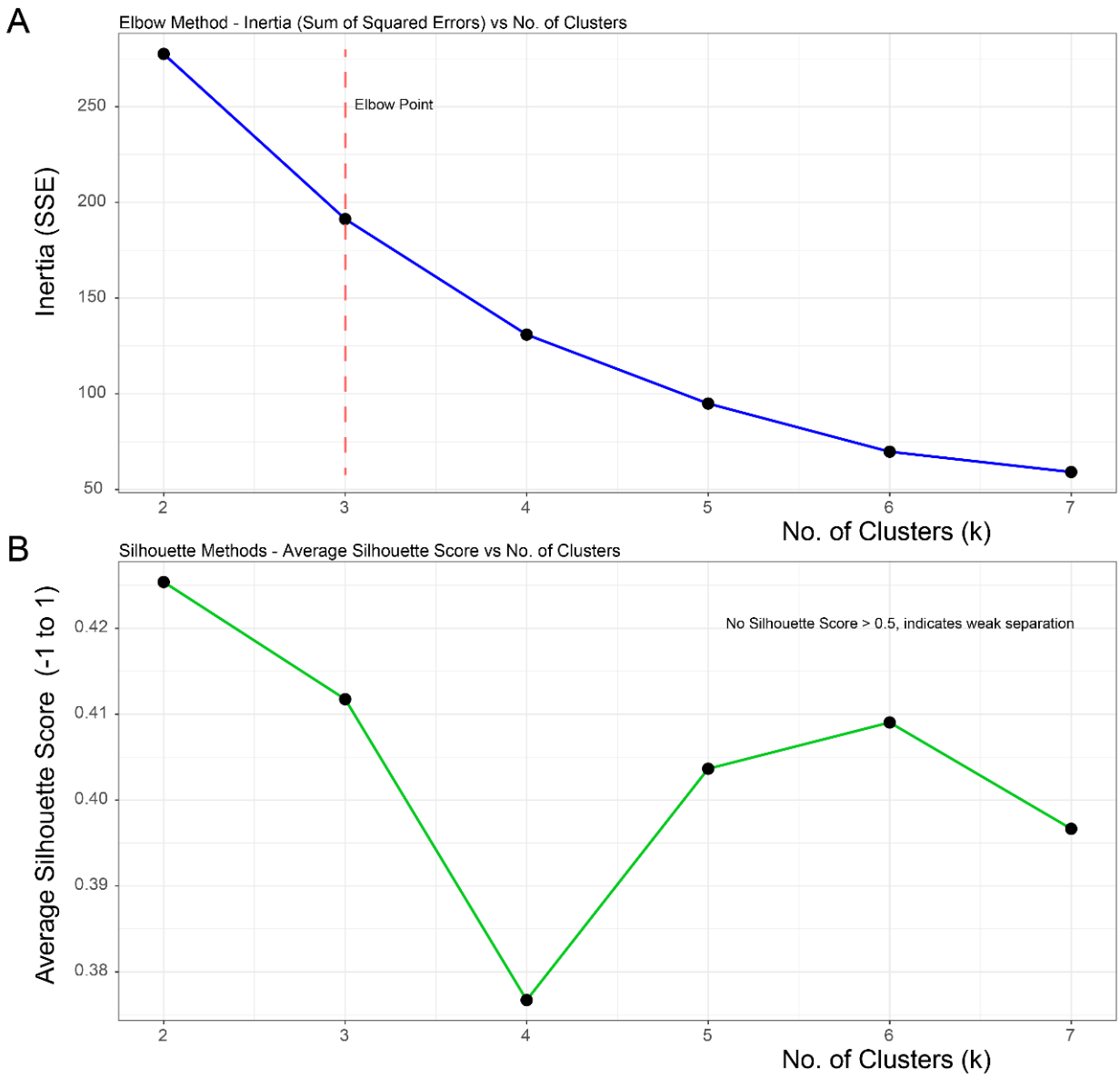

Figure 5.15. Evaluation of optimal numbers of cluster for k-means analysis for the total interspecific sample data. A) Elbow Method plot showing the relationship between the number of clusters, k, and WCSS inertia. B) Average Silhouette Scores for k = 2–7.

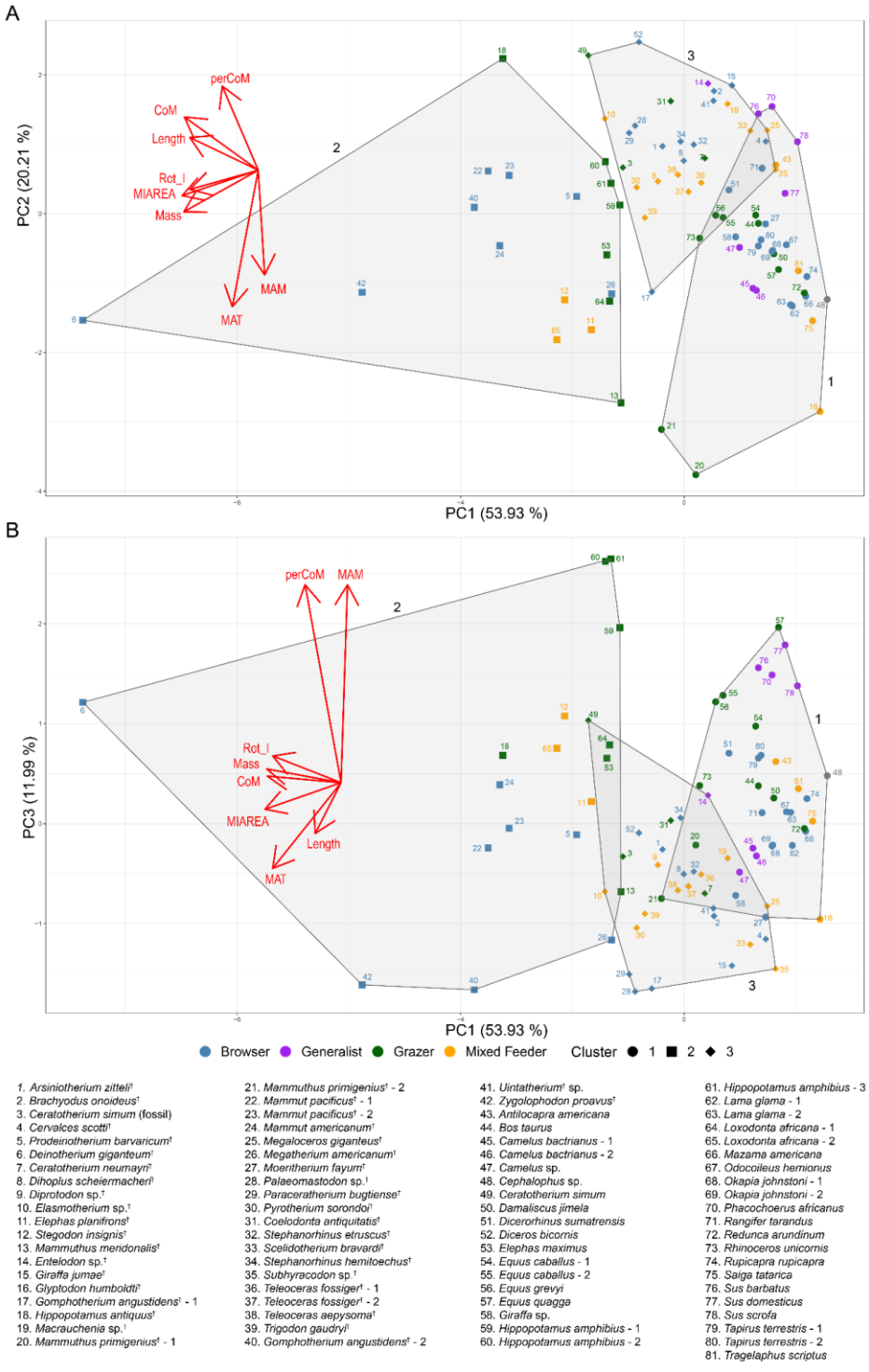

Figure 5.16. PCA of mandibular mechanical and morphological variables across extant and extinct ungulate-grade mammals with k-means clusters. (A) PC1 vs PC2 (explaining 53.93% and 20.21% of total variance, respectively). (B) PC1 vs PC3 (explaining 53.93% and 11.99% of total variance, respectively). Red vectors indicate variable loadings: mandible length, mandible mass, centre of mass (CoM), rotational inertia (Rot_I), masseteric insertion area (MIAREA), masseter (MAM) and temporalis (MAT) mechanical advantage, and the relative position of the CoM (perCoM). Three k-means clusters are identified (1, 2, 3).

5.4.3.1 Results 3 – Addressing Hypothesis 3: Prediction 2: PCA and k-means clustering analysis of mass property, mechanical, anatomical and dietary traits will cluster species by extant or extinct status rather than phylogenetic affinity or dietary category, in clade specific samples of proboscideans and rhinocertoids.

Subset 1: Proboscidea

For the proboscidean subsample, the Elbow Method plot (Figure 15.17 A) shows a reduction in within-cluster sum of squared errors between k = 2 and k = 4. The inflection point, at k = 4, indicates diminishing returns in variance reduction beyond this value of k. However, the average Silhouette Score (Figure 15.17 B) was found to be below 0.5 for all values of k, with the highest score observed at k = 4. Again, these results suggest these data do not exhibit strong cluster structure.

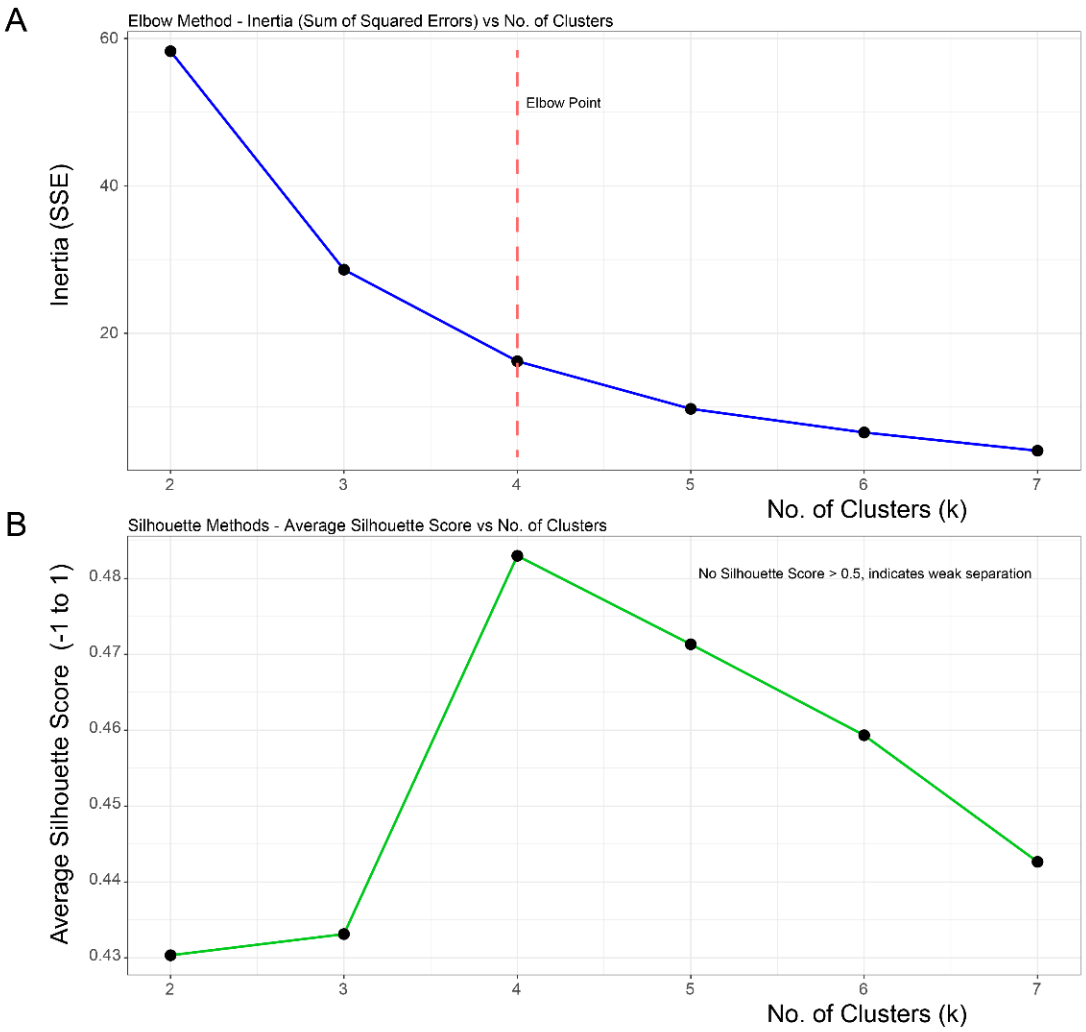

Figure 5.17. Evaluation of optimal numbers of cluster for k-means analysis for the proboscidean subsample data. A) Elbow Method plot showing the relationship between the number of clusters, k, and WCSS inertia. B) Average Silhouette Scores for k = 2–7.

The PCA biplots for the proboscidean dataset (PC1-PC2 and PC1-PC3; Figure 5.18 A–B) collectively explain 88% of the total variance in mandibular morphological and mechanical traits. PC1 (54.79% of variance) primarily reflects size and mass property variables, including mandible mass, rotational inertia, absolute and proportional centre of mass (CoM), masseteric insertion area (MIAREA), and mandible length. PC2 (22.66%) captures variance associated with the mechanical advantages of the masseter (MAM) and temporalis (MAT) muscles, while PC3 (11.48%) represents additional variation in mandible length and proportional CoM displacement.

External validation using purity and silhouette scores indicated moderate agreement between k-means clusters and broad dietary categories (purity = 0.7778 for k = 4), though separation among clusters was weak. These values suggest that the clusters capture some biologically meaningful structure, but variation is largely continuous rather than discrete.

Four clusters were identified, broadly reflecting differences in mandible size, rotational inertia, and mechanical advantage. Cluster 1, solely represented by *Deinotherium giganteum*, exhibits extreme mandibular mass and rotational inertia coupled with high mechanical advantage. Cluster 2 includes the mixed feeding *Elephas maximus*, and the browsing *Gomphotherium, Prodeinotherium,* and *Moeritherium*, showing low rotational inertia and low-to-moderate mechanical advantage. Cluster 3 is comprised entirely of browsing mammutids (i.e., *Zygolophodon*, *Gomphotherium*, *Mammut*). Cluster 4, which includes the grazing mammoths *Mammuthus*, and the mixed feeding *Loxodonta*, *Stegodon*, and *Elephas planifrons*, represents taxa with low rotational inertia and moderate-to-higher mechanical advantage

Overlap is observed between Clusters 2 and 4 along PC3, which contain browsers, mixed feeders and grazers, and are primarily distinguished by differences in lever mechanics. The separation of these clusters along PC2 illustrates a continuum from browsers to mixed feeders to grazers in terms of increasing mechanical advantages of the masseter and temporalis.

The separation between Cluster 2 and Cluster 3 along PC1 is primarily due to increasing mandible length, mass properties, and more anterior centre of mass position. Clusters 3 and 4 are more clearly separated, primarily along PC1 and PC3, where mandible length and proportional CoM exert strong influence. The distribution of clusters and taxa across PC space demonstrates that dietary groups are interspersed among clusters, although a browsers-to-grazer continuum exists along PC2. PC1 clearly separates the extreme mandible of *Deinotherium* (Cluster 1) from the other three clusters, while Cluster 3, consisting of browsing mammutids, is separated from Cluster 2&4 along PC1 and PC3.

Clusters 1&3 are entirely composed of extinct taxa and are clearly separated from all extant species (i.e., *Loxodonta africana*, *Elephas maximus*) which evidence moderate lever efficiency, relatively short and light mandibles, and posteriorly located centres of mass. While the cluster analysis does not cleanly group extant taxa together and separately from extinct taxa, the extant species do occupy a drastically reduced total PC space compared to the extinct taxa. This finding does not support the second prediction of Hypothesis 3 but does indicate extant proboscideans possess a masticatory system adapted for mechanical efficiency, balanced between the more extreme characteristics of specialised browsers (e.g., *Mammathus*) and mandibular-tusked browsers (e.g., *Gomphotherium*, *Prodeinotherium*).

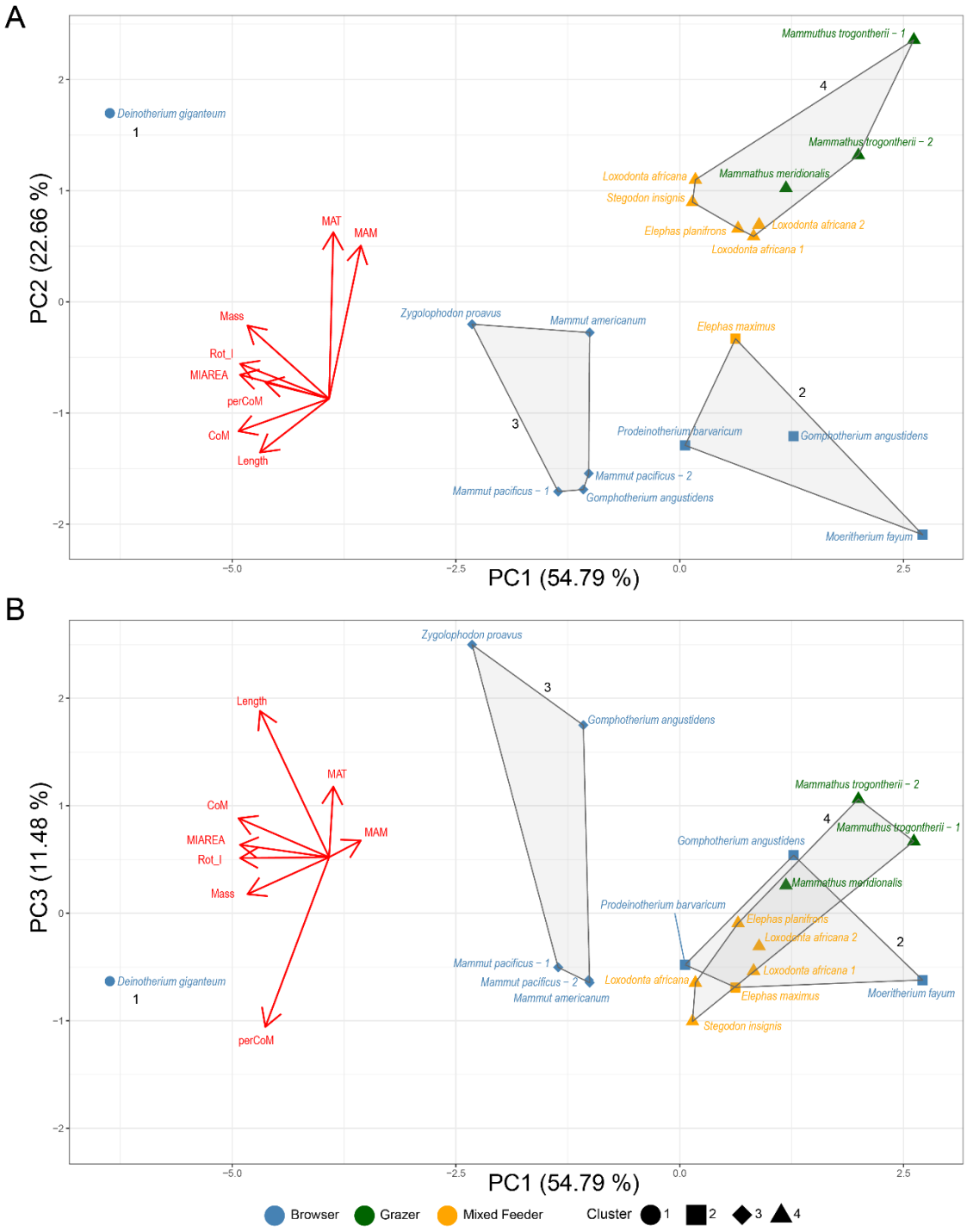

Figure 5.18. Principal Component Analysis (PCA) of mandibular morphological and mechanical variables for extinct and extant proboscidean taxa. (A) PC1–PC2 biplot (54.79% and 22.66% of total variance, respectively). (B) PC1–PC3 biplot (54.79% and 11.48% of variance). Red vectors indicate variable loadings: mandible length, mass, centre of mass (CoM), rotational inertia (Rot_I), relative CoM position (perCoM), masseteric insertion area (MIAREA), and mechanical advantages of the masseter (MAM) and temporalis (MAT). Four k-means clusters (1–4) are illustrated.

Subset 2: Rhinocerotoidea

For the rhinocerotoid subsample, the Elbow Method plot (Figure 5.19 A) shows a steep decline in within-cluster sum of squared error between k = 2 and k = 3, which indicated an inflexion point at k = 3. This result was supported by the Silhouette Score (Figure 5.19 B), with the highest average score seen at k = 3 (approximately 0.59), suggesting three clusters representing the most appropriate solution. Unlike the previous two datasets (i.e., the total interspecific and clade-specific proboscidean datasets), silhouette scores here exceed 0.5 indicating moderate-to-strong cluster separation.

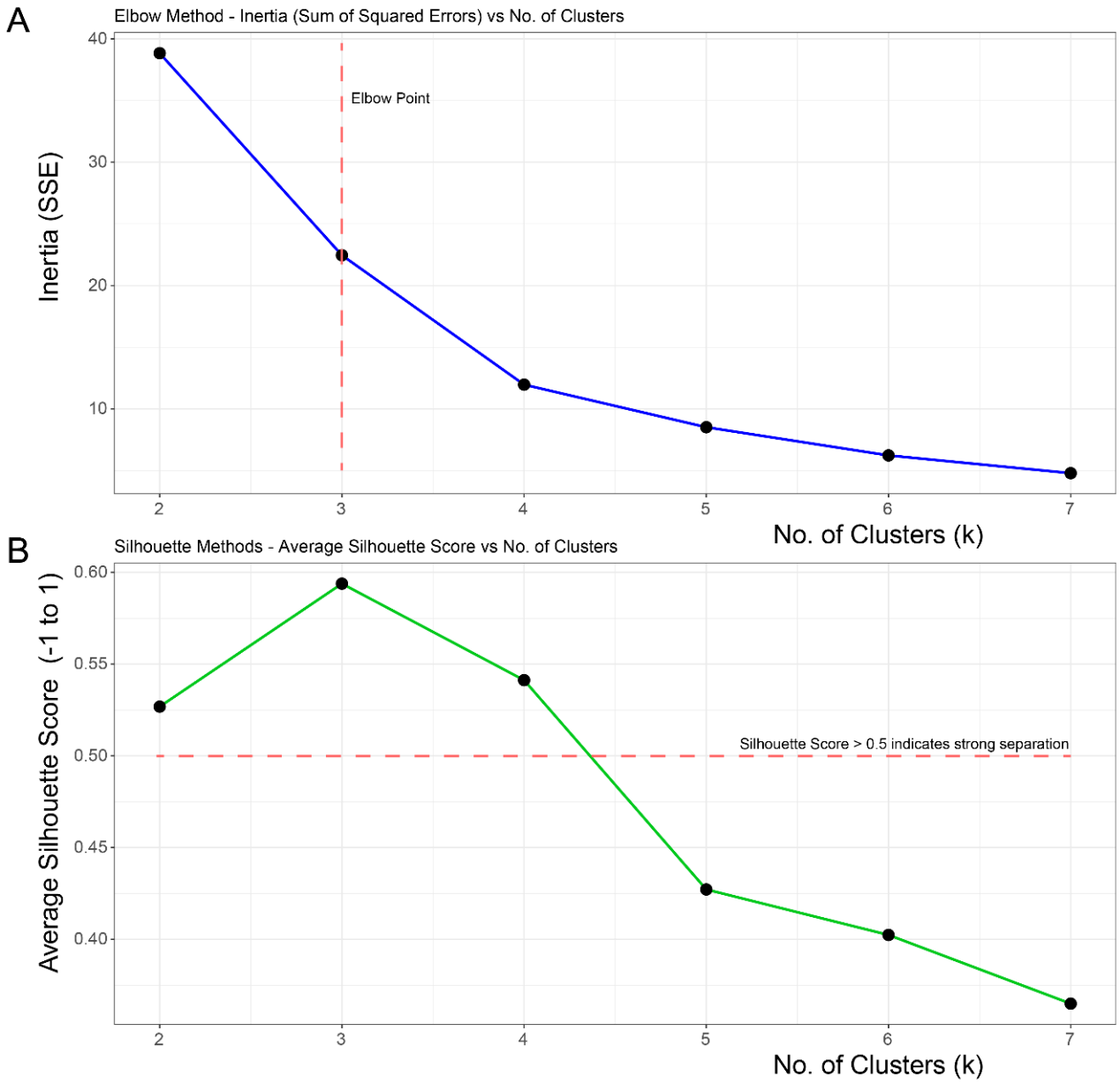

Figure 5.19. Evaluation of optimal numbers of cluster for k-means analysis for the rhinocerotoid subsample data. A) Elbow Method plot showing the relationship between the number of clusters, k, and WCSS inertia. B) Average Silhouette Scores for k = 2–7.

The PCA biplots for the rhinocerotoid dataset, PC1-PC2 (Figure 5.20 A) and PC1-PC3 (Figure 5.20 B), account for 90.52 % of the total variance in the measured mandibular mass property, morphological, and biomechanical variables. PC1 (57.89 % of variance) primarily represents size and mass-related differentiation, with high loadings for mandible length and rotational inertia, and lesser contributions from centre of mass (CoM), proportional centre of mass (perCoM), masseteric insertion area (MIAREA), and mandible mass. PC2 (19.05 %) captures variance largely associated with the mechanical advantages of the masseter (MAM) and temporalis (MAT) muscles, together with both absolute and proportional CoM, while PC3 (13.58 %) represents additional variance in mechanical advantage of the jaw adductor muscles and mandible length.

Three k-means clusters were identified, forming a gradient in mandibular size, mass distribution, and mechanical efficiency. Cluster 1, comprising *Ceratotherium simum* and *Diceros bicornis*, includes the two extant African species characterised by moderate mandibular mass, relatively high mechanical advantage of the masseter, long mandible length, and relatively anterior centres of mass. Cluster 2 contains species belonging to the extinct genera *Coelodota*, *Stephanorhinus*, *Dihoplus*, *Teleoceras*, and the basal *Subhyracodon*, the extinct species *Ceratotherium neumayri*, which has a close phylogenetic affinity to *Ceratotherium simum*, and the extant species *Dicerorhinus sumarensis* and *Rhinoceros unicornis*. This cluster is characterised by short-to-moderate mandible length and rotational inertia, a broad range of lever mechanics, and intermediate centre of mass positions. Cluster 3 includes *Elasmotherium* sp., *Paraceratherium bugtiense*, and a Pleistocene specimen of *Ceratotherium simum*, which occupy the negative extremes of PC1 and PC2, reflecting large mandibular size, high inertia, reduced masseter mechanical advantage, but enlarged masseter insertions areas.

Although moderate-to-strong separation among clusters is evident, external validation revealed no correspondence between k-means clusters and broad dietary categories (purity = 0.375 for k = 3). Substantial overlap occurs among browsers, grazers, and mixed feeders, indicating that diet does not significantly influence the covariation of mandible mass properties with these mechanical and anatomical characteristics. Notably, the two extant African rhinocerotoids cluster closely together, despite contrasting feeding strategies and close phylogenetic relationships with several extinct taxa (i.e., *Ceratotherium simum* (fossil) and *Ceratotherium neumayri*). The extant genera *Dicerorhinus* and *Rhinoceros*, share a closer phylogenetic affinity with the extinct genera *Stephanorhinus*, *Dihoplus*, and *Coelodonta*, and the other extant

genera, and group together in Cluster 2, indicating a strong phylogenetic constraint to the covariation of mass properties, mechanics, and anatomy.

Overall, the distribution of taxa across the PC space demonstrates that mandibular variation in rhinocerotoids is best explained by scaling effects, phylogenetic constraint, and continuous functional gradients rather than discrete dietary or ecological categories, or whether the species in question has survived to the present. As such, these findings do not support the second prediction of Hypothesis 3.

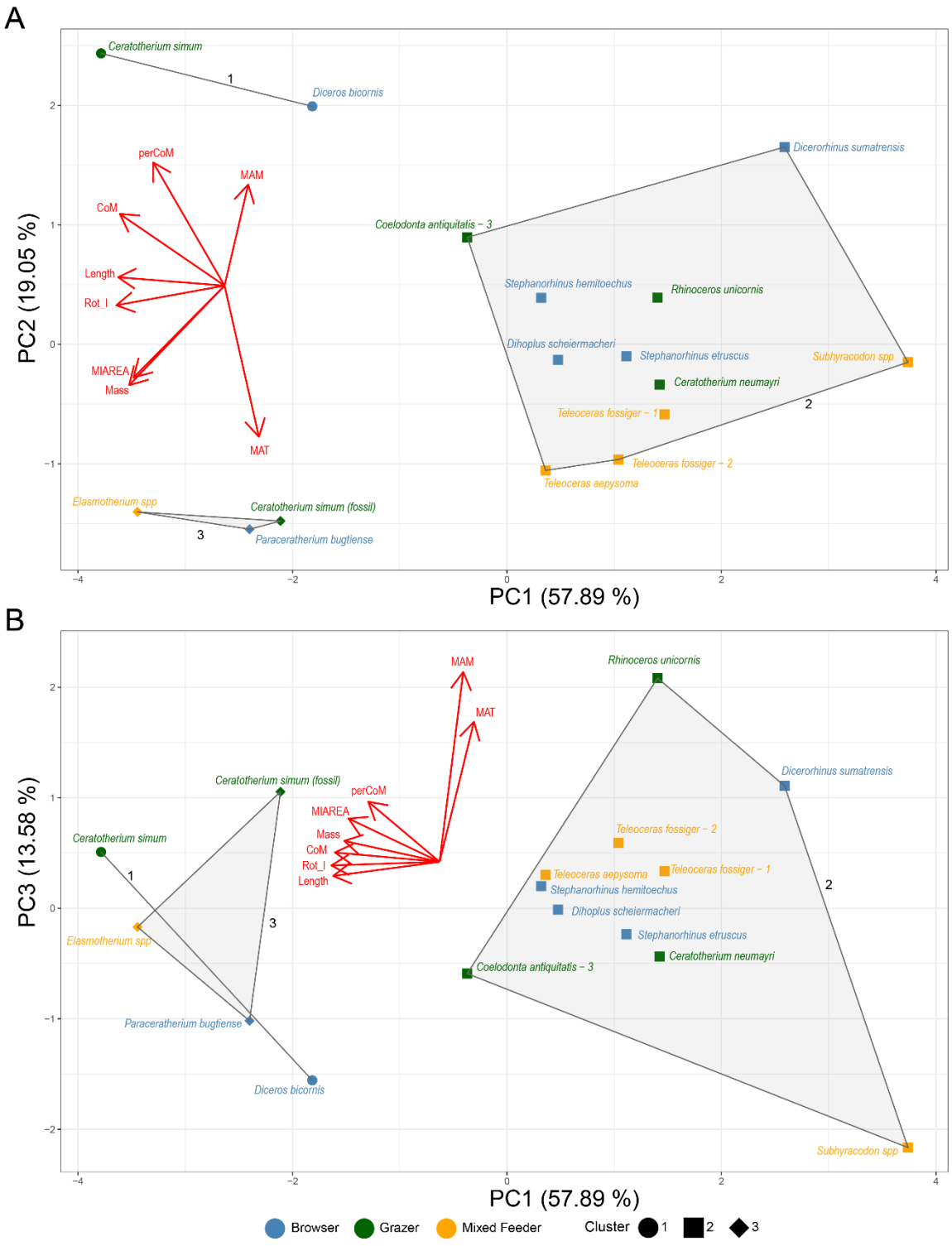

Figure 5.20. Principal Component Analysis (PCA) of mandibular morphological and mechanical variables for extinct and extant rhinocerotoid taxa. (A) PC1–PC2 biplot (explaining 57.89% and 19.05% of total variance, respectively). (B) PC1–PC3 biplot (57.89% and 13.58% of variance). Red vectors indicate variable loadings: mandible length, mass, centre of mass (CoM), proportional CoM (perCoM), rotational inertia (Rot_I), masseteric insertion area (MIAREA), and mechanical advantages of the masseter (MAM) and temporalis (MAT). Three k-means clusters (1–3) are identified.

5.5 Discussion

This study aimed to investigate mandibular mass properties in a broad sample of ungulate-grade mammals and ecologically analogous taxa, with particular emphasis on evaluating scaling relationships, the mechanical cost of mastication, and evolutionary outcomes. Each of the four main research aims was achieved.

Firstly, the interspecific sample utilised in previous chapters was expanded by incorporating a morphologically, ecologically, and phylogenetically diverse sample of ungulate-grade mammals and ecologically similar taxa including *Megatherium*, *Scelidotherium*, *Glyptodon*, and *Diprotodon*. This substantially increased the range of sizes and morphologies available for analysis beyond the limits of the extant sample, and allowed for the quantification of mass properties, as well as anatomical and mechanical traits across broad phylogenetic and temporal scales.

Second, the scaling relationships among mandibular length, mass, centre of mass, rotational inertia, and masseteric insertion area were shown to follow linear allometric trends across all taxa, consistent with the allometric scaling relationships observed in the extant-only interspecific sample. The close agreement among Ordinary Least Squares (OLS), Reduced Major Axis (RMA), and Phylogenetic Generalised Least Squares (PGLS) regressions demonstrates that these relationships represent fundamental mechanical constraints rather than resulting from phylogenetic or sampling bias.

Third, species exhibiting extreme mandibular morphologies, particularly longirostrine proboscideans, displayed high inertia-to-length ratios indicative of increased energetic costs of mastication. These results link mechanical inefficiency to dietary specialisation and provide a functional explanation for the elevated extinction risk of highly specialised megaherbivores.

Fourth, multivariate analyses revealed that variation in mass properties, anatomical and mechanical traits is continuous and governed by co-variation among mass properties, leverage efficiency, and size. This reflects a continuous adaptive gradient rather than discrete ecological or taxonomic divisions, demonstrating that functional diversity influenced adaptability and survivability through mechanical optimisation.

Finally, the survival of extant species to the present day such as *Elephas maximus*, *Loxodonta africana*, *Ceratotherium simum*, and *Diceros bicornis* is associated with mechanically efficient mandibular configurations characterised by reduced inertia and increased leverage when compared to their extinct relatives. These traits likely conferred energetic advantages and are

associated with grazing and mixed feeding diets that contributed to their survival relative to extinct relatives, especially during the reduction in forest habitats and expansion of grassland after the Middle Miocene Climatic Optimum.

5.5.1 Scaling of Mass Properties and Energetic Constraints

Positive allometry in mandibular mass and rotational inertia relative to mandible length demonstrates that as mandible size increases, reinforcement of mandibular structure scales at a disproportionately high rate, likely to maintain robusticity and functional integrity under loading (Alexander 1985; Biewener 2005). Conversely, the isometric scaling of masseteric insertion area with rotational inertia suggests proportional increases in muscle attachment that maintain consistent mechanical efficiency (Turnbull 1967; Mendoza and Palmqvist, 2008) and that the masseter is adapted to generate sufficient torque to contend with mandibular rotational inertia.

High rotational inertia in large extinct species implies considerable energetic cost during mastication. Taxa with anteriorly positioned centres of mass and enlarged symphyses, such as *Deinotherium* and *Zygolophodon*, would have required greater torque to rotate the jaw about the temporomandibular joint, resulting in higher energy expenditure per chewing cycle. In contrast, extant elephantids show reduced mandibular length, more posteriorly positioned centres of mass, and reliance on trunk-mediated food acquisition (Shoshani and Tassy, 2005; Gheerbrant and Tassy, 2009), features that lower cost of work and increase masticatory mechanical efficiency. These results reflect a broader evolutionary shift from both elongate and structurally robust but energetically costly morphologies to more energetically conservative forms.

5.5.2 Phylogenetic Constraint and Functional Convergence

PGLS was not used in Chapters 2 and 4 because those chapters do not test evolutionary relationships among species. Chapter 2 focuses on methodological validation, where the same specimens are compared across methods, so phylogenetic non-independence is irrelevant. Chapter 4 examines the mechanical effects of head posture on mandibular inertia, which is a within-specimen transformation rather than a comparison of independently evolved traits. In contrast, Chapter 3 and Chapter 5 explicitly investigates interspecific scaling, where phylogenetic relatedness affects statistical independence, and therefore PGLS is appropriate.

Mandibular scaling relationships are consistent across Artiodactyla, Perissodactyla, Proboscidea, and Pilosa, demonstrating widespread convergence in the biomechanics of the mandible. PGLS, OLS, and RMA regressions yield nearly identical slopes, indicating that shared ancestry exerts minimal influence on mandibular scaling. These results show that functional optimisation through biomechanical constraint has been a stronger determinant of mandibular evolution than phylogenetic constraint, a pattern mirrored in other aspects of mammal cranial and postcranial morphology (Polly et al. 2013; Cassini et al. 2017; Grossnickle 2020).

5.5.3 Clade-Specific Adaptive Trends

5.5.3.1 Proboscideans

Proboscidean mandibles vary primarily in size, rotational inertia, mechanical advantage, and morphology with many forms (e.g., dinotheres, mammutids) possessing mandibular tusks. The morphological diversity of proboscidean mandibles is illustrated below (Figure 5.21). Extinct browsing species exhibit extremely high rotational inertia and anterior centre of mass positions, whereas extant elephantids cluster within lower-inertia regions of PC morpho-functional space, with improved leverage and mechanical efficiency. This trend suggests that longirostrine forms incurred high energetic costs due to anteriorly weighted mandibles and mandibular tusks.

The transition toward shorter, lighter mandibles with posterior CoM coincided with post-Miocene environmental change and the expansion of open habitats (Figueirido et al., 2011). Mechanically efficient configurations and mixed-feeding strategies likely facilitated survival under more variable environmental conditions. The evolution of the proboscidean trunk may represent a key energetic adaptation: a structure that performed many functions of the mandibular tusks at lower mechanical cost. The shift to trunk-mediated food acquisition reduced calories expended per unit of intake and may have allowed trunked elephantids to outcompete longirostrine lineages (Li et al. 2024).

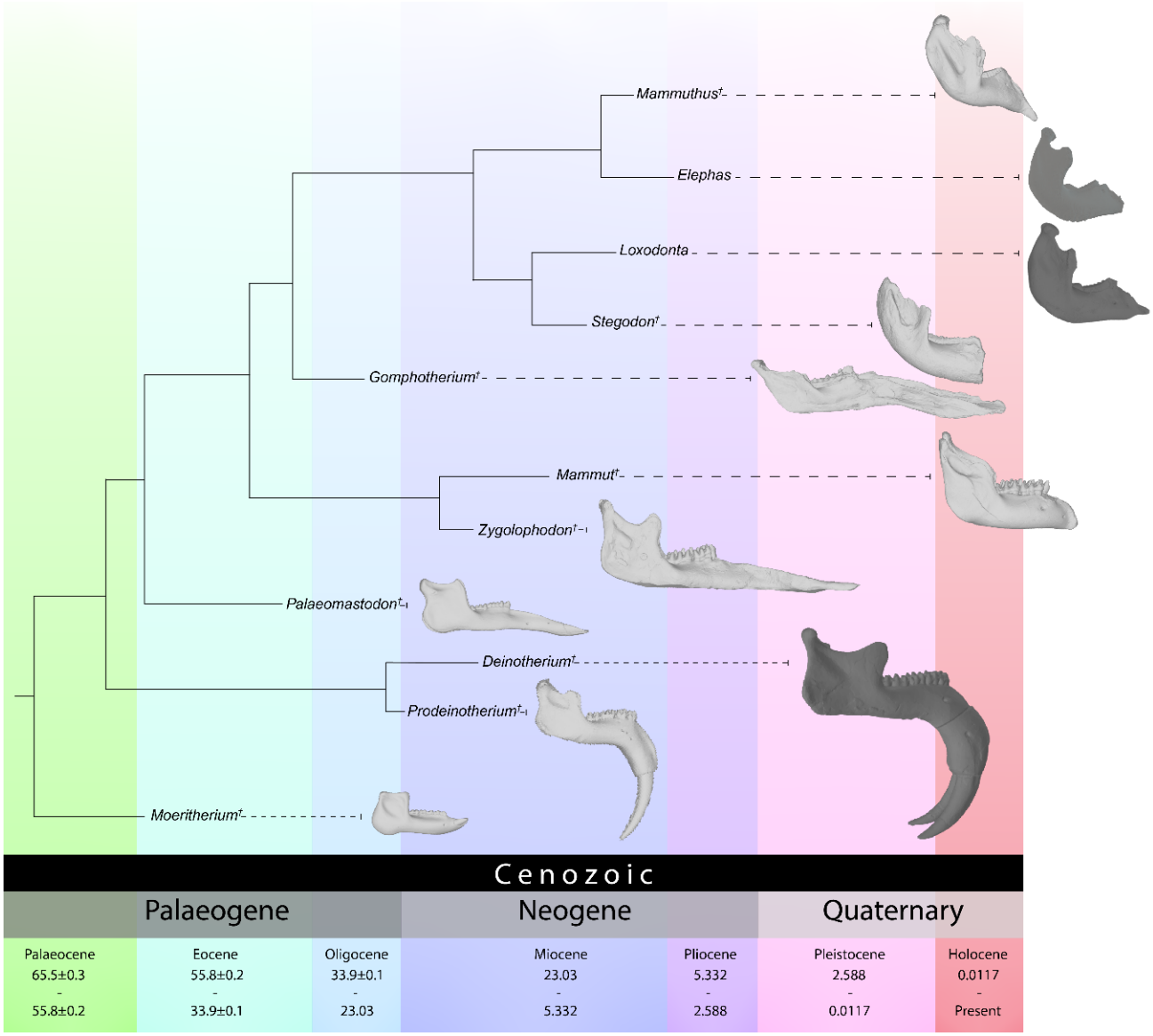

Figure 5.21. Cladogram of proboscideans mapped onto geological time (Palaeocene to Present), with approximate divergence and extinction times indicated. Lateral views of representative mandibles illustrate the contrast between the high past diversity of proboscideans and their limited modern representations.

5.5.3.2 Rhinocerotoids

Rhinocerotoid occupation of PC morpho-function space evidence similar mechanical gradients to those observed in proboscideans. The two extant African species (*Ceratotherium simum*, *Diceros bicornis*) cluster toegther despite divergent diets, reflecting convergence toward mechanically efficient mandibles despite anterior centres of mass due to reduced mass, owing to relatively narrow and slender mandibles, and higher mechanical advantage of the masseter.

Extinct taxa such as *Teleoceras*, *Dihoplus*, and *Chilotherium* occupied intermediate positions, whereas *Paraceratherium* and *Elasmotherium* define high-inertia extremes associated with high mass and poor masseter leverage. The morphological diversity of rhinocerotoids mandibles is illustrated below (Figure 5.22).

The contraction of PC morpho-functional space among extant taxa compared to their extinct relatives indicates a loss of functional and morphological diversity within Rhinocerotoidea. The extinction of most Miocene and Pliocene genera predates human influence and is better explained by environmental change and competition. The decline of *Paraceratherium*, for example, coincided with the expansion of gomphotheres into Asia, whose foraging behaviour and vegetation disturbance likely reduced browse availability in the open grassland habitats and increased competition for resources.

An additional observation concerns the specimen labelled "*Ceratotherium simum* (fossil)," which clusters closer to *Paraceratherium* and *Elasmotherium* than to *Ceratotherium* or *Diceros*. This placement, together with recent taxonomic revisions within Dicerotini, suggests potential misidentification of the museum specimen.

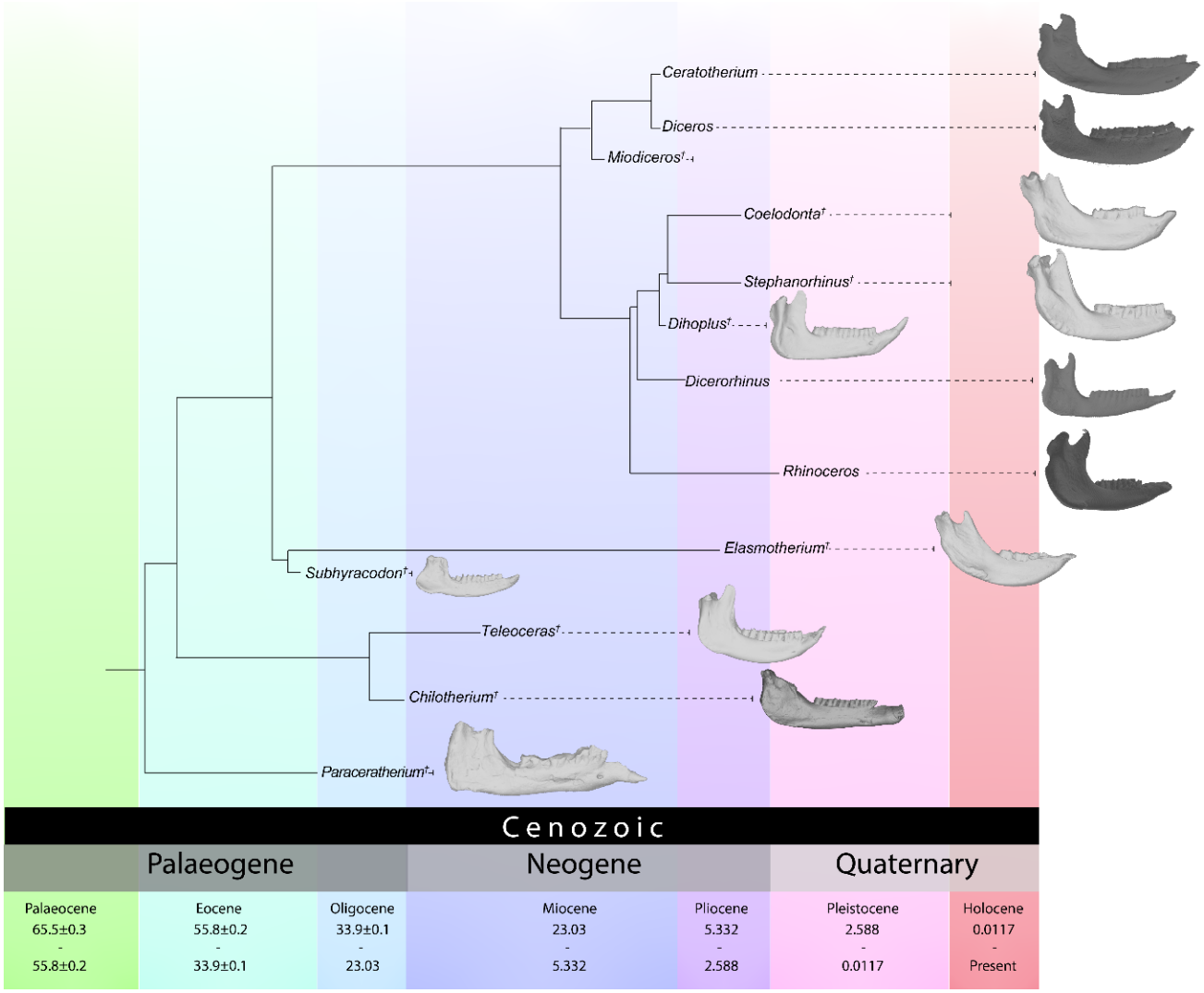

Figure 5.22. Phylogenetic tree of rhinocerotoidea mapped onto geological time (Palaeocene to Present), with approximate divergence and extinction times indicated. Lateral views of representative mandibles illustrate the contrast between the high past diversity of this clade and their limited modern representations.

5.5.4 Methodological Considerations and Future Research

This study employed a simple two-dimensional model of jaw movement and was limited to the hard mineralised tissues of the mandible to facilitate large-scale comparative analysis. Future research should incorporate three-dimensional finite element modelling to evaluate dynamic stress distribution and multi-body dynamic modelling to incorporate three-dimensional jaw kinematics to more fully explore the role of mandible mass properties in mastication and the evolution of the masticatory system. Dissection-based quantification of soft-tissue contributions to mandibular mass and centre of mass in extant taxa would refine mechanical

estimates, as soft tissues substantially increase overall system mass inertia. Dissection of the masseter, and measurement of its physiological cross-sectional area, would also provide a direct evaluation of the use of masseteric insertion area as a coarse proxy for muscular size and torque. However, expanding the depth of analysis in these ways would likely necessitate a reduction in morphological and taxonomic diversity of the study sample. Expanded taxonomic sampling, beyond ungulate-grade mammals and their direct ecological analogues, could further test the universality of scaling patterns, while integration of isotopic or microwear analyses specific to the study specimens would strengthen links between mass properties, mechanical traits and diet.

5.5.5 Concluding Statement

This research represents a comprehensive assessment of mandibular mass properties in ungulate-grade mammals. The findings demonstrate that mandibular form is primarily determined by mechanical and energetic constraints rather than dietary or phylogenetic factors. Across both extant and extinct taxa, positive allometry of mandible mass and rotational inertia with mandible length, and isometric scaling of the masseteric insertion with rotational inertia, indicate consistent biomechanical optimisation through the evolution of ungulate-grade mammals.

Extinct megaherbivores with high inertia and specialised morphologies incurred greater energetic costs and were more vulnerable to environmental change. In contrast, extant taxa exhibit mechanically more efficient jaw configurations that reduce energetic demands and facilitate ecological flexibility. The overall decline in morphological and functional diversity, particularly among proboscideans and rhinocerotoids, reflects the loss of specialised forms and the survival lineages with mechanically conservative masticatory systems.

6. Discussion

This thesis has achieved its aims of establishing and validating digital methodologies for estimating mass distribution, investigating the scaling of mass properties with mandible functional anatomy and the role of head posture on the mechanical costs of mastication, and expanding these analyses to the fossil record by integrating extinct megafaunal taxa.

Chapter 2 validated computed tomography (CT)-based and surface-model approaches for estimating centre of mass (CoM) and rotational inertia.

Chapter 3 investigated how mandibular form scales with biomechanical and anatomical features in extant ungulate-grade mammals, revealing strong and predictable scaling relationships largely independent of diet or phylogeny.

Chapter 4 evaluated how habitual head posture influences mandibular mechanics, demonstrating that posture reduces energetic costs of mastication but does not alter underlying scaling trends, and offers substantial reductions in rotational inertia in species with heavy and anteriorly weighted mandibles.

Chapter 5 extended this framework across the Cenozoic fossil record, integrating ecologically, morphologically, and phylogenetic disparate extinct species to assess whether the observed mechanical patterns reflect fundamental principles or sampling artefacts. The inclusion of ungulate-grade taxa, including extinct megaherbivores, dating from to the Eocene to the present confirmed that these biomechanical trends persist across taxonomic and temporal boundaries, reflecting fundamental constraints governing mandibular evolution.

6.1 Synthesis of Key Findings

6.1.1 Chapter 2 - Methodological Validation and Innovation

Chapter 2 established a methodological foundation for quantifying mandibular mass properties. By validating the voxel-mass specific CT-based centre of mass estimation method (CoM-CT) against the compound-scales method, it demonstrated that digital reconstructions can yield accurate, repeatable, and non-destructive estimates of mass distribution. Critically, CT-derived CoM values were statistically indistinguishable from direct analogue measurements, confirming the method's reliability. The study also showed that volumetric models (CoM-CT) and surface scans (CoM-Surface) provide accurate methods for estimating centre of mass, even when internal density variations are unknown or inaccessible.

These methodological advances have significant implications. They enable large-scale comparative analyses of both extant and extinct taxa mass properties, even those obtained with different methods. They also demonstrate that the external morphology of the mandible sufficiently captures most variation in mass distribution, as internal architecture contributes minimally to overall mass properties. This finding underpins the feasibility of large-scale digital analyses across deep time and phylogeny, supporting the increasing role of open-access 3D repositories (e.g., MorphoSource, Sketchfab) in studies of quantitative functional morphology and in the field of virtual palaeontology.

6.1.2 Chapter 3 - Scaling Relationships and Functional Correlates

The interspecific scaling analysis presented in Chapter 3 demonstrated that the mass properties of the mandible conform to predictable allometric trends consistent with established biomechanical scaling theory (Biewener, 2005; Clemente and Dick, 2023). Mandibular mass scaled approximately isometrically with length, whereas rotational inertia showed positive allometry (slope ≈ 6.1 > 5.0 under isometry), indicating a disproportionate increase in mechanical resistance with size. In contrast, the area of masseteric insertion scaled isometrically with rotational inertia, suggesting proportional muscular adaptation to increased inertial demands.

These relationships were largely independent of diet and phylogeny. Phylogenetic generalised least squares (PGLS) analyses indicated that evolutionary relatedness had limited influence on scaling parameters, implying convergence towards biomechanical optimisation rather than lineage-specific constraint. This convergence is comparable to that observed in limb bones, where bone diameters scale with positive allometry relative to limb length across terrestrial mammals (Christiansen, 2002).

The results indicate that mandibular morphology in herbivorous mammals is primarily governed by mechanical requirements: maintaining structural integrity during masticatory loading while reducing energetic cost. Increases in jaw length and mass, or anterior displacement of the centre of mass, elevate rotational inertia and necessitate greater muscle force to achieve equivalent angular acceleration. Conversely, shorter or lighter mandibles, and those with more posterior centres of mass, reduce inertial load and energy expenditure.

The identified scaling patterns align with biomechanical principles that also apply to other components of the mammalian skeleton. In limb bones, positive allometry of cross-sectional

area relative to length maintains stresses within elastic limits as size increases (Alexander and Jayes, 1983; Biewener and Taylor, 1986). Comparable mechanisms likely operate in the mandible, where structural reinforcement and increased second moments of area counteract the greater bending moments associated with both larger size and higher bite forces. These relationships are consistent with McMahon's (1973) concept of elastic similarity, which proposes that morphological scaling is constrained by the need to preserve constant material stress under increasing load.

The coexistence of positive interspecific allometry and negative intraspecific allometry is not contradictory but reflects the operation of different processes at evolutionary versus developmental scales (Klingenberg, 1996; Voje et al., 2014). At the interspecific level, morphological variation reflects both body-size scaling and adaptive divergence associated with ecology and function (Voje et al., 2014; Klingenberg, 2016). In ungulates and other mammals, larger species commonly exhibit more robust cranio-mandibular morphology and greater estimated bite-force capacity, although the precise expression of these trends varies among clades and feeding systems (Herring, 1993; Law et al., 2018). Where mandibular mass increases and mass is distributed farther from the temporomandibular joint, rotational inertia will also increase; interpreting this as an adaptive consequence of increased body size and feeding load is biomechanically plausible, but the specific link between interspecific mandibular robusticity and rotational inertia is usually inferred rather than tested directly.

In contrast, intraspecific variation largely reflects ontogenetic growth and individual variation within a shared functional and ecological framework (Klingenberg, 1996). Individuals within a species typically share broadly similar feeding strategies, cranial architecture, and functional constraints, so increases in size during growth do not necessarily require fundamentally different mechanical solutions. Instead, ontogenetic and static allometries can differ from evolutionary allometries because they are shaped by developmental covariation, genetic architecture, and the functional requirements maintaining performance within species (Klingenberg, 1996; Voje et al., 2014). Negative intraspecific allometry can therefore be interpreted as consistent with developmental or functional constraints that limit how rapidly particular traits increase relative to body size, although the precise mechanism must be demonstrated for the trait and taxon in question.

The contrast between these patterns indicates that evolutionary and developmental scaling are not expected to be identical. Morphological differences among species are not simply scaled-up versions of within-species growth trajectories; rather, evolutionary allometry may diverge from ontogenetic or static allometry when selection, ecology, and long-term lineage-specific history reshape trait

relationships over macroevolutionary timescales (Klingenberg, 1996; Voje et al., 2014; Klingenberg, 2016). In this sense, disproportionately robust mandibles in larger species are best interpreted as a clade- and function-dependent evolutionary outcome, whereas within-species scaling more often reflects the developmental maintenance of function across differently sized individuals.

6.2.3 Chapter 4 - Behavioural and Postural Compensation

Chapter 4 examined the influence of habitual head posture on the effective mass properties of the mandible. Across a comparative sample of ungulate-grade mammals, adjusting for in vivo head angle displaced the effective centre of mass posteriorly and reduced effective rotational inertia, particularly in large-bodied grazers where anterior head inclination provided substantial mechanical compensation.

Postural adjustment constitutes an additional mechanism for mitigating the mechanical consequences of scaling. Comparative research indicates that habitual head orientation is influenced by vestibular morphology and locomotor energetics. The orientation of the lateral semicircular canal, which approximates neutral head posture, exhibits both phylogenetic and ecological signals (Benoit et al., 2020; Coutier et al., 2017). During locomotion, coordination between head oscillation and stride frequency reduces energetic losses from inertial head motion (Graf et al., 1995; Löscher et al., 2016). These dynamics enable large herbivores to maintain sensory and masticatory stability despite increased cranial mass. Variation in cranio-cervical alignment among feeding types—from the downward-oriented head of the white rhinoceros to the elevated posture of browsers—illustrates how head angle modifies muscle moment arms and jaw loading direction, integrating behavioural, vestibular, and mechanical systems (Schellhorn, 2018; Taylor et al., 2009).

Although these adjustments did not alter general scaling relationships, which remained isometric or positively allometric, they considerably reduced absolute inertia values, in some cases by up to 70–80%. This reduction indicates that habitual feeding posture functions as a biomechanical adaptation to limit the energetic costs associated with large or elongate mandibles. The extent of this effect varied with feeding ecology and body size: grazers with sustained head-down postures showed the greatest reduction, whereas small-bodied species and browsers exhibited limited changes.

These findings correspond with previous evidence linking posture, feeding height, and vigilance behaviour in ungulates (Benoit et al., 2020; Köhler, 1993; Owen-Smith, 1988). The results indicate functional integration between morphological and behavioural traits. Although direct co-evolution of mandibular structure and head posture cannot be inferred, their interaction contributes to maintaining mechanical efficiency within ecological and physiological constraints.

Vestibular evidence further supports the role of posture in influencing mandibular loading. The orientation of the lateral semicircular canal correlates with neutral head posture across ungulates and other mammals, reflecting both phylogenetic and ecological determinants of feeding stance (Benoit et al., 2020; Coutier et al., 2017). During locomotion, synchronisation of head oscillations with stride timing minimises the mechanical cost of supporting and stabilising the head–neck system (Löscher et al., 2016). This interaction among vestibular control, musculoskeletal geometry, and energy use suggests that head posture acts as a biomechanical filter on mandibular mechanics. Incorporating posture into models of mastication may refine estimates of muscle orientation and force direction during feeding (Graf et al., 1995; Taylor et al., 2009).

6.2.4 Chapter 5 - Fossil Integration and Macroevolutionary Perspective

Chapter 5 extended the analysis to the fossil record across 11 mammalian orders to assess whether the mechanical scaling relationships identified in living species are consistent through time. The results demonstrated that positive allometry of mass and inertia, and isometry of muscular insertion area, are maintained across approximately 60 million years of evolutionary history, supporting their interpretation as fundamental biomechanical principles.

Extinct megaherbivores such as *Deinotherium* and *Zygolophodon* exhibited highly anterior centres of mass and elevated rotational inertia relative to mandibular length, reflecting increased energetic costs of mastication. These front-loaded configurations required greater muscular torque for jaw movement and rotation during feeding and occupy the upper limits of rotational-inertia ratios. Their decline and extinction coincides with periods of global climatic aridification and vegetation change during the Miocene and Plio-Pleistocene, respectively. (Fortelius et al., 2006; Figueirido et al., 2011).

In contrast, surviving taxa such as *Elephas maximus*, *Loxodonta africana*, *Ceratotherium simum*, and *Diceros bicornis* occupy a narrower region of morphofunctional space,

characterised by shorter, lighter mandibles and more posterior centres of mass, configurations associated with reduced energetic demand and greater mechanical efficiency. The observed contraction of morphofunctional diversity through time suggests that biomechanical efficiency acted as a selective filter during intervals of environmental stress and ecological competition.

6.3 Methodological Contributions and Implications

This thesis makes several methodological contributions to the study of vertebrate functional morphology.

6.3.1 Digital Methodologies

The validation of digital methods for estimating mass properties establishes a consistent framework for quantifying mandibular mechanics in both extant and extinct taxa. The combined use of CT-based (CoM-CT) and surface-based (CoM-Surface) approaches enables the analysis of extensive comparative datasets without physical handling or destructive procedures. Their demonstrated equivalence increases accessibility to rare, fragile, and digitally archived specimens.

The result that external geometry accounts for most of the variance in mass properties is particularly relevant to palaeontological research, where many mandibles are preserved only as external casts or incomplete specimens. Together with previous evidence supporting the accuracy of digital reconstruction (Lautenschlager, 2016; DeVries et al., 2022), these findings show that reliable functional estimates can be produced at relatively low cost. By combining methodological precision with digital accessibility, this study enhances the feasibility and inclusivity of biomechanical analysis

This thesis does not attempt to establish a universal protocol for all computed tomography (CT)-based analyses of mineralised tissues, but instead develops a practical workflow for analysing specimens that vary in size and originate from multiple scanners and acquisition settings. As such, the priority is the implementation of a standardised and reproducible analytical pipeline in which outputs can be validated and shown to be comparable across datasets. This focus reflects established challenges in quantitative CT, where variability in acquisition and reconstruction can affect measurement consistency.

Firstly, phantom calibration should be used wherever possible, as quantitative CT depends on converting Hounsfield Units (HU) to physical density, which is known to vary with scanner type, acquisition parameters, and object size (Kalender, 2011; Scherberich et al., 2025). Secondly, consistency of acquisition protocol should be prioritised. Parameters such as tube voltage (kVp), reconstruction kernel, scanner model, and imaging geometry are known to influence density estimates and bone mineral measurements (Boone et al., 2001; Prevrhal et al., 2003). Where possible, these parameters should be standardised. However, when replying on online repositories this is rarely possible. In this case, differences should be documented and considered potential sources of error when interpreting results.

Analyses involving specimens of different sizes introduce additional challenges, including partial volume averaging, resolution limits, and size-dependent influences on attenuation, all of which can affect accuracy (Ketcham and Carlson, 2001; Prevrhal et al., 2003). These factors necessitate validation procedures such as sensitivity analyses and careful reporting of methodological limitations.

6.3.2 Masseter Attachment Area as a Proxy for PCSA

Physiological cross-sectional area (PCSA) is the anatomical parameter most directly related to the maximum force-generating capacity of a muscle. In this context, masseter attachment area provides a useful comparative proxy for muscle size, but it is not a precise estimator of PCSA. This is because PCSA is determined not only by the external geometry of the attachment site, but also by internal muscle architecture, particularly fibre length, pennation angle, and muscle thickness or volume, none of which are captured by attachment area alone (van Eijden, Korfage and Brugman, 1997; Lieber and Fridén, 2001). Studies of jaw-muscle architecture likewise show that force-related and excursion-related properties depend on internal architecture rather than attachment surface area alone (Antón, 1999; Antón, 2000).

Muscles with similar attachment areas can differ substantially in architecture. Longer fibres increase shortening capacity, whereas greater pennation allows more fibres to be packed into a given muscle volume, increasing PCSA without requiring a proportional increase in attachment area (Lieber and Fridén, 2001; van Eijden, Korfage and Brugman, 1997). Similarly, increases in muscle thickness can elevate PCSA independently of attachment area. As a result, attachment area alone is not diagnostic of PCSA. In ungulates, the masseter is a dominant component of the masticatory system and is

reflected in mandibular morphology through enlarged attachment regions, but variation in muscle architecture means that attachment area cannot be used to precisely estimate PCSA from bone alone; this conclusion is consistent with broader comparative work on osteological proxies for jaw-muscle size.

Empirical studies indicate that the relationship between muscle attachment area and PCSA is limited rather than exact. In a broad carnivoran sample, estimates based on maximum muscle cross-sectional area correlated more strongly with muscle mass and PCSA than did estimates derived from muscle attachment areas, and the authors explicitly caution that attachment-based approaches should be used carefully across diverse taxa (Dickinson et al., 2021). Accordingly, attachment area captures broad trends in relative muscle investment but does not provide a precise measure of absolute force capacity.

In this thesis, the observation that masseter insertion area scales proportionally with mandibular rotational inertia supports the interpretation of functional covariation between muscle investment and increasing mechanical demand. However, because attachment area is only a coarse proxy for PCSA, this relationship should be interpreted cautiously and used primarily as a comparative metric rather than as a direct estimator of muscle force. That caution is consistent with the current literature on osteological reconstruction of jaw musculature, which shows that internal architecture and muscle thickness materially affect force estimates derived from anatomy.

6.3.3 Integrating Behavioural and Mechanical Modelling

The head posture adjustment model developed in Chapter 4 constitutes a methodological advance by incorporating empirically measured neutral head angles to rotate centre-of-mass coordinates. This provides a physiologically grounded correction for in vivo head and mandible orientation, linking static morphological data to functional context and improving estimates of mechanical cost and comparative energetics.

Although multi-body dynamic simulations could capture three-dimensional kinematics and muscle activation, the two-dimensional rotational model applied here offers an effective comparative framework. It isolates the mechanical component of angular resistance while remaining computationally efficient for large datasets. Future studies may refine this approach by incorporating soft-tissue mass or muscle force data derived from dissections or finite element modelling.

6.3.4 Quantitative Integration of Fossil and Extant Data

A central strength of this thesis is the integration of fossil and extant data within a single analytical framework. Including extinct megafauna enables direct evaluation of whether the identified biomechanical patterns reflect general mechanical principles or depend on the composition of modern taxa. The persistence of consistent scaling relationships across both groups demonstrates that digital biomechanical methods can effectively reveal functional constraints operating over evolutionary timescales.

6.4 Energetic and Functional Determinants of Mandibular Form

The findings of this thesis support a central principle that mandibular evolution is constrained by the energetic cost of moving mandibular mass. The distribution of mineralised tissue, the geometry of the jaw, and the leverage of the adductor musculature jointly determine the torque required for mastication and, by extension, the energetic cost of mastication.

6.4.1 Scaling of Mechanical Cost

The positive allometry of rotational inertia relative to mandibular length indicates that, with increasing body size, the energetic cost of accelerating and decelerating the jaw rises disproportionately. Larger mandibles contain more mass and distribute it farther from the axis of rotation. Without compensatory adaptations—morphological, such as symphyseal shortening, narrowing, or reduced robusticity, or behavioural, such as anterior head inclination—the torque required from the adductor musculature would increase substantially, driving enlargement of the masticatory muscles and further constraining mandibular morphology.

The isometric scaling of the masseteric insertion area with rotational inertia suggests that muscle size increases proportionally with mechanical demand, consistent with stabilising selection maintaining a constant safety factor. This relationship ensures sufficient torque to overcome inertia without excessive energetic cost, paralleling patterns observed in limb musculature, where cross-sectional area scales with body mass to maintain stress limits (Biewener, 2005).

Functional integration between bone and muscle development under mechanical loading is well established in mammalian mastication. Experimental and comparative studies indicate

that mandibular morphology is regulated by maintaining strain within physiological limits (Duncan and Turner, 1995; Frost, 1996, 2003). Bone modelling follows the mechanostat principle, reinforcing regions subjected to habitual stress in proportion to applied strain. This adaptive relationship among muscle mass, fibre composition, and mandibular geometry has been demonstrated in both experimental and anatomical studies (Herring, 1993, 2001; Ross et al., 2007).

Muscle fibre composition contributes to this integration: slow oxidative fibres support sustained and repetitive contraction, whereas fast glycolytic fibres facilitate rapid, high-force movements (Schiaffino and Reggiani, 2011; Salmons, 2009). The dominance of fatigue-resistant fibres in the masseter and pterygoid muscles of herbivorous mammals likely reflects adaptation to continuous mastication, balancing metabolic efficiency with mechanical endurance. Increased bone deposition at the molar row and masseter insertion area would also shift the mandibular centre of mass posteriorly, further optimising mechanical balance.

Reinforcement of the mandibular corpus with increasing body mass accords with the same principles of bone functional adaptation. Experimental and histological evidence shows that bone remodels in response to sustained strain, maintaining stress within physiological limits (Frost, 1996; Duncan and Turner, 1995). In mammalian jaws, cortical thickening corresponds to regions of peak bending stress during chewing (Herring, 1993). Fibre-type composition varies with feeding ecology, with grazers exhibiting higher proportions of oxidative fibres and greater muscle mass (Salmons, 2009). Together, these relationships among muscle physiology, bone structure, and energy use represent an integrated response to the mechanical requirements of repetitive mastication.

6.4.2 Trade-offs between Strength, Efficiency, and Function

Mandibular form represents a balance between mechanical strength, mechanical performance in terms of kinematics, and functional flexibility. Deep, robust jaws, as seen in grazing rhinoceroses and extinct proboscideans, resist bending and torsional stress but exhibit high rotational inertia. In contrast, slender, elongate jaws reduce mass yet may decrease bite force and mechanical advantage and depending on the structure of the diastema and symphysis, may also shift the centre of mass anteriorly, increasing inertia. The consistent scaling of mass, inertia, and masseteric insertion area across taxa indicates that these trade-offs are governed by fundamental mechanical principles rather than by ecological or phylogenetic factors.

6.4.3 Mandible Inertial Properties when Chewing is Slow

Masticatory function in herbivores is characterised by relatively slow, repetitive chewing cycles supported by jaw adductor muscles dominated by fatigue resistant Type 1 fibres (Williams et al., 2007; Kayar et al., 1988; Nishita et al., 1993; Tuxen and Kirkeby, 1990). In this case, performance is constrained less by maximal power output and more by the capacity to contend with repeated loading during prolonged feeding, with large herbivores engaging in chewing activity for many hours per day (Beauchemin, 2018). Increased muscle physiological cross-sectional area (PCSA) enhances maximal force production (Martin et al., 2020) and, although not always explicitly demonstrated in the context of mastication, it is biomechanically plausible that greater PCSA also improves endurance by distributing load across a larger number of fibres, thereby reducing fatigue during sustained chewing. This interpretation is consistent with scaling studies showing that jaw adductor mass and PCSA increase with body size (Perry et al., 2011), and with broader evidence that chewing cycle duration increases and frequency decreases with body size (Druzinsky, 1993; Stover & Williams, 2011). Together, these findings support the inference that increased muscle size in larger taxa contributes not only to force generation but also to maintaining effective mandibular motion under increased mass and inertia, although this latter point remains a biomechanical inference rather than a directly tested hypothesis.

Mechanically, mandibular inertia primarily affects the torque required to accelerate and decelerate the jaw (Ross et al., 2017). When chewing is slow, angular accelerations are small, reducing the inertial contribution to total torque demand. Consequently, differences in inertia are unlikely to produce substantial differences in observable kinematics, such as maximum gape angle, cycle duration, or occlusal trajectory, provided that neuromuscular control compensates through adjustments in muscle recruitment and activation timing (Ross et al., 2009; Ross et al., 2017). Instead, inertial variation is more likely to manifest as differences in muscular effort and loading, including increased torque requirements.

This effect is likely scale-dependent; for small or moderately sized mandibles experiencing low chewing speeds, inertia likely plays a minor role relative to joint mechanics, food material properties, muscle physiology, and neural control (Ross et al., 2017; Virot et al., 2017). In contrast, for large ungulates with massive mandibles and long feeding durations, inertia represents a more substantial mechanical constraint influencing muscular work. This interpretation is consistent with scaling relationships in chewing dynamics and mandibular inertia (Druzinsky, 1993; Ross et al., 2009) but, again, should be regarded as an inference synthesis of available biomechanical evidence rather than direct evidence.

6.4.4 Covariation of Jaw Soft Tissue with Mandible Hard Tissue Mass

Jaw soft tissues, particularly the jaw adductor musculature, generally covary positively with mandibular hard tissue mass, although this relationship is functional rather than strictly geometric. Muscle and bone scale together as components of a mechanical system responsible for generating, transmitting, and resisting forces during mastication (Herring, 1993; van Eijden, 1991). Consequently, muscle size, architecture, and attachment morphology tend to covary with mandibular mass, shape, and structural reinforcement, although the specific relationships are influenced by diet, cranial architecture, and phylogenetic constraints (Ross, 2007).

Across mammals, this covariation reflects the integration of force production and load resistance. In ungulates, it is most strongly expressed in the masseter–mandible complex, as mastication is dominated by masseter and medial pterygoid-driven transverse grinding rather than temporalis-dominated vertical biting typical of many carnivores (Herring, 1993; Ross, 2007). Increases in muscle force capacity are associated with corresponding changes in mandibular architecture, including enlargement of the masseteric fossa, expansion of the angular process, and increased corpus depth, which together increase attachment area and resistance to bending and torsional stresses (van Eijden, 1991; Herring, 1993). This pattern is well documented in mammalian functional morphology, where increased jaw adductor physiological cross-sectional area (PCSA) is associated with more robust mandibles and expanded attachment surfaces (van Eijden, 1991; Ross, 2007).

In herbivorous mammals, particularly ungulates, these relationships are accentuated by the mechanical demands of repetitive mastication of fibrous plant material (Herring, 1993). Species relying on extensive transverse chewing typically exhibit enlarged masseter musculature alongside deeper and more reinforced mandibular corpora, increasing resistance to bending during mastication (Herring, 1993; Ross, 2007). This reflects a functional integration in which mandibular structure accommodates forces generated by large adductor muscles over repeated loading cycles.

Within the context of this thesis, a related pattern is observed in mandibular mass properties. As mandible size increases, rotational inertia increases disproportionately, indicating greater resistance to angular acceleration (Ross et al., 2017). However, masseter insertion area scaling in relation to inertia is not directly established in the literature; the interpretation that muscular torque capacity covaries with increasing mechanical demand is consistent with general principles of musculoskeletal scaling and functional integration (Herring, 1993; Ross, 2007) but should be regarded as a biomechanical inference rather than a directly demonstrated relationship.

6.5 Implications for Chewing Kinematics

6.5.1 Covariation of Jaw Soft Tissue with Mandible Hard Tissue Mass

Chewing cycle duration is best understood as a primarily neuromuscular phenomenon, in which skeletal properties, including mandibular inertia, act as constraints rather than primary determinants. Chewing rhythm is determined by the central pattern generator (CPG) in the brainstem, which produces activation of jaw adductor musculature. The chew period is governed by the oscillatory properties determined by this neural control, together with muscle contraction dynamics and sensory feedback from the teeth, muscles, and joints (Lund and Kolta, 2006). As such, the mandible and its mass properties do no generate chew rhythm but respond to the motor pattern within a closed-loop system linking neural activation, muscle contraction, mandibular motion, and sensory feedback.

Within this framework, muscle dynamics are the primary mechanical constraint on chewing frequency. Jaw closing muscles require sufficient time for activation, force development, the power stroke, and relaxation. If the chew cycle duration is too short, adequate force cannot be generated. The force–velocity relationship further constrains performance, as force declines at high shortening velocities, limiting how quickly effective chewing can occur. Although elastic elements, such as the tendons and aponeuroses of the jaw muscles, periodontal ligament, and articular disc and joint capsule of the temporomandibular joint, may improve mechanical efficiency (Roberts, 2016), they do not determine frequency.

Chewing rhythm is further modulated by sensory feedback, indicating that it is not purely centrally driven. Inputs from periodontal receptors, muscle spindles, Golgi tendon organs, and the temporomandibular joint adjust bite force and timing in response to food properties, with harder foods generally producing slower cycles (Lavigne et al., 1987; Morimoto et al., 1989; Tonni et al., 2020; Al Sayegh et al., 2022;). Thus, chew period is dynamically regulated rather than fixed by skeletal properties.

Inertia influences mechanical demand but not rhythm generation. Increased inertia raises the torque required for a given angular acceleration, but the neuromuscular system compensates by adjusting acceleration, cycle duration, and muscle recruitment (Alexander, 2003; Biewener, 2003). Consequently, inertia affects performance limits and energetic demand, not the neural rhythm itself. Empirical evidence supports this interpretation: chew cycle duration scales only weakly with body size (approximately $T \propto M^{0.1–0.2}$) (Ross et al., 2007; Iriarte-Díaz et al., 2011),

far less steeply than expected if inertia were dominant. This indicates that neuromuscular control compensates for increases in skeletal mass.

Mandibular inertia affects chewing rhythm and kinematics only when mechanical demands approach the limits of neuromuscular compensation. Under typical, slow, force-dominated chewing, neural and muscular dynamics dominate, and inertia acts as a secondary constraint on torque and energetic demand. Only in cases of high acceleration or exceptionally large inertia does it meaningfully influence kinematics. Chewing rhythm is therefore a fundamentally neural-first phenomenon that is constrained, but not determined, by muscular and skeletal properties.

6.5.2 Gape Angle

Gape angle is an important variable in mastication, although its relative importance depends on the phase of the chewing cycle and the aspect of performance considered (e.g., force, kinematics, or energetics) (Herring, 1993; Ross, 2007). While chewing frequency is primarily governed by central pattern generators and neuromuscular control, gape angle influences the mechanical output of the masticatory system by affecting muscle length, moment arms, joint configuration, and bite force transmission (Herring, 1993; Ross, 2007).

Jaw adductor muscles operate under a length–tension relationship, such that muscle force production varies with gape. At large gape angles, muscles are extended beyond optimal fibre length, reducing force-generating capacity, whereas at smaller gape angles, muscles operate closer to optimal length and produce greater force. Consequently, maximum bite force is typically achieved at relatively small gape angles (Herring, 1993). In addition, gape angle affects mechanical advantage through changes in muscle moment arms and joint configuration, further influencing force transmission during the power stroke; this relationship between gape, moment arms, and bite force is well established in biomechanical models and experimental studies of vertebrate feeding systems (Ross, 2007).

Gape angle also interacts with mandibular inertia by influencing angular displacement and acceleration. Larger gape angles involve greater angular excursions and therefore can increase the torque required to accelerate and decelerate the mandible. However, the specific contribution of inertia relative to muscle and joint forces depends on chewing speed and system dynamics (Ross et al., 2017). Changes in mandibular orientation with various gape angles may also affect effective

inertia, affecting total torque requirements, although this effect is likely small relative to muscular force capacity and is not consistently quantified in the mastication literature.

6.6 Behavioural and Postural Modulation of Mechanical Cost

The results presented in Chapter 4 indicate that habitual head posture influences the energetic cost of mastication. An anteriorly inclined head posture, typical of many grazers, shortens the lever arm between the mandible's centre of mass and the temporomandibular joint, thereby reducing rotational inertia and the muscular torque required to accelerate the jaw during chewing. Although this adjustment does not modify the underlying allometric relationships among length, mass, and inertia, it lowers the absolute mechanical load on the masticatory musculature.

Feeding-related head and neck positions correspond closely with ecological behaviour. Browsers generally maintain higher head carriage and a more horizontal jaw orientation, whereas grazers feed with the head lowered toward the ground (Janis, 2008; Owen-Smith, 1973). Vestibular and cranial morphology reflect these differences: the lateral semicircular canal in grazing species, such as the white rhinoceros, is oriented more steeply relative to the skull base than in browsing taxa, indicating a habitual downward-facing posture (Schellhorn, 2018; Benoit et al., 2020). During locomotion, head oscillations are synchronised with stride frequency to minimise muscular effort (Löscher et al., 2016). These relationships show that posture functions both as an ecological adaptation and as a mechanical factor influencing mandibular loading and bite-force direction.

Postural adjustments provide an energetically efficient response to the mechanical challenges of large body size. In grazers that feed for extended periods with the head lowered (Janis, 2008), even small reductions in rotational inertia can produce cumulative energetic savings. Over evolutionary timescales, these advantages may have favoured the integration of posture and mandibular morphology.

Comparative analyses demonstrate that species with heavier or anteriorly weighted mandibles tend to adopt postures that mechanically offset these loads. For example, some rhinocerotids evolved a proportionally narrow mandible thereby reducing mandible mass, while proboscideans evolved the trunk, which separates food acquisition from mandibular movement (Shoshani and Tassy, 2005; Gheerbrant and Tassy, 2009). These examples illustrate how

mechanical and energetic constraints can drive coordinated behavioural and anatomical modifications.

Variation in cranial and mandibular posture among ungulates corresponds to differences in feeding height, habitat structure, and behaviour (Janis, 1982; Owen-Smith, 1973). Grazers typically exhibit downward-oriented skulls, reduced visual overlap, and reinforced nuchal musculature, whereas browsers maintain more horizontal postures associated with greater vertical visual coverage (Benoit et al., 2020; Schellhorn, 2018). These positional differences also affect mandibular mechanics: lowered feeding postures alter the orientation of masticatory muscle vectors and lever arms, modifying stress distribution within the jaw. Over evolutionary timescales, such habitual postures may have contributed to the deepening of the mandibular corpus and the reorganisation of muscle attachments in grazing species.

6.7 Macroevolutionary and Ecological Perspectives

Analyses in Chapter 5 incorporated both extinct and extant ungulate-grade mammals to assess whether the scaling relationships identified in living taxa were maintained through deep time. Using comparable measurements of mandibular length, mass, and rotational inertia, consistent power-law slopes were observed across a broad temporal range. Within the resolution of the dataset, this consistency suggests that relationships among size, mass distribution, and inertia remained stable across multiple lineages.

Comparisons among Perissodactyla, Artiodactyla, Proboscidea, and other groups such as Diprotodontia and Xenarthra revealed broadly overlapping regions of morphofunctional space. Several extinct megaherbivores exhibited anteriorly positioned centres of mass and higher inertia relative to mandibular length than most extant species, while living elephants and rhinoceroses showed shorter mandibles and more posterior centres of mass. These patterns are consistent with functional convergence, although the underlying drivers, including energetic cost, diet, and habitat structure, cannot be determined from these data alone.

The functional trends observed parallel macroevolutionary transitions across multiple ungulate-grade lineages. In rhinocerotids, evolution proceeded from gracile, shallow-jawed browsers such as *Stephanorhinus* and *Dihoplus* in the Miocene to deep-jawed grazing specialists like *Elasmotherium* in the Pleistocene (Cerdeño, 1998; Kosintsev et al., 2019; Deng et al., 2021). Comparable transformations occurred within proboscideans, where mandibular reduction coincided with the transfer of feeding function from the jaws to the trunk (Gheerbrant

and Tassy, 2009; Li et al., 2024). Similar biomechanical outcomes are documented in South American notoungulates and litopterns, which independently developed deep corpora and hypsodont dentitions analogous to those of ruminants and equids (Cassini et al., 2017; Püschel et al., 2023).

These convergent trajectories indicate that variation in mass distribution, inertial loading, and dental anatomy evolved jointly under ecological pressures favouring efficient processing of fibrous vegetation.

6.8 Implications for Human Craniofacial Science

The body of knowledge developed in this thesis, although not focused on human systems, translates directly to human craniofacial science by supporting the framing of the mandible as a load bearing, dynamically controlled system in which muscle, bone, joint mechanics, and motion are tightly integrated. This perspective reinforces that mandibular function is governed by interactions between force generation, load transmission, and mechanical resistance, with practical implications for understanding moment efficiency, muscle torque requirements, and posture-dependent loading.

In prosthodontics, implantology, and temporomandibular joint reconstruction, this integrated view is critical because prosthetic success is determined by functional loading conditions rather than static fit alone. Finite element and clinical studies demonstrate that stress distribution depends on geometry, loading direction, and boundary conditions, highlighting the need to consider how forces are generated and transmitted through the mandible over time. Similarly, TMJ prostheses must replicate joint biomechanics, muscle function and load transfer, to achieve long-term stability.

In orthodontics and dentofacial orthopaedics, the findings support the interpretation that masticatory muscles are part of the mechanical environment shaping mandibular form. The observed covariation between mandibular mass properties and muscle attachment area is consistent with evidence that mandibular geometry reflects muscle function more effectively than simple linear measurements (Raadsheer et al., 1999). Clinically, this implies that treatment outcomes and stability depend on the post-treatment loading regime, and that skeletal patterns should be interpreted as mechanobiological conditions influenced by muscle function (Kiliaridis, 1995).

In forensics and bioanthropology, the thesis supports the view that the mandible is mechanically and developmentally informative, with variation in mass distribution and inertia being related to functional loading and biomechanical demand. This supports established findings that mandibular morphology can be used for sex estimation and population analysis (Franklin et al., 2006; Franklin et

al., 2008), while reinforcing that such interpretations should be multivariate and functionally informed, as mandibular form reflects an integrated signal of size, function, and development (Krishan et al., 2016).

In biomedical engineering, the work addresses a key limitation in existing approaches by demonstrating that mandibular mechanics depend not only on static bite forces but also on mass distribution and rotational inertia. This highlights the importance of incorporating dynamic factors to improve the accuracy of simulations used in implant design, surgical planning, and patient-specific modelling.

This thesis demonstrates that similar external morphologies can differ in internal mass distribution and inertia, while existing literature demonstrates that overall geometry better reflects muscle-related function than simple measurements. At the same time, bone-muscle relationships are shown to be functional but not deterministic, as attachment area remains an imperfect proxy for muscle force capacity.

6.9 Limitations, Parameters Not Investigated, Future Work

6.9.1 Limitations

The modelling framework used in this study treated the mandible as a rigid, two-dimensional lever rotating about a fixed axis. This simplified approach excluded three-dimensional kinematics, temporomandibular joint translation, and the contributions of soft-tissue mass and forces. While effective for broad comparative analyses, these simplifications limit the precision of mechanical estimates. Future work employing multi-body dynamics or finite-element methods could address these limitations and evaluate the sensitivity of results to model assumptions. Incorporating dynamic musculoskeletal simulations and load-path analyses would enable direct estimation of stress transmission through mandibular bone, offering greater insight into structural performance under masticatory loading. Such approaches have been successfully applied to three-dimensional models of jaw and hyoid systems (Hannam et al., 2008; Langenbach and Hannam, 1999), while recent load-path optimisation techniques allow quantification of how mandibular geometry affects the mechanical efficiency of force transmission during chewing (Wilken et al., 2024). Integrating these biomechanical methods with volumetric mass models would enhance understanding of how the distribution of mass influences mechanical function. In addition, validation of physiological cross-sectional area estimates through combined digital and in vivo approaches (Ginor and Blanke, 2024) would

improve the accuracy of bite-force reconstructions and strengthen functional interpretations of fossil mandibles.

Assumptions of uniform bone density facilitated comparative analyses but may have introduced bias in absolute mass estimates. Incorporating species-specific density values derived from micro-CT or QCT data would refine these estimates and clarify how bone microstructure contributes to whole-mandible mechanical behaviour. Similarly, refinement of dietary categories would improve ecological resolution. The use of broad browser–grazer distinctions likely obscure finer-scale variation related to seasonality or habitat; applying stable-isotope or microwear data to the same specimens would provide a more detailed ecological context.

Sampling biases also constrain interpretation. Fossil assemblages are often dominated by large, robust mandibles, limiting representation of mid-sized and gracile taxa. Expanding taxonomic coverage would allow more comprehensive testing of scaling relationships and improve understanding of functional diversity. Ontogenetic and phylogenetic effects remain another important source of variation. Ontogenetic series, such as those available for *Diceros bicornis*, indicate that centre of mass position and rotational inertia can shift through development. Comparative analyses of ontogenetic trajectories could therefore clarify how developmental and evolutionary processes interact to shape mandibular mechanics.

6.9.2 Parameters Not Investigated

Direct measurement of muscle physiological cross-sectional area (PCSA) was not undertaken in this thesis, as it requires dissection or advanced imaging. However, it represents an important avenue for future research, particularly in controlled systems such as domesticated species where diet and loading can be manipulated. In the present study, masseter attachment area was used as a coarse proxy for muscle size, although this provides only an indirect estimate of force capacity because PCSA depends on internal architecture (van Eijden, 1991; Lieber and Fridén, 2000). Inclusion of additional parameters, such as muscle PCSA, joint morphology, ligament behaviour, and chewing kinematics, is therefore essential, as these are central components of the masticatory system and clarify why mandibular inertia alone cannot determine chewing dynamics.

Chewing mechanics are best understood as arising from four interacting subsystems: neural control, which generates rhythm; muscle mechanics, which produces torque; joint mechanics, which constrains motion and transmits force; and skeletal mass properties, which determine resistance to

motion (Lund and Kolta, 2006; Ross, 2007). The parameters considered here primarily relate to muscle and joint mechanics within this framework.

The geometry and mobility of the temporomandibular joint strongly constrain mandibular motion. The mandible undergoes rotation, translation, and transverse or mediolateral displacement, with joint morphology determining axis of rotation, range of motion, muscle leverage, and stress distribution. Carnivores typically exhibit hinge-like joints with limited lateral motion and rapid closure, whereas herbivores possess flatter condyles that permit greater translation and transverse grinding (Herring, 1993). Greater displacements during chewing generally reduce angular acceleration and increase cycle duration, consequently diminishing the relative influence of inertia.

Joint ligaments provide passive constraints that stabilise the system and introduce viscoelastic behaviour. By adding stiffness and damping, they cause the mandible to function as a spring-mass-damper system, smoothing and stabilising oscillations and reducing the energetic cost of reversing the direction of motion (Hylander, 1979; Herring, 1993).

Mandibular angular acceleration and chewing frequency are key determinants of mechanical demand. Because torque is proportional to inertia and angular acceleration, the effect of inertia depends strongly on acceleration. Larger mammals typically chew more slowly, reducing angular acceleration and partially compensating for increased inertia (Ross et al., 2009).

Muscle PCSA determines maximal force production and therefore muscular torque capacity. Increased mandibular inertia requires greater torque, which is accommodated through larger PCSA, mechanically efficient lever arms, and increased mandibular robusticity. Herbivores, particularly grazers, exhibit large masseter PCSAs and high bite force capacities, whereas carnivores rely more on the temporalis for rapid closure (Herring, 1993; van Eijden, 1991).

These factors interact through a torque balance in which muscular force must overcome inertial resistance to angular acceleration, gravitational loading, food resistance, as well as joint and ligament forces. Chewing performance therefore depends on the balance between torque demand and muscular capacity. Within this system, mandibular inertia is only one component of mechanical demand and can be accommodated through compensatory changes in muscle size, kinematics, joint mechanics, and behaviour.

These considerations support the interpretation that mandibular rotational inertia is best understood as a mechanical demand variable rather than a determinant of chewing behaviour. A complete framework is one in which mass distribution defines demand, muscle PCSA and lever arms define

capacity, joint mechanics constrain motion, and neural control governs rhythm, with function emerging from their interaction.

6.9.3 Future Work

The energetic implications of mandibular design remain to be directly tested. Measuring chewing energetics in living species would help determine whether mechanical proxies accurately reflect metabolic cost. Future research would benefit from computational and imaging approaches capable of quantifying internal stress and strain within the mandible under realistic muscle loads. Advances in dynamic modelling now allow anatomically accurate simulations of masticatory motion, incorporating muscle paths and temporomandibular-joint mechanics (Hannam et al., 2008; Langenbach and Hannam, 1999). Finite-element load-path analyses can capture how bone geometry distributes forces along functional axes (Wilken et al., 2024), while validated three-dimensional estimates of muscle cross-sectional area and in vivo bite forces (Ginor and Blanke, 2024) provide a means of linking virtual models with experimental data. Together, these approaches will help clarify how variation in mandibular mass distribution affects mechanical performance, integrating morphology, physiology, and evolutionary adaptation within a unified biomechanical framework.

Future research could build on the findings of this thesis by employing domesticated or experimentally tractable species to directly test the relationships between mandibular mass properties, muscle function, and mechanical loading under controlled conditions. The present thesis demonstrates that mandibular inertia varies with size and head posture, that masseter attachment area covaries with mechanical demand, and that mandibular morphology reflects functional loading shaped by adaptive processes. However, these conclusions are derived from comparative datasets and therefore remain inferences rather than direct tests of causality.

The use of controlled model systems would allow experimental manipulation of key variables that are otherwise unknown or uncontrolled in comparative studies, particularly chewing behaviour and food material properties. In domesticated species, diet hardness, toughness, volume, and feeding frequency can be standardised and measured, enabling direct investigation of how mechanical loading influences mandibular structure and muscle development during ontogeny. Such systems would also permit direct measurement of muscle function through electromyography (EMG), bite force, and estimation of muscle PCSA via dissection or imaging, allowing validation of muscle attachment area as a proxy for force capacity and testing of the relationship between muscle force, inertia, and torque demand.

In addition, domesticated species provide opportunities for longitudinal and ontogenetic studies, enabling tracking of changes in mandibular shape, mass distribution, and inertial properties through growth. This would allow assessment of whether intraspecific scaling patterns arise primarily from developmental processes or from responses to mechanical loading. Controlled settings also enable investigation of head posture and behavioural factors, including their influence on mandibular loading, muscle recruitment, and mechanical demand over time. Furthermore, such datasets could be integrated with finite element and multibody dynamic analyses, extending the modelling approaches developed in this thesis.

In summary, the use of controlled experimental systems would enable a shift from comparative inference to direct testing of causality, allowing the relationships between mandibular inertia, muscle function, and mechanical demand to be quantified under known conditions. This would strengthen and refine the interpretations presented in this thesis by providing a more mechanistic understanding of how loading, development, and behaviour interact to shape mandibular structure and function.

6.10 Concluding Remarks

Across the analyses, external geometry was a strong predictor of mandibular mass properties, while internal structural variation had limited influence at the whole-mandible scale. Mass and rotational inertia scaled with length with positive allometry, in-excess of geometrical expectations, and masseter insertion area increased proportionally with inertial demand. Adjusting for habitual head posture altered absolute inertia values but did not change overall scaling relationships. The inclusion of fossil taxa showed that these relationships persisted through time.

The findings indicate that mandibular form is primarily governed by mechanical requirements, with behavioural factors modifying but not overriding these constraints. Future research combining higher resolution ecological data, three-dimensional kinematic modelling, and direct energetic measurements would expand the scope and increase the precision of these analyses.

Overall, the results correspond with broader comparative and palaeobiological evidence showing that structural and inertial scaling in the mandible reflects general biomechanical consequences of herbivorous feeding strategies. From the Palaeogene diversification of true

ungulates to convergent groups such as rhinocerotids, proboscideans, and South American meridiungulates, similar principles of ecological adaptation, stress regulation, material optimisation, and mechanical performance appear to have guided the evolution of mastication.

References

Adams, N.F., Candy, I. & Schreve, D.C., 2022. An Early Pleistocene hippopotamus from Westbury Cave, Somerset, England: support for a previously unrecognized temperate interval in the British Quaternary record. *Journal of Quaternary Science*, 37(1), pp.28–41. https://doi.org/10.1002/jqs.3375

Al Sayegh, S., Christidis, N., Kumar, A., Svensson, P. and Grigoriadis, A., 2022. Masticatory performance in patients with jaw muscle pain: A case–control study. *Frontiers in Dental Medicine*, *3*, p.963425.

Alexander, R.M. & Jayes, A.S., 1983. A dynamic similarity hypothesis for the gaits of quadrupedal mammals. *Journal of Zoology*, 201(1), pp.135–152. https://doi.org/10.1111/j.1469-7998.1983.tb04266.x

Alexander, R.M., 2003. *Principles of animal locomotion*. Princeton university press.

Altman, D.G. & Bland, J.M., 1983. Measurement in medicine: the analysis of method comparison studies. *Journal of the Royal Statistical Society. Series D (The Statistician)*, 32(3), pp.307–317. Available at: https://www.jstor.org/stable/2987937

Antón, S.C., 1999. Macaque masseter muscle: internal architecture, fiber length and cross-sectional area. *International Journal of Primatology*, *20*(3), pp.441-462.

Asher, R.J., Bennett, N. and Lehmann, T., 2009. The new framework for understanding placental mammal evolution. *Bioessays*, *31*(8), pp.853-864.

Avedik, A. & Clauss, M., 2023. Chewing, dentition and tooth wear in Hippopotamidae (*Hippopotamus amphibius* and *Choeropsis liberiensis*). *PLoS ONE*, 18(10), e0291825. https://doi.org/10.1371/journal.pone.0291825

Bai, B., Meng, J., Zhang, C., Gong, Y-X. & Wang, Y-Q., 2020. The origin of Rhinocerotoidea and phylogeny of Ceratomorpha (Mammalia, Perissodactyla). *Communications Biology*, 3, 509. https://doi.org/10.1038/s42003-020-01205-8

Baleka, S., Varela, L., Tambusso, P.S., Paijmans, J.L., Mothé, D., Stafford, T.W., Fariña, R.A. and Hofreiter, M., 2022. Revisiting proboscidean phylogeny and evolution through total evidence and palaeogenetic analyses including Notiomastodon ancient DNA. *Iscience*, *25*(1).

Ballatore, M. & Breda, M., 2013. *Stephanorhinus hundsheimensis* (Rhinocerotidae, Mammalia) teeth from the early Middle Pleistocene of Isernia La Pineta (Molise, Italy) and comparison with

coeval British material. *Quaternary International*, 302, pp.169–183. https://doi.org/10.1016/j.quaint.2013.02.002

Barghusen, H.R. & Hopson, J.A., 1970. Dentary-squamosal joint and the origin of mammals. *Science*, 168(3931), pp.573–575.

Bargo, M.S., Vizcaíno, S.F. & Kay, R.F., 2009. Predominance of orthal masticatory movements in the early Miocene *Eucholaeops* (Mammalia, Xenarthra, Tardigrada, Megalonychidae) and other megatherioid sloths. *Journal of Vertebrate Paleontology*, 29(3), pp.870–880. https://www.jstor.org/stable/20627097

Bargo, M.S., Vizcaíno, S.F., Archuby, F.M. & Blanco, R.E., 2000. Limb bone proportions, strength and digging in some Lujanian (Late Pleistocene–Early Holocene) mylodontid ground sloths (Mammalia, Xenarthra). *Journal of Vertebrate Paleontology*, 20(3), pp.601–610. https://doi.org/10.1671/0272-4634(2000)020[0601:LBPSAD]2.0.CO;2

National Center for Biotechnology Information (NCBI), 2023. *The NCBI Handbook [Internet]. 2nd edition*. Bethesda (MD): National Center for Biotechnology Information (US). Available at: https://www.ncbi.nlm.nih.gov/books/NBK541027 [Accessed 27 October 2025].

Beauchemin, K.A., 2018. Invited review: Current perspectives on eating and rumination activity in dairy cows. *Journal of dairy science*, *101*(6), pp.4762-4784.

Benoit, J., Manger, P.R., Norton, L., Fernandez, V. & Rubidge, B.S., 2017. Synchrotron scanning reveals the palaeoneurology of the head-butting *Moschops capensis* (Therapsida, Dinocephalia). *PeerJ*, 5, e3496. https://doi.org/10.7717/peerj.3496

Benoit, J., Legendre, L.J., Farke, A.A., Neenan, J.M., Mennecart, B., Costeur, L., Merigeaud, S. & Manger, P.R., 2020. A test of the lateral semicircular canal correlation to head posture, diet and other biological traits in “ungulate” mammals. *Scientific Reports*, 10, 19602. https://doi.org/10.1038/s41598-020-76757-0

Bettinardi, V., Castiglioni, I., De Bernardi, E. & Gilardi, M.C., 2014. PET quantification: strategies for partial volume correction. *Clinical and Translational Imaging*, 2(3), pp.199–218. https://doi.org/10.1007/s40336-014-0066-y

Biewener, A.A. and Patek, S., 2003. Animal locomotion: Oxford university press.

Biewener, A.A., 2005. Biomechanical consequences of scaling. *Journal of Experimental Biology*, *208*(9), pp.1665-1676.

Biewener, A.A. & Taylor, C.R., 1986. Bone strain: a determinant of gait and speed? *Journal of Experimental Biology*, 123, pp.383–400.

Blanco, F., Lazagabaster, I.A., Sanisidro, Ó., Bibi, F., Heckeberg, N.S., Ríos, M., Mennecart, B., Alberdi, M.T., Prado, J.L., Saarinen, J. and Silvestro, D., 2025. Two major ecological shifts shaped 60 million years of ungulate faunal evolution. *Nature Communications*, *16*(1), p.4648.

Blender Foundation. (2025) *Blender (Version 4.5.2)* [Computer software]. Amsterdam, The Netherlands.. Available at: https://www.blender.org/

Boone, J.M., Nelson, T.R., Lindfors, K.K. and Seibert, J.A., 2001. Dedicated breast CT: radiation dose and image quality evaluation. *Radiology*, *221*(3), pp.657-667.

Bouvier, M. and Hylander, W.L., 1981. Effect of bone strain on cortical bone structure in macaques (Macaca mulatta). *Journal of Morphology*, *167*(1), pp.1-12.

Buckley, L.B., Hurlbert, A.H. and Jetz, W., 2012. Broad-scale ecological implications of ectothermy and endothermy in changing environments. *Global Ecology and Biogeography*, *21*(9), pp.873-885.

Buckley, M., 2015. Ancient collagen reveals evolutionary history of the endemic South American 'ungulates'. *Proceedings of the Royal Society B: Biological Sciences*, *282*(1806), p.20142671.

Burger, B.J., 2015. The systematic position of the saber-toothed and horned giants of the Eocene: the uintatheres (Order Dinocerata). *Utah State University, Conference Poster*.

Cassini, G.H., Vizcaíno, S.F. and Bargo, M.S. (2012) 'Body mass estimation in Early Miocene native South American ungulates: a predictive equation based on 3D landmarks', *Journal of Zoology*, 287, pp. 53–64.

Cassini, G.H., Cerdeño, E., Villafañe, A.L. and Muñoz, N.A. (2017) 'Paleobiology of Santacrucian native ungulates (Meridiungulata: Astrapotheria, Litopterna and Notoungulata)', in Vizcaíno, S.F., Kay, R.F. and Bargo, M.S. (eds.) *Early Miocene Paleobiology in Patagonia: High-Latitude Paleocommunities of the Santa Cruz Formation*. Cambridge: Cambridge University Press, pp. 243–260.

Cerdeño, E. (1998) 'Diversity and evolutionary trends of the family Rhinocerotidae', *Palaeogeography, Palaeoclimatology, Palaeoecology*, 141, pp. 13–34.

Christiansen, P., 2002. Mass allometry of the appendicular skeleton in terrestrial mammals. *Journal of Morphology*, *251*(2), pp.195-209.

Christiansen, P. and Wroe, S., 2007. Bite forces and evolutionary adaptations to feeding ecology in carnivores. *Ecology*, *88*(2), pp.347-358.

Christiansen, P., 2004. Body size in proboscideans, with notes on elephant metabolism. *Zoological journal of the Linnean Society*, *140*(4), pp.523-549.

Clauss, M., Lechner-Doll, M. & Streich, W.J. (2003) 'Ruminant diversification as an adaptation to the physicomechanical characteristics of forage: a reevaluation of an old debate and a new hypothesis', *Oikos*, 102, pp. 253–262. doi:10.1034/j.1600-0706.2003.12406.x.

Clemente, C.J. (2014) 'The evolution of bipedal running in lizards suggests a consequential origin may be exploited in later lineages', *Evolution*, 68(7), pp. 2014–2028. doi:10.1111/evo.12447

Clemente, C.J. and Dick, T.J., 2023. How scaling approaches can reveal fundamental principles in physiology and biomechanics. *Journal of Experimental Biology*, *226*(7), p.jeb245310.

Copes, L.E. & Schwartz, G.T. (2010). "The scale of it all: postcanine tooth size, the taxon-level effect, and the universality of Gould's scaling law." *Paleobiology*, 36(2), 188–203.

Coutier, F., Hautier, L., Billet, G., de Muizon, C. & Goswami, A., 2017. Orientation of the lateral semicircular canal in Xenarthra and its links with head posture and phylogeny. *Journal of Morphology*, 278(4), pp.486–499. doi:10.1002/jmor.20649.

Crompton, A.W. & Park, R., 1978. Evolution of the mammalian masticatory apparatus. *American Scientist*, 66(2), pp.192–201.

Crompton, A.W., 1962. The evolution of the mammalian jaw. *Evolution*, 17(4), pp.431–439. doi:10.1111/j.1558-5646.1963.tb03299.x.

Damuth, J. & Janis, C.M., 2011. On the relationship between hypsodonty and feeding ecology in ungulate mammals, and its utility in palaeoecology. *Biological Reviews*, 86(3), pp.733–758. doi:10.1111/j.1469-185X.2011.00176.x.

Damuth, J.D. and MacFadden, B.J. eds., 1990. *Body size in mammalian paleobiology: estimation and biological implications*. Cambridge University Press.

Dauncey, M.J. & Ingram, D.L., 1988. Influence of environmental temperature and energy intake on skeletal muscle respiratory enzymes and morphology. *European Journal of Applied Physiology and Occupational Physiology*, 58(3), pp.239–244. doi:10.1007/BF00417256.

De Muizon, C., Billet, G., Argot, C., Ladevèze, S. and Goussard, F., 2015. Alcidedorbignya inopinata, a basal pantodont (Placentalia, Mammalia) from the early Palaeocene of Bolivia: anatomy, phylogeny and palaeobiology. *Geodiversitas*, *37*(4), pp.397-634.

DeVries, R.P., Sereno, P.C., Vidal, D. and Baumgart, S.L., 2022. Reproducible digital restoration of fossils using blender. *Frontiers in Earth Science*, *10*, p.833379.

Dellanini, L., Hawkins, D., Martin, R.B. & Stover, S., 2003. An investigation of the interactions between lower-limb bone morphology, limb inertial properties and limb dynamics. *Journal of Biomechanics*, 36(6), pp.913–919. doi:10.1016/S0021-9290(03)00076-9.

Deng, T., Lu, X., Wang, S., Flynn, L.J., Sun, D., He, W. and Chen, S., 2021. An Oligocene giant rhino provides insights into *Paraceratherium* evolution. *communications Biology*, *4*(1), p.639.

Dickinson, E., Davis, J.S., Deutsch, A.R., Patel, D., Nijhawan, A., Patel, M., Blume, A., Gannon, J.L., Turcotte, C.M., Walker, C.S. and Hartstone-Rose, A. (2021) 'Evaluating bony predictors of bite force across the order Carnivora', *Journal of Morphology*, 282(10), pp. 1499–1513. https://doi.org/10.1002/jmor.21400

Dittrich, L., 2007. Food presentation in relation to behaviour in ungulates. In: *Principles of Zoo Animal Feeding*. Berlin: Blackwell, pp.48–53.

Druzinsky, R.E., 1993. The time allometry of mammalian chewing movements: chewing frequency scales with body mass in mammals. *Journal of Theoretical Biology*, *160*(4), pp.427-440.

Duncan, R.L. & Turner, C.H., 1995. Mechanotransduction and the functional response of bone to mechanical strain. *Calcified Tissue International*, 57(5), pp.344–358. doi:10.1007/BF00302070.

Erdal, O., Antoine, P.O. and Sen, S., 2016. New material of Palaeoamasia kansui (Embrithopoda, Mammalia) from the Eocene of Turkey and a phylogenetic analysis of Embrithopoda at the species level. *Palaeontology*, *59*(5), pp.631-655.

Estes, R.D. (2012) The Behavior Guide to African Mammals: Including Hoofed Mammals, Carnivores, Primates. 20th Anniversary ed. Berkeley: University of California Press.

Figueirido, B., Janis, C.M., Pérez-Claros, J.A., De Renzi, M. and Palmqvist, P., 2012. Cenozoic climate change influences mammalian evolutionary dynamics. *Proceedings of the National Academy of Sciences*, *109*(3), pp.722-727.

Franklin, D., O'Higgins, P., Oxnard, C.E. and Dadour, I., 2006. Determination of sex in South African Blacks by discriminant function analysis of mandibular linear dimensions: a preliminary investigation using the Zulu local population. *Forensic science, medicine, and pathology*, *2*(4), pp.263-268.

Franklin, D., O'Higgins, P., Oxnard, C.E. and Dadour, I., 2008. Discriminant function sexing of the mandible of indigenous South Africans. *Forensic science international*, *179*(1), pp.84-e1.

Fortelius, M., Eronen, J., Liu, L., Pushkina, D., Tesakov, A., Vislobokova, I. and Zhang, Z., 2006. Late Miocene and Pliocene large land mammals and climatic changes in Eurasia. *Palaeogeography, Palaeoclimatology, Palaeoecology*, *238*(1-4), pp.219-227.

Fortelius, M., 1985. Ungulate cheek teeth: developmental, functional, and evolutionary interrelations. *Acta Zoologica Fennica*, 180, pp.1–76. Helsinki: Finnish Zoological Publishing Board.

Niehaus, A.J. (ed.), 2022. *Fowler's Medicine and Surgery of Camelids*. 4th ed. Hoboken, NJ: John Wiley & Sons, Inc.

Fox, E.A., van Schaik, C.P., Sitompul, A. & Wright, D.N., 2004. Intra- and interpopulational differences in orangutan (Pongo pygmaeus) activity and diet: Implications for the invention of tool use. *American Journal of Physical Anthropology*, 125(2), pp.162–174. doi:10.1002/ajpa.10386.

Frost, H.M., 1996. Perspectives: A proposed general model of the "mechanostat" (suggestions from a new skeletal-biologic paradigm). *The Anatomical Record*, 244(2), pp.139–147. doi:10.1002/(SICI)1097-0185(199602)244:2<139::AID-AR1>3.0.CO;2-X.

Frost, H.M., 2003. Bone's mechanostat: A 2003 update. *The Anatomical Record Part A: Discoveries in Molecular, Cellular, and Evolutionary Biology*, 275(2), pp.1081–1101. doi:10.1002/ar.a.10119.

van der Geer, A.A.E., van den Bergh, G.D., Lyras, G.A., Prasetyo, U.W., Awe Due, R., Setiyabudi, E. & Drinia, H., 2016. The effect of area and isolation on insular dwarf proboscideans. *Journal of Biogeography*, 43(8), pp.1656–1666. doi:10.1111/jbi.12743.

Gerstner, G.E. & Gerstein, J.B., 2008. Chewing rate allometry among mammals. *Journal of Mammalogy*, 89(4), pp.1020–1030. doi:10.1644/07-MAMM-A-324.1.

Gheerbrant, E., Schmitt, A. and Kocsis, L., 2018. Early African fossils elucidate the origin of embrithopod mammals. *Current Biology*, *28*(13), pp.2167-2173.

Gheerbrant, E. & Tassy, P., 2009. *Origin and evolution of proboscideans*. In: W.F. Perrin, B. Würsig & J.G.M. Thewissen, eds. *Encyclopedia of Marine Mammals*. 2nd ed. London: Academic Press, pp. 873–879.

Gheerbrant, E., 2009. Paleocene emergence of elephant relatives and the rapid radiation of African ungulates. *Proceedings of the National Academy of Sciences*, 106(26), pp.10717–10721. doi:10.1073/pnas.0900251106.

Ginor, S. & Blanke, A., 2024. A comparison of dissection and 3D approaches to estimate muscle physiological cross-sectional area, validated by in vivo bite forces. *Journal of Experimental Biology*, 227(2), jeb246341. doi:10.1242/jeb.246341.

Graf, W., de Waele, C. & Vidal, P.P., 1995. Functional anatomy of the head-neck movement system of quadrupedal and bipedal mammals. *Journal of Anatomy*, 186, pp.55–74

Grand, T.I., 1977. Body weight: Its relation to tissue composition, segment distribution, and motor function. I. Interspecific comparisons. *American Journal of Physical Anthropology*, 47(2), pp.211–240. doi:10.1002/ajpa.1330470204.

Gröcke, D.R., 2017. Stable-isotope studies on the collagenic and hydroxylapatite components of fossils. *Palaeogeography, Palaeoclimatology, Palaeoecology*, 485, pp.1–14. doi:10.1016/j.palaeo.2016.09.001

Grigg, G., Nowack, J., Bicudo, J.E.P.W., Bal, N.C., Woodward, H.N. & Seymour, R.S., 2022. Whole-body endothermy: ancient, homologous and widespread among the ancestors of mammals, birds and crocodylians. *Biological Reviews*, 97(2), pp.766–801. https://doi.org/10.1111/brv.12822

Grimal, Q. & Laugier, P., 2019. Quantitative ultrasound assessment of cortical bone properties beyond bone mineral density. *IRBM*, 40(1), pp.16–24. https://doi.org/10.1016/j.irbm.2018.10.006

Grossnickle, D.M., 2020. Feeding ecology has a stronger evolutionary influence on functional morphology than on body mass in mammals. *Evolution*, 74(3), pp.610–628. doi:10.1111/evo.13933

Hadjidakis, D.J. and Androulakis, I.I., 2006. Bone remodelling. *Annals of the New York Academy of Sciences*, 1092, pp.385–396. doi:10.1196/annals.1365.035.

Hall-Martin, A.J., von la Chevallerie, M. and Skinner, J.D., 1977. Carcass composition of the giraffe *Giraffa camelopardalis giraffa*. *South African Journal of Animal Science*, 7, pp.55–64

Hannam, A.G., Stavness, I., Lloyd, J.E. and Fels, S., 2008. A dynamic model of jaw and hyoid biomechanics during chewing. *Journal of Biomechanics*, 41(5), pp.1069–1076. doi:10.1016/j.jbiomech.2007.12.001

Healy, W.B. and Ludwig, T.G., 1965. Ingestion of soil by sheep in New Zealand in relation to wear of teeth. *Nature*, 208, pp.806–807

Heglund, N.C. and Taylor, C.R., 1988. Speed, stride frequency and energy cost per stride: how do they change with body size and gait? *Journal of Experimental Biology*, 138, pp.301–318.

Heglund, N.C., Taylor, C.R. and McMahon, T.A., 1974. Scaling stride frequency and gait to animal size: mice to horses. *Science*, 186(4169), pp.1112–1113

Heglund, N.C., Cavagna, G.A. and Taylor, C.R., 1982. Energetics and mechanics of terrestrial locomotion. III. Energy changes of the centre of mass as a function of speed and body size in birds and mammals. *Journal of Experimental Biology*, 97, pp.41–56. doi:10.1242/jeb.97.1.41

Herring, S.W., 1985. The ontogeny of mammalian mastication. *American Zoologist*, 25(2), pp.339–349. https://doi.org/10.1093/icb/25.2.339

Herring, S.W., 1993. Formation of the vertebrate face epigenetic and functional influences. *American Zoologist, 33*(4), pp.472-483.

Herring, S.W., 1993. Functional morphology of mammalian mastication. *American Zoologist*, 33(3), pp.289–299

Herring, S.W., Rafferty, K.L., Liu, Z.J. and Marshall, C.D., 2001. Jaw muscles and the skull in mammals: the biomechanics of mastication. *Comparative Biochemistry and Physiology Part A*, 131(1), pp.207–219

Hildebrand, M. & Hurley, J.P., 1985. Energy of the oscillating legs of a fast-moving cheetah, pronghorn, jackrabbit, and elephant. *Journal of Morphology*, 184(1), pp.23–31. https://doi.org/10.1002/jmor.1051840103

Hiraiwa, T., 1978. Histochemical properties of masticatory muscles of growing rat and of matured mammals. *Comparative Biochemistry and Physiology Part A: Physiology*, 59(3), pp.231–238. https://doi.org/10.1016/0300-9629(78)90152-4

Hofmann, R.R., 1989. Evolutionary steps of ecophysiological adaptation and diversification of ruminants: a comparative view of their digestive system. *Oecologia*, 78, pp.443–457. https://doi.org/10.1007/BF00378733

Hudson, P.E., Corr, S.A., Payne-Davis, R.C., Clancy, S.N., Lane, E. & Wilson, A.M., 2011. Functional anatomy of the cheetah (Acinonyx jubatus) forelimb. *Journal of Anatomy*, 218(4), pp.375–385. https://doi.org/10.1111/j.1469-7580.2011.01348.x

Hullar, T.E., 2006. Semicircular canal geometry, afferent sensitivity, and animal behavior. *Anatomical Record Part A: Discoveries in Molecular, Cellular, and Evolutionary Biology*, 288(4), pp.466–472. https://doi.org/10.1002/ar.a.20304

Hullot, M., Antoine, P.-O., Spassov, N., Koufos, G.D. & Merceron, G., 2022. Late Miocene rhinocerotids from the Balkan-Iranian province: ecological insights from dental microwear textures and enamel hypoplasia. *Historical Biology*. https://doi.org/10.1080/08912963.2022.2086323

Huttunen, K., 2002. Systematics and taxonomy of the European Deinotheriidae (Proboscidea, Mammalia). *Annalen des Naturhistorischen Museums in Wien, Serie A*, 103, pp.237–250.

Huttunen, K., 2004. On a *Prodeinotherium bavaricum* (Proboscidea, Mammalia) skeleton from Franzenbad, Czech Republic. *Annalen des Naturhistorischen Museums in Wien, Serie A*, 105, pp.375–396.

Hylander, W.L., 1979. The functional significance of primate mandibular form. *Journal of Morphology*, *160*(2), pp.223-239.

Iriarte-Díaz, J., Reed, D.A. and Ross, C.F., 2011. Sources of variance in temporal and spatial aspects of jaw kinematics in two species of primates feeding on foods of different properties. *Integrative and Comparative Biology*, *51*(2), pp.307-319.

Isler, K. & van Schaik, C.P., 2006. Metabolic costs of brain size evolution. *Biology Letters*, 2(4), pp.557–560. https://doi.org/10.1098/rsbl.2006.0538

Janis, C.M., Scott, K.M. & Jacobs, L.L. (eds.), 1998. *Evolution of Tertiary Mammals of North America. Volume 1: Terrestrial Carnivores, Ungulates, and Ungulate-like Mammals*. Cambridge: Cambridge University Press.

Janis, C.M., 1982. Evolution of horns in ungulates: ecology and paleoecology. *Biological Reviews*, 57(3), pp.261–318. https://doi.org/10.1111/j.1469-185X.1982.tb00370.x

Janis, C.M., Scott, K.M. & Jacobs, L.L. (eds.), 1998. *Evolution of Tertiary Mammals of North America. Volume 1: Terrestrial Carnivores, Ungulates, and Ungulate-like Mammals*. Cambridge: Cambridge University Press.

Janis, C.M., 1990. Correlation of cranial and dental variables with dietary preferences in mammals: a comparison of macropodoids and ungulates. *Memoirs of the Queensland Museum*, 28, pp.349–366

Janis, C.M., 2008. An evolutionary history of browsing and grazing ungulates. In: Gordon, I.J. & Prins, H.H.T. (eds.) *The Ecology of Browsing and Grazing*, Ecological Studies 195. Springer, Berlin, pp.21–45

Jin, Y. & Qian, H., 2022. U.PhyloMaker: An R package that can generate large phylogenetic trees for plants and animals. *Ecography*, 45(5), pp.675–684. https://doi.org/10.1111/ecog.05896

Kalender, W.A., 2011. *Computed tomography: fundamentals, system technology, image quality, applications*. John Wiley & Sons.

Kayar, S.R., Hoppeler, H., Essen-Gustavsson, B. and Schwerzmann, K., 1988. The similarity of mitochondrial distribution in equine skeletal muscles of differing oxidative capacity. *Journal of Experimental Biology*, *137*(1), pp.253-263.

Ketcham, R.A. and Carlson, W.D., 2001. Acquisition, optimization and interpretation of X-ray computed tomographic imagery: applications to the geosciences. *Computers & Geosciences*, *27*(4), pp.381-400.

Kiliaridis, S., 1995. Masticatory muscle influence on craniofacial growth. *Acta Odontologica Scandinavica*, *53*(3), pp.196-202.

Kleiber, M., 1932. Body size and metabolism. *Hilgardia*, 6(11), pp.315–353.

Klingenberg, C.P., 1996. Multivariate allometry. In *Advances in morphometrics* (pp. 23-49). Boston, MA: Springer US.

Klingenberg, C.P., 2016. Size, shape, and form: concepts of allometry in geometric morphometrics. *Development genes and evolution*, *226*(3), pp.113-137.

Köhler, M., 1993. *Skeleton and habitat of recent and fossil Ruminants*. München: Verlag Dr. Friedrich Pfeil.

Kosintsev, P., Mitchell, K.J., Devièse, T., van Der Plicht, J., Kuitems, M., Petrova, E., Tikhonov, A., Higham, T., Comeskey, D., Turney, C. and Cooper, A., 2019. Evolution and extinction of the giant rhinoceros *Elasmotherium sibiricum* sheds light on late Quaternary megafaunal extinctions. *Nature ecology & evolution*, *3*(1), pp.31-38.

Krishan, K., Chatterjee, P.M., Kanchan, T., Kaur, S., Baryah, N. and Singh, R.K., 2016. A review of sex estimation techniques during examination of skeletal remains in forensic anthropology casework. *Forensic science international*, *261*, pp.165-e1.

Kurtén, B., 2017. *Pleistocene mammals of Europe*. Routledge.

Langenbach, G.E.J. and Hannam, A.G., 1999. The role of passive muscle tensions in a three-dimensional dynamic model of the human jaw. *Archives of Oral Biology*, *44*(7), pp.557-573.

Larramendi, A., 2015. Shoulder height, body mass, and shape of proboscideans. *Acta Palaeontologica Polonica*, *61*(3), pp.537-574.

Laurie, W.A., Lang, E.M. and Groves, C.P., 1983. Rhinoceros unicornis. *Mammalian species*, (211), pp.1-6.

Lavigne, G., Kim, J.S., Valiquette, C. and Lund, J.P., 1987. Evidence that periodontal pressoreceptors provide positive feedback to jaw closing muscles during mastication. *Journal of neurophysiology*, *58*(2), pp.342-358.

Lautenschlager, S., 2016. Reconstructing the past: methods and techniques for the digital restoration of fossils. *Royal Society Open Science*, *3*(10), p.160342.

Law, C.J., Duran, E., Hung, N., Richards, E., Santillan, I. and Mehta, R.S., 2018. Effects of diet on cranial morphology and biting ability in musteloid mammals. *Journal of Evolutionary Biology*, *31*(12), pp.1918-1931.

Lehmann, J., Korstjens, A. and Dunbar, R., 2008. Time management in great apes: implications for gorilla biogeography. *Evolutionary Ecology Research*, *10*(4).

Li, C., Deng, T., Wang, Y., Sun, F., Wolff, B., Jiangzuo, Q., Ma, J., Xing, L., Fu, J., Zhang, J. and Wang, S., 2024. The trunk replaces the longer mandible as the main feeding organ in elephant evolution. *Elife*, *12*, p.RP90908.

Li, S., Jiangzuo, Q. and Deng, T., 2022. Body mass of the giant rhinos (Paraceratheriinae, Mammalia) and its tendency in evolution. *Historical Biology*, pp.1-12.

Lieber, R.L. and Fridén, J., 2001. Clinical significance of skeletal muscle architecture. *Clinical Orthopaedics and Related Research®*, *383*, pp.140-151.

Liu, A.G., Seiffert, E.R. and Simons, E.L., 2008. Stable isotope evidence for an amphibious phase in early proboscidean evolution. *Proceedings of the National Academy of Sciences*, *105*(15), pp.5786-5791.

Liu, S., Westbury, M.V., Dussex, N., Mitchell, K.J., Sinding, M.H.S., Heintzman, P.D., Duchêne, D.A., Kapp, J.D., Von Seth, J., Heiniger, H. and Sánchez-Barreiro, F., 2021. Ancient and modern genomes unravel the evolutionary history of the rhinoceros family. *Cell*, *184*(19), pp.4874-4885.

Löscher, D.M., Meyer, F., Kracht, K. and Nyakatura, J.A., 2016. Timing of head movements is consistent with energy minimization in walking ungulates. *Proceedings of the Royal Society B: Biological Sciences*, *283*(1843), p.20161908.

Lucas, P.W., 2004. Dental Functional Morphology: How Teeth Work.

Lund, J.P. and Kolta, A., 2006. Generation of the central masticatory pattern and its modification by sensory feedback. *Dysphagia, 21*(3), pp.167-174.

Ma, J., Wang, S. and Deng, T., 2024. When the woolly rhinoceroses roamed East Asia: a review of isotopic paleoecology of the genus Coelodonta from the Tibetan Plateau to northern Eurasia. *Frontiers in Ecology and Evolution*, *12*, p.1377000.

Macaulay, S., Hutchinson, J.R. and Bates, K.T., 2017. A quantitative evaluation of physical and digital approaches to centre of mass estimation. *Journal of anatomy*, *231*(5), pp.758-775.

Mallet, C., Billet, G., Houssaye, A. and Cornette, R., 2020. A first glimpse at the influence of body mass in the morphological integration of the limb long bones: an investigation in modern rhinoceroses. *Journal of Anatomy*, *237*(4), pp.704-726.

Mallet, C., Billet, G., Cornette, R. and Alexandra Houssaye, A., 2022. Adaptation to graviportality in Rhinocerotoidea? An investigation through the long bone shape variation in their hindlimb. *Zoological Journal of the Linnean Society*, *196*(3), pp.1235-1271.

Martin, M.L., Travouillon, K.J., Fleming, P.A. & Warburton, N.M., 2020. Review of the methods used for calculating physiological cross-sectional area (PCSA) for ecological questions. *Journal of Morphology*, 281(7), pp.778–789. https://doi.org/10.1002/jmor.21139

Martínez-Navarro, B., Barrena, P.P., Malapeira, J.M., Montoya, S.R., Ortiz, M.P.E., Torregrosa, V. and Claros, J.A.P., 2010. La fauna de grandes mamíferos de Fuente Nueva-3 y Barranco León-5: Estado de la cuestión. In *Ocupaciones humanas en el Pleistoceno inferior y medio de la Cuenca de Guadix-Baza* (pp. 197-236).

Marugán-Lobón, J., Chiappe, L.M. and Farke, A.A., 2013. The variability of inner ear orientation in saurischian dinosaurs: testing the use of semicircular canals as a reference system for comparative anatomy. *PeerJ*, *1*, p.e124.

McMahon, T., 1973. Size and shape in biology: elastic criteria impose limits on biological proportions, and consequently on metabolic rates. *Science*, *179*(4079), pp.1201-1204.

Mead, A.J. and Wall, W.P., 1998. Dietary implications of jaw biomechanics in the rhinocerotoids Hyracodon and Subhyracodon from Badlands National Park, South Dakota. *United States Department of the Interior• National Park Service• Geological Resource Division*, p.23.

E. H. W. Meijering, W. J. Niessen, M. A. Viergever., 2001. Quantitative Evaluation of Convolution-Based Methods for Medical Image Interpolation. Medical Image Analysis, vol. 5, pp. 111-126.

Mendoza, M. and Palmqvist, P., 2008. Hypsodonty in ungulates: an adaptation for grass consumption or for foraging in open habitat?. *Journal of Zoology*, *274*(2), pp.134-142.

Minetti, A.E., Ardigo, L.P., Reinach, E. and Saibene, F., 1999. The relationship between mechanical work and energy expenditure of locomotion in horses. *Journal of Experimental Biology*, *202*(17), pp.2329-2338.

Morales-García, N.M., Säilä, L.K. and Janis, C.M., 2020. The Neogene savannas of North America: A retrospective analysis on artiodactyl faunas. *Frontiers in Earth Science*, *8*, p.191.

Morimoto, T., Inoue, T., Masuda, Y. and Nagashima, T., 1989. Sensory components facilitating jaw-closing muscle activities in the rabbit. *Experimental brain research*, *76*(2), pp.424-440.

Myers, M.J. and Steudel, K., 1985. Effect of limb mass and its distribution on the energetic cost of running. *Journal of Experimental biology*, *116*(1), pp.363-373.

Myers, M.J. and Steudel, K., 1997. Morphological conservation of limb natural pendular period in the domestic dog (Canis familiaris): implications for locomotor energetics. *Journal of Morphology*, *234*(2), pp.183-196.

Nardelli, F., 2014. The last chance for the Sumatran rhinoceros? *Pachyderm*, *55*, pp.43-53.

Newsom, L.A. and Mihlbachler, M.C., 2006. Mastodons (Mammut americanum) diet foraging patterns based on analysis of dung deposits. In *First floridians and last mastodons: The page-ladson site in the Aucilla river* (pp. 263-331). Dordrecht: Springer Netherlands.

Nishita, T., Goto, T., Kimura, H. and Asari, M., 1993. Carbonic anhydrase III content in various equine muscles. *Comparative Biochemistry and physiology. B, Comparative Biochemistry*, *106*(1), pp.199-202.

Northey, R.D., Hawley, J.G. and Suckling, G.W., 1975. The tooth to pad relationship in sheep-some mechanical considerations. *New Zealand Journal of Agricultural Research*, *18*(2), pp.133-138.

Owen-Smith, R.N. and Smith, R.N.O., 1973. *The behavioural ecology of the white rhinoceros* (Doctoral dissertation, University of Wisconsin).

Owen-Smith, R.N., 1988. *Megaherbivores: the influence of very large body size on ecology*. Cambridge university press.

Pandolfi, L., Rivals, F. and Rabinovich, R., 2020. A new species of rhinoceros from the site of Bethlehem: 'Dihoplus' bethlehemsis sp. nov. (Mammalia Rhinocerotidae). *Quaternary International*, *537*, pp.48-60.

Perry, J.M., Hartstone-Rose, A. and Wall, C.E., 2011. The jaw adductors of strepsirrhines in relation to body size, diet, and ingested food size. *The Anatomical Record: Advances in Integrative Anatomy and Evolutionary Biology*, *294*(4), pp.712-728.

Peters, R.H., 1986. *The ecological implications of body size* (Vol. 2). Cambridge university press.

Picard, B., Robelin, J., Pons, F. and Geay, Y., 1994. Comparison of the foetal development of fibre types in four bovine muscles. *Journal of Muscle Research & Cell Motility*, *15*(4), pp.473-486.

Polly, P.D., Lawing, A.M., Fabre, A.C. and Goswami, A., 2013. Phylogenetic principal components analysis and geometric morphometrics. *Hystrix*, *24*(1), p.33.

Prevrhal, S., Engelke, K. and Kalender, W.A., 1999. Accuracy limits for the determination of cortical width and density: the influence of object size and CT imaging parameters. *Physics in Medicine & Biology*, *44*(3), pp.751-764.

Price, S.A. and Bininda-Emonds, O.R., 2009. A comprehensive phylogeny of extant horses, rhinos and tapirs (Perissodactyla) through data combination. *Zoosystematics and Evolution*, *85*(2), pp.277-292.

Prothero, D.R. and Sereno, P.C., 1982. Allometry and paleoecology of medial Miocene dwarf rhinoceroses from the Texas Gulf Coastal Plain. *Paleobiology*, *8*(1), pp.16-30.

Prothero, D.R., 2005. *The evolution of North American rhinoceroses*. Cambridge University Press.

Püschel, H.P., Shelley, S.L., Williamson, T.E., Perini, F., Wible, J.R. and Brusatte, S.L., 2022. NEW PHYLOGENY OF LITOPTERNA AND "ARCHAIC" PALEOGENE UNGULATES ENLIGHTENS THE INTERFAMILIARY AFFINITIES WITHIN THE ORDER. *Journal of vertebrate paleontology*.

Pullen, A.H., 1977. The distribution and relative sizes of three histochemical fibre types in the rat tibialis anterior muscle. *Journal of Anatomy*, *123*(Pt 1), p.1.

Raadsheer, M.C., Van Eijden, T.M.G.J., Van Ginkel, F.C. and Prahl-Andersen, B., 1999. Contribution of jaw muscle size and craniofacial morphology to human bite force magnitude. *Journal of dental research*, *78*(1), pp.31-42.

Raafat, A., Pickford, M., Sileem, A., AbdelGawad, M. and Mekawy, M., 2024. New Moeritherium material from the Fayum area, Egypt. *Egyptian Journal of Geology*, *68*(1), pp.47-56.

Rabey, K.N., Green, D.J., Taylor, A.B., Begun, D.R., Richmond, B.G. and McFarlin, S.C., 2015. Locomotor activity influences muscle architecture and bone growth but not muscle attachment site morphology. *Journal of Human Evolution*, *78*, pp.91-102.

Raia, P., Carotenuto, F., Meloro, C., Piras, P. and Pushkina, D., 2010. The shape of contention: adaptation, history, and contingency in ungulate mandibles. *Evolution*, *64*(5), pp.1489-1503.

Raichle, M.E. and Gusnard, D.A., 2002. Appraising the brain's energy budget. *Proceedings of the National Academy of Sciences*, *99*(16), pp.10237-10239.

Raichlen, D.A., 2006. Effects of limb mass distribution on mechanical power outputs during quadrupedalism. *Journal of Experimental Biology*, *209*(4), pp.633-644.

Raichlen, D.A., 2004. *The relationship between limb muscle mass distribution and the mechanics and energetics of quadrupedalism in infant baboons (Papio cynocephalus)*. The University of Texas at Austin.

Raichlen, D.A., 2005a. Ontogeny of limb mass distribution in infant baboons (Papio cynocephalus). *Journal of Human Evolution*, *49*(4), pp.452-467.

Raichlen, D.A., 2005b. Effects of limb mass distribution on the ontogeny of quadrupedalism in infant baboons (Papio cynocephalus) and implications for the evolution of primate quadrupedalism. *Journal of human evolution*, *49*(4), pp.415-431.

Raichlen, D.A., 2006. Effects of limb mass distribution on mechanical power outputs during quadrupedalism. *Journal of Experimental Biology*, *209*(4), pp.633-644.

Ravosa, M.J., Ross, C.F., Williams, S.H. and Costley, D.B., 2010. Allometry of masticatory loading parameters in mammals. *The Anatomical Record: Advances in Integrative Anatomy and Evolutionary Biology*, *293*(4), pp.557-571.

Reilly, S.M. and Lauder, G.V., 1992. Morphology, behavior, and evolution: comparative kinematics of aquatic feeding in salamanders. *Brain, Behavior and Evolution*, *40*(4), pp.182-196.

Revell, L.J., 2012. phytools: an R package for phylogenetic comparative biology (and other things). *Methods in ecology and evolution*, (2), pp.217-223.

Richard, B.A. and Wainwright, P.C., 1995. Scaling the feeding mechanism of largemouth bass (Micropterus salmoides): kinematics of prey capture. *Journal of Experimental Biology*, *198*(2), pp.419-433.

Rivals, F. and Lister, A.M., 2016. Dietary flexibility and niche partitioning of large herbivores through the Pleistocene of Britain. *Quaternary Science Reviews*, *146*, pp.116-133.

Rivals, F., Prilepskaya, N.E., Belyaev, R.I. and Pervushov, E.M., 2020. Dramatic change in the diet of a late Pleistocene Elasmotherium population during its last days of life: Implications for its catastrophic mortality in the Saratov region of Russia. *Palaeogeography, Palaeoclimatology, Palaeoecology*, *556*, p.109898.

Roberts, T.J., 2016. Contribution of elastic tissues to the mechanics and energetics of muscle function during movement. *Journal of Experimental Biology, 219*(2), pp.266-275.

Rockenfeller, R., Günther, M., Clemente, C.J. and Dick, T.J., 2024. Rethinking the physiological cross-sectional area of skeletal muscle reveals the mechanical advantage of pennation. *Royal Society Open Science*, *11*(9), p.240037.

Ross, C.F. and Iriarte-Diaz, J., 2014. What does feeding system morphology tell us about feeding?. *Evolutionary Anthropology: Issues, News, and Reviews*, *23*(3), pp.105-120.

Ross, C.F., Reed, D.A., Washington, R.L., Eckhardt, A., Anapol, F. and Shahnoor, N., 2009. Scaling of chew cycle duration in primates. *American Journal of Physical Anthropology: The Official Publication of the American Association of Physical Anthropologists*, *138*(1), pp.30-44.

Ross, C.F., Iriarte-Diaz, J., Platts, E., Walsh, T., Heins, L., Gerstner, G.E. and Taylor, A.B., 2017. Scaling of rotational inertia of primate mandibles. *Journal of human evolution*, *106*, pp.119-132.

Ross, C.F., Dharia, R., Herring, S.W., Hylander, W.L., Liu, Z.J., Rafferty, K.L., Ravosa, M.J. and Williams, S.H., 2007. Modulation of mandibular loading and bite force in mammals during mastication. *Journal of Experimental Biology*, *210*(6), pp.1046-1063.

Rubes, J., Musilova, P., Kopecna, O., Kubickova, S., Cernohorska, H. and Kulemsina, A.I., 2012. Comparative molecular cytogenetics in Cetartiodactyla. *Cytogenetic and Genome Research*, *137*(2-4), pp.194-207.

Sakagami, R. and Kawabe, S., 2020. Endocranial anatomy of the ceratopsid dinosaur Triceratops and interpretations of sensory and motor function. *PeerJ*, *8*, p.e9888.

Salmons, S., 2009. Adaptive change in electrically stimulated muscle: a framework for the design of clinical protocols. *Muscle & Nerve: Official Journal of the American Association of Electrodiagnostic Medicine*, *40*(6), pp.918-935.

Sanders, W.J., 2023. *Evolution and fossil record of African Proboscidea*. CRC Press.

Schaffer, W.M. and Reed, C.A., 1972. The co-evolution of social behavior and cranial morphology in sheep and goats (Bovidae, Caprini).

Schellhorn, R., 2018. A potential link between lateral semicircular canal orientation, head posture, and dietary habits in extant rhinos (Perissodactyla, Rhinocerotidae). *Journal of Morphology*, *279*(1), pp.50-61.

Scherberich, J., Windfelder, A.G., Steinbart, J. and Krombach, G.A., 2025. Measurement accuracy of CT systems: The importance of calibration phantoms. *Plos one*, *20*(9), p.e0332263.

Schiaffino, S. and Reggiani, C., 2011. Fiber types in mammalian skeletal muscles. *Physiological reviews*, *91*(4), pp.1447-1531.

Schiffmann, C., Hatt, J.M., Hoby, S., Codron, D. and Clauss, M., 2019. Elephant body mass cyclicity suggests effect of molar progression on chewing efficiency. *Mammalian Biology*, *96*, pp.81-86.

Schindelin, J., Arganda-Carreras, I., Frise, E., Kaynig, V., Longair, M., Pietzsch, T., Preibisch, S., Rueden, C., Saalfeld, S., Schmid, B. and Tinevez, J.Y., 2012. Fiji: an open-source platform for biological-image analysis. *Nature methods*, *9*(7), pp.676-682.

Schmid, B., Schindelin, J., Cardona, A., Longair, M., & Heisenberg, M. (2010). A high-level 3D visualization API for Java and ImageJ. *BMC Bioinformatics*, *11*(1). doi:10.1186/1471-2105-11-274

Schoch, R.M. and Lucas, S.G., 1985. The phylogeny and classification of the Dinocerata (Mammalia, Eutheria). *Bulletin of the Geological Institutions of the University of Uppsala*, *11*, pp.31-58.

Schulte, P.M., 2015. The effects of temperature on aerobic metabolism: towards a mechanistic understanding of the responses of ectotherms to a changing environment. *The Journal of experimental biology*, *218*(12), pp.1856-1866.

Schultz, J.A., Engels, S., Schwermann, L.C. and v Koenigswald, W., 2020. *Evolutionary trends in the mastication patterns in some perissodactyls, cetartiodactyls, and proboscideans* (pp. 215-230). Verlag Dr. Friedrich Pfeil.

Sereno, P.C., Wilson, J.A., Witmer, L.M., Whitlock, J.A., Maga, A., Ide, O. and Rowe, T.A., 2007. Structural extremes in a Cretaceous dinosaur. *PloS one*, *2*(11), p.e1230.

Seymour, R.S., 2016. Cardiovascular physiology of dinosaurs. *Physiology*, *31*(6), pp.430-441.

Sharp, A.C., 2014. Three dimensional digital reconstruction of the jaw adductor musculature of the extinct marsupial giant Diprotodon optatum. *PeerJ*, *2*, p.e514.

Shoshani, J., 1998. Understanding proboscidean evolution: a formidable task. *Trends in Ecology & Evolution*, *13*(12), pp.480-487.

Shoshani, J. and Tassy, P., 2005. Advances in proboscidean taxonomy & classification, anatomy & physiology, and ecology & behavior. *Quaternary International*, *126*, pp.5-20.

Smith, B.H., 1991. Dental development and the evolution of life history in Hominidae. *American Journal of Physical Anthropology*, *86*(2), pp.157-174.

Solounias, N., Danowitz, M., Buttar, I. and Coopee, Z., 2019. Hypsodont crowns as additional roots: A new explanation for hypsodonty. *Frontiers in Ecology and Evolution*, *7*, p.135.

Stevens, K.A., 2013. The articulation of sauropod necks: methodology and mythology. *PLoS One*, *8*(10), p.e78572.

Stover, K.K. and Williams, S.H., 2011. Intraspecific scaling of chewing cycle duration in three species of domestic ungulates. *Journal of Experimental Biology*, *214*(1), pp.104-112.

Suraprasit, K., Jongautchariyakul, S., Yamee, C., Pothichaiya, C. and Bocherens, H., 2019. New fossil and isotope evidence for the Pleistocene zoogeographic transition and hypothesized savanna corridor in peninsular Thailand. *Quaternary Science Reviews*, *221*, p.105861.

Taylor, C.R., Shkolnik, A.M.I.R.A.M., Dmi'el, R.A.Z.I., Baharav, D. and Borut, A.R.I.E.H., 1974. Running in cheetahs, gazelles, and goats: energy cost and limb configuration. *American Journal of Physiology-Legacy Content*, *227*(4), pp.848-850.

Taylor, M.P., Wedel, M.J. and Naish, D., 2009. Head and neck posture in sauropod dinosaurs inferred from extant animals. *Acta Palaeontologica Polonica*, *54*(2), pp.213-220.

Turnbull, W.D., 1967. *The mammalian masticatory apparatus* (Doctoral dissertation, The University of Chicago).

Tuxen, A. and Kirkeby, S., 1990. An animal model for human masseter muscle: histochemical characterization of mouse, rat, rabbit, cat, dog, pig, and cow masseter muscle. *Journal of oral and maxillofacial surgery*, *48*(10), pp.1063-1067.

Upham, N.S., Esselstyn, J.A. and Jetz, W., 2019. Inferring the mammal tree: species-level sets of phylogenies for questions in ecology, evolution, and conservation. *PLoS biology*, *17*(12), p.e3000494.

Valerio, S.O., Hummel, J., Codron, D., Hatt, J.M. and Clauss, M., 2022. The ruminant sorting mechanism protects teeth from abrasives. *Proceedings of the National Academy of Sciences*, *119*(49), p.e2212447119.

Van Der Klaauw, C.J., 1952. Size and position of the functional components of the skull. A contribution to the knowledge of the architecture of the skull, based on data in the literature. *Archives Néerlandaises de Zoologie*, *9*(1), pp.1-556.

Van Eijden, T.M.G.J., 1991. Three-dimensional analyses of human bite-force magnitude and moment. *Archives of oral biology*, *36*(7), pp.535-539.

Van Eijden, T.M.G.J., Korfage, J.A.M. and Brugman, P., 1997. Architecture of the human jaw-closing and jaw-opening muscles. *The Anatomical Record: An Official Publication of the American Association of Anatomists*, *248*(3), pp.464-474.

Vidal, P.P., Graf, W. and Berthoz, A., 1986. The orientation of the cervical vertebral column in unrestrained awake animals: I. Resting position. *Experimental Brain Research*, *61*(3), pp.549-559.

Virot, E., Ma, G., Clanet, C. and Jung, S., 2017. Physics of chewing in terrestrial mammals. *Scientific reports*, *7*(1), p.43967.

Vøillestad, N.K., Tabata, I. and Medbø, J.I., 1992. Glycogen breakdown in different human muscle fibre types during exhaustive exercise of short duration. *Acta physiologica scandinavica*, *144*(2), pp.135-141.

Voje, K.L., Hansen, T.F., Egset, C.K., Bolstad, G.H. and Pélabon, C., 2014. Allometric constraints and the evolution of allometry. *Evolution*, *68*(3), pp.866-885.

Von Koenigswald, W., 2011. Diversity of hypsodont teeth in mammalian dentitions–construction and classification. *Palaeontographica Abteilung A*.

Von Koenigswald, W., Widga, C. and Göhlich, U.B., 2023. New mammutids (Proboscidea) from the Clarendonian and Hemphillian of Oregon – a survey of Mio-Pliocene mammutids from North America. *Bulletin of the Museum of Natural History, University of Oregon*, 30, pp.1–63.

Walker, R.H., Hutchinson, M.C., Potter, A.B., Becker, J.A., Long, R.A. and Pringle, R.M., 2023. Mechanisms of individual variation in large herbivore diets: Roles of spatial heterogeneity and state-dependent foraging. *Ecology*, *104*(2), p.e3921.

Welker, F., Collins, M.J., Thomas, J.A., Wadsley, M., Brace, S., Cappellini, E., Turvey, S.T., Reguero, M., Gelfo, J.N., Kramarz, A. and Burger, J., 2015. Ancient proteins resolve the evolutionary history of Darwin's South American ungulates. *Nature*, *522*(7554), pp.81-84.

Wilken, A.T., Schultz, J.A., Luo, Z.X. and Ross, C.F., 2024. A new biomechanical model of the mammal jaw based on load path analysis. *Journal of Experimental Biology*, *227*(18), p.jeb247030.

Williams, S.H. and Kay, R.F., 2001. A comparative test of adaptive explanations for hypsodonty in ungulates and rodents. *Journal of Mammalian Evolution*, *8*(3), pp.207-229.

Williams, S.H., Vinyard, C.J., Wall, C.E. and Hylander, W.L., 2007. Masticatory motor patterns in ungulates: a quantitative assessment of jaw-muscle coordination in goats, alpacas and horses. *Journal of Experimental Zoology Part A: Ecological Genetics and Physiology*, *307*(4), pp.226-240.

Wroe, S., McHenry, C. and Thomason, J., 2005. Bite club: comparative bite force in big biting mammals and the prediction of predatory behaviour in fossil taxa. *Proceedings of the Royal Society B: Biological Sciences*, *272*(1563), pp.619-625.

Zeuner, F.E., 1934. *Die Beziehungen zwischen Schadelform und Lebensweise bei den rezenten und fossilen Nashornern*. Lippert & Company.

Zhang, F., Langenbach, G.E.J., Hannam, A.G. and Herring, S.W., 2001. Mass properties of the pig mandible. *Journal of dental research*, *80*(1), pp.327-335.

Zhang, F., Peck, C.C. and Hannam, A.G., 2002. Mass properties of the human mandible. *Journal of biomechanics*, *35*(7), pp.975-978.

Zhang, H., Wang, Y., Janis, C.M., Goodall, R.H. and Purnell, M.A., 2017. An examination of feeding ecology in Pleistocene proboscideans from southern China (Sinomastodon, Stegodon, Elephas), by means of dental microwear texture analysis. Quaternary International, 445, pp.60-70

Zhanxiang, Q. and Banyue, W., 2007. Paracerathere fossil of china. *PalaeontologiaSinica, newseriesc*, *29*, pp.1-396.

Zhegallo, V., Kalandadze, N., Shapovalov, A., Bessudnova, Z., Noskova, N. and Tesakova, E., 2005. On the fossil rhinoceros Elasmotherium (including the collections of the Russian Academy of Sciences). *Cranium*, *22*(1), pp.17-40.

Zhou, Z., Winkler, D.E., Fortuny, J., Kaiser, T.M. and Marcé-Nogué, J., 2019. Why ruminating ungulates chew sloppily: biomechanics discern a phylogenetic pattern. *PLoS One*, *14*(4), p.e0214510.